THE PRODUCTION OF POLYMER/NANOCOMPOSITE PROTON CONDUCTING MEMBRANES FOR POLYMER ELECTROLYTE MEMBRANE FUEL CELL (PEMFC) APPLICATIONS

by

Ayşe ASLAN

A thesis submitted to

The Graduate School of Sciences and Engineering

of

Fatih University

in partial fulfillment of the requirements for the degree of

Doctor of Philosophy

in

Chemistry

December 2013
Istanbul, Turkey

APPROVAL PAGE

This is to certify that I have read this thesis written by Ayşe ASLAN and that in my opinion it is fully adequate, in scope and quality, as a thesis for the degree of Doctor of Philosophy in Chemistry.

_____

Prof. Dr. Ayhan BOZKURT
Thesis Supervisor

I certify that this thesis satisfies all the requirements as a thesis for the degree of Doctor of Philosophy in Chemistry.

_____

(Assoc. Prof. Dr. Abdulhadi BAYKAL)
Head of Department

Examining Committee Members

Prof. Dr. Ayhan BOZKURT   _____

Prof. Dr. Turgay SEÇKİN   _____

Prof. Dr. Ali ATA   _____

Assoc. Prof. Dr. Ali Ekrem MÜFTÜOĞLU   _____

Assoc. Prof. Dr. Kurtuluş GÖLCÜK   _____

It is approved that this thesis has been written in compliance with the formatting rules laid down by the Graduate School of Sciences and Engineering.

_____

(Assoc. Prof. Dr. Nurullah ARSLAN)
Director

December 2013

THE PRODUCTION OF POLYMER/NANOCOMPOSITE PROTON CONDUCTING MEMBRANES FOR POLYMER ELECTROLYTE MEMBRANE FUEL CELL (PEMFC) APPLICATIONS

AYŞE ASLAN

Ph.D. Thesis - Chemistry
December 2013

Thesis Supervisor: Prof. Dr. Ayhan BOZKURT

ABSTRACT

Proton exchange membrane fuel cell (PEMFC) is widely used as alternative mobile and stationary power sources. The proton exchange membrane (PEM) is the key component in a proton exchange membrane fuel cell that can be sandwiched between catalytic composite electrodes to construct PEMFC. The great effort has been done for the development of novel proton exchange membranes. In this context, polymer nanocomposite membranes containing inorganic moieties have attracted great attention because of their dual nature stemming from the flexibility of the organic polymer backbone and the thermal and chemical stability of the inorganic additive.

In this thesis, proton conducting nanocomposite electrolytes containing poly(vinylphosphonic acid) (PVPA) and SiO_2 were prepared by two different methods. In the anhydrous state, the proton conductivity of PVPA(10)SiO_2 (*in situ*) was found to be 0,009 (Scm^{-1}) at 120°C. The proton conductivity of PVPA(10)SiO_2 increased to 0.08 (Scm^{-1}) at 50 % relative humidity. The SiO_2 nanoparticles in the composite membranes improved the thermal properties and increased the proton conductivity. proton conducting nanocomposite electrolytes containing Poly(vinylphosphonic acid) (PVPA) and TiO_2 have been prepared and characterized. In the nanocomposite materials, the TiO_2 content was varied from 5 to 20 percentage (w/w) to improve mechanical strength and stability. The thermal, proton conducting as well as morphology of the electrolytes were investigated. The results suggest that proton conduction is occurred between surface of the nano-titania particles with the aid of sulfonic acid and phosphonic acid units of PVPA.

The materials were prepared via two different approaches where in the first, a binary system was produced by mixing of poly(1-vinyl 1,2,4-triazole) (P(VTri))/sulfated nanotitania (TS) and poly(vinylphosphonic acid) (P(VPA))/ sulfated nanotitania (TS) composites. In the second, ternary nano composite membranes including P(VTri)/TS/P(VPA) were produced at several compositions to get P(VTri)-TS-P(VPA)$_x$ where x designates the molar ratio of the polymer repeating units and sulfated nanotitania ratio. The conductivity of is P(VTri)-TS-P(VPA)$_4$ found to be 0.003 (Scm^{-1}) at 150°C. Proton conducting nano-composite membranes included binary and ternary mixtures of sulfated nano-titania (TS), poly(vinyl alcohol) (PVA) and nitrilotri(methyl phosphonic acid) (NMPA) are discussed. The maximum proton conductivity has been measured for PVA-TS-(NMPA)$_3$ as 0.003 Scm^{-1} at 150 ^{o}C Proton conducting nano-composite membranes were prepared via ternary mixtures comprising sulfated nanotitania (TS), sulfonated polysulfone (SPSU) and nitrilotri(methyl phosphonic acid) (NMPA).The maximum proton conductivity of SPSU-TS-NMPA is 0.002 Scm^{-1} at 150 ^{o}C.

In another approach, azole functional PGMA grafted hollow silica sphere nanoparticles as a proton conducting bio-inspired membranes. For the preparation of hollow silica particles (HSS), a two-step method based on the sol–gel process was used in this study. HSS grafted with Poly(glycidyl methacrylate) (PGMA) by free radical polymerization of (glycidyl methacrylate) (GMA) and HSPGMA (Poly(glycidyl methacrylate) (PGMA) grafted hallow silica spheres) modified with 5-aminotetrazole (ATet), 3-amino-1,2,4-triazole (ATri) and 1H-1,2,4-triazole (Tri) in order to obtain 1,2,4-triazole functional PGMA grafted hallow silica spheres (HSPGMA-Tri), 5-aminotetrazole functional PGMA grafted hallow silica spheres (HSPGMA-Tet) and 5-Amino-Triazole functional PGMA grafted hallow silica spheres (HSPGMA-ATri) molecules via ring opening of the epoxide ring. The proton conductivitiy of the composite membranes are approximately 10^{-3} Scm^{-1} at 150 ^{o}C. As another type azol functional nanoparticles azol functional SiO$_2$ were synthesized and chracterizated.

In this thesis the functional nanoparticles were synthesized and the nanocomposite membranes were obtained. The characterization results indicated that the functional nanoparticles in the composite membranes improved the thermal and mechanical stability and enhanced the proton conductivity.

Keywords: Proton Exchange Membran Fuel Cell (PEMFC), Proton Conducting Nanocomposite Membranes, Functional Nano Particles, PVPA, SPSU, PVTri, PGMA, Hallow silica, SiO$_2$, TiO$_2$

PROTON İLETKEN MEMBRAN YAKIT HÜCRELERİ UYGULAMARI İÇİN PROTON İLETKEN POLİMER/NANOKOMPOZİT MEMBRANLARIN ÜRETİLMESİ

Ayşe ASLAN

Doktora Tezi - Kimya
Aralık 2013

Tez Danışmanı: Prof. Dr. Ayhan BOZKURT

ÖZ

Proton iletken membran yakıt hücreleri taşınabilir alternatif enerji depolama sistemleri olması, çevre duyarlılığı gibi sebepler göz önünde bulundurulduğunda enerjikaynağı olarak büyük bir öneme sahiptir. Proton iletken yakıt hücresinde protonun anottan katota geçişini sağlayan membran, yakıt hücresinin en önemli bölümünü oluşturmaktadır. Bu sebeple kimyasal ve termal kararlılığı yüksek maliyeti düşük yeni membranların üretilmesi anlamında çok fazla çalışma yapılmaktadır. Bu kapsamda, organik ve inorganik yapıların avantajlarını bir araya getiren polimer nanokompozit membranlar alternetif membranlar görülmektedir.

Bu tez çalışması kapsamında, ilk olarak SiO_2 nano parçacıkları ve poli(vinilfosfonik asit) (PVPA) polimeri kullanılarak $PVPA(x)SiO_2$ nanokompozit membranlar sentezlendi. Membranlar mekanik karıştırma ve in situ yöntemleri kullanılarak değişen oranlarda sentezlendi. Her membran için karakterizasyon çalışmaları yapıldı. $PVPA(10)SiO_2$ (*in situ*) membranına ait proton iletkenlik değeri nemsiz ortamda 120°C'de 0,009 (Scm^{-1}) ve %50 nem içeren $PVPA(10)SiO_2$ membranına ait iletkenlik değeri 100 °C' de 0.08 (Scm^{-1}) olarak öçüldü. TiO_2 nano parçacıkları ve poli(vinilfosfonik asit) (PVPA) polimeri kullanılarak mekanik karıştırma ve in situ yöntemleri ile değişen oranlarda $PVPA(x)TiO_2$ nanokompozit membranlar sentezlendi. Her membran için karakterizasyon çalışmaları yapıldı. Yapılan karakterizasyon çalışmaları sonucunda TiO_2 nanoparçacıklarının yüzeyi ile fosfonik asit grupları arasındaki etkileşim tespit edildi ve bu etkileşime bağlı olarak PVPA(x)TiO nanokompozit mebranlarının proton iletken ve termal özelliklerinin nano partiküller sayesinde arttığı belirlendi.

Poli(1-vinil 1,2,4-triazol) (P(VTri))/sulfonlanmış titanyum(TS) and poli(vinilfosfonik asit) (P(VPA))/ sulfonlanmış titanyum (TS) kompozitleri iki ve üç bileşenli olarak P(VTri)-TS-P(VPA)$_x$ sentezlendi. Sentezlenen herbir nanokompozit polimer membran için karakterizasyon testleri yapıldı. Üçlü sistemlere bir diğer örnek olarak sülfonlanmış nanotitanyum (TS), poli(vinil alkol) (PVA) ve nitrilotri(metiltrifosfonik asit) (NMPA) PVA-TS-(NMPA) nanokompozit membanları sentezlendi ve karakterizaston testleri yapıldı. Ayrıca sülfonlanmış polisülfone (SPSU), sülfonlanmış nanotitanyum (TS) ve nitrilotri(metiltrifosfonik asit) (NMPA) nanokompozit membanları sentezlendi ve karakterizaston testleri yapıldı. Yapılan karakterizasyon sonuçlarına göre sulfonik asit gruplarının proton iletkenliği artırdığı belirlendi.

Diğer bir çalışmada, küresel silika (HSS) yapıları Poli(glisidil metakrilat) (PGMA) polimeri ile dallanmış hale getirldi. PGMA ile modifiye edilmiş olan HSS daha sonra azol grupları (5-aminotetrazoe (ATet), 3-amino-1,2,4-triazol (ATri) and 1H-1,2,4-triazol (Tri)) ile PGMA üzerindeki epoksi gruplarının halka açılma reaksiyonu ile açılarak fonksiyonel hale getirildi. Fonksiyonel hale getirilen HSS yapıları daha sonra fosforik asit (H$_3$PO$_4$) ile dop edilerek proton iletken nanokompozit membranlar sentezlendi.

Anahtar Kelimeler: Proton İletken Yakıt Hücreleri (PEMFC), Proton İletken Nanokompozit Membran, Fonksiyonel Nano Partiküller, PVPA, SPSU, PVTri, PGMA, Hallow Silika, SiO$_2$, TiO$_2$.

To my parents

ACKNOWLEDGEMENT

I would like to express my sincere gratitude to my advisor, Prof. Dr. Ayhan BOZKURT, for taking me in as his graduate student and introducing me to fuel cell and nanotechnology. His creative thinking, insight, and drive have been inspirational. His expertise in nanostructured and polymer materials along with his vision of nanotechnology has been the source of inspiration to me for further research in the field.

I specially thank to Prof. Dr. Turgay SEÇKIN for his generous assistance and insightful discussions during my study. In addition his valuable times of consultation and editing that went into the completion of this dissertation were unbelievably helpful.

I am also very grateful to my colleagues Dr. Sevim ÇELIK, Ms. Hamide AYDIN, Mrs. Zehra DURMUŞ, Ms. Emine DOĞANAY and Ms. Ümran KURTAN. I highly appreciate their friendship and support.

I would like to thank Professor Dr.Ali ATA, Assoc. Professors Dr. GÖLCÜK and MÜFTÜOĞLU for serving on my thesis supervisory committee. I am grateful to them for their careful and critical reading of my thesis and invaluable suggestions.

I would also like to thank to TUBITAK-BIDEB 2211 scholarship programme during my PhD education.

I express my thanks to my friends Mrs. Gülsen SÜSLÜ, Ms. Gökşen KAPLAN, and Ms. Hilal YANARDAĞ, for their friendship and moral support.

Finally, I would like to thank my parents and my brothers for their love, patience and encouragement.

TABLE OF CONTENTS

LIST OF TABLES

TABLE

LIST OF FIGURES

FIGURE

LIST OF SYSMBOLS AND ABBREVIATIONS

SYMBOL/ABBREVIATION

ATet	5-Aminotetrazole
ATri	3-Amino-1,2,4-triazole
BnIm	Benzimidazole
DSC	Differential Scanning Calorimetry
FTIR	Fourier Transform Infrared Radiation
HSS	Hallow Silica Sphere
MeIm	1-Methylimidazole
P4VI	Poly(4-vinylimidazole)
PAMPSA	Poly(2-acrylamido-2-methyl-1-propane sulfonic acid)
PEMFCs	Polymer electrolyte membrane fuel cells
PEMs	Polymer electrolyte membranes
PGMA	Poly(glycidil Methacrilate)
PVBBA	Poly (vinyl benzene boronic acid)
PVBPA	Poly(vinyl benzyl phosphonic acid)
PVPA	Poly(vinyl phosphonic acid)
PVTri	Polyvinyl triazole
Py	Pyrazole
RH	Relative humidity
SEM	Scanning Electron Microscopy
SPSU	Sulfonated Polysulfone
TA	Triflic acid
Tet	Tetrazole

TGA	Thermogravimetric Analysis
Tri	Triazole
TS	Sulfated Titania

CHAPTER 1

INTRODUCTION

1.1 INTRODUCTION

Proton exchange membrane fuel cell (PEMFC) is widely used as alternative mobile and stationary power sources. Fuel cells have become an important energy conversion technology because of their high electrical efficiency, low emissions, and easy operations this technology experienced several cycles of intense research activity (Barbir and Gómez 1996, Li, Zhou et al. 2005, Aslan, Celik et al. 2009, Celik, Bozkurt et al. 2012). The significant requirement in attaining optimum performance from PEMFCs is to achieve effective humidification of the ionomeric structure of the membrane. Great improvements have been made to the preparation and modification of polymer electrolyte membranes (PEMs) in the past decades (Bao, Ouyang et al. 2006, Hagihara, Uchida et al. 2006).

The proton exchange membrane (PEM) is the key component in a proton exchange membrane fuel cell which has a capability to transport protons from anodic to cathodic side (Barbir and Gómez 1996, Bozkurt, Meyer et al. 2003).The best known example of PEMs is DuPont's perfluorosulfonic acid type membrane (Nafion) which is most widely used both in fuel cell research and industry. In addition, the materials which have non-perfluorinated backbone chains were also developed a alternative materials to Nafion.

The great effort has gone into the development of proton exchange membranes which are more stable than commercial Nafion. As a consequence, polymeric/inorganic composite

membranes were identified and achieved by many research groups. The polymer nano composite membranes have a lot of advantages because of their dual functionality like specific chemical reactivity and flexibility of the organic polymer backbone, as well as the mechanical properties and thermal stability of the inorganic backbone. As well known, Polysulfones (PS) are commonly used materials, because of their mechanical properties, low cost, ease of processing thermal and chemical stability. Producing proton conducting materials these aromatic polymers have been sulfonated by treatment with various sulfonating methods.

Highly stable PEMs are developed by optimizing the degree of functionalization, interactions between two segments (organic–organic and organic–inorganic), controlled cross-linking and chemical or surface modifications. In this context, polymer composite membranes containing inorganic moieties have attracted great attention because of their dual nature stemming from the flexibility of the organic polymer backbone, and the thermal and chemical stability of the inorganic additive (Aslan and Bozkurt 2009, Celik, Bozkurt et al. 2012).

Polymer nanocomposites are promising materials which include inorganic nanoscale particles providing the advantages of rigidity, thermal stability and organic polymers supplying the flexibility, dielectric, ductility, and processibility (Krishnamoorti and Vaia 2007). The interest toward organic–inorganic composite materials increased due to their extraordinary properties arising from the relation between the organic moiety and the inorganic moiety(Mauritz and Jones 1990, Wen and Mark 1995, Ahmad, Sarwar et al. 1997, Ahmad, Sarwar et al. 1998). However, proton conductivity usually decreases with an increase in filler content due to the rather low proton conductivity of the fillers themselves (Suryani and Liu 2009). In addition, the conductivity may also be affected by interaction between the additive with proton-exchange groups in the original polymer matrix.

Inorganic units provide high mechanical and thermal stability as well as electrical and magnetic activity, while organic domains provide flexibility, multi-functional reactivity, and facilitate machining at low temperature. Additional novel properties can be introduced using nanocomposite materials. Even at low loadings this interfacial area creates a

significant volume fraction of interfacial polymer with properties different from the bulk polymer (Balazs, Emrick et al. 2006, Caseri 2006, Krishnamoorti and Vaia 2007, Schadler, Kumar et al. 2007). The structural and physicochemical properties of organic–inorganic composites depend on their composition, the size of the inorganic particles/filler, interfacial interactions, etc. (Schaefer and Justice 2007).

The increasing attention is presently being devoted to polymer nanocomposites due to the possibility of production of homogeneous membranes that can be applied in PEMFCs. In earlier studies inorganic fillers such as TiO_2 and SiO_2 have been frequently used where these fillers are indeed effective in improving mechanical properties of the composite membranes (Watanabe, Uchida et al. 1996, Yang, Srinivasan et al. 2001, Uchida, Ueno et al. 2003, Baglio, Arico et al. 2005, Chalkova, Pague et al. 2005, Jalani, Dunn et al. 2005, Chuang, Hsu et al. 2007). The ionic conductivity of polymer membranes including metal oxides, i.e., TiO_2, increases for a large temperature range.

Modifying inorganic fillers by inorganic sulphonic or phosphoric acid has become a promising way to enhance proton conductivity of membranes under intermediate temperature and low relative humidity or even anhydrous conditions (Hogarth, da Costa et al. 2005, Jin, Qiao et al. 2007, Rusanov, Kostoglodov et al. 2008, Wang, McDermid et al. 2008). Titania is usually used in the form of nanoparticles with high surface area, activity and excellent chemical stability(Yang, Chiu et al. 2008, Santiago, Isidoro et al. 2009). Moreover, acid-modified oxides such as sulfated titania and zirconia have been proposed as super acids where ionic conductive groups exist on its solid surface(Hino and Arata 1979, Hino and Arata 1980). Acid modified nanoparticles have better performance to improve the proton conductivity than unmodified filler. Super acids such as acid-modified oxides titania and zirconia have been preferred as filler for conducting membranes because of conductive groups exist on its solid surface (Baglio, Arico et al. 2005, Chalkova, Pague et al. 2005). Embedding acid-functionalized fillers can potentially enhance or preserve proton conductivity. Also as a new type of polymer nanocomposite membrane, acid modified nanoparticles have been introduced into polymers improving the proton conductivity. Previously, Munakata et al. have reported sulfuric acid-modified porous silica (Munakata, Chiba et al. 2005), and Wu et al. have reported a titania-based material (Wu, Hou et al.

2010). The sulfated nanoparticles are expected to show the highest proton conductivity when they dispersed in a suitable polymer matrices(Hino and Arata 1980).

As an organic moiety, Poly(vinyl alcohol) (PVA), one of the most commonly used matrices, has extensively been investigated with different kinds of nanofillers (Godovsky 2000, Kumar, Elgamiel et al. 2001, Qian, Yin et al. 2001). These studies showed that the introduction of nanosized particles into PVA altered its physicochemical properties. For example, incorporation of magnetite nanoparticles, synthesized by a sonochemical method, into PVA (Baglio, Arico et al. 2005) was found to reduce the glass transition temperature of PVA by 15 °C and the thermal stability by 28 °C. However, in the presence of montmorillonite (MMT) nanofiller, glass transition increased by 25 °C and the thermal degradation was unaffected up to 50 % of initial weight loss (Strawhecker and Manias 2000, Yu, Lin et al. 2003). More recently, PVA-based nanocomposites have been developed to improve the properties of the polymer for use in a variety of applications (Nakane, Yamashita et al. 1999, Cendoya, Lopez et al. 2001, Lin, Watanabe et al. 2003).

The phosphate-functional polymers and their derivatives have attracted considerable attention for fuel cell applications. Vinylphosphonic acid monomer can be polymerized with high yield by free radical polymerization in the absence of oligomeric by-products. The polymer matrix PVPA has interesting properties due to their acidic phosphate group(Pu, Pan et al. 2010). Both, PVPA homopolymer and its composite membranes exhibited high proton conductivity, moderate swelling property and ion exchange capacity(Aslan and Bozkurt 2009, Aslan and Bozkurt 2011). Functional polymers based on vinylphosphonic acid and derivatives have been recognized as promising materials in energy conversion. Poly(vinylphosphonic acid) (PVPA) is the simplest polymer in which one phosphonic acid group is tethered to each repeat unit of a macromolecule. Poly(vinylphosphonic acid) is an appropriate alternative for H_3PO_4 because it is the polymer with the highest concentration of immobilized phosphonic acid used in order to prevent self-condensation of acid groups up to 150 ^{0}C. Phosphonic acid functional polymers are commonly used for preparation of proton conductive membranes such as phosphonated siloxane matrices (Tripathi, Saxena et al. 2008), polyphosphazanes (Smitha, Sridhar et al. 2005) and polysulfone (Abu-Thabit, Ali et al. 2010). Among them

poly(vinylphosphonic acid) (P(VPA)) has emerged as an interesting candidate because of its extremely high concentration of phosphonic acid which is directly attached to a flexible polymer chain(Schuster, Rager et al. 2005, Gubler, Kramer et al. 2007, Steininger, Schuster et al. 2007). The conducting properties of novel polymer complex electrolytes consisting of poly(vinylphosphonic acid) and different polymers were studied different research groups (Schuster and Meyer 2003). As a polymer electrolyte vinyl phosphonic acid and 1-vinyl-1,2,4-triazole copolymer was synthesized and a proton conductivity of 10^{-3} Scm^{-1} at 120 ^{o}C was reported(Aslan, Celik et al. 2009). Additionaly, Kreuer confirmed the presence of Grotthuss proton transport mechanism in poly(vinyl phosphonic acid)(Kreuer 1996).

Amoung the azole-containing electrolyte systems, P(VTri) has greating interest due to its thermal stability and proton conducting capability. In the polymer/polymer and polymer/acid system P(VTri) commonly used (Celik, Bozkurt et al. 2012). Previously, the proton conductivity of Nafion–P(VTri) blend membranes was 5.3×10^{-4} Scm^{-1} (at 220 ◦C) in anhydrous state. The conductivity of blend increased at least three orders of magnitude upon hydration and exceeded 10^{-3} S cm^{-1} (at ambient temperature) with RH = 50% (Kim, Mori et al. 2007). In similar work, Özden et al. developed polymer electrolyte membranes based on P(VTri), doping it with p-toluenesulfonic acid, the conductivity rises to 2×10^{-2} Scm^{-1} (at 110 ◦C) (Ozden, Celik et al. 2010).

In this study, inorganic-organic nanocomposite membranes were produced via embedding of nanoparticles into polymer and functionalization of nanoparticles surface with polymer or phosphonic and sulfonic acid units. In addition novel nanocomposite membranes were synthesized using 1,2,4-triazole, 5-amino-tetrazol and 5-amino-1,2,4-triazol by ring opening reaction of epoxide on the surface of Silica. Hallow silica nanoparticles were grafted with poly(glycidyl methacrylate) (PGMA) and were doped with phosphoric acid to facilitate the proton transport.

The samples were characterized with NMR, FT-IR and elemental analysis. The thermal properties of the samples were analyzed with TGA and DSC. Morphology of nanocomposite membranes was investigated with SEM, AFM and TEM. The proton conductivity of the membranes was studied using impedance spectrometer.

1.2 FUEL CELLS

A fuel cell is a device that converts the chemical energy from a fuel into electricity through a chemical reaction with oxygen or another oxidizing agent. A fuel cell is like a battery in that it generates electricity from an electrochemical reaction but fuel cells are different from batteries in that the fuel cells, use an external supply of chemical energy and can run indefinitely, as long as it is supplied with a source of hydrogen and a source of oxygen (usually air).According to the nature of the electrolyte, fuel cells are classified each type requiring particular materials and fuel.

There are several different types of fuel cell but they are all based around a central design. A fuel cell unit consists of a stack, which has two electrodes, one positive and one negative, called the cathode and the anode. The electricity is produced via reactions that take place at the electrodes. The solid or a liquid electrolyte is the key component in the fuel cell which has a capability to transport ions from anodic to cathodic side.

The concept of a fuel cell had effectively been demonstrated in the early nineteenth century by Humphry Davy. Physicist William Grove developed the first crude fuel cells in 1839. The term fuel cell was first used in 1889 by Charles Langer and Ludwig Mond, who researched fuel cells using coal gas as a fuel.

1801
Humphry Davy demonstrates the principle of what became fuel cells.

1839
William Grove invents the 'gas battery', the first fuel cell.

1889
Charles Langer and Ludwig Mond develop Grove's invention and name the fuel cell.

1950s
General Electric invents the proton exchange membrane fuel cell.

1959
Francis Bacon demonstrates a 5 kW alkaline fuel cell.

1960s
NASA first uses fuel cells in space missions.

1970s
The oil crisis prompts the development of alternative energy technologies including PAFC.

1980s
US Navy uses fuel cells in submarines.

1990s
Large stationary fuel cells are developed for commercial and industrial locations.

2007
Fuel cells begin to be sold commercially as APU and for stationary backup power.

2008
Honda begins leasing the FCX Clarity fuel cell electric vehicle.

2009
Residential fuel cell micro-CHP units become commercially available in Japan. Also thousands of portable fuel cell battery chargers are sold.

Figure 1.1 The history of Fuell Cells.

NASA and industrial partners, began developing fuel cell generators for manned space missions at the end of the 1950s then, the first fuel cell have been developed with Willard Thomas Grubb at General Electric (GE) in cooperation with NASA, and was used in the Gemini space programme of the mid-1960s in many other applications. Also in the 1980s, substantial technical and commercial development continued into the use of fuel cells for transport applications. In the 1990s, PEMFC and SOFC technology were promoted by governments to clean transport also helped drive the development of PEMFC for automotive and small stationary applications. The fuel cells was characterised by increasing concerns on the part of governments, business and consumers over energy security, energy efficiency, and carbon dioxide ($CO2$) emissions. Fuel cells began to become commercial in a variety of applications in 2007. Fuel cells are used for primary and backup power for commercial, industrial and residential buildings and in remote or inaccessible areas. They are used to power fuel cell vehicles, including automobiles, buses, forklifts, airplanes, boats, motorcycles and submarines.

1.2.1 Polymer Electrolyte Membrane Fuel Cell (PEMFC)

PEMFC is the most useful type for transportation applications (Starz et al., 1999). The PEMFC has very high power density and a relatively low operating temperature (20 - 100 ^{o}C). Therefore PEMFC is self-starting without the need of external warm up and readily generating electricity which makes it particularly promising. A hydrogen-powered PEMFC consists of two electrodes and a separator polymer membrane as shown in Figure 1.2.
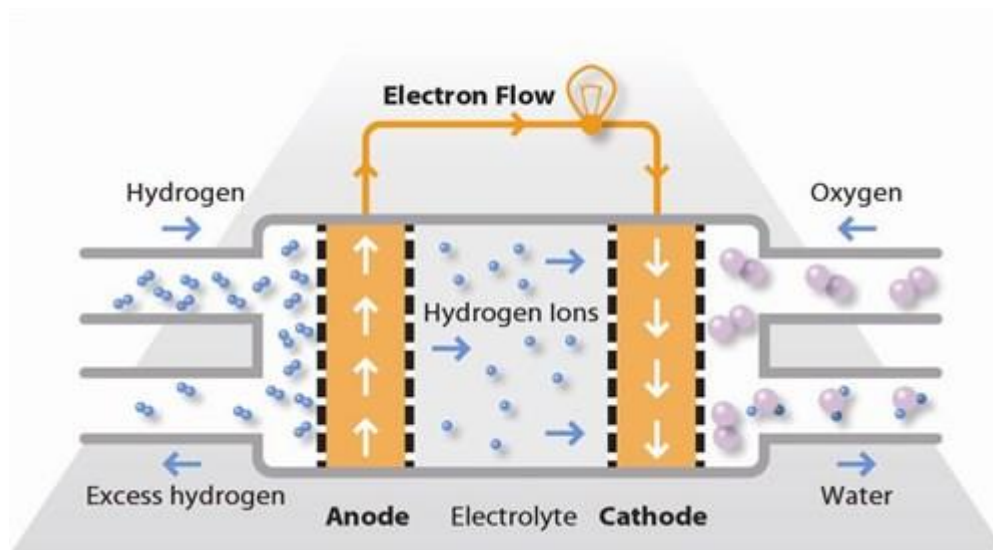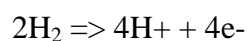
Anode Reactions:	$2H_2 => 4H+ + 4e-$
Cathode Reactions:	$O_2 + 4H+ + 4e- => 2 H_2O$
Overall Cell Reactions:	$2H_2 + O_2 => 2 H_2O$
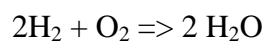
Figure 1.2 Schematic illustration of an individual fuel cell (fuel cell today, 2012).

Hydrogen is supplied to the anode and air is channeled to the cathode. At the anode, a platinum catalyst causes the hydrogen to split into positive hydrogen ions (protons) and negatively charged electrons. The polymer electrolyte membrane (PEM) permits only the transfer of proton to the cathode. The electrons travel along an external circuit to the cathode and create an electrical current. At the cathode, the electrons and protons combine with oxygen to form water which is the only waste product of hydrogen fueled PEMFCs.

1.2.2 Solid Oxide Fuel Cell (SOFC)

Solid oxide fuel cells are considered as the best useful fuel cell for stationary power generators that could provide electricity and heat for houses, factories or towns (Singhal, 2008). The operation temperature is very high (700-1000 ^{o}C) for this type of fuel cell.

1.2.3 Alkaline Fuel Cell (AFC)

Alkaline fuel cell is one of the oldest designs for fuel cells; use an aqueous solution of potassium hydroxide in a porous stabilized matrix as an electrolyte. The operating temperature ranges from 65 to 200 ^{o}C (Van den Broeck, 1993). It is also very expensive, so this type of fuel cell is unlikely to be commercialized, but research has revisited this type of fuel cells recently again (Jiang , 2009).

1.2.4 Molten-Carbonate Fuel Cell (MCFC)

Like the SOFC, molten-carbonate fuel cells are also useful for large stationary power generators (Bischoff, 2006). The fuel cells use molten alkaline carbonate (e.g., sodium bicarbonate NaHCO3) as electrolyte. The operating temperature is 600 ^{o}C.

1.2.5 Phosphoric-Acid Fuel Cell (PAFC)

The phosphoric-acid fuel cell has its potential use in small stationary power-generation systems (Kumura, 2004). Molten phosphoric acid (H3PO4) is used as electrolyte.. Therefore, it is not possible to use them in cars.

1.2.6 Direct-Methanol Fuel Cell (DMFC)

Methanol fuel cells are comparable to a PEMFC in regards to its operating temperature (90-120 ^{o}C), but yet are not as efficient (Bolufer, 2008). They use a polymer membrane as electrolyte. (Jiang, 2009).

1.3 POLYMER ELECTROLYTE MEMBRANE (PEM) FOR FUEL CELLS

1.3.1 SiO_2 Nanocomposite Membranes

The name silica comprises a large family of products with general formula SiO_2 or SiO_2xH_2O. It is a naturally occurring material found in minerals, such as quartz and flints. But silica used in chemical applications has a synthetic origin. There are two form of silica,

crystalline and amorphous. The crystalline form involves a high degree of ordering. The active surface, which may participate in any chemical or physical interaction, is limited to the external surface of the crystalline particles. Amorphous silica occurs in various forms likes fibers, sheets, sols, gels and powders. fabricated according to the application.Amain feature of interest is the porosity of the amorphous silica forms. Porosity introduces a large surface area inside the silica particles. As interphase processes require a large surface/mass ratio. So, amorphous silica is far more interesting for chemical and physical applications than their crystalline counterparts. It is commonly used in modifying the properties of the ionic polymers. The silica has an extremely large surface area and smooth nonporous surface, which could promote strong physical contact between the filler and the polymer matrix.

Hydrophilic silica nanoparticles improved hydrophilicity, methanol barrier and proton conductivity, while hydrophobic silica nanoparticles compensated against excessive water swelling (Macarie and Ilia 2010). The size of dispersed particles plays a significant role in controlling the physical and electrochemical properties of nanocomposite materials. In addition the dispersion of small fraction of filler inorganic particles in polymer nanocomposites can increase the ionic conductivity by 1-2 orders of magnitude and may substantially increase the mechanical stability (Pandey, Hashmi et al. 2008). Nafion-SiO_2 composite membrane were synthesized by self-assembly process that showed high water retention and durability. It was reported that SiO_2 nanoparticle content and hydrolysis conditions influenced the nanoparticle distribution and phase segregation yielding highest proton conductivity of $0.090 Scm^{-1}$(Kumar, Elgamiel et al. 2001).

The addition of inorganic oxides MO_2 (M = Si, Ti, Zr) into polymer matrices has been reported in previous studies as an effective method to enhance the water retention capability of membranes, such as Nafion (Weston and Steele 1982, Croce, Appetecchi et al. 1998, Yang, Srinivasan et al. 2001, Moskwiak, Giska et al. 2006). Studies on Nafion/SiO_2 composite membranes have attracted the attention of many research groups. Their results show that the morphological properties of the filler play a major role in the performance of the composite membranes at a high operating temperature (Hagihara, Uchida et al. 2006, Pandey, Hashmi et al. 2008, Pu, Pan et al. 2010).

1.3.2 TiO$_2$ Nanocomposite Membranes

TiO$_2$ is believed to be the most promising material at the present because of its powerful oxidation strength, high photostability, and nontoxicity (Chalkova, Pague et al. 2005, Liu, Guo et al. 2006). TiO$_2$ has been demonstrated as appropriate inorganic filler for developing composite proton exchange membrane because of its significant behavior in composites (Chen, Han et al. 2007, Carbone, Sacca et al. 2008). Studies on Nafion/TiO$_2$ composite membranes have attracted the attention of many research groups. Their results show that the morphological properties of the filler play a major role in the performance of the composite membranes at a high operating temperature (Baglio, Arico et al. 2005, Saccà, Carbone et al. 2005, Trakanprapai, Esposito et al. 2005, Chen, Han et al. 2007). Santiago et al. (Santiago, Isidoro et al. 2009) incorporated TiO$_2$ into Nafion by sol–gel method to form a composite membrane that showed an improved cell performance at 130 ^{0}C.

In previous studies about SPSU/TiO$_2$ composite membranes for high operating temperature showed that the filler has a major role in the morphological performance of the composite membranes (Kobayashi, Rikukawa et al. 1998, Devrim, Erkan et al. 2009, Jun, Zarrin et al. 2011). The increase in the nano particles content in the polymer matrix, results in the decrease in proton conductivity the reason can be attributed to low proton conductivity of the fillers which may also blocks the diffusion of the H+ ions themselves. Embedding acid-functionalized fillers can potentially enhance or preserve proton conductivity, reduce methanol permeability and optimize the interfacial compatibility of the polymer electrolyte membranes (Ren, Sun et al. 2006, Jin, Qiao et al. 2007, Wu, Zheng et al. 2007, Gosalawit, Chirachanchai et al. 2008, McKeen, Yan et al. 2008, Wang, McDermid et al. 2008, Suryani and Liu 2009, Wang, Zhang et al. 2009). In this context, as a new type of polymer nanocomposite membrane, acid modified nanoparticles have been introduced into polymers improving the proton conductivity. Acid-modified oxides such as sulfated titania and zirconia have been proposed as super acids where ionic conductive groups exist on its solid surface (Hino and Arata 1979). Previously, Kanamura et al. have reported sulfuric acid-modified porous silica, and Miyayama et al. have reported a zirconia-based material (Munakata, Chiba et al. 2005). These sulfated nanoparticles are expected to show the highest proton conductivity when they dispersed in the membranes.

The inorganic additive, TiO_2, is believed to be the most promising material at present due to its powerful oxidation strength, high photostability, and nontoxicity(Chen, Han et al. 2007, Carbone, Sacca et al. 2008). However, upon embedding TiO_2 into polymer matrices, proton conductivity usually decreases with an increase in filler content due to the rather low proton conductivity of the fillers themselves and their considerable dilution effect on the proton-exchange groups in the original polymer matrix. To overcome this problem, modified nanoparticles possessing different functional groups were employed. Bifunctional nanoparticles, having been embedded into polymers, play a role in the construction of novel nanocomposite membranes with enhanced proton conductivities(Nogami, Matsushita et al. 2000, Wang, Holmberg et al. 2002, Munakata, Chiba et al. 2005). In the previous work, we proved that the presence of acidic functional units enhanced the proton conductivity of polymer membranes and according to the XRD results the size of sulfated titania nanoparticles was 10-15 nm (Aslan and Bozkurt 2012, Aslan, Golcuk et al. 2012).

In addition, inclusion of TiO_2 filler into PVA matrix has effectively reduced the swelling ratio of the composite polymer membrane (Yang and Lin 2002, Tuncer, Sauers et al. 2007, Venckatesh, Balachandaran et al. 2012) Furthermore, Yang synthesized a crosslinked PVA composite polymer membrane to be applied in alkaline DMFCs (Gasa, Boob et al. 2006, Boroglu, Celik et al. 2011). Their results showed that the morphological properties of the filler played a major role in the performance of the composite membranes at higher operating temperatures.

Proton conducting membranes including functional nano-titania have been reported (Smitha, Sridhar et al. 2004, Li, Zhou et al. 2005) .High concentration of phosphonic acid groups, which were bonded by oxygen bridges with acid modified nano-titania, increased the proton conductivity and thermal stability of the nanocomposite membranes.

1.3.3 Functional Nanocomposite Membranes

The modification of the particles with functional polymer is a creative method to synthesize alternative polymer composite. The importance of this system is connected to its multifunctionality, where the same macromolecule has functional groups reactive with the nanoparticle and functional groups available for further chemical reactions(Taniguchi,

Shirai et al. 2005, Marini, Pourabbas et al. 2008, Sakai, Kajitani et al. 2010, Liu, Li et al. 2013). The developed strategy allows the functionalization of the nanoparticles by a polymer carrying functional groups capable of reacting with the nanoparticle surface and various molecules such as azole compounds(Alahmadi, Mohamad et al. 2012).

In this context, Hah et al. demonstrated a two-step method to prepare monodisperse hollow silica particles. Pu et al reported the functionalizing of HSS and developed composite membrane as proton conducting systems (Hah, Kim et al. 2003, Pu, Pan et al. 2010). Additionally, Tsyalkovsky et al. have reported the grafting of surface of nanoparticles with PGMA (Tsyalkovsky, Klep et al. 2007).

The special structure in the spheres and functional groups may hold more locked water and reduce the loading of the inorganic components, which may be beneficial for the water retention and improvement on the proton conductivity of the membranes. Due to advantages of functionalization as a new azole functional polymer composite, the azole based membranes was developed which have dramatically increased due to their fundamental properties of chemical energy conversion in industrial devices such as proton exchange membrane fuel cells (PEMFC)(Chuang, Hsu et al. 2007, Celik, Aslan et al. 2008, Aslan and Bozkurt 2012, Celik, Bozkurt et al. 2012). An interesting approach can be the proton solvent comprising functional polymers that are thermally stable and having proton transport pathway. From this point of view, polymer grafting HSS composite membranes including azole units would be interesting where azole units and H_3PO_4 these can be used as the proton charge carriers in the membrane under anhydrous condition.

1.3.4   Mechanisms of Proton Transport

The mechanism of proton transport in water molecules has been studied extensively (Eigen, 1964; Agmon, 1995; Agmon, 1996). The proton transport based on the "Grotthuss mechanism" (also called the "hopping mechanism", "chain mechanism" or "structure diffusion") comprises rapid intermolecular proton transfers (hopping) down a chain of hydrogen bonds, for which the transfer events are assumed to be highly correlated, with reorientation of water dipoles to produce a configuration which allows for the next hopping event (Grotthuss, 1806; Kreuer, 1997). The latter avoids strong solvent effects that tend to

suppress proton transfer reactions (Kreuer, 1996; Kreuer, 1997). However, this mechanism cannot explain all abnormal proton conductive systems. Based on NMR spectra and self-diffusion coefficients, Kreuer et al. proposed a "Vehicle mechanism", also called molecular diffusion, for the interpretation of the conductivity of fast proton conductors, such as zeolites, Nafion etc (Kreuer et al., 1982). According to this model the proton does not migrate as H^+ but as H_3O^+, NH_4^+, etc., bonded to a " vehicle" such as H_2O, NH_3, etc. The unloaded vehicles move in the opposite direction. Sequential hydrogen bonds are not necessary for proton transport with this model.

CHAPTER 2

EXPERIMENTAL

2.1 SYNTHESIS OF PVPA-SIO$_2$ NANOCOMPOSITE MEMBRANES

Vinylphosphonic acid (> 97%, Aldrich) DMF, (> 99%, Fluka) SiO$_2$ nanoparticles (10-20 nm, 99,5%, Aldrich) and $\alpha - \alpha$'- Azodiisobutyramidine dihydrochloridine (98%, Fluka) were used as received. PVPA was synthesized by free radical polymerization of vinyl phosphonic acid (Lee et al. 2007). Two different approaches were used for the preparation of nanocomposite materials. In the first approach, PVPA (see Figure 2.1.) and SiO$_2$ nanoparticles were mixed at several ratios to obtain PVPA(x)SiO$_2$ composite membranes where x was the percent (w/w) ratio of SiO$_2$ nanoparticles in the polymer ranging from 5 to 20. Then the mixture was further stirred under nitrogen atmosphere at 80 ^{o}C for 24 h, i.e., until getting a homogeneous milky solutions. The polymer films were cast onto polished poly(tetrafluoroethylene) (PTFE) plates and dried under vacuum at 50 ^{o}C and then stored in a glove box. Hygroscopic and free standing PVPA(x)SiO$_2$ films were obtained (see Figure2.1.).

In the second approach, the composites were synthesized by in situ polymerization of VPA with $\alpha - \alpha$- azodiisobutyramidine dihydrochloride as the initiator in the existence of SiO2 nanoparticles with various weight ratios. The reaction mixtures were further stirred under nitrogen atmosphere at 85 oC for 24 h, until the mixtures became homogeneous white gels. The polymer gels were cast onto polished PTFE then stored in a glove box.

Hygroscopic materials were obtained and denoted as PVPA(x)SiO2 (in situ). The polymeric nanocomposite films were stored in a glove box prior to all measurements
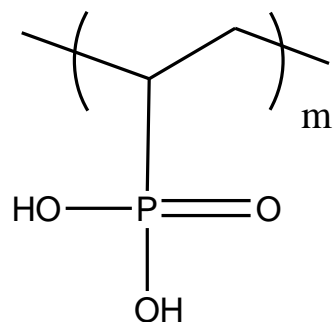
Figure 2.1 The Structure of PVPA.
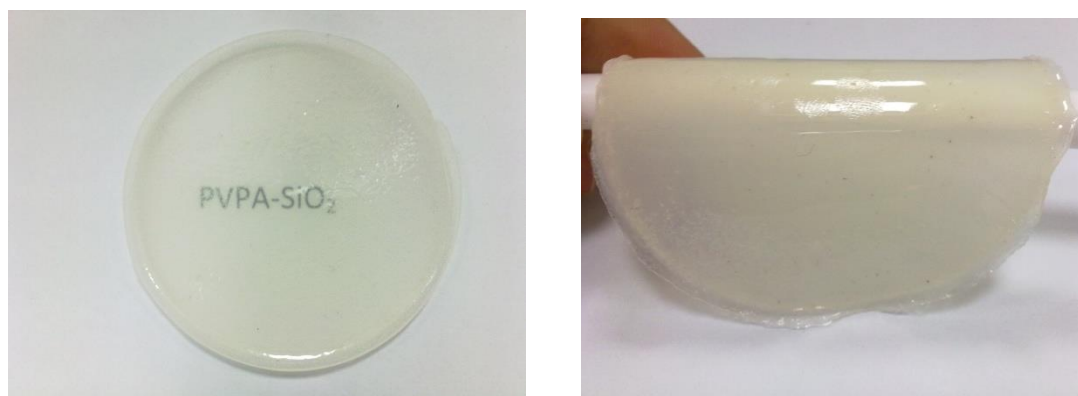
Figure 2.2 Free standing film of PVPASiO$_2$ composite membranes.

2.2 SYNTHESIS OF PVPA-TIO₂ NANOCOMPOSITE MEMBRANES

Vinylphosphonic acid (> 95%, Fluka) DMF, (> 99%, Fluka) TiO_2 nano particles (10-50nm- 99,5%, Aldrich) and $\alpha - \alpha$'- Azodiisobutyramidine dihydrochloridine (98%, Fluka) were used as received.

PVPA was synthesized by free radical polymerization of vinyl phosphonic acid according to previous work PVPA (Bingol, Meyer et al. 2006) (see Figure 2.3.) and TiO_2 nanoparticles were admixed at various percentage ratios to obtain PVPA(x)TiO_2 composite membranes x = 5,10,15,20) where x is the percentage (w/w) ratio of TiO_2 nanoparticles in PVPA matrix. Then the mixture was further stirred under nitrogen atmosphere at 80 ^{0}C for 24 h, i.e., until getting a homogeneous milky solutions. The polymer films were cast onto polished poly(tetrafluoroethylene) (PTFE) plates and dried under vacuum at 50 ^{0}C and then stored in a glove box.

In the second approach, the composites were synthesized by *in situ* polymerization of VPA with $\alpha - \alpha$'- Azodiisobutyramidine dihydrochloride as the initiator in the presence of TiO_2 nanoparticles. The reaction mixtures were further stirred under nitrogen atmosphere at 85 ^{o}C for 24 h, until the mixtures became homogeneous white viskos mixture. The polymers were cast onto polished PTFE plates, dried under vacuum at 50 ^{0}C and then stored in a glove box. Hygroscopic and free standing films were denoted as PVPA(x)TiO_2 (*in situ*). Prior to all measurements, polymer films were stored in a glove box.
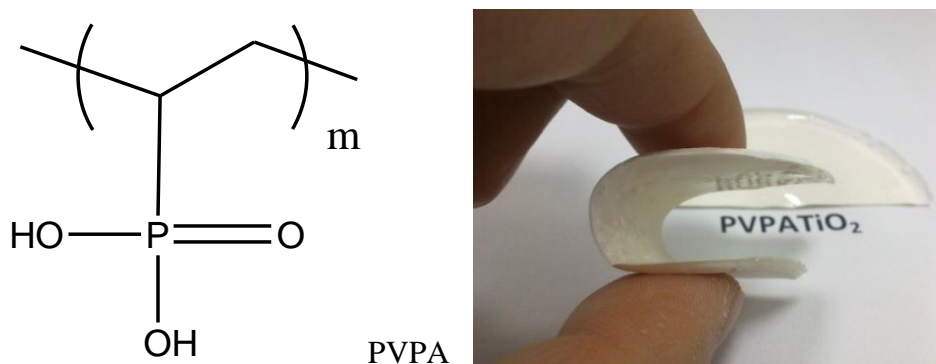
Figure 2.3 Structure of PVPA and picture of composite membrane.

2.3 SYNTHESIS OF PVPA-TIO$_2$SO$_3$H NANOCOMPOSITE MEMBRANES

Vinylphosphonic acid (> 95%, Fluka) DMF, (> 99%, Fluka) and $\alpha - \alpha$'-Azodiisobutyramidine dihydrochloridine (98%, Fluka) were used as received. PVPA was synthesized by free radical polymerization of vinyl phosphonic acid (Sevil and Bozkurt, 2004).

Sulfated nano-titania was prepared according to following procedure have reported by Sakai et al (Sakai, Kajitani et al. 2010). First, 5 g of titanyl sulfate (TiOSO4·nH2O, n=1–2) was dissolved into 200 mL of water and stirred continuously for 40 min. The solution was then heated under continuous stirring, resulting in a white precipitate at around 70 °C. The white precipitate was collected by suction filtration, washed several times with distilled water, the resultant powder was stored in glove box (Sakai, Kajitani et al. 2010). The amount of sulfate groups in the sample powder was to be about 1×10^{-3} molg^{-1} from the acid–base titration.

PVPA and sulfated nano-titania were mixed at various concentrations to get PVPATS$_x$ (see Figure 2.4) where x designates the molar ratio of the polymer repeating unit to sulfate units and varied from 1 to 4. Then the mixture was further stirred under nitrogen atmosphere at 50 ^{o}C for 24 h, i.e., until getting a homogeneous milky solutions. The polymer films were cast onto polished PTFE plates, dried under vacuum at 50 ^{o}C and then

stored in a glove box. Hygroscopic and free standing films were obtained and the materials and were denoted as PVPATS$_x$. Prior to all measurements, polymer films were stored in a glove box.
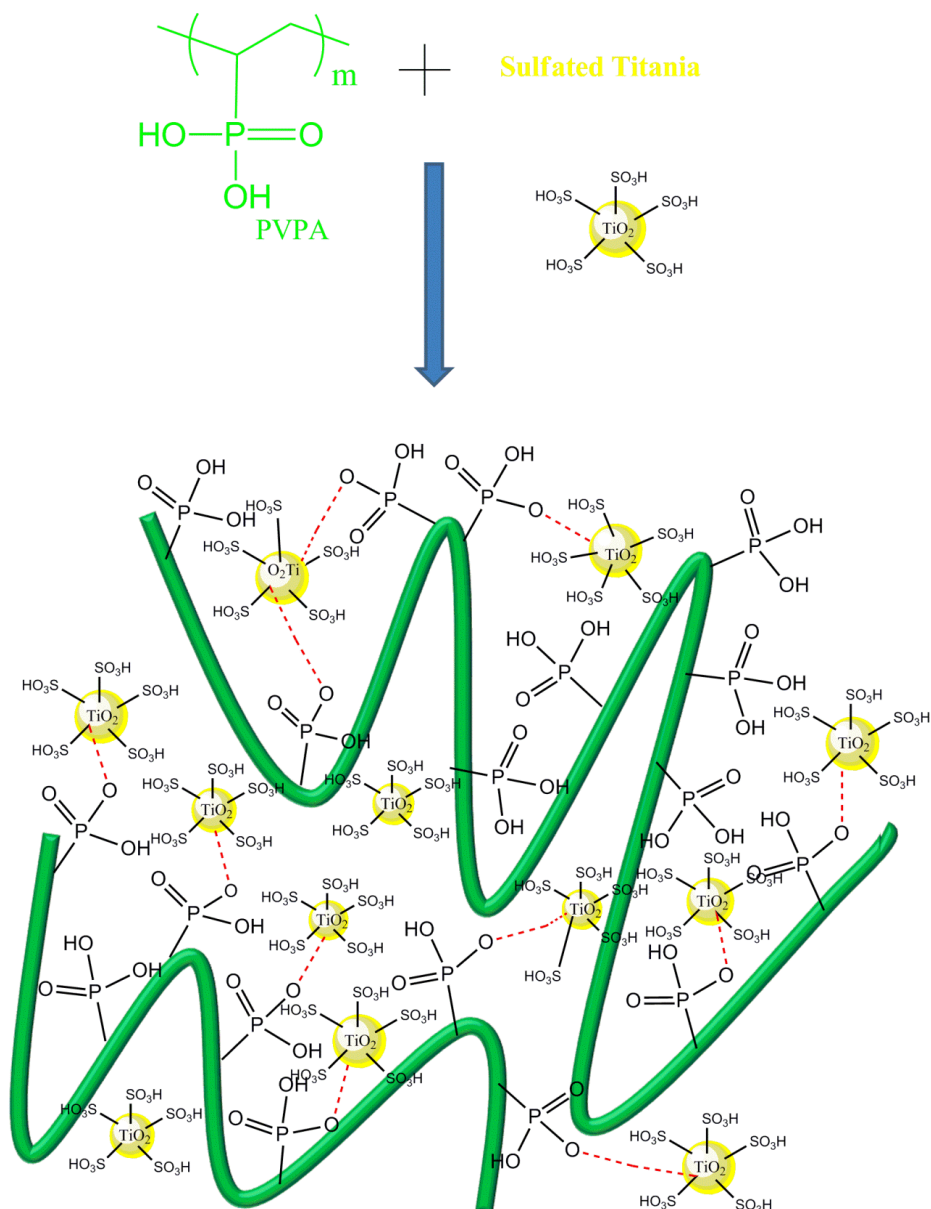
Figure 2.4 The model structure of PVPA/TS nanocomposites membranes.

2.4 SYNTHESIS OF NAFION-TS NANOCOMPOSITE MEMBRANES

DMF, (> 99%, Fluka) and $\alpha - \alpha$'- Azodiisobutyramidine dihydrochloridine (98%, Fluka) were used as received. PVPA was synthesized by free radical polymerization of vinyl phosphonic acid (Sevil and Bozkurt 2004).

Sulfated nano-titania was prepared according to following procedure have reported by Sakai et al (Sakai, Kajitani et al. 2010). First, 5 g of titanyl sulfate (TiOSO4·nH2O, n=1–2) was dissolved into 200 mL of water and stirred continuously for 40 min. The solution was then heated under continuous stirring, resulting in a white precipitate at around 70 °C. The white precipitate was collected by suction filtration, washed several times with distilled water, the resultant powder was stored in glove box (Sakai, Kajitani et al. 2010). The amount of sulfate groups in the sample powder was to be about 1×10^{-3} molg^{-1} from the acid–base titration.

Nafion and sulfated nano-titania were mixed at various concentrations to get Nafion-TS$_x$ (see Figure 2.5) where x designates the % ratio of the weight of the Nafion and varied from 5 to15. Then the mixture was further stirred under nitrogen atmosphere at 50 °C for 24 h, i.e., until getting a homogeneous milky solutions. The polymer films were cast onto polished PTFE plates, dried under vacuum at 50 °C and then stored in a glove box. Hygroscopic and free standing films were obtained and the materials and were denoted as Nafion-TS$_x$. Prior to all measurements, polymer films were stored in a glove box.
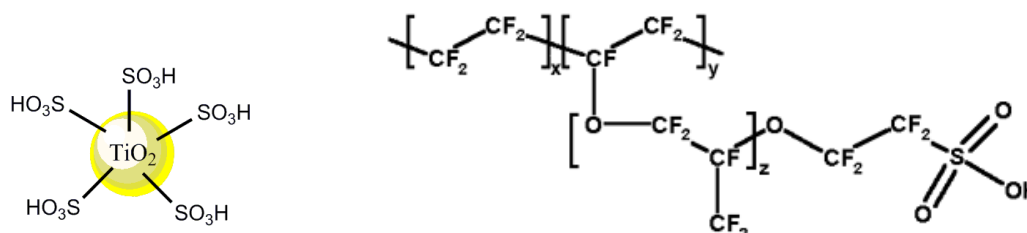
Figure 2.5 The structure of TS and Nafion.

2.5 SYNTHESIS OF PVTRI-TS-PVPA NANOCOMPOSITE MEMBRANES

1-Vinyl-1,2,4-triazole, VTri (> 97%, Fluka), Vinylphosphonic acid, VPA (> 95%, Fluka) and DMF (> 99%, Fluka) were used as received. Azobisisobutyronitrile (AIBN; Merck) was recrystallized from THF. The P(VTri), was successfully produced via free-radical polymerization in toluene with a high yield (> 85%). Poly(vinyl phosphonic acid) was produced by free radical polymerization of vinyl phosphonic acid (Bingol, Meyer et al. 2006).

Sulfated nano-titania was prepared according to the procedure reported by Sakai et al. (Sakai, Kim et al. 2012) 5 g of titanyl sulfate ($TiOSO4 \cdot nH2O$, n=1–2) was dissolved into 200 ml of water and stirred continuously for 40 min. The solution was then heated under continuous stirring, resulting in a white precipitate at around 70 °C. The white precipitate was collected by suction filtration, washed several times with distilled water, the resultant powder was stored in glove box (Sakai, Kim et al. 2012).

The membrane materials were produced by two different approaches. According to previous studies, at higher contents (10-20%) of additive materials (TS), the proton conductivity decreased because of their blocking effect as well as interactions between host guest systems and additive materials. For P(VTri)-TS-P(VPA)$_x$ composite membranes 5% (w/w) is the optimum composition. In the first, P(VTri) /TS membrane was prepared by dissolving 5% w/w sulfated titania into P(VTri) host polymer (see Figure 2.7.) and also P(VPA)/TS membrane was prepared by dissolving 5% (w/w) sulfated titania into P(VPA) host polymer. Then the solutions were stirred under nitrogen atmosphere for 24 h, i.e., until getting a homogeneous milky solutions. The films were cast onto polished poly(tetrafluoroethylene), PTFE plates and dried under vacuum at 50 ^{o}C and then stored in a glove box.
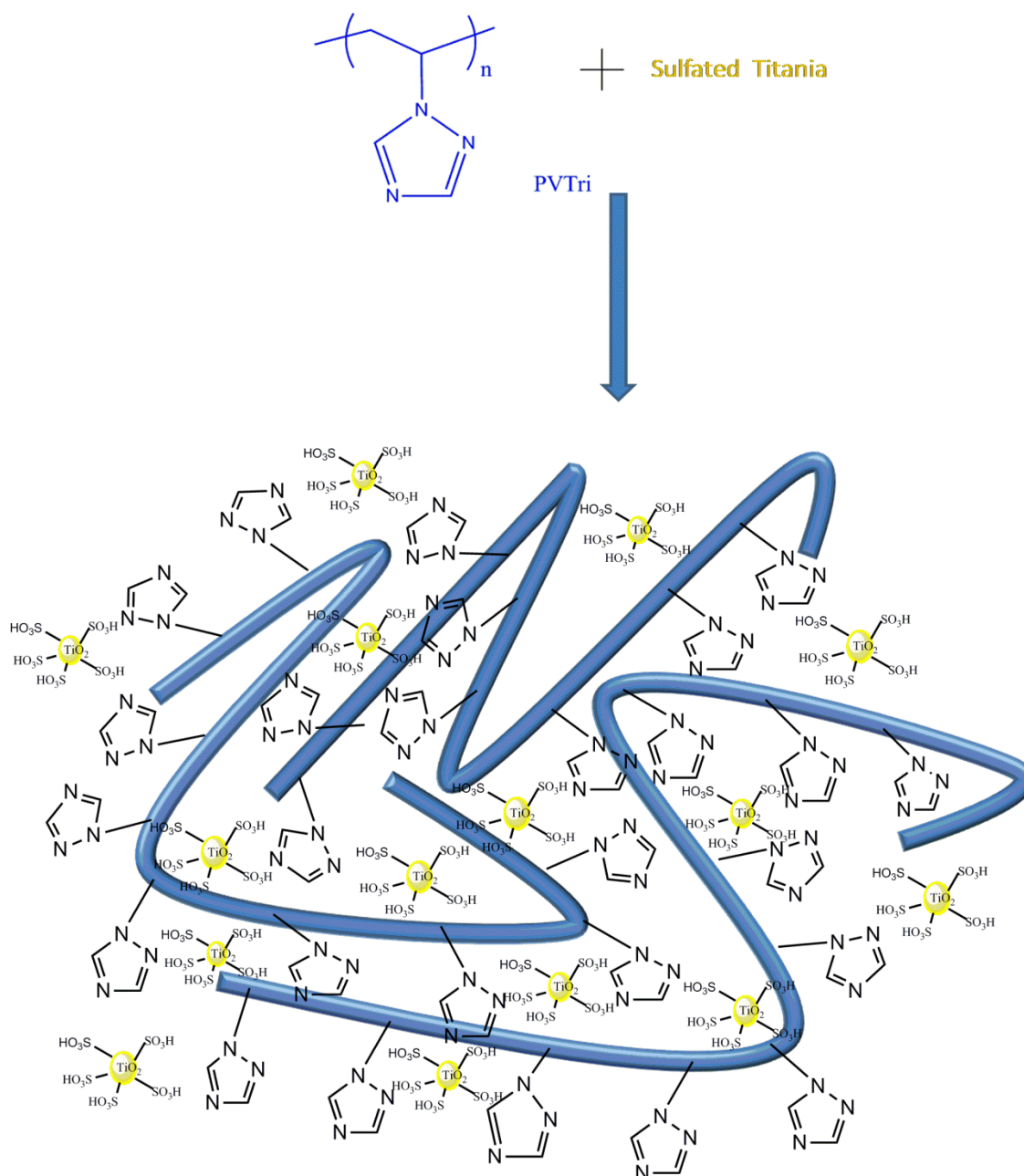
Figure 2.6 The model structure of PVTri-TS composite membranes.

In the second approach stoichiometric amounts of P(VPA) were added into first solution system to get P(VTri)-TS-P(VPA)$_x$; x=1,2,4) where x is the molar ratio of the corresponding monomers. The complex polymer electrolytes were isolated in the solution as white gel. Then the solutions were further stirred under nitrogen atmosphere for 24 h,

i.e., until getting a homogeneous milky solutions. The films were cast onto polished Poly(tetrafluoroethylene) PTFE plates and dried under vacuum at 50 ^{o}C .Then the films were stored in a glove box. Transparent, hygroscopic and free standing films were obtained and the samples denoted as P(VTri)-TS-P(VPA)$_x$.

2.6 SYNTHESIS OF PVA-TS-NMPA NANOCOMPOSITE MEMBRANES

The solvents, methanol (Sigma-Aldrich), and dimethylformamide (DMF; Merck) were used as received.

Sulfated nano-titania was produced according to a previously reported procedure (Aslan and Bozkurt, 2012). Firstly, 5 g of titanyl sulfate (TiOSO$_4 \cdot$nH$_2$O, n=1–2) was dissolved in 200 mL of water and stirred for about 50 min. The solution temperature was slowly increased up to 70 °C and the white precipitate was collected by suction filtration, and washed several times with distilled water. The obtained powder was carefully dried and stored in a glove box. In the powder sample, the amount of sulfate groups was calculated by acid–base titration, which was about 1×10^{-3} mol/g.

Binary and ternary proton conductive polymer nanocomposite membranes were produced using two different procedures. According to previous studies, at higher contents (10-20%) of additive materials (TS), the proton conductivity decreased because of their blocking effect as well as interactions between host guest systems and additive materials. The former membranes were prepared by mechanical mixing of sulfated nano-titania (TS) (5% (w/w)) and poly(vinyl alcohol) in DMF, while the latter ones were obtained by addition of the dopant nitrilotri(methyl triphosphonic acid) (NMPA) (see Figure 2.8.) into PVA/TS system at several stoichiometric ratios. The homogeneous solutions were stirred overnight at ambient temperature. The membranes were prepared by casting of the solution on a polished poly(tetrafluoro ethylene), and the solvent was slowly evaporated at 80 ^{o}C for 24 h. To ensure complete solvent removal, the membranes were placed under vacuum at 80 ^{o}C for 48 h. Homogeneous and yellowish free standing films were obtained.
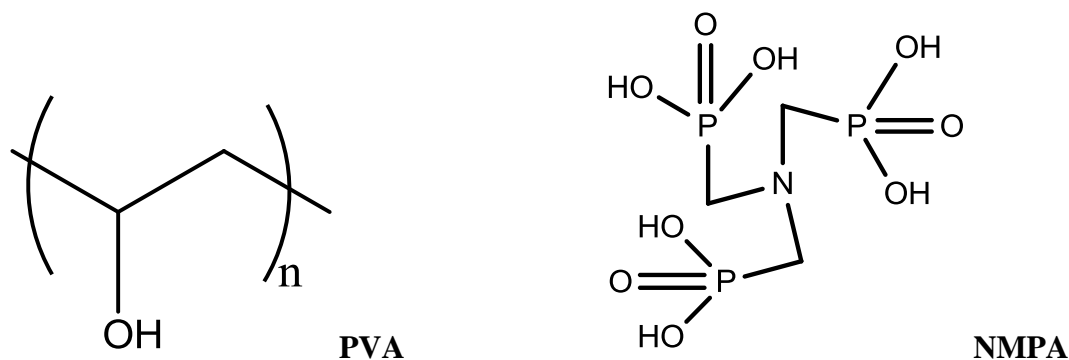
Figure 2.7 Structure of PVA and NMPA.

2.7 SYNTHESIS OF SPSU-TS-NMPA NANOCOMPOSITE MEMBRANES

The commercial polysulfone (PSU; Aldrich),1,2-dichloroethane (DCE; Merck), methanol (Sigma-Aldrich), and dimethylformamide (DMF; Merck) were used as received.

Acid modified TiO_2 was synthesized by hydrolysis and precipitation of $TiOSO_4$ (Sakai et al., 2010). The amount of sulfate groups of the resultant powder was found to be about 1×10^{-3} molg^{-1} from the acid–base titration.

Sulfonated polysulfone (SPSU) (see Figure 2.8.) was prepared according to literature (Gustian et al., 2012). The polysulfone sulfonation degree (DS) of was measured by acid-base titrimetric method. The sulfonation ratio of sulfonated polysulfone was calculated as 104 % (mol SO_3H/repeat unit) x100).

The preparation of proton conductive composite membranes includes two steps which are as follows. Firstly, mechanical mixing of sulfated nanotitania (5wt%) and sulfonated polysulfone were prepared in DMF. Then the dopant nitrilotri(methyl triphosphonic acid) (NMPA) was added of at several stoichiometric ratios in DMF, i.e., SPSU:dopant; 1:1, 1:2, 1:3, 1:4. The homogeneous solutions were stirred overnight with mechanical stirring at 80 ^{o}C. Solvent was evaporated in vacuum oven at 60 ^{o}C. To ensure complete solvent

removal, the membranes were placed in glove box at 50 ^{o}C. The thicknesses of the films were measured as 250-500 µm.
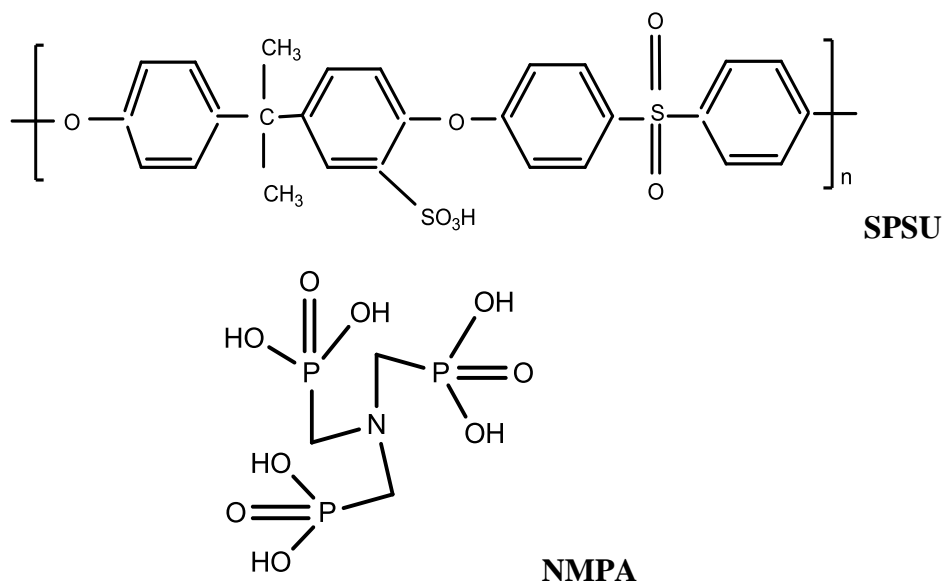
Figure 2.8 The structure of the SPSU and NMPA.

2.8 SYNTHESIS OF AZOL GROUPS FUNCTIONAL PGMA GRAFTED HALLOW SILICA SPHERES NANOCOMPOSITE MEMBRANES

Glycidyl methacrylate (>97%), were supplied from SigmaAldrich Chemical Company. Ortho-Phosphoric acid (>99%), Diethlyether (>99.5%) and DMF (>99.5%) were purchased from Merck. Azobisisobutyronitrile (AIBN; Merck) was recrystallized from THF prior to use.

It is well known that the sol–gel process has been commonly used to prepare silica and other metal oxide particles (Marini et al. 2008; Taniguchi et al., 2005). In this study, hollow silica particles were prepared by sol–gel process via two-step method. Firstly, HSS particles were prepared according to following procedure have reported by Hah et al (Hah et al., 2003). Then the hydrolysis of phenyltrimethoxysilane (PTMS) was performed under

acidic conditions. Hydrolysis time plays an important role in the formation of hollow particles. In the second step the condensation of the silane progressed under basic conditions. The resultant particles were collected with a membrane filter and washed with water and ethanol several times.

HSS was dissolved in DMF and Poly(glycidyl methacrylate) was grafted by free radical polymerization of glycidyl methacrylate (Aslan and Bozkurt, 2010; Çelik and Bozkurt, 2008) using 1% AIBN. The temperature was set to 85 ^{o}C (see Figure 2.10.). The HSPGMA were obtained after precipitation with THF and washed with water several times. Then, it was filtered and dried at 70 ^{o}C under vacuum and white and rigid polymers were obtained.
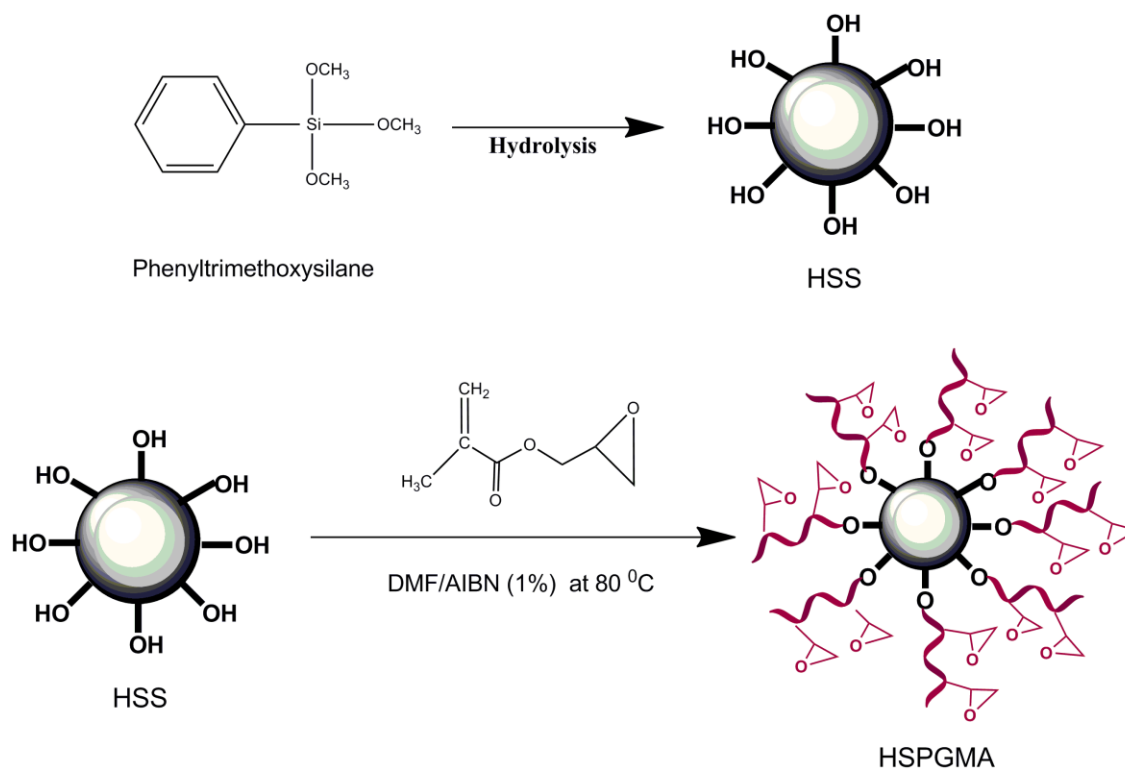
Figure 2.9 Synthesis of the PGMA grafted HSS.

In order to prepare 1,2,4-Triazole functional HSPGMA, the HSPGMA was dissolved in DMF and stoichiometric amounts of 1,2,4-Triazole were added to the solution. The temperature was set to 80 ^{0}C and the mixture was stirred under nitrogen atmosphere for 24 hours. The resulting solid mixture was filtered and dialyzed against water to remove excess 1,2,4-Triazole.

The 1,2,4-Triazole functional PGMA grafted HSS (HSPGMA-Tri) (see Figure 2.10.) were dried at 80 ^{o}C under vacuum.The azole functional polymer was dissolved in hot DMSO and phosphoric acid at different ratios, x=1, 2 (i.e. x is the number of moles of acid per moles of azole unit in the polymer). The polymer films were cast onto polished PTFE plates, dried under vacuum at 80 ^{o}C and then stored in a glove box. Light yellow and free standing films were obtained and prior to all measurements, polymer films were stored in a glove box.
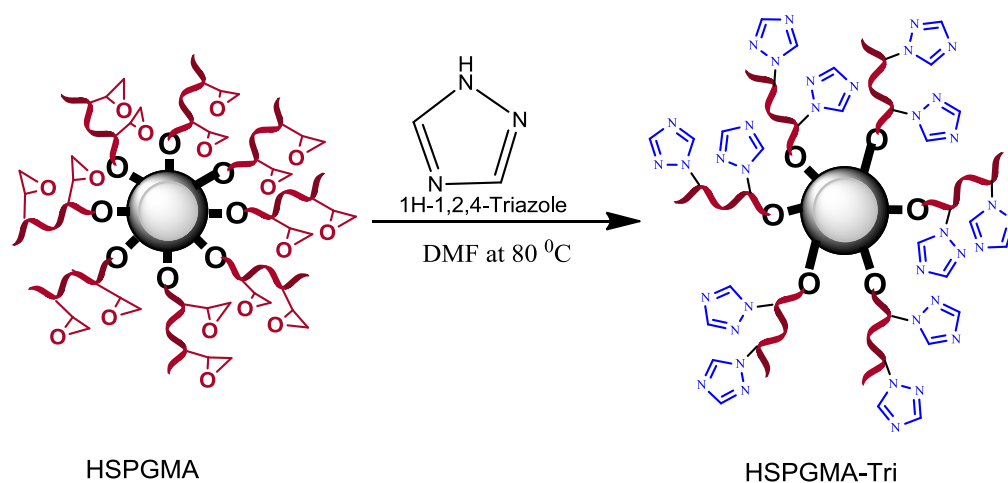
Figure 2.10 Synthesis of the 1,2,4-Triazole functional PGMA grafted hallow silica spheres (HSPGMA-Tri).

In order to prepare 5-Amino-Triazole functional HSPGMA, the HSPGMA was dissolved in DMF and stoichiometric amounts of 5-Amino-1,2,4-Triazole were added to the solution. The temperature was set to 80 ^{0}C and the mixture was stirred under nitrogen

atmosphere for 24 hours. The resulting solid mixture was filtered and dialyzed against water to remove excess 5-Amino-1,2,4-Triazole.

The 5-Amino-Triazole functional PGMA grafted HSS (HSPGMA-ATri) (see Figure 2.11.) were dried at 80 ^{o}C under vacuum. The 5-Amino-Triazole functional polymer was dissolved in hot DMSO and phosphoric acid at different ratios, x=1, 2 (i.e. x is the number of moles of acid per moles of azole unit in the polymer). The polymer films were cast onto polished PTFE plates, dried under vacuum at 80 ^{o}C and then stored in a glove box. Light yellow and free standing films were obtained and prior to all measurements, polymer films were stored in a glove box.
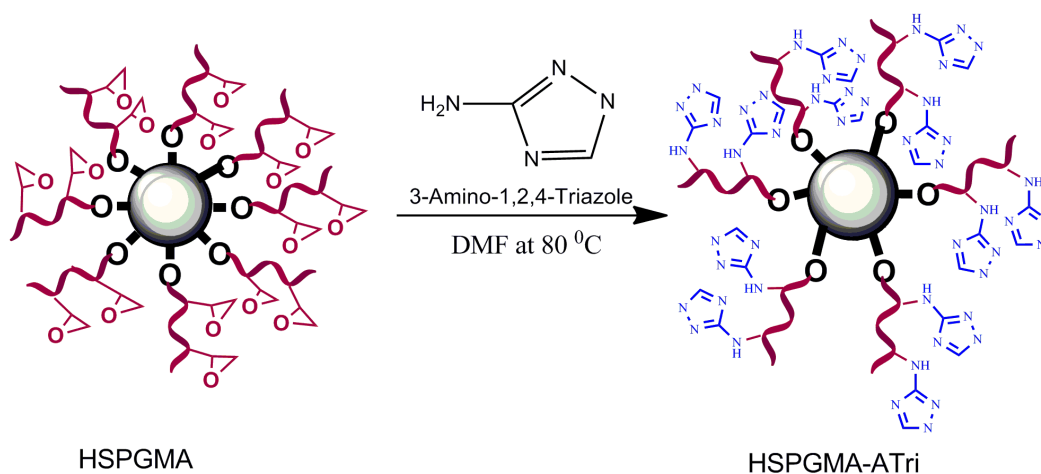
Figure 2.11 Synthesis of the 5-Amino-1,2,4-Triazole functional PGMA grafted hallow silica spheres (HSPGMA-ATri).

In order to prepare 5-Aminotetrazole functional HSPGMA, the HSPGMA was dissolved in DMF and stoichiometric amounts of 5-Aminotetrazole were added to the solution. The temperature was set to 80 ^{0}C and the mixture was stirred under nitrogen atmosphere for 24 hours. The resulting solid mixture was filtered and dialyzed against water to remove excess 5-Amino-Triazole.

The 5-Aminotetrazole functional PGMA grafted HSS (HSPGMA-ATet) (see Figure 2.12.) were dried at 80 ^{o}C under vacuum. The 5-Aminotetrazole functional polymer was dissolved in hot DMSO and phosphoric acid at different ratios, x=1, 2 (i.e. x is the number of moles of acid per moles of azole unit in the polymer). The polymer films were cast onto polished PTFE plates, dried under vacuum at 80 ^{o}C and then stored in a glove box. Light yellow and free standing films were obtained and prior to all measurements, polymer films were stored in a glove box.

HSPGMA   HSPGMA-ATet
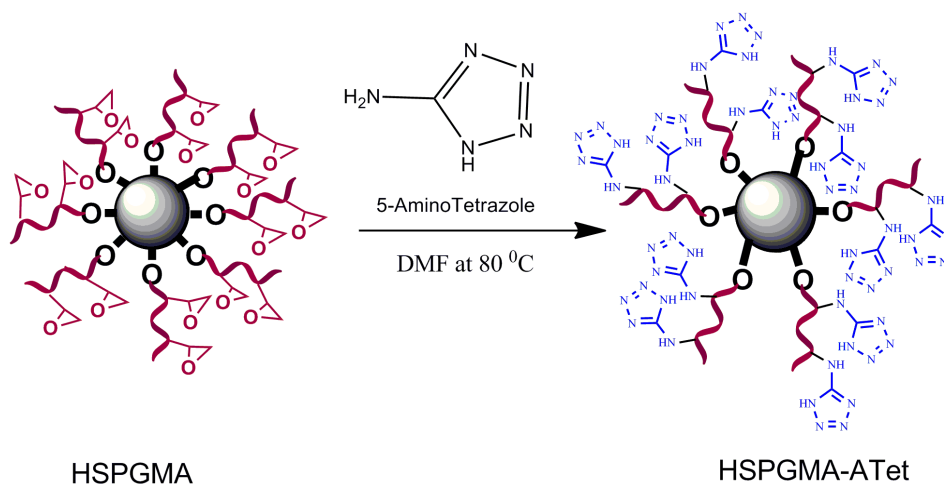
Figure 2.12 Synthesis of the 5-Aminotetrazole functional PGMA grafted hallow silica spheres (HSPGMA-Tet).

2.9 SYNTHESIS OF AZOL FUNCTIONAL SIO$_2$ NANOCOMPOSITE MEMBRANES

The intention of the present work was to develop a one-pot method for the synthesis of modified silica nanoparticles starting from fundamental molecules instead of using already synthesized silica nanoparticles. For this purpose, TEOS which has been the starting molecule for the synthesis of silica nanoparticles in Stöber reaction (Stöber, Fink et al. 1968, Rao, El-Hami et al. 2005, Rahman, Vejayakumaran et al. 2007).The resultant

particles were collected with a membrane filter and washed with water and ethanol several times.
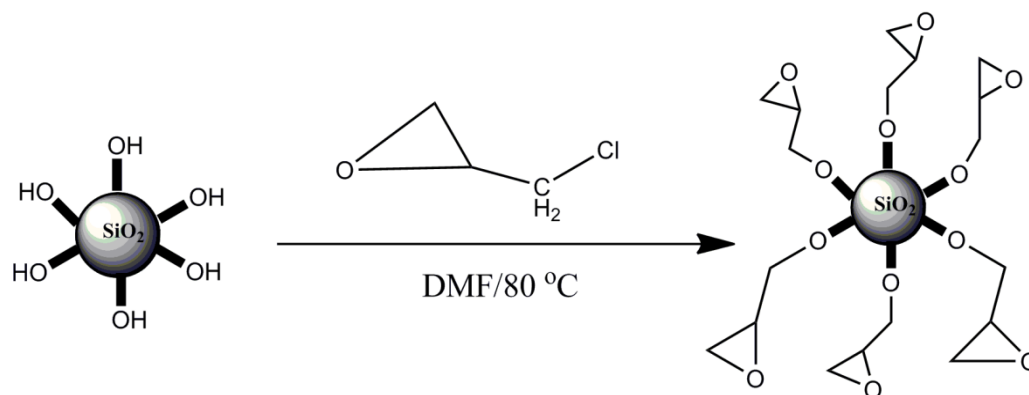
Figure 2.13 Synthesis of the epichlorohydrin modified SiO_2 nanoparticles.

SiO$_2$ was dissolved in THF and epichlorohydrin was added to solution. When the reaction occurred between epiclhorohydrin and surface of silica, the HCl was bubbled to NaOH solution to measure using epichlorohydrin. The temperature was set to 85 ^{o}C (see Figure 2.14.). The modified silica nanoparticles were obtained after precipitation and washed with water/methanol solution several times. Then, it was filtered and dried at 70 ^{o}C under vacuum.

In order to prepare 1,2,4-Triazole functional SiO$_2$ (see Figure 2.14), the modified silica was dissolved in DMF and stoichiometric amounts of 1,2,4-Triazole were added to the solution. The temperature was set to 100 ^{0}C and the mixture was stirred under nitrogen atmosphere for 24 hours. The resulting solid mixture was filtered and dialyzed against water to remove excess 1,2,4-Triazole.
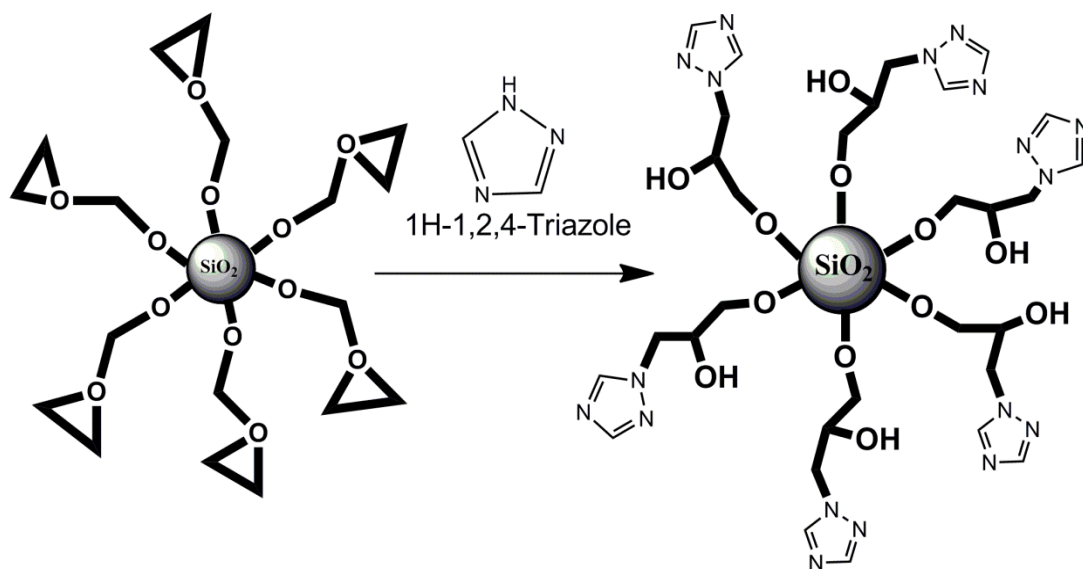
Figure 2.14 Synthesis of the 1,2,4-Triazole functional SiO_2 nanoparticles (Tri- SiO_2).

In order to prepare 5-Amino-1,2,4-Triazole functional SiO_2 (see Figure 2.15), the modified silica was dissolved in DMF and stoichiometric amounts of 5-Amino-1,2,4-Triazole were added to the solution. The temperature was set to 100 ^{0}C and the mixture was stirred under nitrogen atmosphere for 24 hours. The resulting solid mixture was filtered and dialyzed against water to remove excess 5-Amino-1,2,4-Triazole.
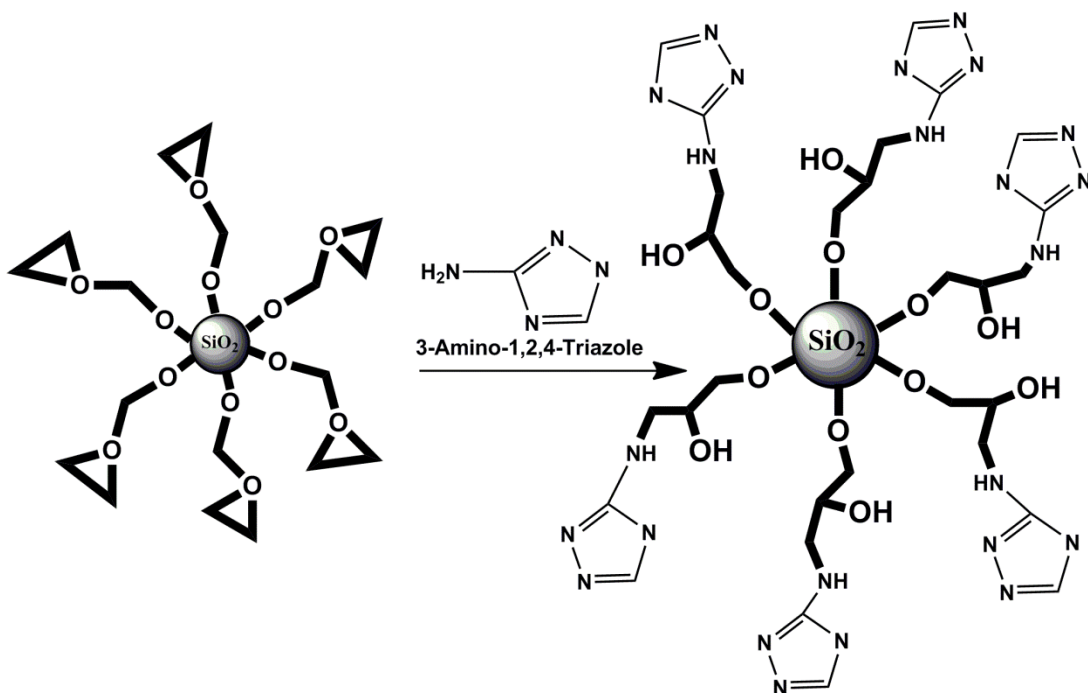
Figure 2.15 Synthesis of the 5-Amino-1,2,4-Triazole functional SiO_2 nanoparticles (ATri- SiO_2).

In order to prepare 5-Amino-Tetrazol functional SiO_2 (see Figure 2.16), the modified silica was dissolved in DMF and stoichiometric amounts of 5-Amino-Tetrazol were added to the solution. The temperature was set to 100 ^{0}C and the mixture was stirred under nitrogen atmosphere for 24 hours. The resulting solid mixture was filtered and dialyzed against water to remove excess 5-Amino-Tetrazol.
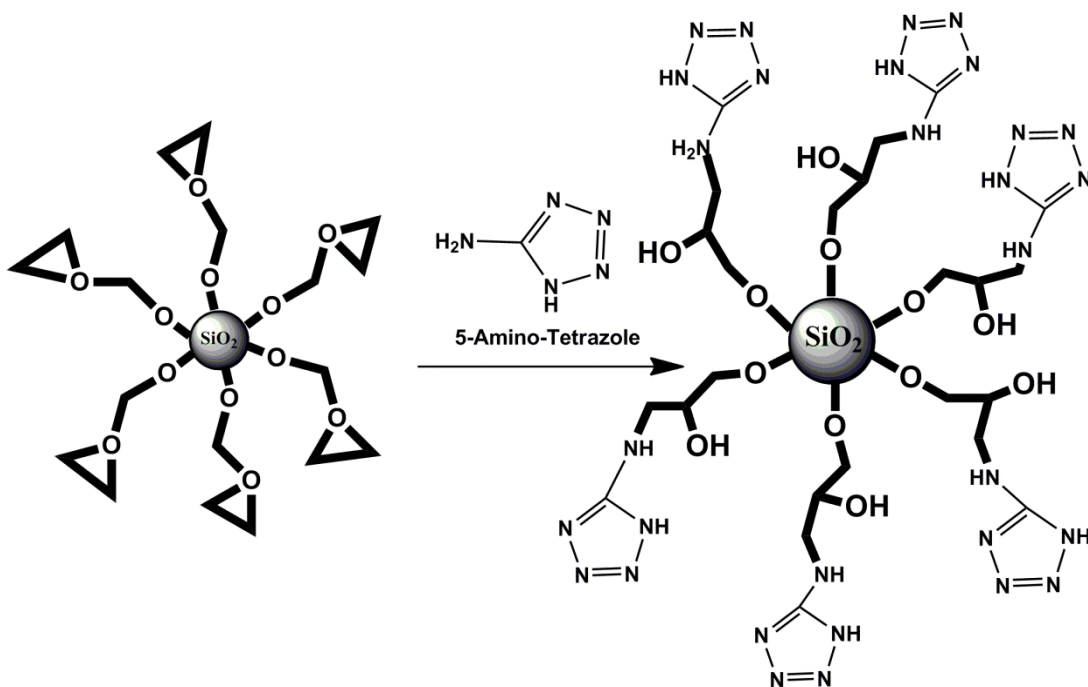
Figure 2.16 Synthesis of the 5-Amino-Tetrazol functional SiO$_2$ nanoparticles (Tet- SiO$_2$).

2.10 CHARACTERIZATIONS

Fourier-Transform IR (FTIR) is most useful for identifying chemicals that are either organic or inorganic. It can be utilized to quantitate some components of an unknown mixture. It can be applied to the analysis of solids, liquids, and gasses. The term Fourier Transform Infrared Spectroscopy (FTIR) refers to a fairly recent development in the manner in which the data is collected and converted from an interference pattern to a spectrum. FTIR can be used to identify chemicals from spills, paints, polymers, coatings, drugs, and contaminants. FTIR is perhaps the most powerful tool for identifying types of chemical bonds (functional groups). The wavelength of light absorbed is characteristic of the chemical bond as can be seen in this annotated spectrum. FT-IR spectra were recorded on a Bruker Alpha-P in ATR in range of 4000 cm^{-1}-400 cm^{-1}.

The content of carbon, hydrogen, and nitrogen in the polymers was determined by elemental analysis using a LECO CHNS-932 instrument.

Thermogravimetry analysis (TGA) is based on the measurement of the weight loss of the material as a function of temperature, or isothermally as a function of time, in an atmosphere of nitrogen, helium, air, other gas, or in vacuum. TGA curve provides information concerning the thermal stability of the initial sample, intermediate compounds that may be formed and of the residue if any. In addition to thermal stability, the weight losses observed in TGA can be quantified to predict the pathway of degradation or to obtain compositional information. The ability to vary atmosphere during the TGA evaluation, particularly from an inert to a reactive gas, provides additional information about a material composition and its stability. The experimental data offer more sophisticated understanding of reactions occurring at materials heating. Thermal stabilities of the polymer electrolytes were examined by a Perkin Elmer STA 6000 Thermal Analyzer. The samples (~10 mg) were heated from room temperature to 750 °C under N_2 atmosphere at a scanning rate of 10 °C/min.

DSC measures the temperatures and heat flow associated with transitions in materials as a function of time and temperature. It determines transition temperatures, melting and crystallization, and heat capacity. In heat flux instruments, the sample and reference are heated from the same source and the temperature difference is measured. In amorphous polymers DSC shows the glass transition temperature (Tg) and presence of single Tg verifies the homogeneity of the polymer. DSC measurements were carried out on a Perkin Elmer Jade DSC under N_2 atmosphere and heating-cooling curves were recorded at a rate of 10 °C/min. The second heating curves were evaluated.

A scanning electron microscope (SEM) is a type of electron microscope that images a sample by scanning it with a beam of electrons in a raster scan pattern. The electrons interact with the atoms that make up the sample producing signals that contain information about the sample's surface topography, composition, and other properties such as electrical conductivity. For conventional imaging in the SEM, specimens must be electrically conductive, at least at the surface, and electrically grounded to prevent the accumulation of electrostatic charge at the surface. Nonconductive materials are therefore usually coated with an ultrathin coating of electrically conducting material (e.g. gold), deposited on the sample either by low-vacuum sputter coating or by high-vacuum evaporation. The

morphology of the membranes was observed by scanning electron microscopy (SEM) type JEOL 7001 FESEM. The samples were previously coated with gold in a sputtering device.

The tapping mode AFM images of the membranes were acquired using a Park AFM (XE-100, Park AFM, Korea), supported on a Minus-K (25BM-6, Minus-K, Inglewood, CA) vibration isolation base. The AFM parameters to obtain the images were carefully set to minimize the pressure of tip on the membranes. A commercial Si tip was used with the nominal radius <10 nm, resonant frequency nominal of 330 kHz, a nominal spring constant of 42N/m (PPP-NCHR, Nanosensors, Switzerland). 20 × 20 □m images were acquired at a resolution of 512×512 points within the range of 0.5-0.8 Hz scan rate and were subjected to first-order flattening. Surface roughness was calculated by using the Root Mean Square (RMS), that is, the standard deviation of the Z values within a given area, defined by Eq. 2.1

$$RMS = \sqrt{\frac{\sum_{i=1}^{N}(Z_i - Z_{ave})^2}{N}}$$

(2.1)

Where Z_{ave} is the average, Z_i is the current Z value, and N is the number of points within the analyzed area. It was noted that the surface roughness depends on the curvature and size of the AFM tip and on the image processing (Sedin and Rowlen 2001) therefore we applied the same procedure for each image. The RMS mean values and the standard deviations were obtained by analyzing at AFM images.

Methanol permeability was measured using our homemade diaphragm diffusion cell with a volume of 4 ml. The cell was filled with a pure methanol. Methanol vapor in equilibrium with the liquid diffused along the concentration gradient through the membrane, which was clamped between the mouth of glass and the cap. The cap has a hole with a 0.82cm diameter so that the methanol diffused through the membrane could escape. The weight loss is recorded as a function of time and the data were used for permeability calculations.

Water uptake (WU) measurement was determined by the weight difference between the fully hydrated membranes and dried membranes. The dried membranes (W_{dry}) were weighed and then wetted until the weight remained constant. The wet or saturated weights of the membranes (Wwet) were measured quickly after removing or wiping out any remaining surface water with a paper. . The water uptake was calculated according to the equation (2.2):

$$Water\ uptake\ (WU) = \frac{W_{wet} - W_{dry}}{W_{dry}} \times 100\%$$ (2.2)

The oxidative stability of the membranes was tested by immersing the films into Fenton's reagent (3% H_2O_2 aqueous solution containing 2 ppm $FeSO_4$). The dissolved time of the membranes into the reagent were used to evaluate their oxidative stability.

The proton conductivity studies of the samples were performed using a Novocontrol dielectric-impedance analyzer. The films were sandwiched between platinum blocking electrodes and the conductivities were measured in the frequency range 1 Hz-3 MHz at 10 °C intervals. The temperature was controlled with a Novocontrol cryosystem using liquid nitrogen, which is applicable between -150 and 250 °C.

The frequency-dependent AC conductivities, σac (ω), of the polymer blends were calculated using Eq 2.3:

$$\sigma^{'}(\omega) = \sigma_{ac}(\omega) = \varepsilon^{''}(\omega)\ \omega\ \varepsilon_o$$ (2.3)

where $\sigma^{'}(\omega)$ is the real part of conductivity, $\omega = 2\pi f$ is the angular frequency, ε_o is the vacuum permittivity ($\varepsilon_o = 8.852 \times 10^{-14}$ F/cm), and $\varepsilon^{''}$ is the imaginary part of complex dielectric permittivity (ε^{*}).

CHAPTER 3

RESULTS AND DISCUSSION

3.1 CAHARACTERIZATION OF PVPA-SIO$_2$ NANOCOMPOSITE MEMBRANES

3.1.1 FTIR Studies

The homopolymer of PVPA was prepared by free-radical polymerization of vinylphosphonic acid. Figure 3.1 shows the FTIR spectra of PVPASiO$_2$ nanocomposite membranes. The FTIR spectrum of PVPA shows strong bands between 1040-910 cm^{-1} due to asymmetric stretching vibrations of the P-OH group. The peak at 1150 cm^{-1} corresponds to P=O stretching(Celik, Aslan et al. 2008, Goktepe, Celik et al. 2008). The P–O–H vibration at 930 cm^{-1} decreases as the PVPA ratio increases, indicating the existence of excess acidic protons. Additionally, phosphonic acid units give rise to broad bands with medium intensity between 1700-1590 cm^{-1} and 2850-2750 cm^{-1} region. The band at 918 cm^{-1} is ascribed to vibration of terminal SiOH groups. The broad and strong peak at about 1136 cm^{-1} is attributed to the overlapping of the combined results of the Si-O band vibrations and/or stretching in SiO$_2$ particles(Ou and Seddon 1997, Parler, Ritter et al. 2001). Typical absorption peaks of SiO$_2$ (1100 and 466 cm^{-1}) did not only overlap by those of PVPA but also shifted to 972 and 440 cm^{-1}, respectively. This may also indicate that the PVPA matrix and SiO$_2$ nanoparticles are not simply mixed, but complexation interactions exist. The broad band between 3500 cm^{-1} - 2500 cm^{-1} is the hydrogen bonding network which is necessary for proton conduction(Celik, Akbey et al. 2008).
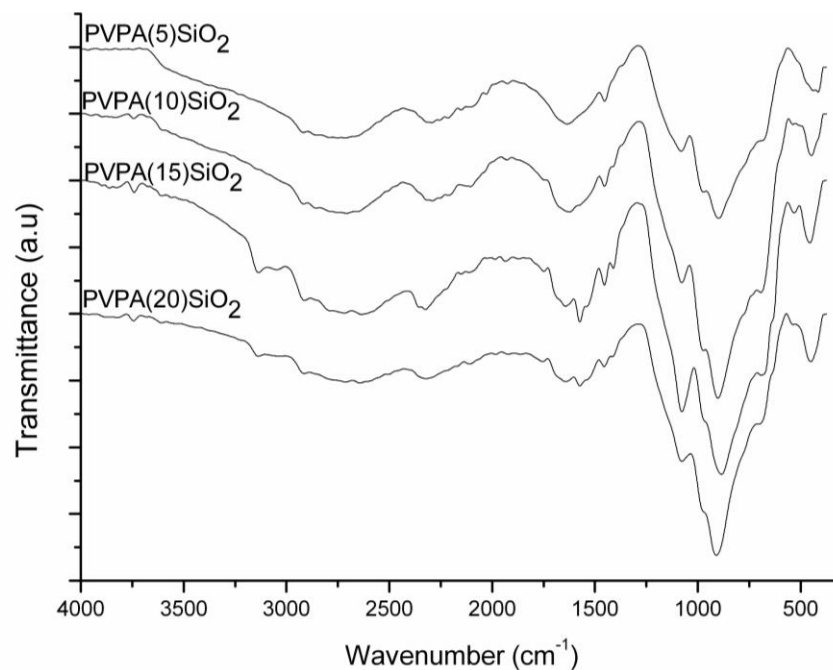
Figure 3.1 FT-IR spectra of the PVPASiO$_2$ composite membranes.

3.1.2 AFM

The selected AFM images of membranes are shown in Figure 3.2. The mean values of surface roughness of membranes are listed together with SiO$_2$ content membranes in Table 3.1.

Table 3.1 The mean RMS roughness values with the standard deviations and the DC conductivity of membranes.

Membranes	Roughness (nm)	SiO$_2$ content (weight %)
PVPA	2.4 ± 6.1	-----
PVPA(5)SiO$_2$	19.8 ± 6.4	%5
PVPA(10)SiO$_2$	283.2 ± 14.7	%10
PVPA(15)SiO$_2$	173.8 ± 13.21	%15
PVPA(20)SiO$_2$	48.4 ± 12.3	%20

The RMS roughness drastically increased from 19.8 nm to 283.2 nm when the SiO_2 content was increased from 5 % to 10 %. However, addition of more SiO_2 did not cause to increase RMS roughness. Bigger granular domains are clearly seen on the surface of PVPA(10)SiO_2 (see Figure 3.2b). Cho *et al.* modified the surface of Nafion by ion beam bombardment to improve the fuel cell performance (Cho, Cho et al. 2006). They found that the increase in the effective surface area resulted in higher proton conductivity of Nafion. We surprisingly observed in this study that the RMS roughness of membranes followed the same trend with the DC conductivity values. Hydrophobic surface can be preferential for fuel cell applications because water should be properly removed from the electrode catalyst layer (Wagner, Manhart et al. 2009). The higher RMS roughness value might be attributed to the production of bigger of hydrophobic granules on the surface (Aslan, Gölcük et al.2012).
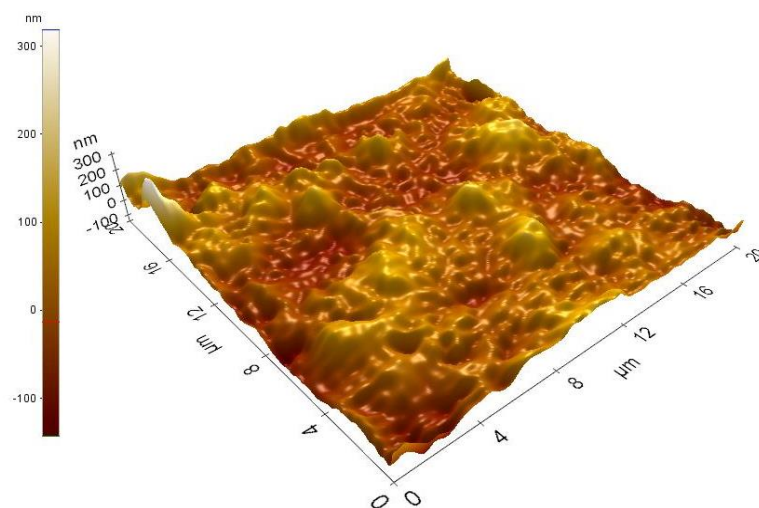
Figure 3.2 AFM images of the PVPA and PVPA(20)SiO_2 composite membranes.
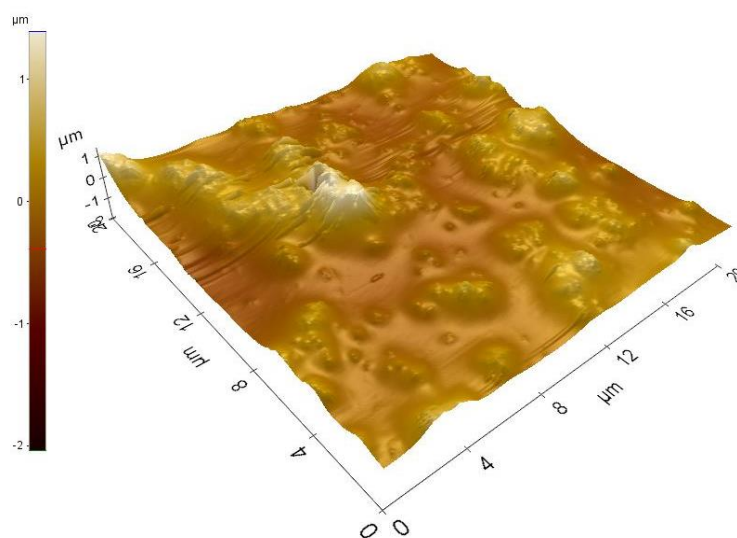
Figure 3.3 AFM images of the PVPA and PVPA(10)SiO$_2$ composite membranes.
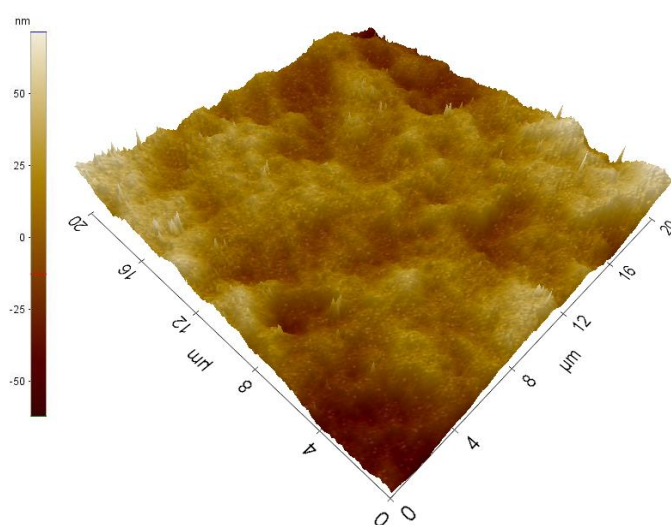
Figure 3.4 AFM images of the PVPA and PVPA(5)SiO$_2$ composite membranes.
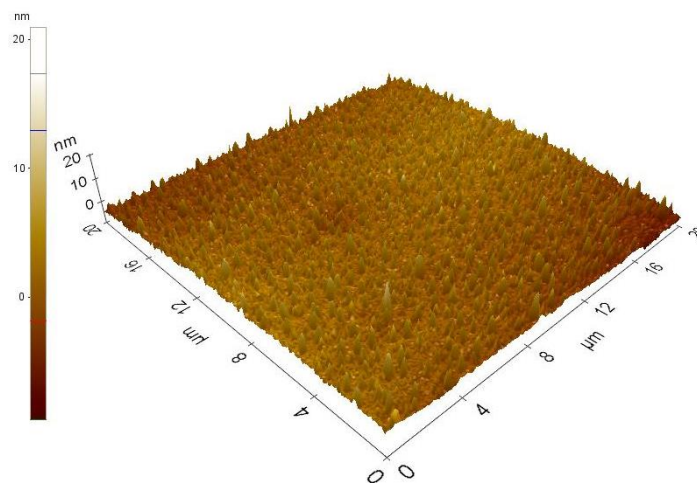
Figure 3.5 AFM images of the PVPA membranes.

3.1.3   TEM

Figure 3.6 shows a typical TEM image of the PVPA(10)SiO$_2$ nanocomposite membrane The additive SiO$_2$ particles were uniformly distributed in the membrane. There is no obvious SiO$_2$ aggregation in the PVPA matrix, and the SiO$_2$ particles, ranging from 20 to 50 nm, are distributed in PVPA matrices uniformly (Aslan, Gölcük et al. 2012).
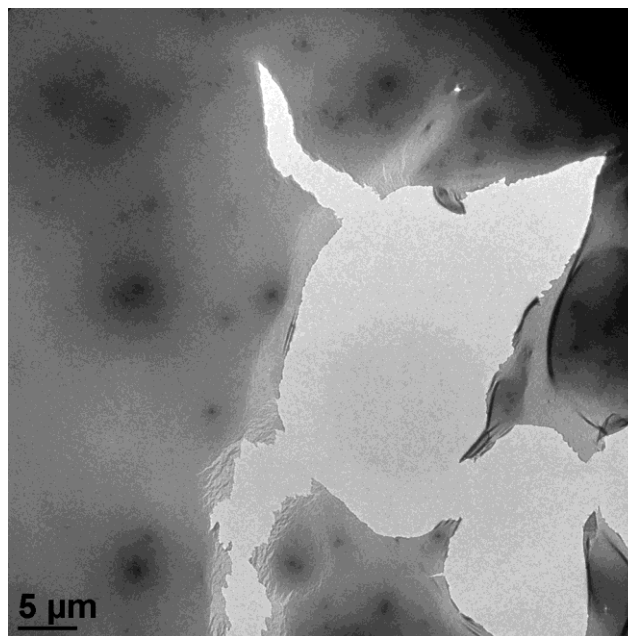
Figure 3.6 The TEM pictures of PVPA(10)SiO$_2$ composite membranes.

3.1.4 Thermal analysis

Table 3.2 lists the glass transition temperatures of the PVPA(x)SiO$_2$ nanocomposites. PVPA exhibits a glass transition at around -23°C (Celik, Akbey et al. 2008) and the PVPA(x)SiO$_2$ nanocomposite membranes have definite glass transition temperatures between 84°C and 100°C. The DSC results indicate that the glass transition temperatures of the samples shift to higher temperatures as the quantity of SiO$_2$ increases. This shift can be due to complexation interaction between host polymer and nanoparticles. The glass transition temperatures of PVPA(x)SiO$_2$ (*in situ*) composite membranes are ranging from 57 $^\circ$C to 93 $^\circ$C. The lower glass transition temperature values can be due to the low molecular weight of the host polymer (Aslan, Gölcük et al. 2012).

Table 3.2 Max. Proton conductivity and Tg (^{o}C) values for the all membranes.

Sample Name	SiO$_2$ content (w/w%)	Relative Humidity (%)	Tg (^{o}C)	Max. Proton Conductivity (Scm^{-1})
PVPA(5)SiO$_2$	5 %	---	100 ^{o}C	7,2 x10^{-8} (Scm^{-1})at 120°C
PVPA(10)SiO$_2$	10 %	---	96 ^{o}C	1,1 x10^{-7} (Scm^{-1})at 120°C
PVPA(15)SiO$_2$	15 %	---	87 ^{o}C	8,5 x10^{-8} (Scm^{-1})at 120°C
PVPA(20)SiO$_2$	20 %	---	84 ^{o}C	8,2 x10^{-8} (Scm^{-1})at 120°C
PVPA(5)SiO$_2$	5 %	50	---	0,0034 (Scm^{-1})at 100°C
PVPA(10)SiO$_2$	10%	50	---	0,08 (Scm^{-1})at 100°C
PVPA(15)SiO$_2$	15%	50	---	0,007 (Scm^{-1})at 100°C
PVPA(20)SiO$_2$	20%	50	---	0,003 (Scm^{-1})at 100°C
PVPA(5)SiO$_2$ (in situ)	5 %	---	93 ^{o}C	0,001 (Scm^{-1})at 120°C
PVPA(10)SiO$_2$ (in situ)	10%	---	61 ^{o}C	0,009 (Scm^{-1})at 120°C
PVPA(15)SiO$_2$ (in situ)	15%	---	57 ^{o}C	0,003 (Scm^{-1})at 120°C

The thermogravimetry (TG) results of the PVPA(x)SiO$_2$ are illustrated in Figure 3.7. The TG curves showed that the materials have no weight loss up to 140 ^{o}C. The slightly weight change at about 180 ^{o}C can be attributed to anhydride formation for dry PVPA(10)SiO$_2$ and PVPA(20)SiO$_2$ membranes(Celik, Akbey et al. 2008). Clearly, the dried materials are thermally stable up to 200 ^{o}C and then they decompose.
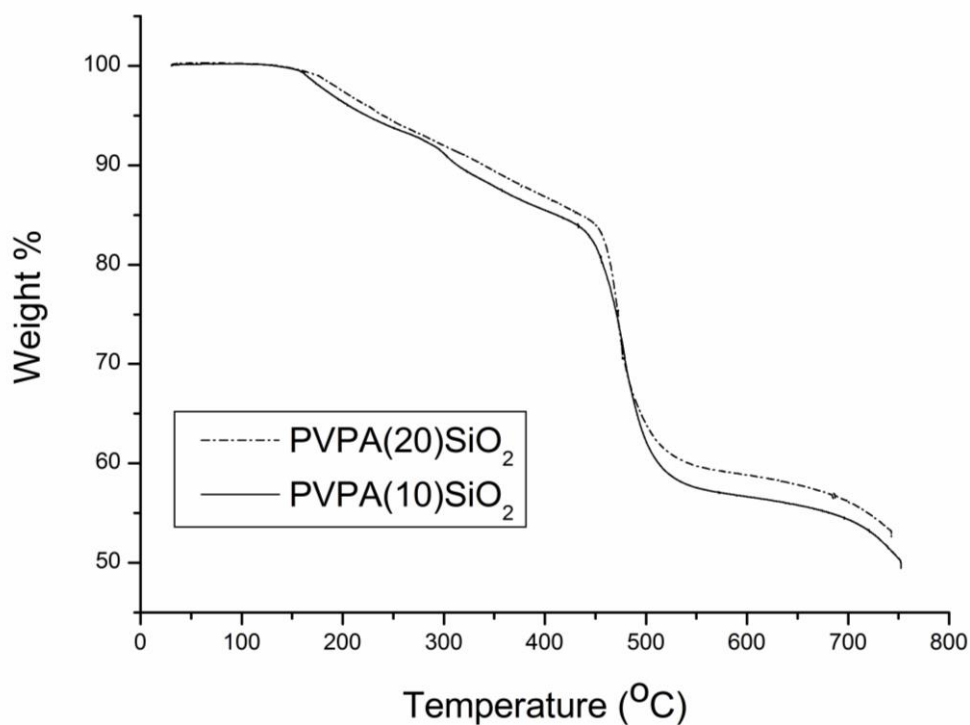
Figure 3.7 TG thermograms of PVPA(x)SiO$_2$ composite membranes recorded at a heating ^{o}C/min under a nitrogen atmosphere.

Similarly, Figure 3.8. shows the thermogravimetry (TG) results of the PVPA(x)SiO$_2$ (*in situ*). The PVPA(x)SiO$_2$ (*in situ*) membranes have no weight change up to 100 ^{o}C. The thermograms of PVPA(10)SiO$_2$ (*in situ*) and PVPA(20)SiO$_2$ (*in situ*) are showed that the materials are thermally stable up to 180 ^{o}C.
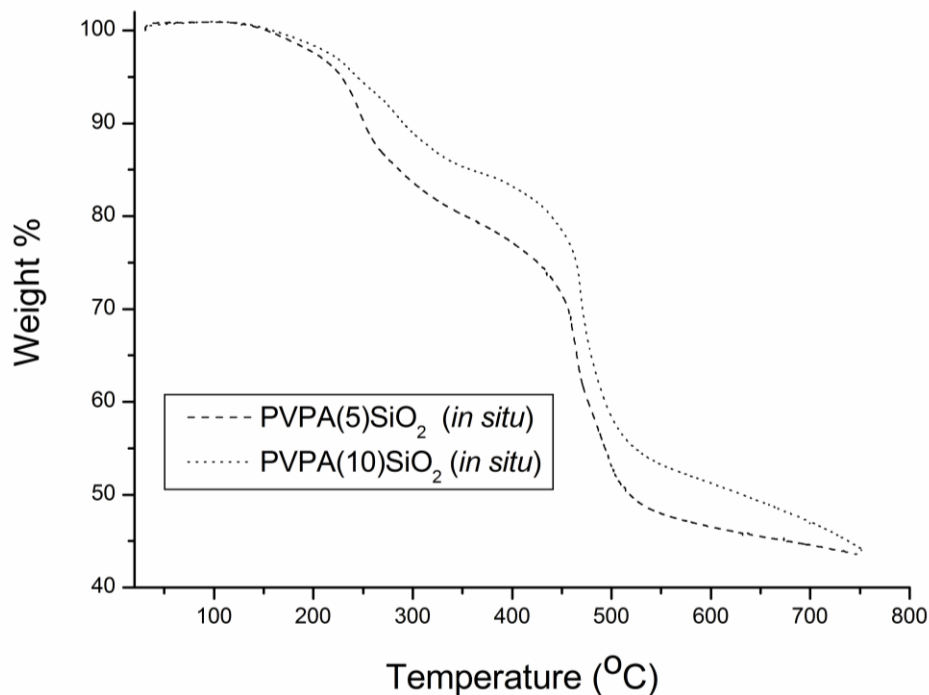
Figure 3.8 TG thermograms of triazole functional materials recorded at a heating rate of 10 ^{o}C/min under a nitrogen atmosphere.

3.1.5 Methanol Permeability

Methanol crossover is still a problem in direct methanol fuel cells, especially for portable applications where the current densities are relatively low. Fuel crossover at high methanol concentrations from anode side to the cathode side causes polarization losses. In this study, methanol permeability of the blend membranes was measured by simple homemade diaphragm diffusion cell similar to the study of (Munakata, Chiba et al. 2005, Gasa, Boob et al. 2006). The cell is filled with a pure methanol and the mass flow is recorded as a function of time (see Figure 3.9.). Molar methanolflux (J) through PVPA(10)SiO$_2$ blend was calculated using Eq. (3.1). Nafion112 with known permeability is used as reference for blend membranes. Methanol permeability of blend membranes may be calculated using molar flux (J) shown in Eqs. (3.1) and 3.2) (Boroğlu et al., 2006, (Aslan, Gölcük et al. 2012).).

$$J = \frac{W}{M_w \times A \times t} \tag{3.1}$$

$$\frac{J_1 l_1}{J_2 l_2} = \frac{P_1}{P_2} \tag{3.2}$$

where J: flux, MW:molecular weight,W: weight loss (g), P: permeability, l: thickness (cm), A: area (cm^2), t: time (s).

Thickness of the films was taken into account leading the cancellation of the thickness values (l) in Eq. (3.2). Therefore, permeability is directly proportional to the molar flux. The measure methanol permeability PVPA(10)SiO$_2$ was 2,4x10^{-7} cm^2 s^{-1}, respectively. It is clearly seen that the methanol crossover in the blended membrane is lower than commercial Nafion 112. Our results are comparable with the literature(Lin, Wycisk et al. 2007, Lin, Wu et al. 2008,).
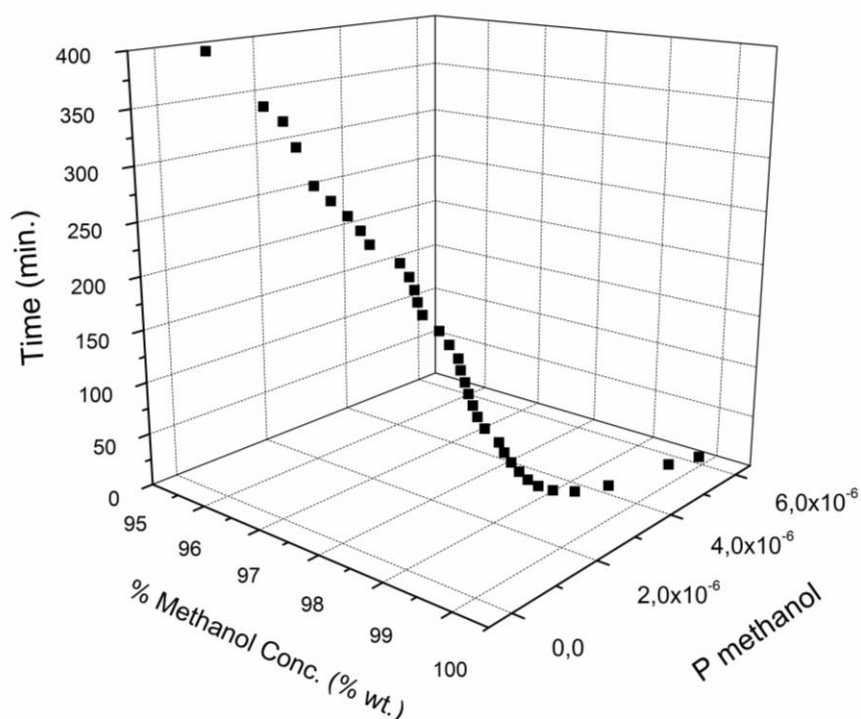
Figure 3.9 Methanole permeability of PVPA(10)SiO$_2$ composite membrane.

3.1.6 Proton conductivity

Figure 3.10. shows the AC conductivity of the sample versus frequency at several temperatures. The σ_{ac} versus frequency curves change with the frequency where in the low frequency region, the reduction in the conductivity is due to polarization of the blocking electrodes. The proton conductivity increases as temperature increases. The DC conductivity (σ_{dc}) of the samples was derived from the plateaus of log σ_{ac} versus log F by linear fitting of the data.
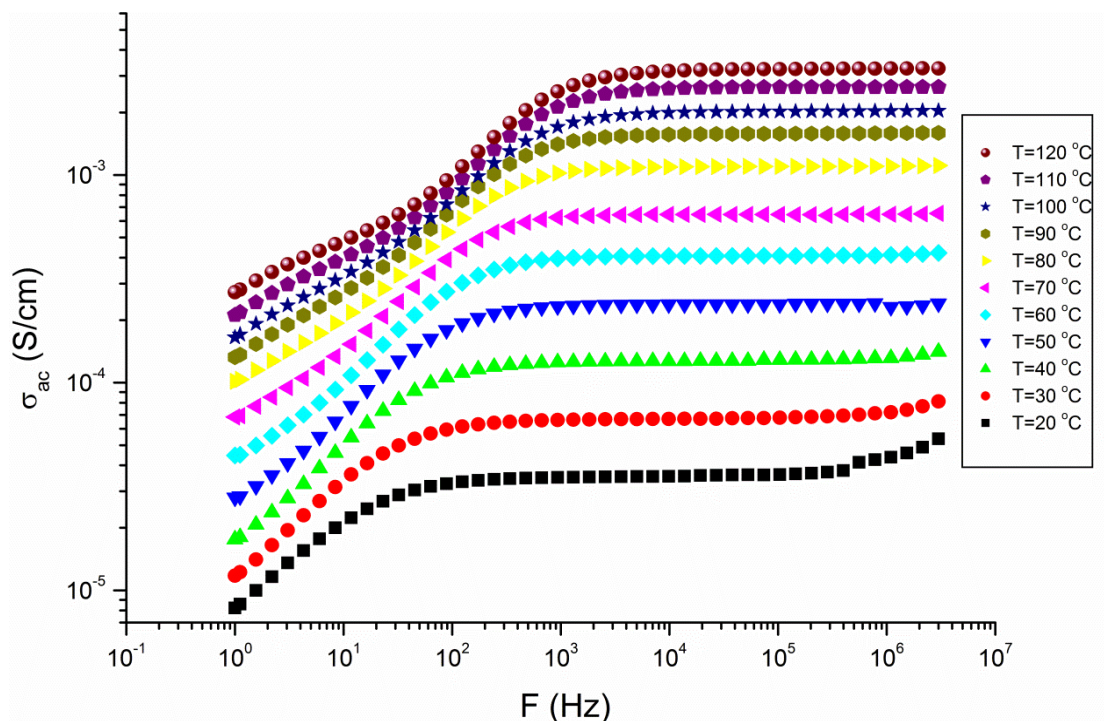
Figure 3.10 AC conductivity of PVPA(10)SiO$_2$ composite membrane.

The AC conductivities, σ_{ac} (ω) of the polymers were measured at several temperatures using impedance analyzer. The frequency dependent AC conductivities (σ_{ac} (ω)) were calculated using Eq. (3.3);

$$\sigma^{'}(\omega) = \sigma_{ac}(\omega) = \varepsilon^{''}(\omega)\,\omega\,\varepsilon_o \qquad\qquad (3.3)$$

where $\sigma^{'}(\omega)$ is the real part of conductivity, $\omega = 2\pi f$ is the angular frequency, ε_o is the vacuum permittivity and $\varepsilon^{''}$ is the imaginary part of complex dielectric permittivity (ε^{*}). The proton conductivities of PVPA(x)SiO$_2$ anhydrous nanocomposite polymer electrolytes were measured from 20°C to 120°C.

The proton conductivities of all anhydrous samples were compared in Figure 3.11. The DC conductivity strongly depends on increment of temperature and ratio of PVPA in the composite membranes.

Previously, solid-state NMR was studied to elucidate the structure and the local proton diffusion of the PVPA (Wagner et al., 2009). The results were demonstrated that the proton migration through host polymer was mediated by acidic protons through hydrogen bonding network(Celik, Akbey et al. 2008, Wagner, Manhart et al. 2009).
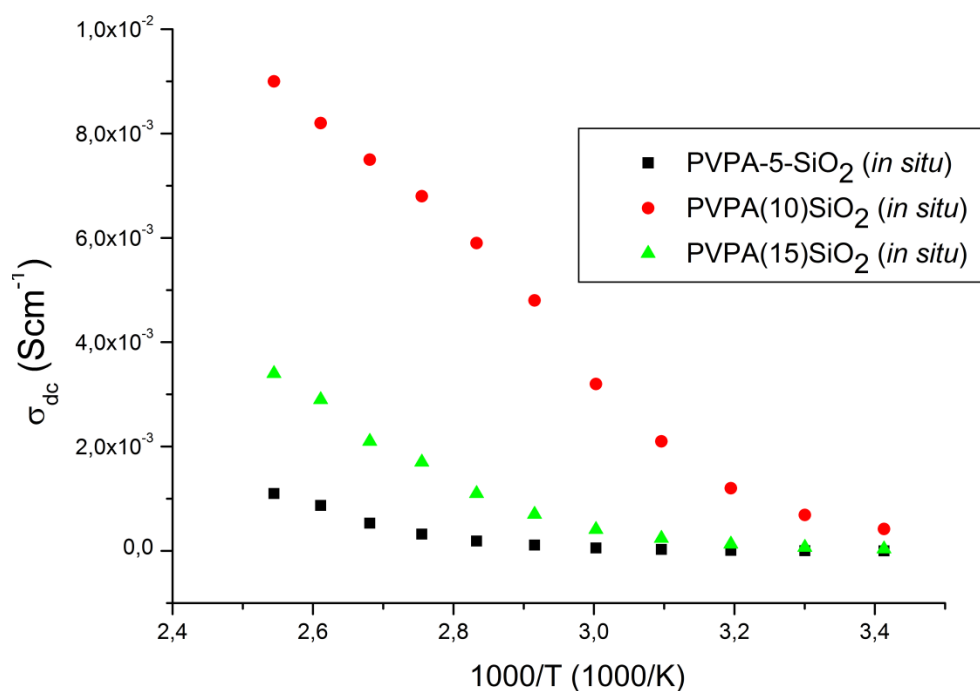
Figure 3.11 DC conductivity of PVPA(x)SiO$_2$ *(in situ)* composite membrane.

Clearly, proton conductivities of these samples increase with PVPA content (see Figure 3.12.). The maximum proton conductivity was measured for PVPA(10)SiO$_2$ (*in situ*) and found to be 0,009 (Scm^{-1}) at 120°C in the dry state. The proton conductivity of PVPA(10)SiO$_2$ (*in situ*) is almost identical to PVPA(15)SiO$_2$ (*in situ*) except with a slight deviation at higher temperatures. The material with x=10 was considered to be the optimum composition as the complex polymer electrolyte. Conductivity results showed that the PVPA content was highly effective on the proton conductivity of PVPA(10)SiO$_2$ (*in situ*) systems. Although the major part of proton transport is provided over phosphonic acid units coordinated with SiO$_2$,the decrease in conductivity for samples with higher nanoparticle content can be attributed to threshold composition of SiO$_2$ (Aslan, Gölcük et al. 2012).

3.1.7 Effect of Humidity on Conductivity

Previously, Kaltbeitzel *et al.* reported that maximum proton conductivity of 10^{-3} Scm^{-1} was reached under a pressure of 1 bar and in H$_2$O atmosphere (Kaltbeitzel, Schauff et al. 2007).
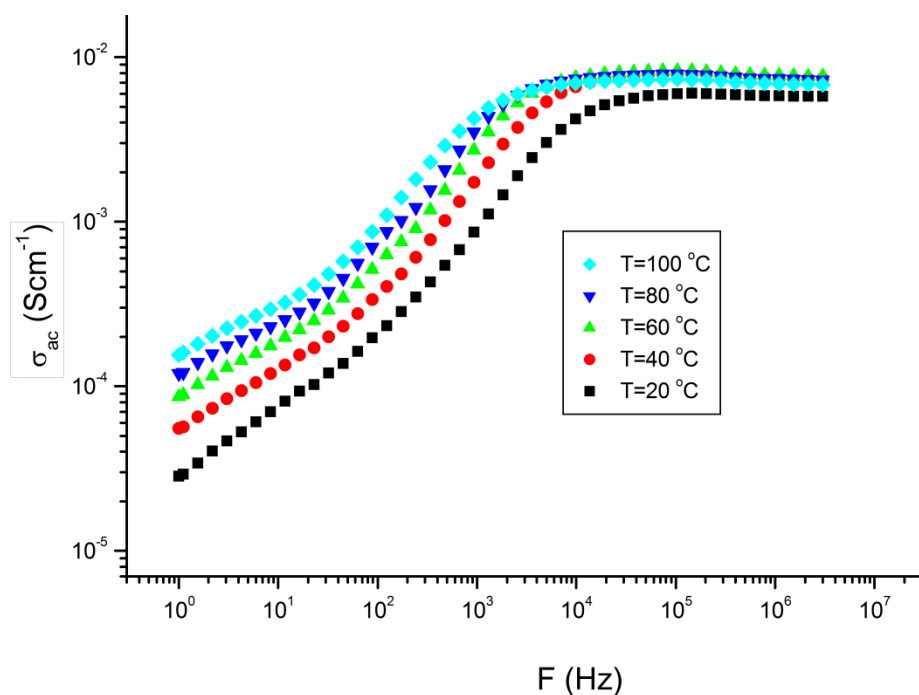
Figure 3.12 AC conductivity of PVPA(15)SiO$_2$ composite membranes (RH=50%) versus reciprocal temperature.
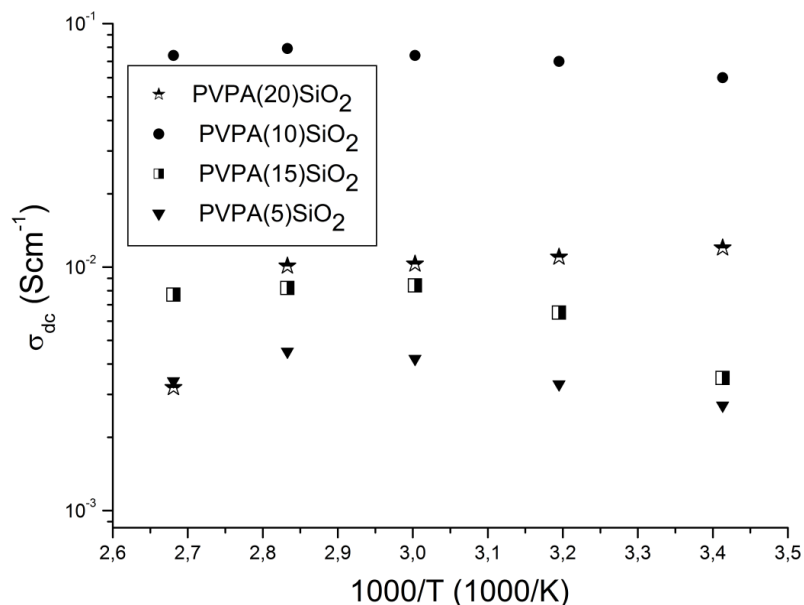
Figure 3.13 DC conductivity of PVPASiO$_2$ composite membranes (RH=50%) versus reciprocal temperature.

Similarly, the proton conductivity of Nafion 117 depends on temperature as well as humidity levels. When the membrane was fully humidified, the proton conductivity of Nafion 117 membrane was increased to 0.11 Scm^{-1} at room temperature and to 0.20 Scm^{-1} at elevated temperatures (Takimoto, Wu et al. 2009). The proton conductivity of Nafion 117 at 50 % relative humidity was approximately 0.03 Scm^{-1} at 40°C (Casciola, Alberti et al. 2006). As seen in Figure 3.13. the proton conductivity of the nanocomposite polymer electrolyte PVPA(x)SiO$_2$ membranes strongly depends upon the humidity. As shown in Figure 3.13., the proton conductivity of the humidified nanocomposite polymer electrolyte PVPA(x)SiO$_2$ membranes slightly changes with the temperature. The proton conductivity of hydrated PVPA(10)SiO$_2$ was measured to be 0.08 Scm^{-1} at 100 °C. The hydrated and anhydrous form of PVPA(10)SiO$_2$ have slightly higher proton conductivity than the other samples. Compared to pristine PVPA, the composite membranes with SiO$_2$ nanoparticles show higher proton conductivity at all temperatures. However, the proton conductivity of the composite membrane with higher SiO$_2$ content increases distinctively at higher temperatures. At lower temperatures the proton conductivity of the composite membranes

mainly depends upon water content of the membranes. As the temperature increases, the free water in the membranes begins to evaporate and the contribution of the water absorbed in SiO_2 becomes more important (Aslan, Gölcük et al. 2012).. From these results it can be concluded that PVPA(10)SiO_2 is the optimum composition.

3.2 CHARACTERIZATION OF PVPA-TIO$_2$ NANOCOMPOSITE MEMBRANES

3.2.1 FTIR studies

The homopolymer of PVPA was prepared by free-radical polymerization of vinylphosphonic acid. Figure 3.14. shows the FTIR spectra of PVPATiO$_2$ nanocomposite membranes. The FTIR spectrum of PVPA shows strong bands between 1040-910 cm^{-1} that belong to asymmetric stretching vibrations of the P-OH group. The P–O–H vibration at 930 cm^{-1} decreases as the PVPA ratio increases, indicating the existence of excess acidic protons (Sevil and Bozkurt 2004). Additionally, phosphonic acid units give rise to broad bands with medium intensity between 1700-1590 cm^{-1} and 2850-2750 cm^{-1} region(Bozkurt, Meyer et al. 2003, Celik, Akbey et al. 2008). The intensities of these peaks increase as the concentration of TiO$_2$ particles increases. The broad and strong peak at about 600 cm^{-1} is attributed to the overlapping of the combined results of the Ti-O band vibrations and/or stretching in TiO$_2$ particles (Mallakpour and Barati 2011). The new bands at 1075 and 1140 cm^{-1} can be attributed to the P–O–Ti and P O stretching vibrations, respectively. The bands at 1330 and 1427 cm^{-1} can be attributed to the weak phosphoryl (P O) frequency and P–C stretching vibrations(Wu, Hou et al. 2010). It could be deduced from these results that PVPA had formed chemical bonds with the Ti atom at the titania surface via phosphonate groups. Both the characteristic peaks of PVPA and TiO$_2$ can be clearly seen in all these composite spectra. The broad band between 3500 cm^{-1} - 2500 cm^{-1} is the hydrogen bonding network which is necessary for proton conduction.
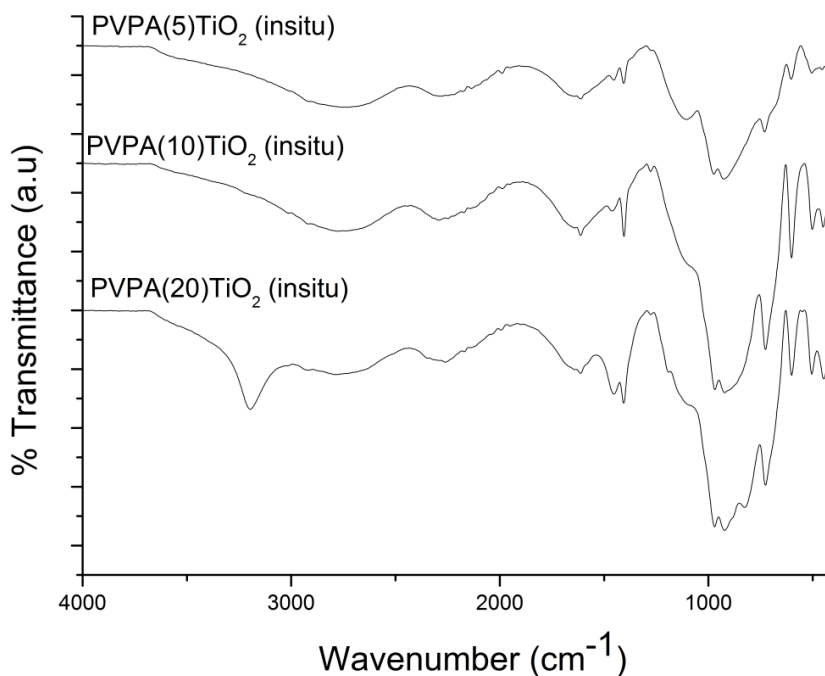
Figure 3.14 FT-IR spectra of PVPA(x)TiO$_2$ (*in situ*) composite membranes.

3.2.2   SEM

In order to examine the microstructures and nano filler distribution within the nanocomposites, SEM analysis was conducted. Typical surface SEM photographs of PVPATiO$_2$ nanocomposite were illustrated in Figure 3.15. From Figure 3.15, it was observed that TiO$_2$ were homogenously dispersed in the PVPA matrix. Moreover, from these figures, it can be seen that PVPA and TiO$_2$ being well distributed throughout the matrix. This result is also consistent with the DSC curves of blend membranes that no separate T$_g$ transition of impregnated PVPA was observed (Aslan and Bozkurt 2012).
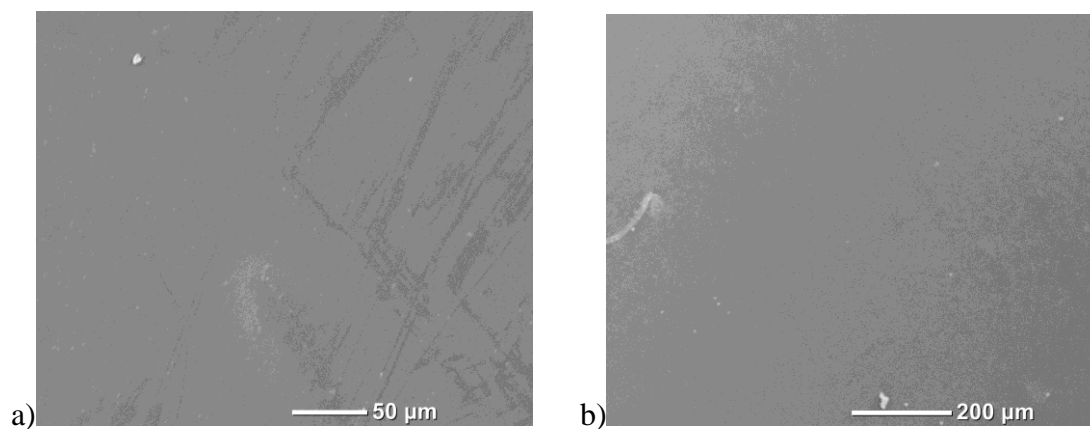
Figure 3.15 SEM micrographs of the surface of PVPATiO$_2$ composite membranes (a) 50 μm (b) 200 μm.

3.2.3   Thermal analysis

Table 3.3 lists the glass transition temperatures of the PVPA(x)TiO$_2$ nanocomposites. The PVPA(x)TiO$_2$ nanocomposite polymer membranes have definite glass transition temperatures between 126 ^{0}C and 85 ^{0}C (Table 3.3.). The results indicate that the glass transition temperatures of the samples shift to lower temperatures as the quantity of TiO$_2$ increases.

Table 3.3 Max. Proton conductivity and Tg (^{o}C) values for the PVPA(x)TiO$_2$ composite membranes

Sample Name	TiO$_2$ content (w/w %)	Tg (^{o}C)	Max. Proton Conductivity (Scm^{-1}) at 120°C
PVPA(5)TiO$_2$	5	96	2 x10^{-5} (Scm^{-1}) at 120°C
PVPA(10)TiO$_2$	10	123	1,2 x10^{-5} (Scm^{-1}) at 120°C
PVPA(20)TiO$_2$	20	130	0,004 (Scm^{-1}) at 120°C
PVPA(5)TiO$_2$ (*in situ*)	5	103	0,002 (Scm^{-1}) at 120°C
PVPA(10)TiO$_2$ (*in situ*)	10	120	0,004 (Scm^{-1}) at 120°C
PVPA(20)TiO$_2$ (*in situ*)	20	126	0,002 (Scm^{-1}) at 120°C

The PVPA(x)TiO$_2$ (*in situ*) composite membranes have glass transition temperatures between 103 ^{0}C and 125 ^{0}C. The reason can be attributed to inhibition of intra and inter chain condensation. This increase of Tg suggests improved thermal stability and hence provides potential advantages during the PEM fuel cell operation at high temperatures. The reason of such increment in Tg can be expressed by the free volume theory (Peighambardoust and Pourabbas 2007). Based on this theory, thermal expansion of free volumes, the space that is not occupied by polymer chains, occurs above glass transition temperature, and chains begin to fill the free volumes as a result of enhanced thermally motivated segmental motions of the chains. Incorporation of TiO$_2$ particles in polymer matrix would fill these free volumes and would cause need to more energy for starting segmental motions, which would make Tg to increase (Aslan and Bozkurt 2012).

Figure 3.16. shows the thermogravimetry (TG) results of the PVPA(x)TiO$_2$. Both PVPA(10)TiO$_2$ and PVPA(20)TiO$_2$ have no weight change up to approximately 150 ^{0}C. Then an elusive weight loss up to 180 ^{0}C can be attributed to anhydride formation. Clearly, the dried materials are thermally stable up to 200 ^{0}C, then they decompose (Aslan and Bozkurt 2012).
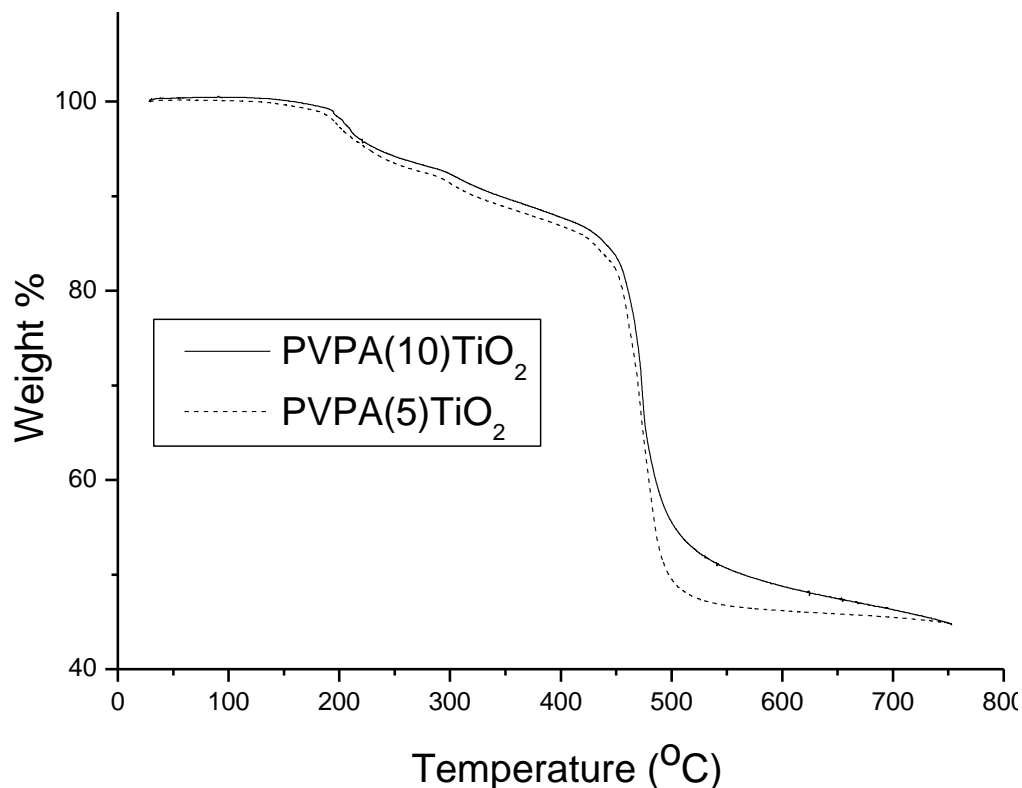
Figure 3.16 TG thermograms of PVPATiO$_2$ composite membranes recorded at a heating rate of 10 ^{o}C/min under nitrogen atmosphere.

Figure 3.17. shows the thermogravimetry (TG) results of the PVPA(x)TiO$_2$ (*in situ*). Both PVPA(10)TiO$_2$ (*in situ*) and PVPA(20)TiO$_2$ (*in situ*) have no weight change up to approximately 150 ^{0}C. The TG graphs show an elusive weight loss up to 150 ^{0}C which can be attributed to anhydride formation. It is clear that the dried polymers are thermally stable up to 200 ^{0}C, then they decompose. The TiO$_2$ nano particles improved the thermal stability of the PVPA nano composite membranes.
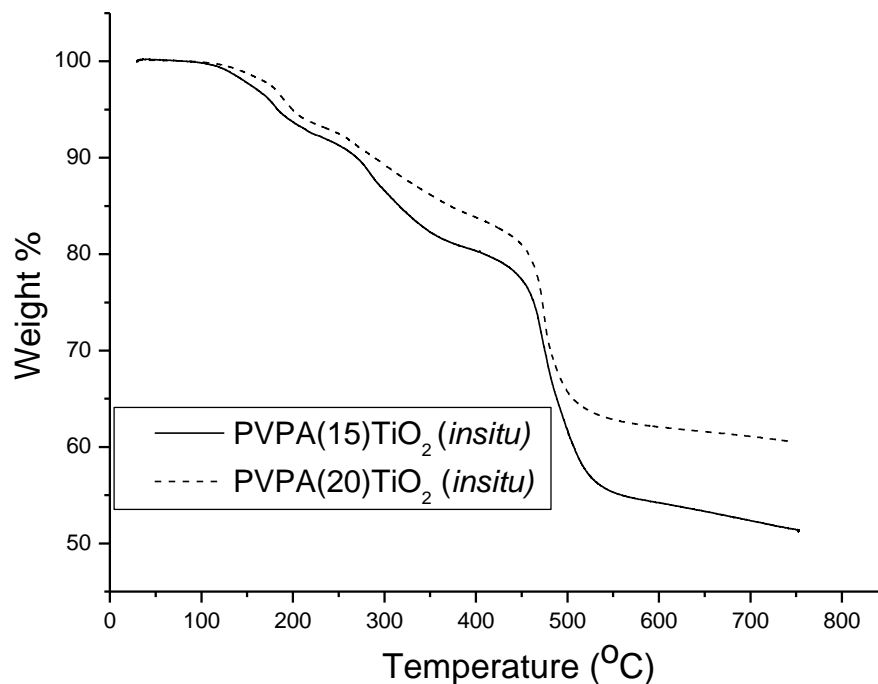
Figure 3.17 TG thermograms of PVPATiO$_2$ (*in situ*) composite membranes recorded at a heating rate of 10 ^{o}C/min under nitrogen atmosphere.

3.2.3 Proton conductivity

The proton conductivities of PVPA(x)TiO$_2$ anhydrous nanocomposite polymer electrolytes were measured from 20 ^{o}C to 120 ^{o}C. The AC conductivity of PVPA(5)TiO$_2$ and PVPA(20)TiO$_2$ composite membranes are shown in Figure 3.18 and Figure 3.19.
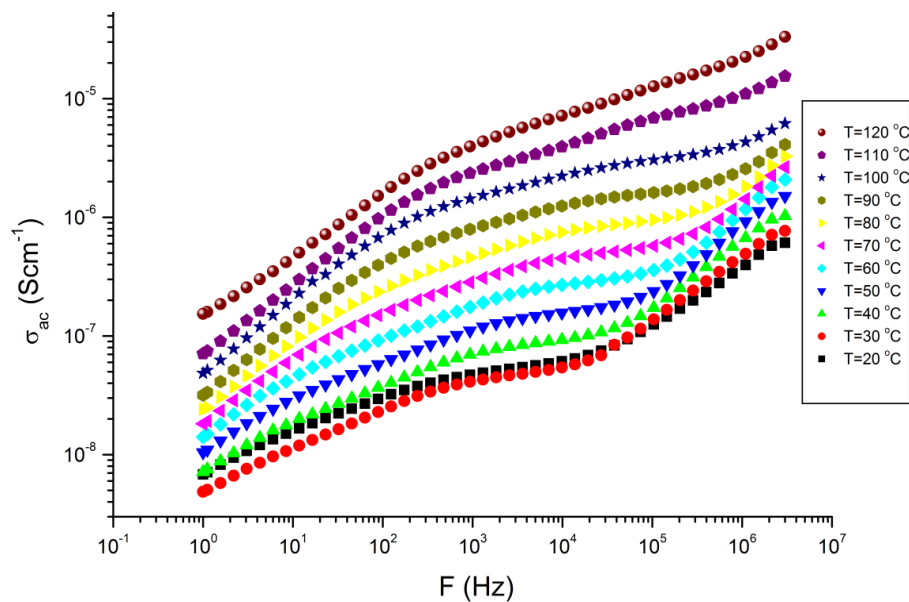
Figure 3.18. AC Conductivity of PVPA(5)TiO$_2$ composite membranes.
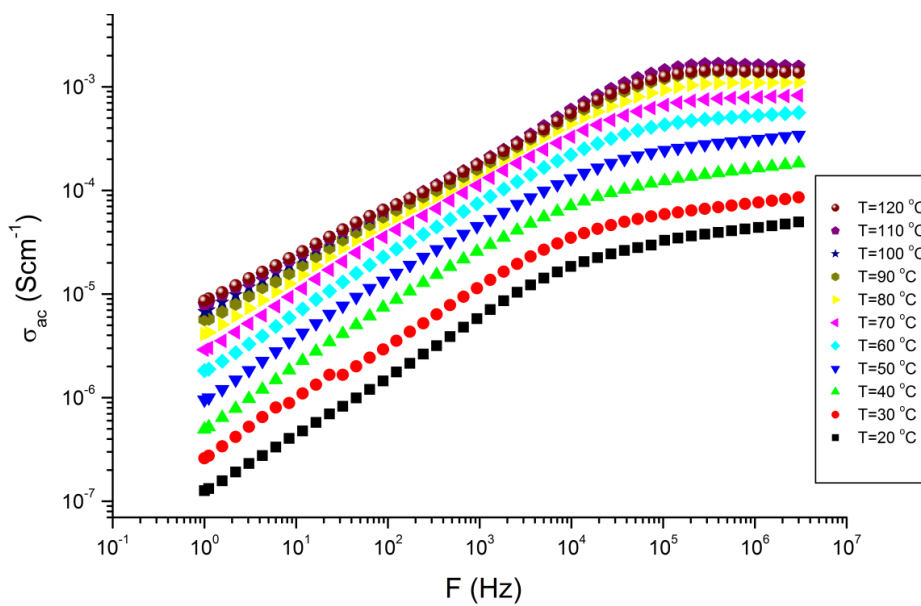
Figure 3.19. AC Conductivity of PVPA(20)TiO$_2$ composite membranes.

The proton conductivities of PVPA(x)TiO$_2$composite membranes were compared in Figure 3.20. The conductivity isotherm illustrates that the DC conductivity strongly depends on temperature as well as the ratio of TiO$_2$.
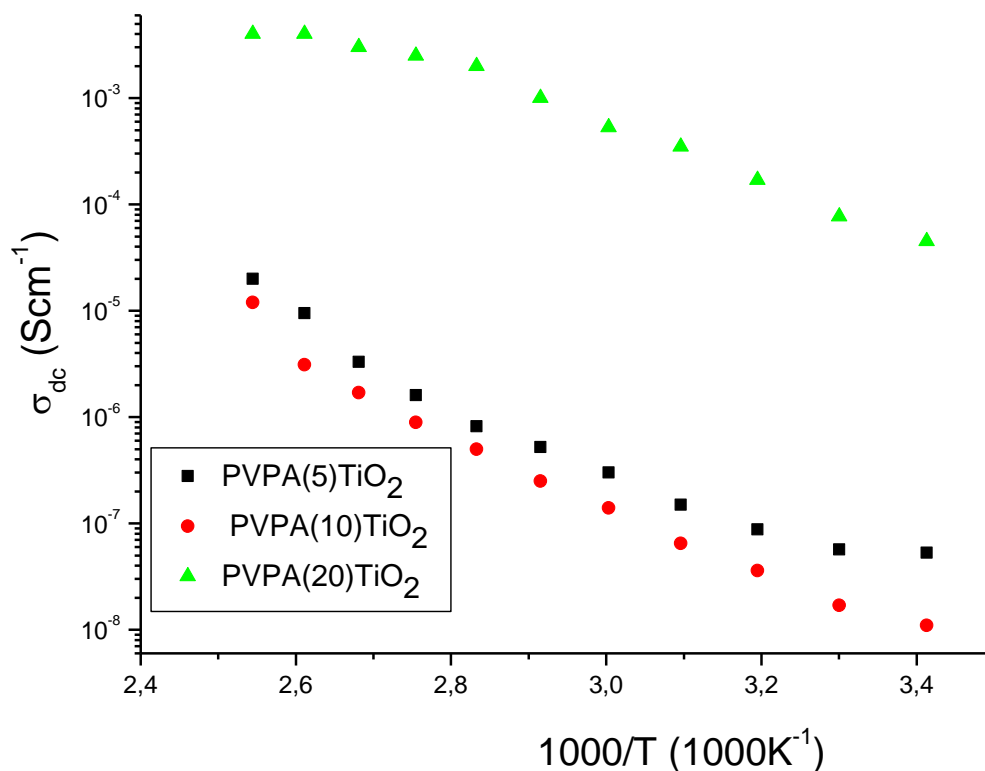
Figure 3.20 DC Conductivity Measurements of PVPATiO$_2$ composite membranes versus reciprocal temperature.

The AC conductivity of PVPA(10)TiO$_2$ (*in situ*) and PVPA(20)TiO$_2$ (*in situ*) composite membranes are shown in Figure 3.21. and Figure 3.22. The maximum proton conductivity was measured for PVPA(10)TiO$_2$ (*in situ*) and found to be 0,004 (Scm^{-1}) at 120 ^{o}C in the dry state in Figure 3.23. The material with x=10 was considered to be the optimum composition as the complex polymer electrolyte.
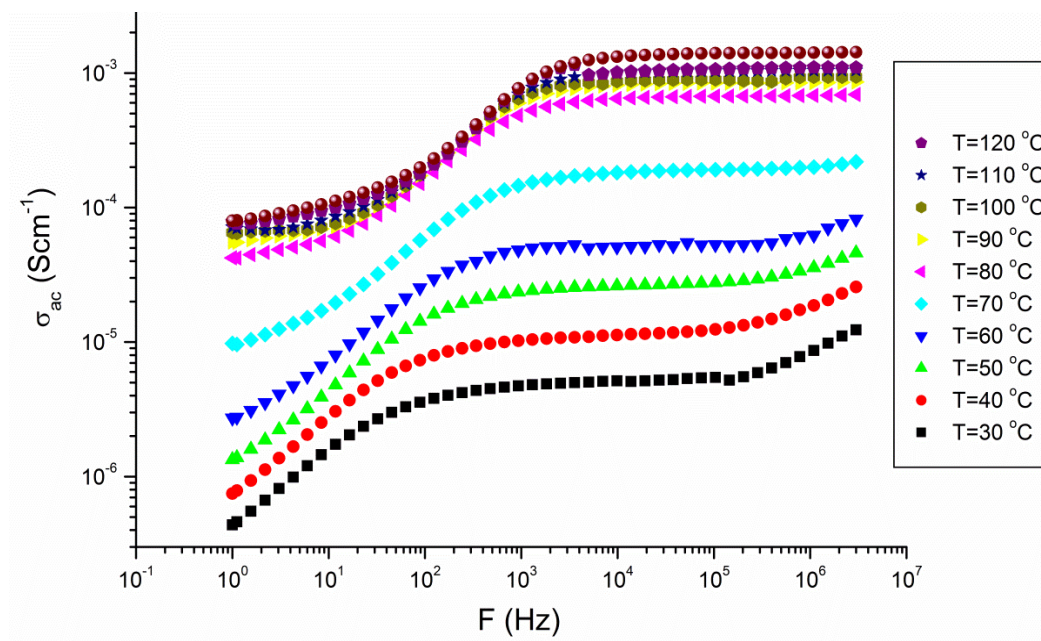
Figure 3.21 AC Conductivity Measurements of PVPA(10)TiO$_2$ (*in situ*) composite membranes versus reciprocal temperature.
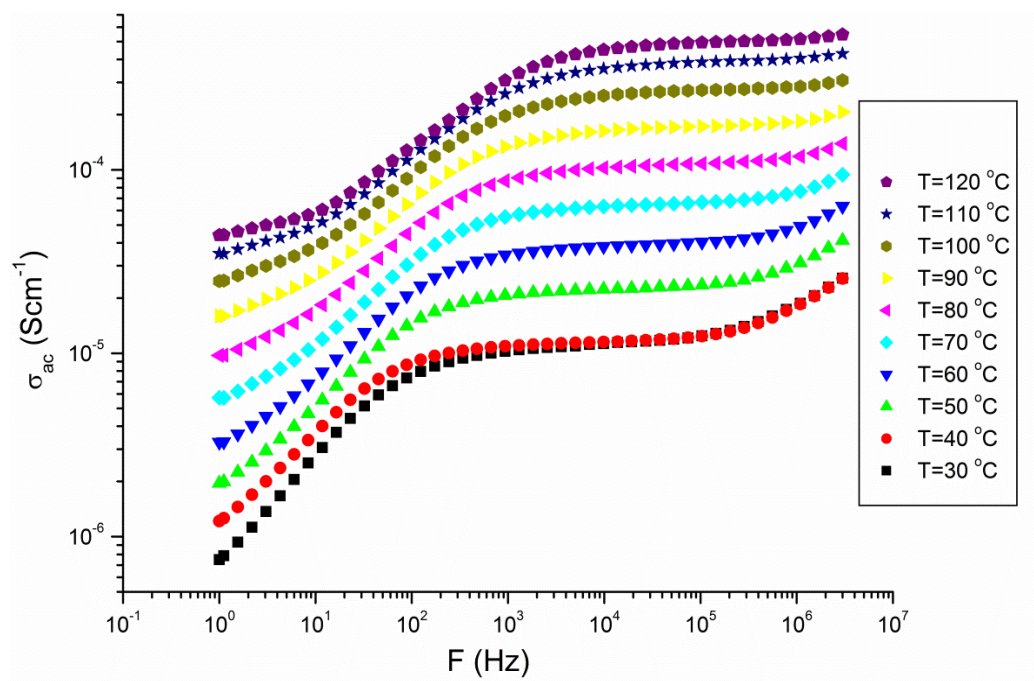
Figure 3.22 AC Conductivity Measurements of PVPA(20)TiO$_2$ (*in situ*) composite membranes versus reciprocal temperature.
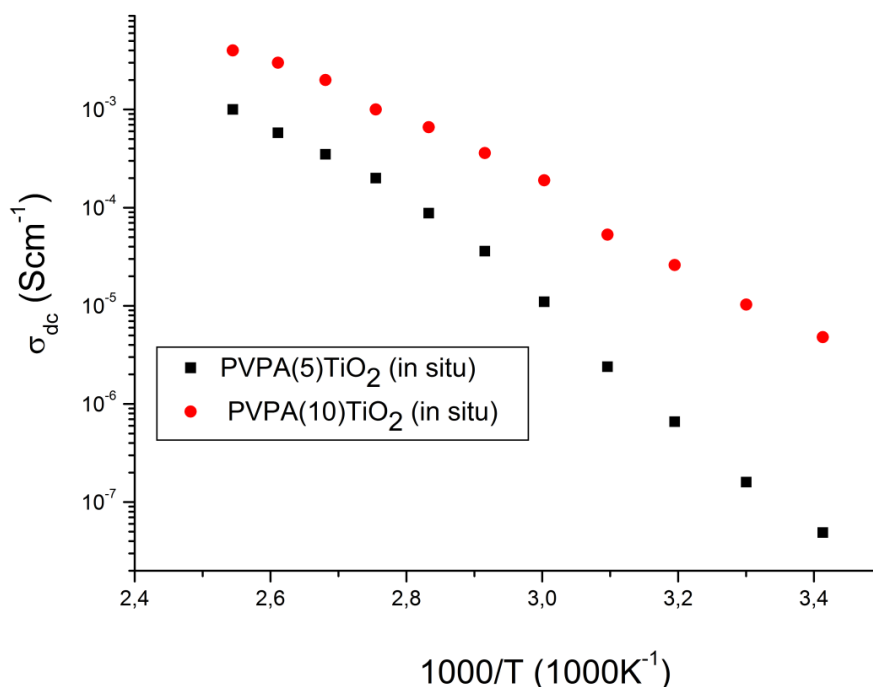
Figure 3.23 DC Conductivity Measurements of PVPATiO$_2$ (*in situ*) composite membranes versus reciprocal temperature.

Conductivity results showed that the PVPA composition is highly effective on the proton conductivity of the samples in the PVPA(10)TiO$_2$ (*in situ*) systems. Although the major part of proton transport is provided over both phosphonic acid coordinated with TiO$_2$ in Figure 3.24. The increasing of the conductivity of nanocomposite polymer membrane was explained that the nano particle fillers in the polymer matrix. Nonconducting TiO$_2$ particles which remain embeded in the channels connecting the diffusion of protons (Eikerling, Kornyshev et al. 2001). Moreover, the interactions between phosphonic units of PVPA and nanoparticles improve the protons transport. The decrease in conductivity for samples with higher TiO$_2$ content can be attributed to segmental relaxation inhibited by complexation (Aslan and Bozkurt 2012).. Previously work, Wu et al. explained the interaction, between the nanoparticle and phosphonic acid units, improved the proton conductivity(Wu, Hou et al. 2010). Another earlier work showed the nanoparticle content is an important factor on proton conductivity and thermal stability of nanocomposite membranes (Devrim, Erkan et al. 2009).
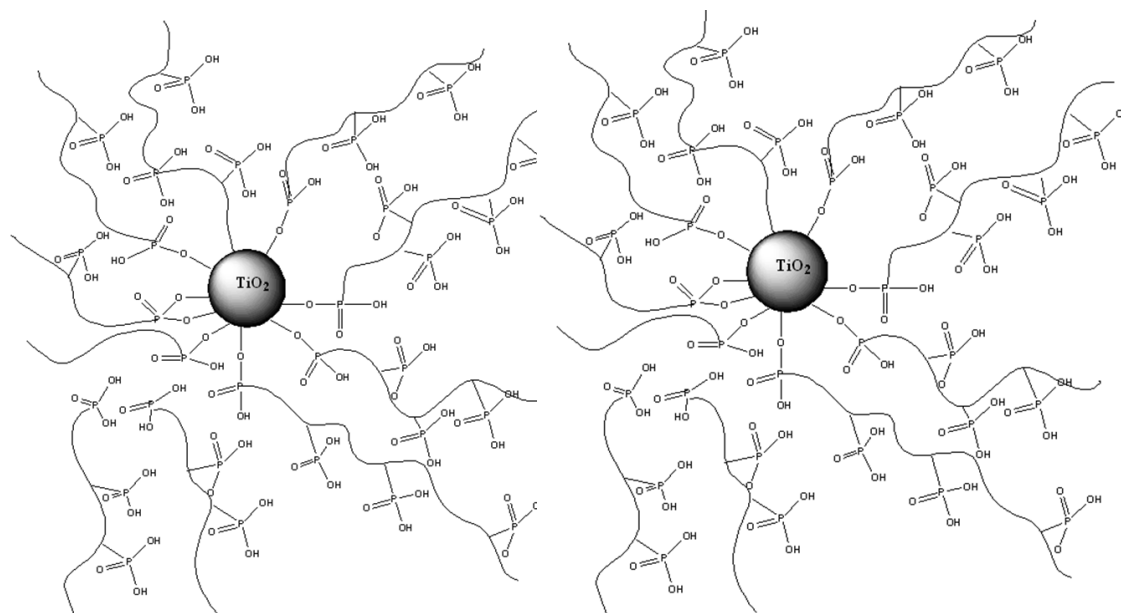
Figure 3.24 Model structure of PVPATiO$_2$ composite membranes.

3.3 CHARACTERIZATION OF PVPA-TIO$_2$SO$_3$H NANOCOMPOSITE MEMBRANES

3.3.1 FTIR studies

Figure 3.25 shows the FTIR spectra of PVPATS$_x$ nanocomposite membranes. The FTIR spectrum of PVPA shows strong bands between 1040-910 cm^{-1} that belong to asymmetric stretching vibrations of the P-OH group. The peak at 1150 cm^{-1} corresponds to P=O stretching. Additionally, phosphonic acid units give rise to broad bands with medium intensity between 1700-1590 cm^{-1} and 2850-2750 cm^{-1} region. FT-IR spectra of sulfuric acid modified nano-titania shows charateristic peaks around 1650cm-1 and at 980-1250 cm^{-1}. The peaks at 980 - 1250 cm^{-1} was attributed to bidentate sulfate coordination on the titania surface (980-990, 1040, 1130-1150 and 1210-1230 cm^{-1}) (Arata and Hino 1990, Jiang, Herricks et al. 2003, Wu, Hou et al. 2010) These peaks are overlapped with the corresponding peaks of phosphonic acid units of host matrix and became more intense (Aslan and Bozkurt 2012). The S=O vibration at 1393 cm^{-1}, can be clearly observed from the sample sulfated nano-titania (Navarrete et al. 1996). The broad band between 3500 cm^{-1}

^{1}-2500 cm^{-1} is the hydrogen bonding network which is necessary for proton conduction (Celik, Akbey et al. 2008).
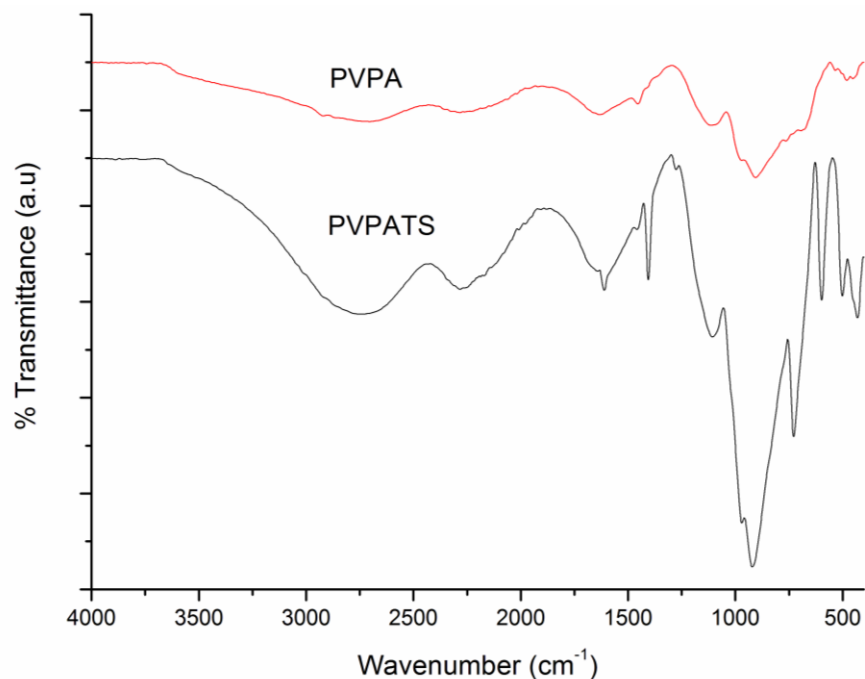
Figure 3.25 FT-IR spectra of the PVPA and PVPATS composite membranes.

3.3.2   XRD

Phase investigation of the crystallized product was performed by XRD and the diffraction pattern is presented in Fig. 3.26. The XRD pattern indicates that the product is sulfated nano-titania, and the diffraction peaks are broadened owing to very small crystallite size (Aslan and Bozkurt 2012).. According to Scherrer's equation was approximately 10-15 nm. The similar results reported in previous articles(Sakai, Kajitani et al. 2010).
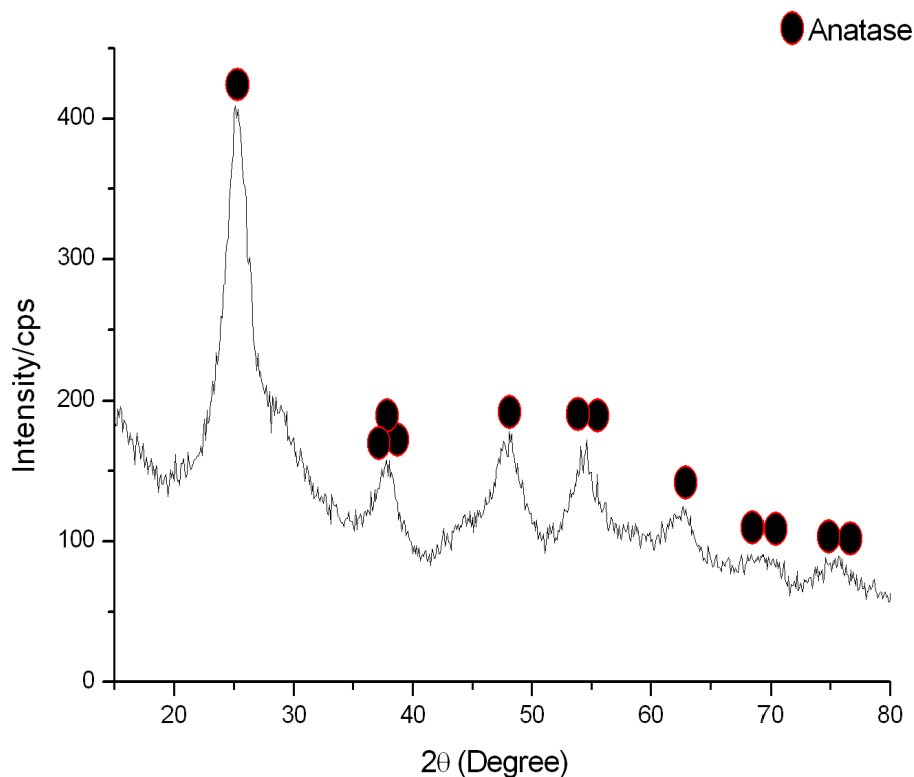
Figure 3.26 XRD pattern of the TiO$_2$SO$_3$H nanoparticles.

3.3.3 SEM

In order to examine the microstructures and nanofiller distribution within the nanocomposites, SEM analysis was conducted. Typical surface SEM photographs of PVPATS nanocomposite were illustrated in see Figure 3.27 a) and b). From Figure 3.27, it was observed that sulfated nano-titania were homogenously dispersed and embedded in the PVPA matrix. Moreover, from these figures, it can be seen that PVPA beads and sulfated nano-titania being well distributed throughout the matrix (Aslan and Bozkurt 2012). This result is also consistent with the DSC curves of the impregnated membranes that has no separate T$_g$ transition.

a)
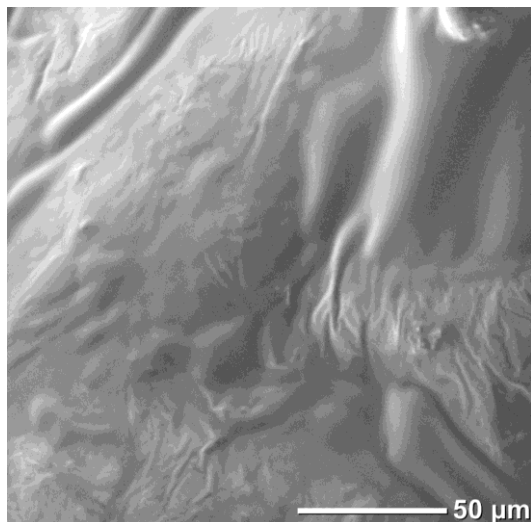
b)
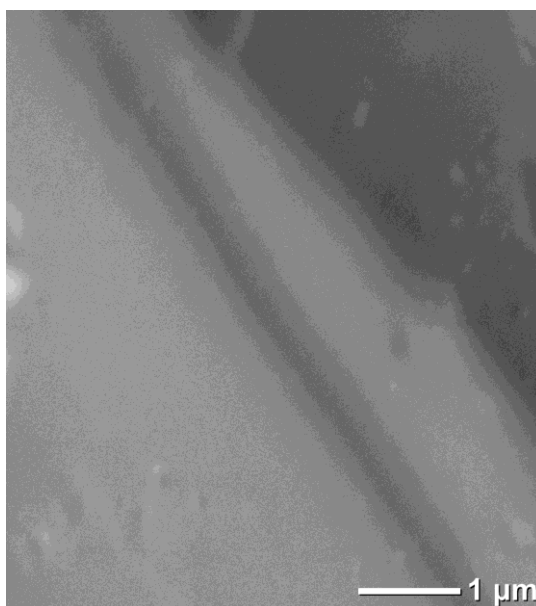
Figure 3.27 The SEM pictures of PVPATS composite membranes.

3.3.4 Thermal analysis

Table 3.4 lists the glass transition temperatures of the $PVPATS_x$ nanocomposites. PVPA exhibits a glass transition at around -23 ^{o} (Celik, Akbey et al. 2008). $PVPATS_x$

nanocomposite polymer membranes have definite glass transition temperatures between 84 ^{o}C and 100 ^{o}C. The results indicate that the glass transition temperatures of the samples shift to higher temperatures as the quantity of sulfated nano-titania increases. The reason can be attributed to inhibition of segmental relaxations due to complexation.

Table 3.4 Max. Proton conductivity and Tg (^{o}C) values for the all membranes.

Sample Name	PVPA:TS (molar ratio)	Tg (^{o}C)	Max. Proton Conductivity (Scm^{-1})
PVPATS	1:1	78 ^{o}C	0,03 (Scm^{-1}) at 150°C
PVPATS$_2$	1:2	82°C	5 $x10^{-3}$ (Scm^{-1}) at 150°C
PVPATS$_4$	1:4	94°C	0,01 (Scm^{-1}) at 150°C

Figure 3.28 shows the thermogravimetry (TG) results of the composite membranes under inert conditions. The TG graphs show an elusive weight loss up to 150 ^{o}C which can be attributed to anhydride formation (Celik, Akbey et al. 2008). It is clear that the dried polymers are thermally stable up to 200 ^{o}C, then they decompose. As the nanoparticle content increases, the degradation temperature slightly shifts to higher temperature which may be due to inhibition of anhydride formation (Aslan and Bozkurt 2012)..
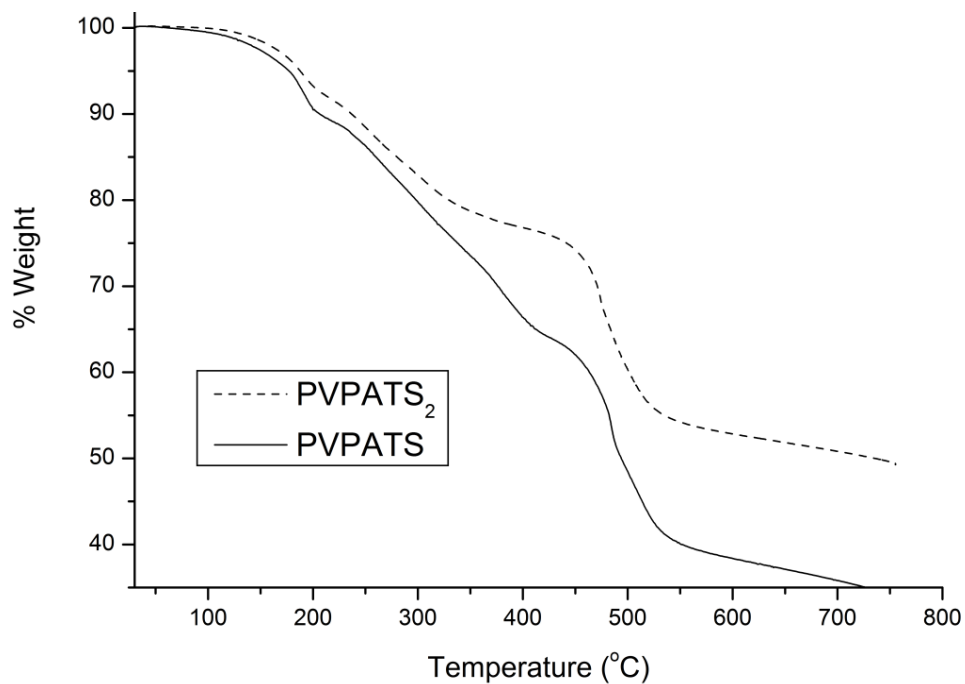
Figure 3.28 TG thermograms of PVPATS composite membranes recorded at a heating rate of 10 ^{o}C/min under a nitrogen atmosphere.

3.3.5   Proton conductivity

The proton conductivities of PVPATS$_x$ anhydrous nanocomposite polymer electrolytes were measured between 20-150 ^{o}C. The AC conductivity of PVPATS$_x$ composite membrane is shown in Figure 3.29, 3.30 and 3.31.
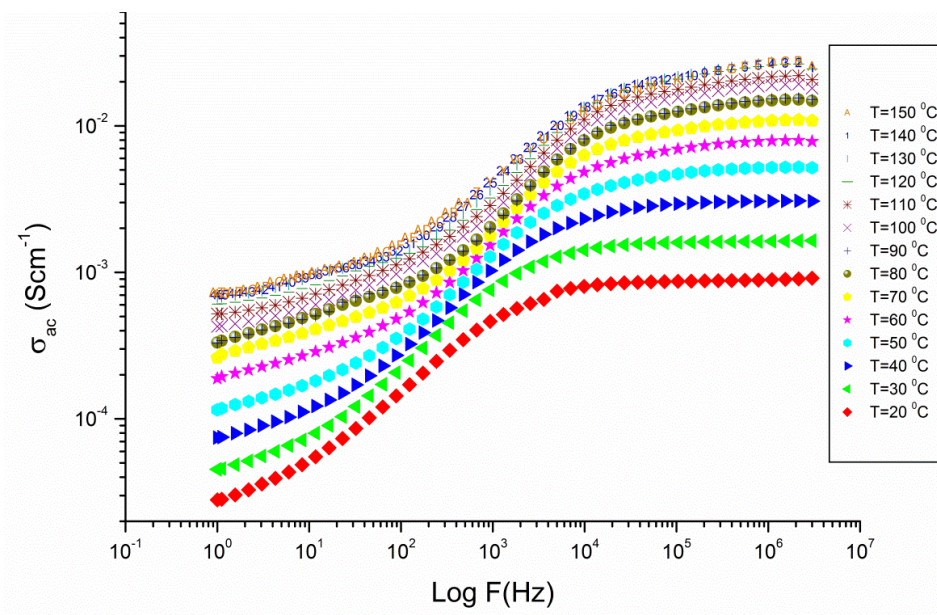
Figure 3.29 AC Conductivity of PVPATS composite membrane.
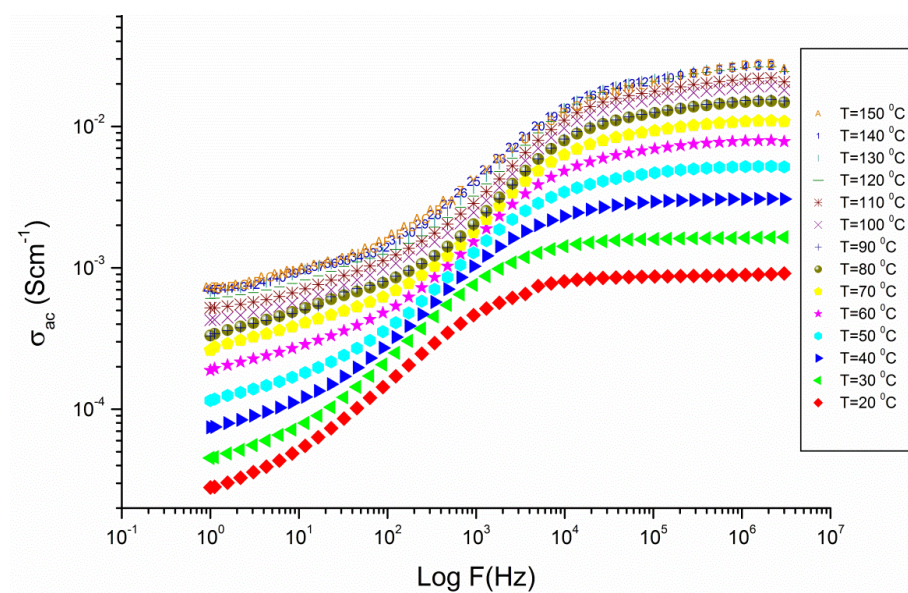
Figure 3.30 AC Conductivity of PVPATS composite membranes.
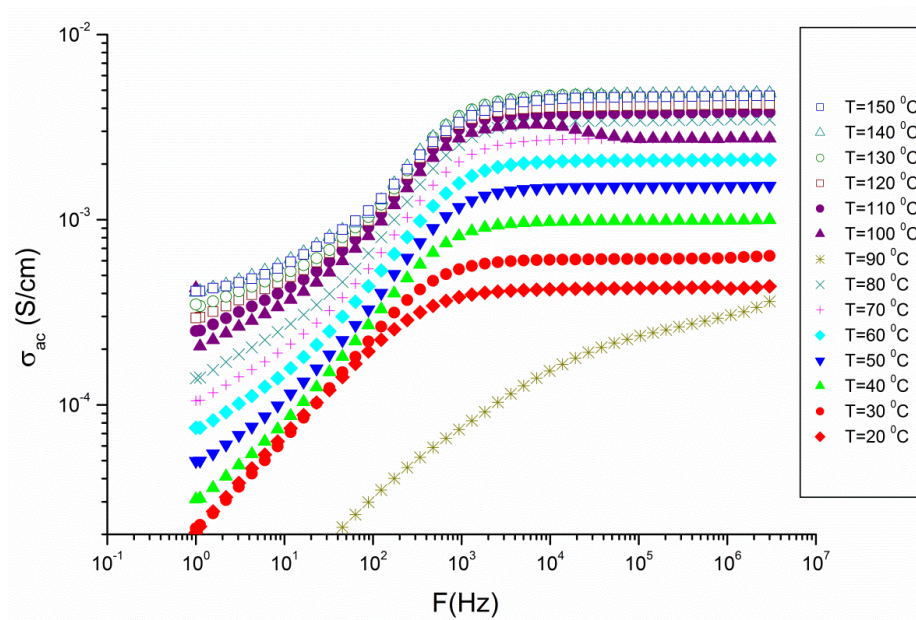
Figure 3.31 AC Conductivity of PVPATS$_2$ composite membrane.
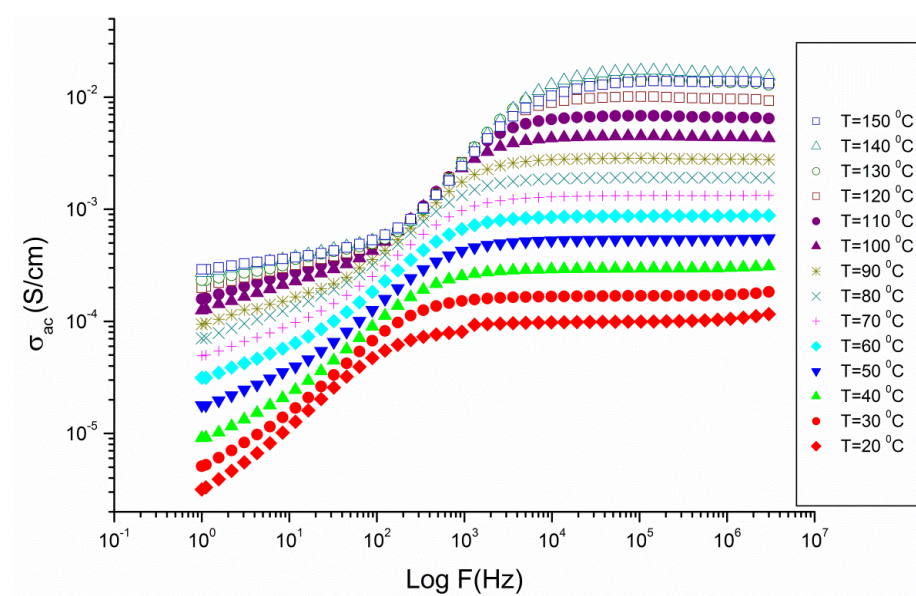
Figure 3.32 AC Conductivity of PVPATS$_4$ composite membrane.

The proton conductivities of all anhydrous samples were compared in Figure 3.33. The conductivity isotherm illustrates that the DC conductivity strongly depends on temperature as well as the ratio of PVPA (Aslan and Bozkurt 2012)..
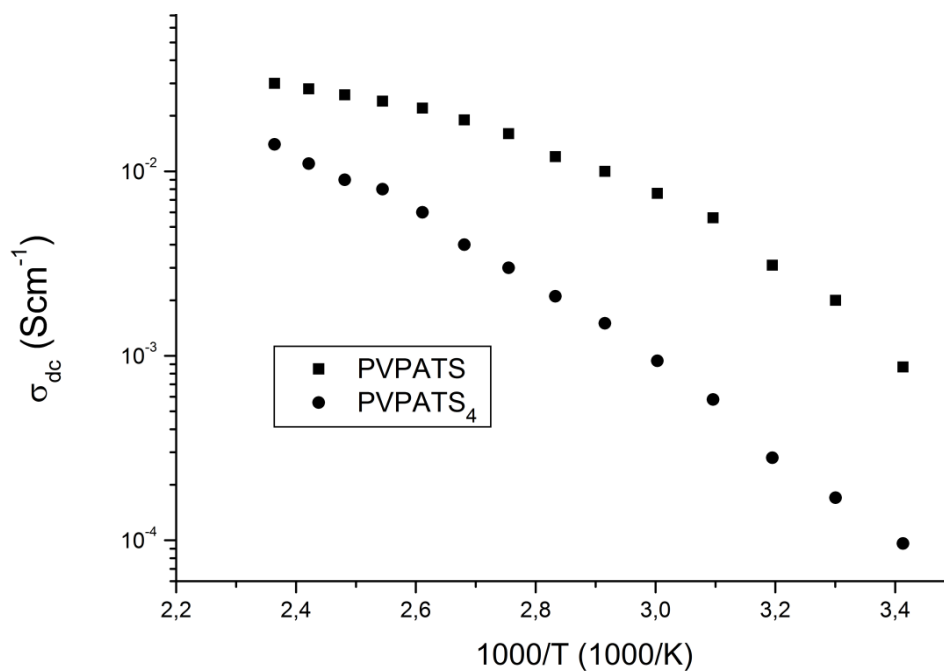
Figure 3.33 DC Conductivity of PVPATS composite membrane.

The relation between self-condensation and proton conductivity of PVPA was investigated by Kaltbeitzel et al (Kaltbeitzel, Schauff et al. 2007). Maximum proton conductivity for pristine PVPA was reached under 1 bar H_2O atmosphere. The proton conductivities of Nafion 117 membrane were ranged form 0.11 Scm^{-1} at room temperature to 0.20 Scm^{-1} at elevated temperatures when the membrane was fully hydrated. The proton conductivity of Nafion117 at 50 % relative humidity was approximately 0.03 Scm^{-1} at 40 ^{o}C (Kreuer 2001, Casciola, Alberti et al. 2006, Takimoto, Wu et al. 2009).

Previously, Wu et al. have reported organophosphorylated titania and chitosan composite membranes which exhibit an increased proton conductivity to an acceptable

level of 0.01 S cm^{-1} (RH= 80 %) for DMFC (Wu, Hou et al. 2010). These organophosphorylated titania nanoparticles were enhanced the proton conductivity when they dispersed in the membranes at low temperatures in humidified conditions .

The proton conductivities of these samples increase with PVPA content and increasing temperature. The maximum proton conductivity was measured for PVPATS$_x$ and found to be 0.03 (Scm^{-1}) at 150 ^{o}C in the dry state. The material with x=1 was considered to be the optimum composition as the complex polymer electrolyte. Conductivity results showed that the PVPA composition is highly effective on the proton conductivity of the samples in the PVPATS$_x$ systems. The major part of proton transport is provided over both phosphonic acid coordinated with sulfated nano-titania (Aslan and Bozkurt 2012).. Previously, the structure and the local proton transport of the host matrix, PVPA were studied by solid-state NMR (Lee, Bingoel et al. 2007).

In the current system, proton transfer can be facilitated by the additional sulfated groups on titania fillers. From the FT-IR, composite membranes as well as conductivity data, it can be concluded that a Grotthuss mechanism (structural diffusion) is the possible pathway for the total proton diffusion. This continuous pathway may convey proton mobility over the –POH groups and sulfate groups may reduce the energy barrier for proton transport (see Figure 3.34). The proton could travel along the ionic bonds from one functional group to another (Smitha, Sridhar et al. 2004, Ramirez-Salgado 2007).
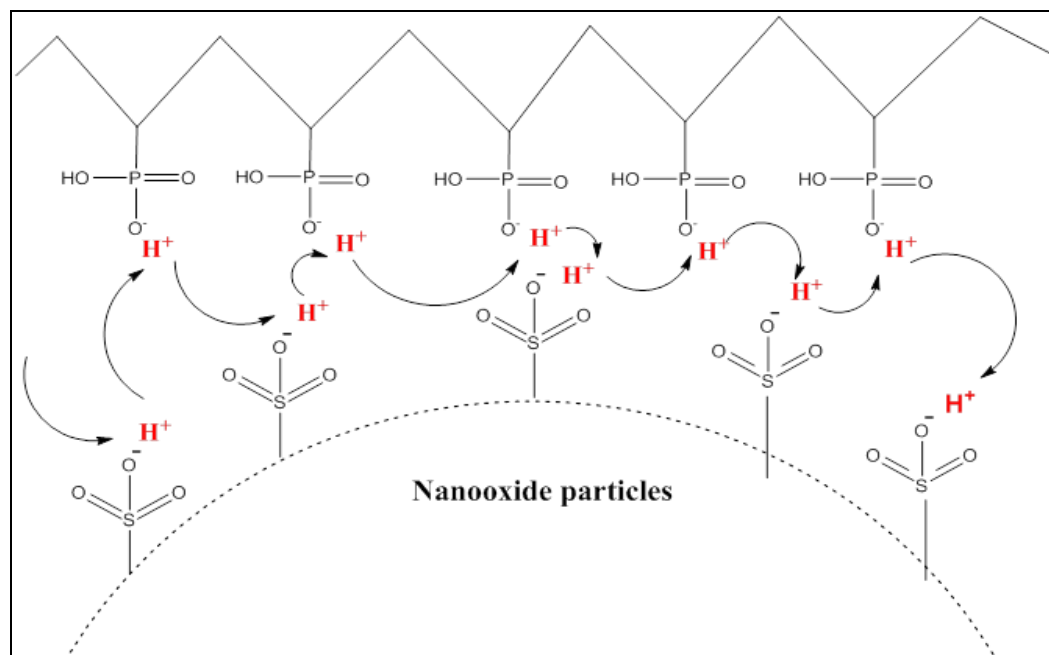
Figure 3.34 Proton transfer mechanism in PVPATS composite membranes.

3.4 CHARACTERIZATION OF NAFION-TS NANOCOMPOSITE MEMBRANES

3.4.1   FTIR studies

Figure 3.35. shows the FTIR spectra of Nafion-TS nanocomposite membranes. The Additionally, Sulfonic acid units give rise to broad bands with medium intensity between 1700-1590 cm^{-1} and 2850-2750 cm^{-1} region (Bozkurt et al., 2003: Çelik et al., 2008). The intensities of these peaks increase as the concentration of TS particles increases. The broad and strong peak at about 600 cm^{-1} is attributed to the overlapping of the combined results of the Ti-O band vibrations and/or stretching in TS particles (Mallakpour and Barati, 2011). The new bands at 1075 and 1140 cm^{-1} can be attributed to the S–O–Ti and S O stretching vibrations, respectively. (Wu et al., 2010). It could be deduced from these results that nafion matrix had formed chemical bonds with the Ti atom at the titania surface via phosphonate groups. Both the characteristic peaks of Nafion and TS can be clearly seen in all these composite spectra. The broad band between 3500 cm^{-1} - 2500 cm^{-1} is the hydrogen bonding network which is necessary for proton conduction (Aslan and Bozkurt 2012)..
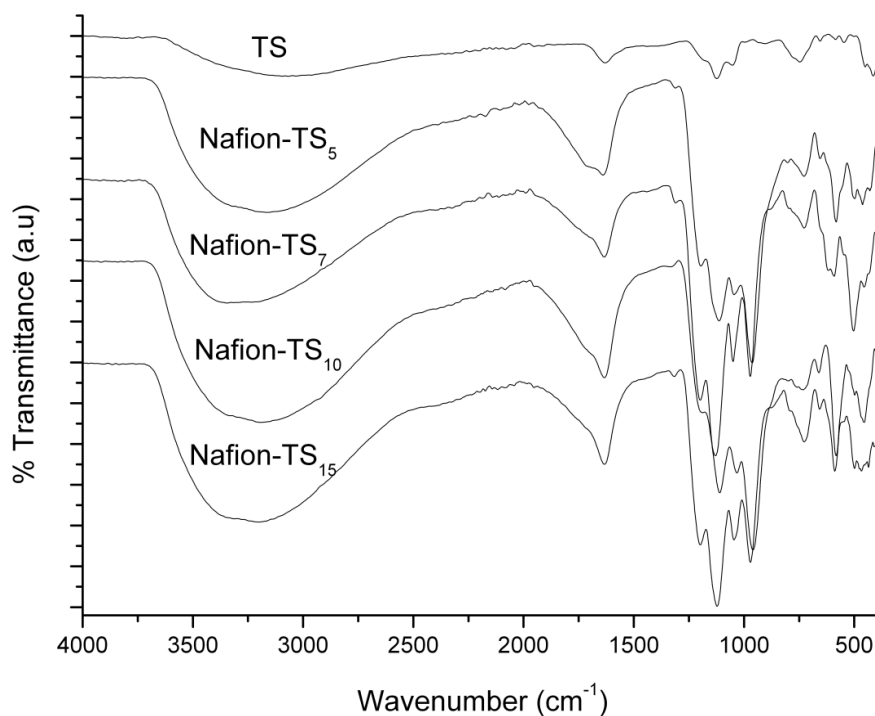
Figure 3.35 FT-IR spectra of the TS and Nafion-TS$_x$ composite membranes.

3.4.2   SEM

In order to examine the microstructures and nano filler distribution within the nanocomposites, SEM analysis was conducted. Typical surface SEM photographs of Nafion-TS nanocomposite were illustrated in Figure 3.36. From Figure 3.36., it was observed that TiO$_2$ were homogenously dispersed in the Nafion matrix. Moreover, from these figures, it can be seen that Nafion and TS being well distributed throughout the matrix.

a)
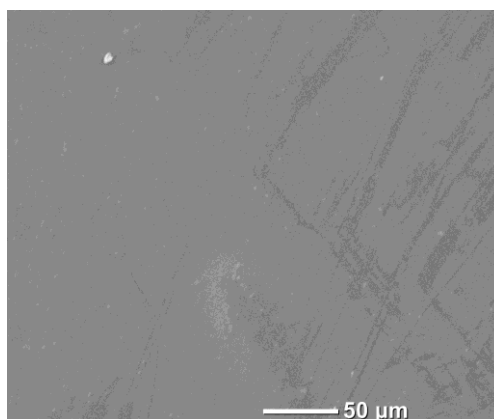
b)
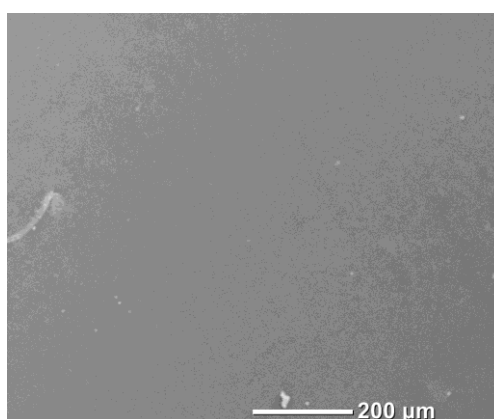
Figure 3.36 SEM micrographs of the surface of Nafion-TS composite membranes (a) 50 □m □(b) 200 □m.

3.4.3   Thermal analysis

Table 3.5 lists the glass transition temperatures of the Nafion-TS_x nanocomposites. Nafion-TS_x nanocomposite polymer membranes have definite glass transition temperatures between 126 ^{0}C and 85 ^{0}C. The results indicate that the glass transition temperatures of the samples shift to lower temperatures as the quantity of TS increases.

Table 3.5 Max. Proton conductivity and Tg (^{o}C) values for the Nafion-TS composite membranes.

Sample Name	TS content (w/w %)	Tg (^{o}C)	Max. Proton Conductivity (Scm^{-1}) at 120°C
Nafion-TS$_5$	5	96	2×10^{-5} (Scm^{-1}) at 120°C
Nafion-TS$_7$	7	123	$1,2 \times 10^{-5}$ (Scm^{-1}) at 120°C
Nafion-TS$_{10}$	10	130	$0,004$ (Scm^{-1}) at 120°C
Nafion-TS$_{15}$	15	103	$0,002$ (Scm^{-1}) at 120°C

The Nafion-TS$_x$ composite membranes have glass transition temperatures between 103 ^{0}C and 125 ^{0}C. The reason can be attributed to inhibition of intra and inter chain condensation. This increase of Tg suggests improved thermal stability and hence provides potential advantages during the PEM fuel cell operation at high temperatures. The reason of such increment in Tg can be expressed by the free volume theory (Peighambardoust and Pourabbas, 2007). Incorporation of TiO$_2$ particles in polymer matrix would fill these free volumes and would cause need to more energy for starting segmental motions, which would make Tg to increase.

Figure 3.37. shows the thermogravimetry (TG) results of the Nafion-TS$_x$. An elusive weight loss up to 180 ^{0}C can be attributed to anhydride formation. Clearly, the dried materials are thermally stable up to 300 ^{0}C, then they decompose.
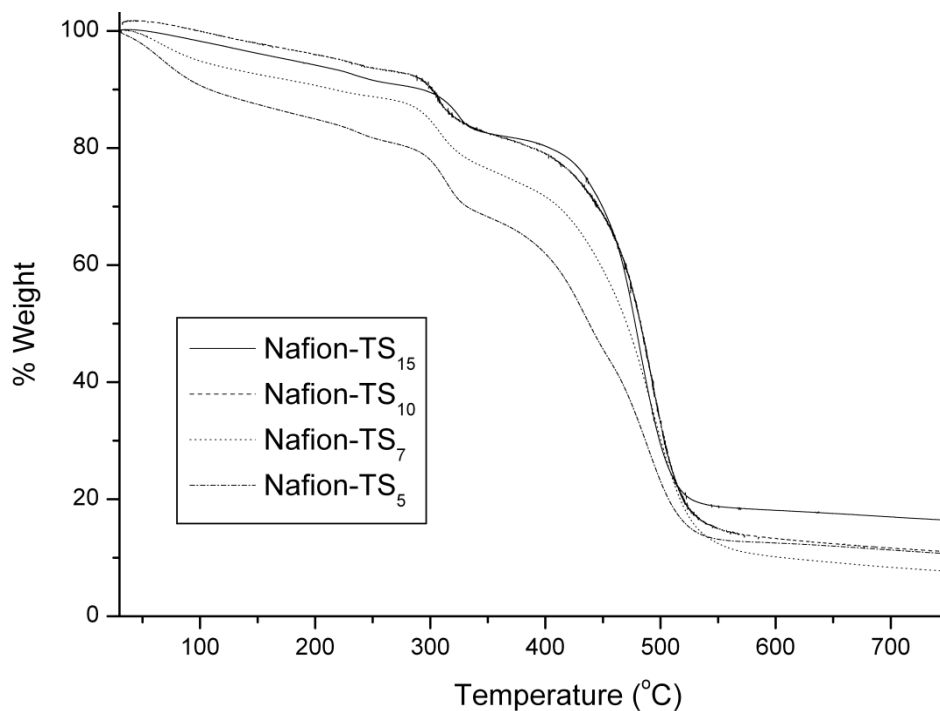
Figure 3.37 TG thermograms of Nafion-TS composite membranes recorded at a heating rate of 10 $^{\circ}$C/min under a nitrogen atmosphere.

3.4.5 Water/Methanol Uptake

The water/methanol uptake of the membranes is a major parameter influencing proton conductivity, mechanical property and stability. Solution uptakes of the Nafion-TS samples are shown in Figure 3.38. As can be seen, water/methanol uptake increase with increasing TS content. The sample has the highest water uptake value (250 %). This result showed that the increasing swelling character with TS content it may be attributed to water retention behaviour of sulfonic acid units in the nanocomposite membranes.
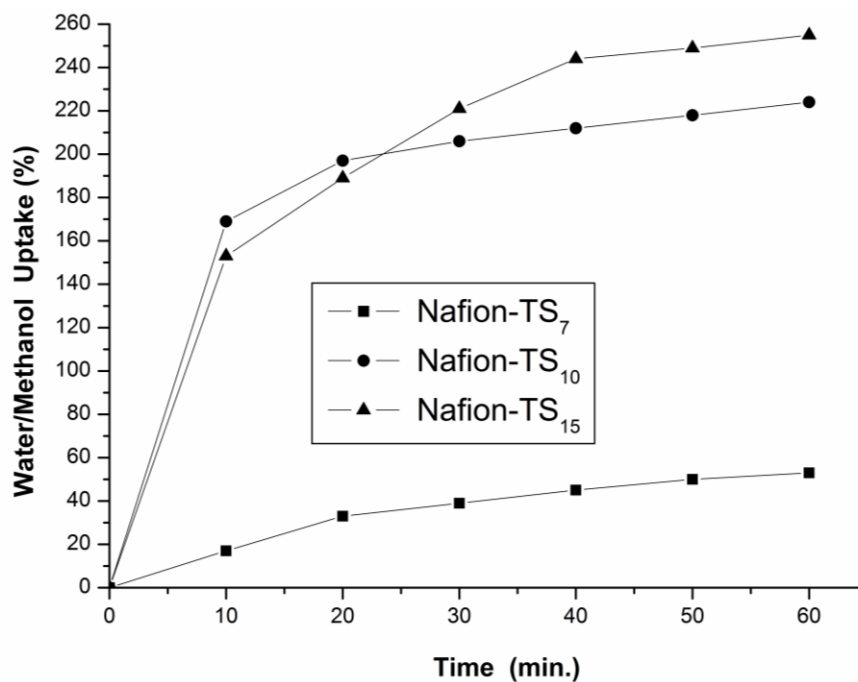
Figure 3.38 Water/Methanol uptake of Nafion-TS nanocomposite membranes.

3.4.6 Proton conductivity

The proton conductivities of Nafion-TS$_x$ anhydrous nanocomposite polymer electrolytes were measured from 20 ^{o}C to 120 ^{o}C. The AC conductivity of Nafion-TS$_{10}$ and Nafion-TS$_{15}$ composite membranes are shown in Figure 3.39 and Figure 3.40.
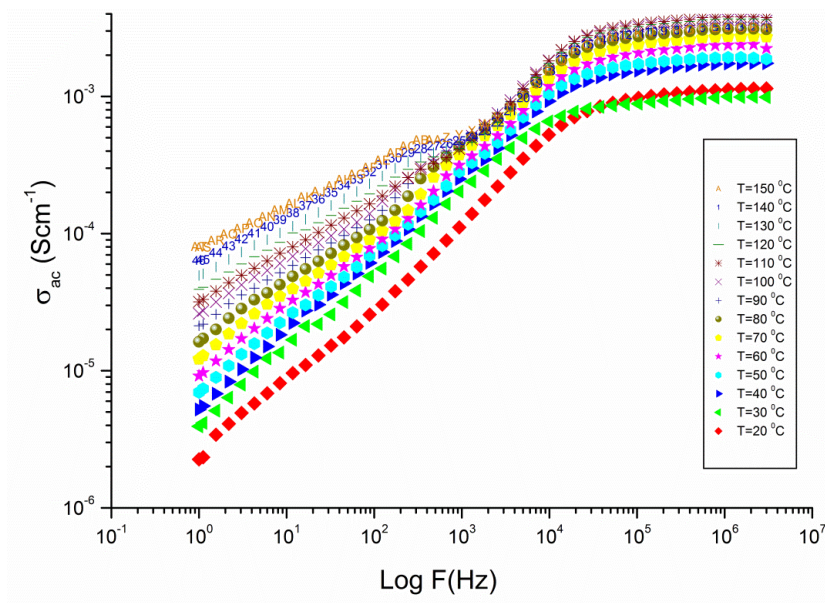
Figure 3.39 AC Conductivity of Nafion-TS$_{10}$ composite membranes.
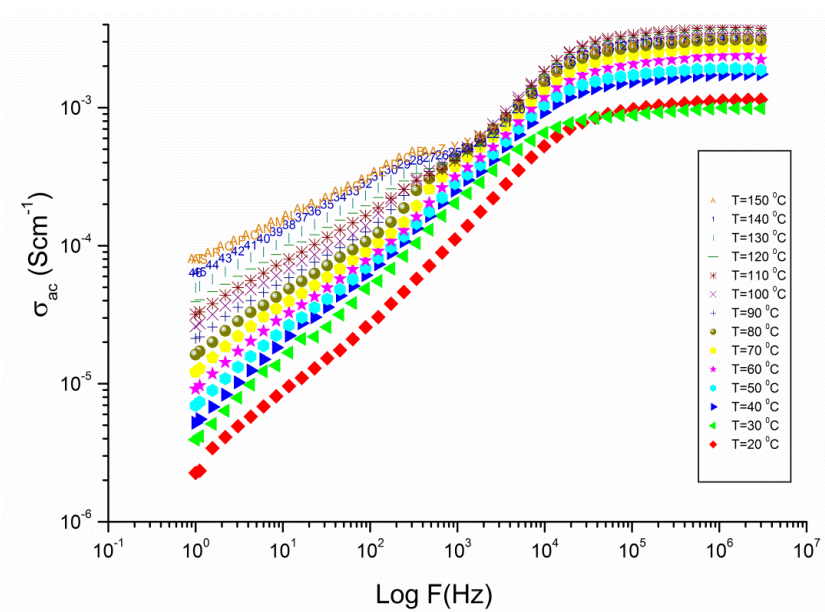
Figure 3.40 AC Conductivity of Nafion-TS$_{15}$ composite membranes.

The proton conductivities of Nafion-TS$_x$ composite membranes were compared in Figure 3.41. The conductivity isotherm illustrates that the DC conductivity strongly depends on temperature as well as the ratio of TiO_2SO_3H.
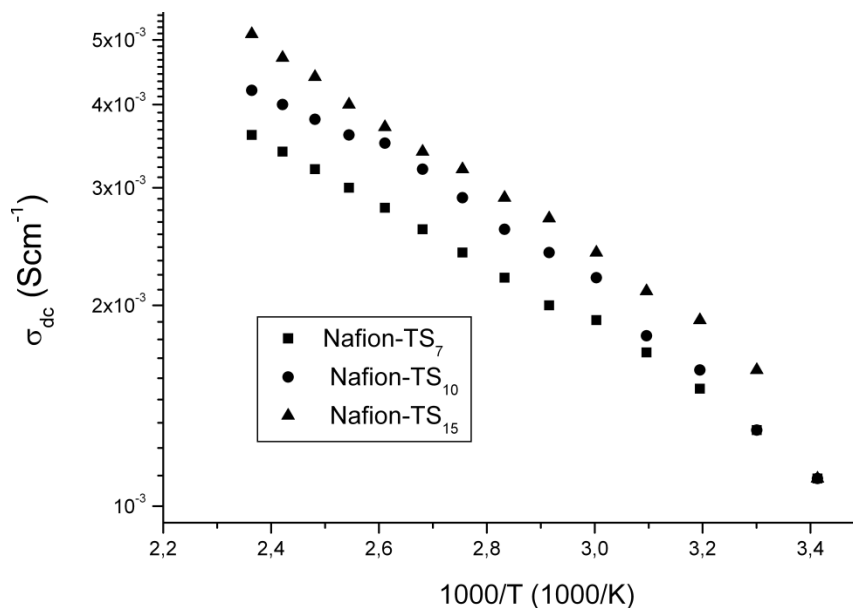
Figure 3.41 DC Conductivity Measurements of Nafion-TS composite membranes versus reciprocal temperature.

In the current system, proton transfer can be facilitated by the additional sulfated groups on titania fillers. From the FT-IR, composite membranes as well as conductivity data, it can be concluded that a Grotthuss mechanism (structural diffusion) is the possible pathway for the total proton diffusion. This continuous pathway may convey proton mobility over the –POH groups and sulfate groups may reduce the energy barrier for proton transport. The proton could travel along the ionic bonds from one functional group to another (Aslan and Bozkurt 2012)..

3.5 CHARACTERIZATION OF PVTRI-TIO$_2$SO$_3$H-PVPA NANOCOMPOSITE MEMBRANES

3.5.1 FTIR studies

Figure 3.42. shows the FT-IR spectra of P(VTri)-TS, P(VTri)-TS nanocomposite polymer electrolytes. In P(VTri)-TS, the triazole units show several medium or strong peaks in the 1430-1650 cm^{-1} range due to ring stretching (C-N, C=N) vibrations. The peak at 1270 cm^{-1} is due to the ring N-N stretching. The IR spectrum of P(VPA) shows strong bands at 1040-910 cm^{-1} that belong to asymmetric stretching vibrations of the P-OH group and at 1150 cm^{-1} that corresponds to P=O stretching (Nagarale, Shin et al. 2010). Additionally, phosphonic acid units give rise to broad bands with medium intensity at 1700-1590 cm^{-1} and 2850-2750 cm^{-1}. FT-IR spectra of sulfuric acid modified nano-titania shows characteristic peaks around 1650 cm^{-1} and at 980-1250 cm^{-1}. The peaks at 980 - 1250 cm^{-1} were attributed to bidentate sulfate coordination on the titania surface (980-990, 1040, 1130-1150 and 1210-1230 cm^{-1}) (Arata and Hino 1990, Jiang, Herricks et al. 2003, Wu, Hou et al. 2010). These peaks are overlapped with the corresponding peaks of phosphonic acid units of host matrix and became more intense. The S=O vibration at 1393 cm^{-1}, can be clearly observed from the sample sulfated nano-titania (Sakai, Kim et al. 2012). The new sharp bands at 1075 and 1140 cm^{-1} can be attributed to the P–O–Ti and P O stretching vibrations, respectively. The bands at 1330 and 1427 cm^{-1} can be attributed to the weak phosphoryl (P O) frequency and P–C stretching vibrations, respectively (Baglio, Arico et al. 2005). It could be deduced from these results that P(VPA) had replaced the original bidentate position of SO$_3$H and formed chemical bond interaction with the Ti atom at the titania surface via phosphonate groups (Aslan and Bozkurt 2012).
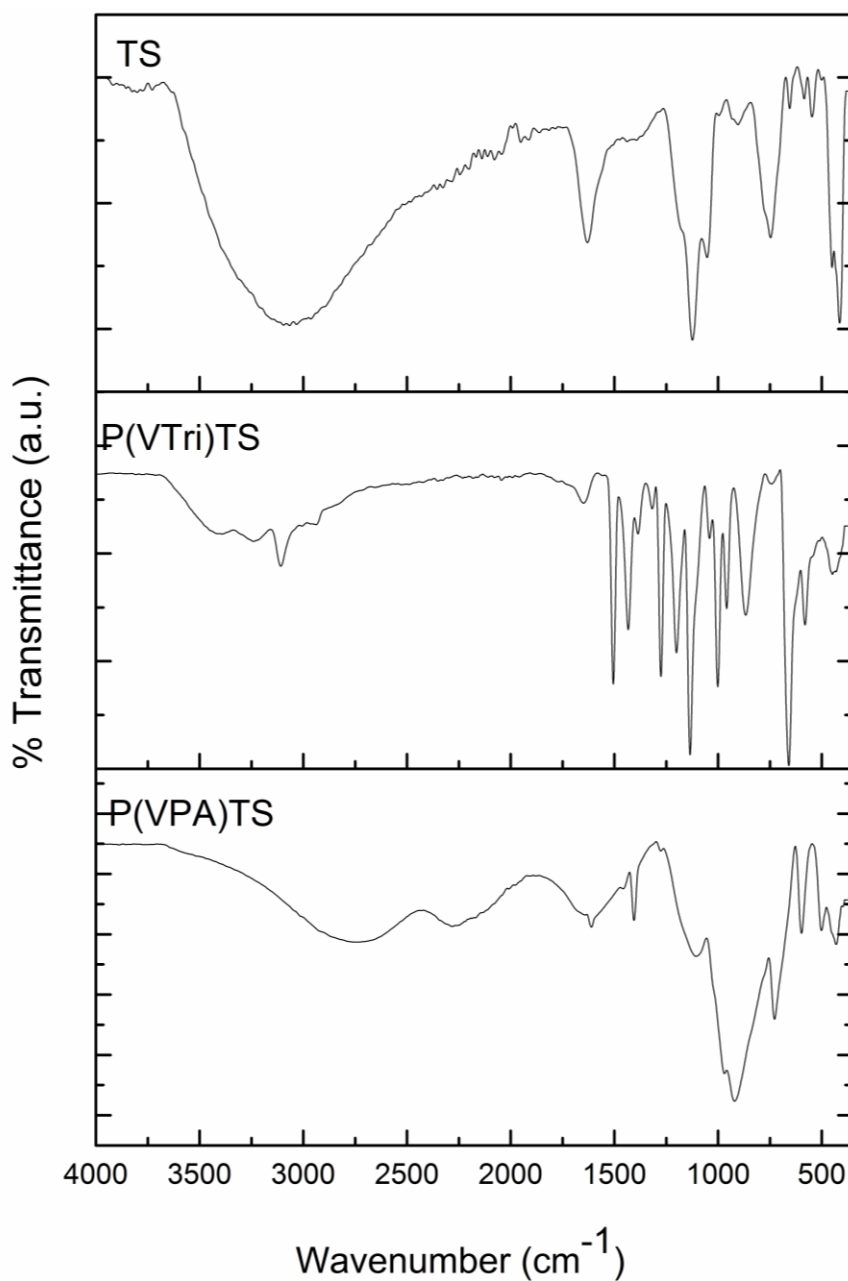
Figure 3.42 FT-IR spectra of the TS, PVTri-TS and PVPA-TS nanocomposite membranes.

Figure 3.43 is the FT-IR results of P(VTri)-TS-P(VPA)$_x$ nanocomposite electrolytes. At higher P(VPA) ratio the P–O–H vibration at 930 cm^{-1} becomes stronger, indicating the existence of excess acidic protons (Aslan and Bozkurt 2014). The broad bands are shown at between 800-1000 cm^{-1} this broading may also attributed to interaction of SO$_3$H groups and

phosphonic acid units of P(VPA) (Aslan and Bozkurt 2012). Additionally the broad bands with medium intensity at 1700-1500 cm^{-1} and 2850-2750 cm^{-1} increased in parallel with the concentration of P(VPA). The broad band between 3500 cm^{-1}-2500 cm^{-1} is the hydrogen bonding network which is necessary for proton conduction (Aslan and Bozkurt 2009).
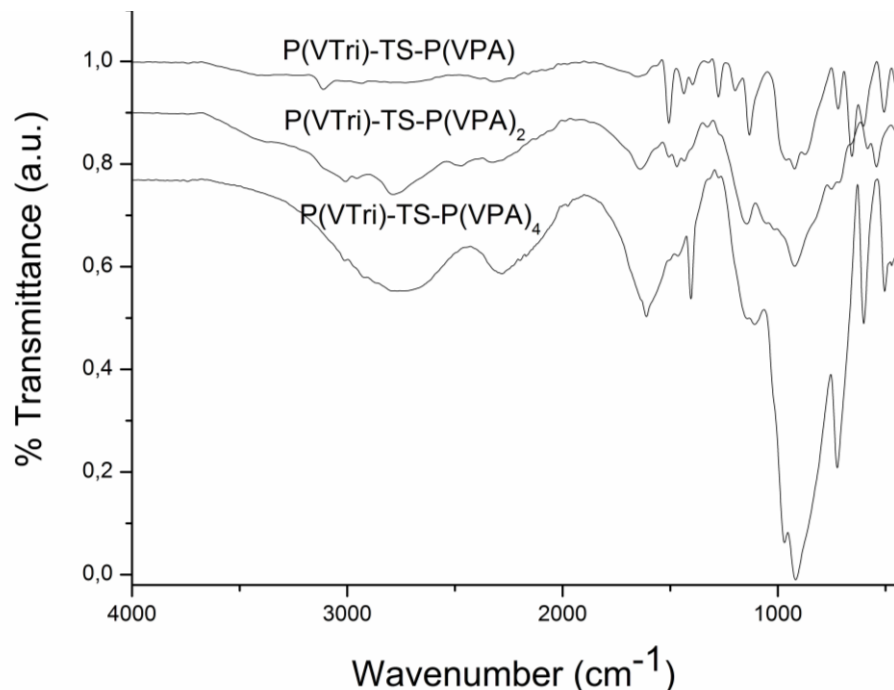

Figure 3.43 FT-IR spectra of the P(VTri)-TS-P(VPA) nanocomposite membranes.

3.5.2 XRD

The XRD patterns of hydrous sulfated nano-titania and b) P(VTri)/sulfated nanotitania composite are shown in Figure 3.44 and the diffraction peaks are broadened owing to small crystallite size. The mean size of the crystallites was estimated from the diffraction pattern by line profile fitting method using the equation given by Pielaszek et al. (Pielaszek 2004, Wejrzanowski, Pielaszek et al. 2006).

The line profile, shown in Figure 3.43a was fitted for observed 7 peaks with the following miller indices: (101), (004), (200), (211), (204), (116), (203) and (215) which are in accordance with the anatase structure of TiO_2 (Zhang, Li et al. 2008, Aslan and Bozkurt 2012). The average crystallite, size, D and σ, was obtained as 7 ±3 nm as a result of this line profile fitting. When P(VTri)-sulfated nano-titania prepared as mechanical mixing, the intense diffraction peak at $2\theta = 25^o$ was significantly weakened as seen at Figure 3.44b. When 5% nanoparticles were incorporated into P(VTri), the peak at 25° becomes more shaper because of the superimposition of peaks of P(VTri) and nanoparticles(Deng, Ding et al. 2002). The XRD data of the composite indicate that the sulfated TiO_2 nanoparticles embedded in P(VTri) are in the anatase structure. Because the diffraction peak at around 25° for anatase is overlapped with that for the sulfated TiO_2 doped P(VTri) (Aslan and Bozkurt 2012)..
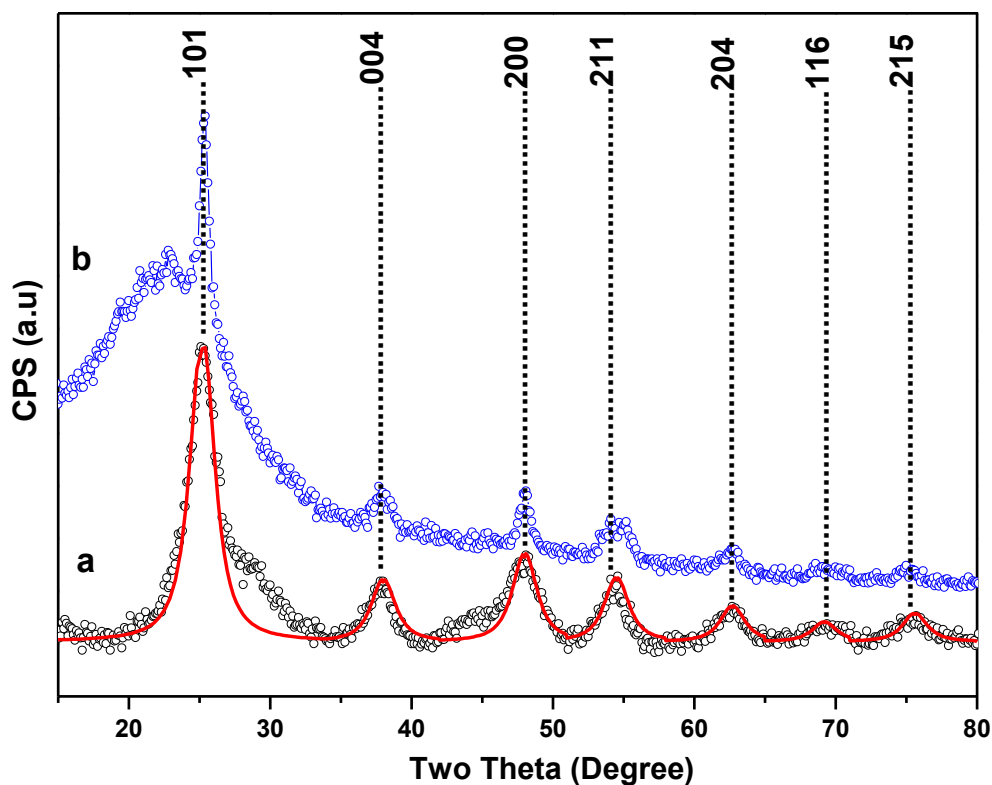
Figure 3.44 XRD pattern of hydrous a) sulfated nano-titania (TS) b) PVTri-sulfated nano-titania composite (PVTri-TS)

3.5.3 SEM

Surface morphology of P(VTri)-TS-P(VPA) nanocomposite polymer membrane was investigated by scanning electron microscopy (see Figure 3.45a and Figure 3.45b). Due to strong interaction between of phosphonic acid groups of P(VPA) and the triazole units of P(VTri), no phase separation occurred during solvent evaporation, hence homogeneous and transparent films formed. It was observed that sulfated nano-titania were quite well dispersed and embedded in the polymer matrix. This result is also consistent with the DSC results of blend membranes that no separate T_g transition of impregnated polymer was observed (Kickelbick 2003).

a)   b)
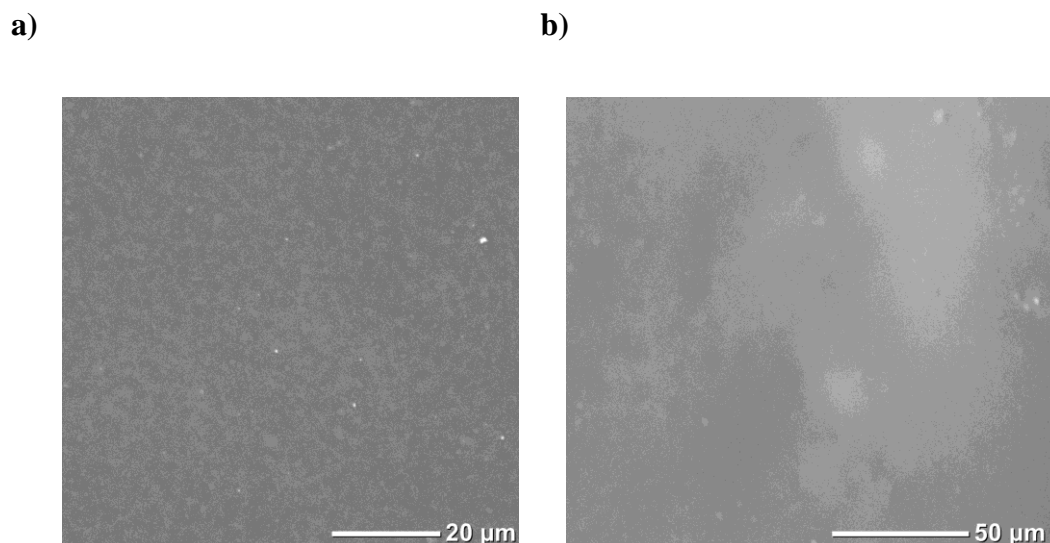
Figure 3.45 SEM pictures of P(VTri)-TS-P(VPA) nanocomposite membranes.
 a) 20μm b) 50μm

3.5.4   Thermal analysis

The glass transition temperature of the P(VTri) was reported at around 160 ^{o}C. P(VPA) exhibits a glass transition at around -23^{0}C(Sevil and Bozkurt 2004). In the P(VPA) and P(VTri) homopolymers, no melting transition can be detected, probably because the investigated samples are rather amorphous. T_g of P(VTri)-TS and P(VPA)-TS membranes were measured at 130 ^{o}C and 67 ^{o}C, respectively. The T_g values of the nano composite membranes are shown in Table 3.6.

Table 3.6 Maximum proton conductivity and T_g values of the nanocomposite membranes.

Sample Name	P(VTri)-TS-P(VPA) ratio	Tg (^{o}C)	Max. Proton Conductivity (Scm^{-1})
P(VTri)-TS	1-%5	130 ^{O}C	8,5x10^{-8} Scm^{-1} at 150°C
P(VPA)-TS	1-%5	67 ^{O}C	3,1x 10^{-3}Scm^{-1} at 150°C
P(VTri)-TS-P(VPA)	1-%5-1	121 ^{O}C	2,5x10^{-5} Scm^{-1} at 150°C
P(VTri)-TS-P(VPA)$_2$	1-%5-2	106 ^{O}C	2,6x10^{-4} Scm^{-1} at 150°C
P(VTri)-TS-P(VPA)$_4$	1-%5-4	86°C	0,003 Scm^{-1} at 150°C

The complex polymer electrolytes have definite glass transition temperatures at 121°C for x=1, 106 ^{o}C for x=2 and 86°C for x=4. PVPA has lower Tg and may have showed softening effect in the matrix. The results demonstrated that as the quantity of P(VPA) increased, the glass transition temperature of the samples shifted to lower temperatures.

Thermal stability of the nanocomposite membrane samples could be inferred from their TGA thermograms in Figure 3.46. P(VTri)-TS has a considerable thermal stability under inert conditions. Above 250 $^{\circ}$C, a remarkable weight loss derives from the thermal decomposition of triazole groups and the polymer main chain. The P(VPA)-TS curves illustrated that the composite membrane is thermally stable up to approximately 180 $^{\circ}$C, then the composite decomposes. The dried nanocomposite P(VTri)-TS-P(VPA)$_x$ materials are thermally stable up to approximately 300 $^{\circ}$C. In addition, P(VTri)-TS-P(VPA)$_x$ nanocomposite membranes possess better thermal stability than P(VTri)-P(VPA) polymer electrolyte membranes(Baglio, Arico et al. 2005), this may also be attributed to the presence of sulfated titania in the membrane matrices inhibited the condensation of phosphonic acid units up to 300 $^{\circ}$C(Wagner, Manhart et al. 2009).
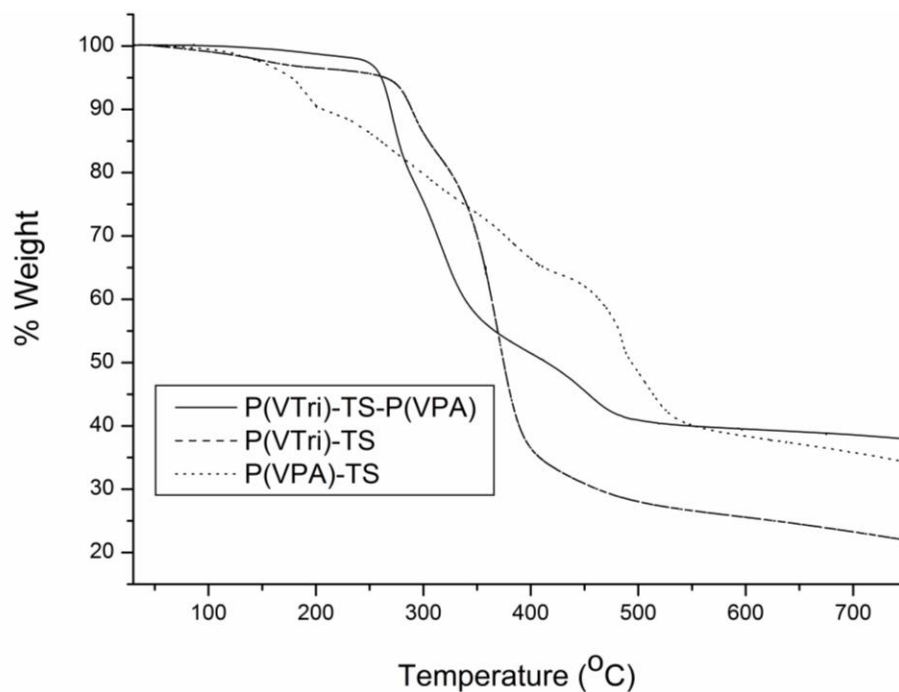
Figure 3.46 TG thermograms of P(VTri)-TS-P(VPA), P(VTri)-TS and P(VPA)-TS composite membranes recorded at a heating rate of 10 $^{\circ}$C/min under a nitrogen atmosphere.

3.5.6 Proton conductivity

The AC conductivities, σ_{ac} (ω) of the polymers were measured at several temperatures using impedance spectroscopy. The AC conductivity of P(VTri)-TS-P(VPA) and P(VTri)-TS-P(VPA)$_2$ is shown in Figure 3.47. and 3.48. Frequency dependent AC conductivities (σ_{ac} (ω)) were measured using Eq. (3.5);

$$\sigma^{'}(\omega) = \sigma_{ac}(\omega) = \varepsilon^{''}(\omega)\, \omega\, \varepsilon_o \qquad (3.5)$$

where $\sigma^{'}$ (ω) is the real part of conductivity, $\omega = 2\pi f$ is the angular frequency, ε_o is the vacuum permittivity ($\varepsilon_o = 8.852 \times 10^{-14}$ F/cm), and $\varepsilon^{''}$ is the imaginary part of complex dielectric permittivity (ε^{*}). The proton conductivities of anhydrous nanocomposite polymer electrolytes were measured from 20 ^oC to 150 ^oC.
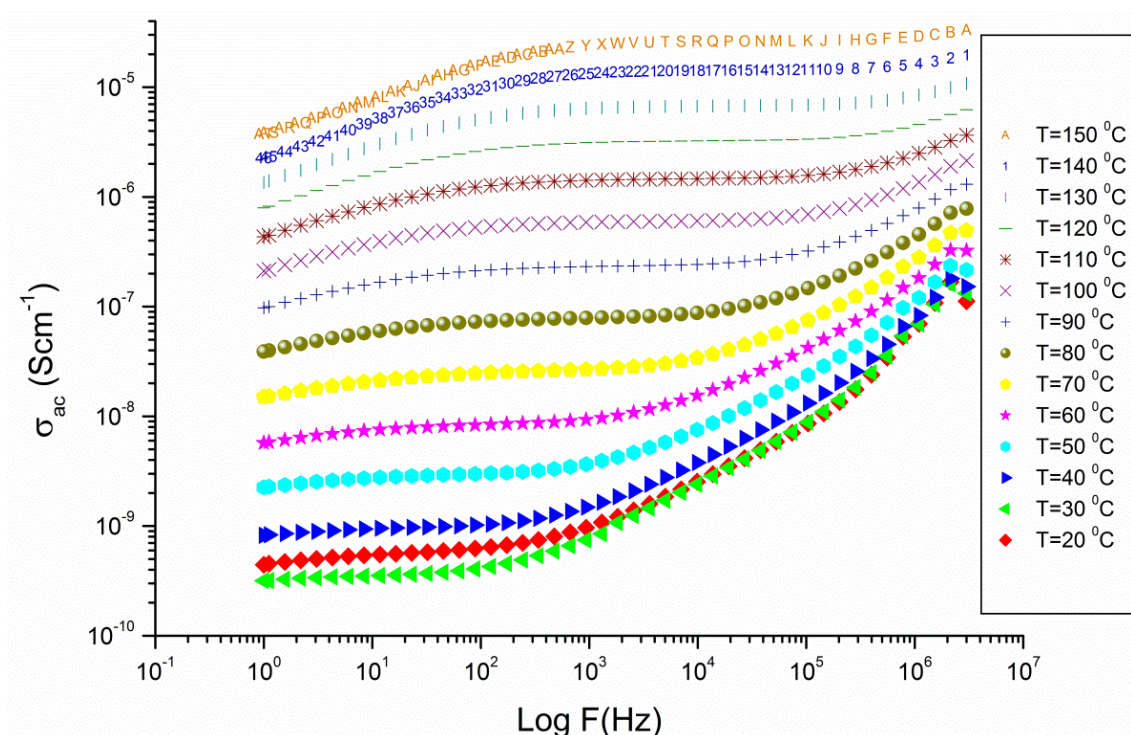
Figure 3.47 AC Conductivity of P(VTri)-TS-P(VPA) composite membranes.
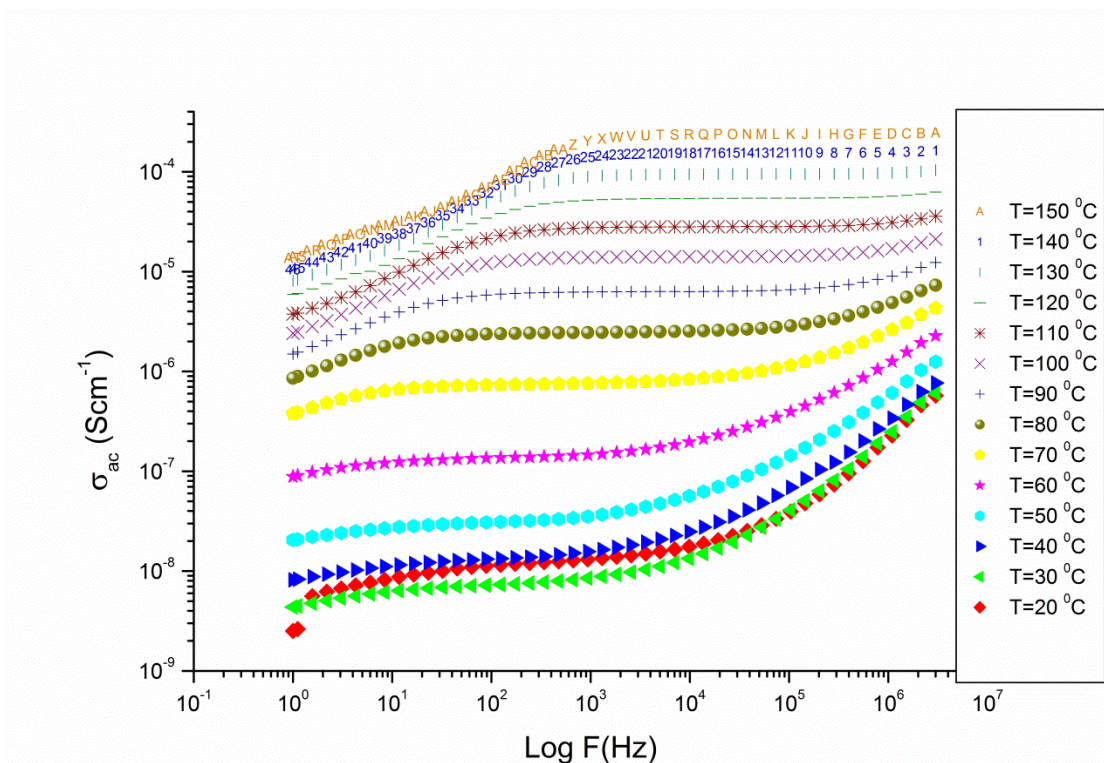
Figure 3.48 AC Conductivity of P(VTri)-TS-P(VPA)$_2$ composite membranes.

The proton conductivity of the P(VTri)-TS depends on the increasing temperature. In the anhydrous conditions, the proton conductivity of P(VTri)-TS was measured as 5,9 x10^{-14} S cm^{-1} at 20 ^{o}C and 8,5x10^{-8} Scm^{-1} at 150 ^{o}C. Low conductivity can be attributed to low concentration of functional nanoparticles which was 5% (w/w).

The proton conductivity of all anhydrous P(VTri)-TS-P(VPA)$_x$ samples were compared in Figure 3.49. The conductivity results illustrate that the DC conductivity strongly depends on temperature as well as the ratio of P(VPA). As seen, the proton conductivity of these samples is improved with P(VPA) content and maximum proton conductivity was measured for P(VTri)-TS-P(VPA)$_4$ and found to 0.003 at 150 ^{o}C. The material with x=4 is the optimized composition in terms of conductivity as well as thin film formation. Conductivity results showed that in the P(VTri)-TS-P(VPA) systems, the P(VPA) composition and sulfated nano titania are highly effective on the proton conductivity of the samples. The previously work, it was reported that for P(VPA)/P(VTri)

blends, P(VTri)P(VPA)$_2$ was the optimum composition and showed a proton conductivity of 2.5x 10^{-5} S/cm at 180 ^{o}C in the anhydrous state (Aslan and Bozkurt 2009). This results verified the sulfated nano titania increased P(VPA) content as well as enhanced the proton conductivity and thermal stability of the nanocomposite membrane. Moreover, Wang et al. (Wang, McDermid et al. 2008) and Li et al.(Li, Sun et al. 2006) confirmed that the modified nanoparticles more increased the proton conductivity than unmodified nanoparticles via their functional groups (Aslan and Bozkurt 2012).
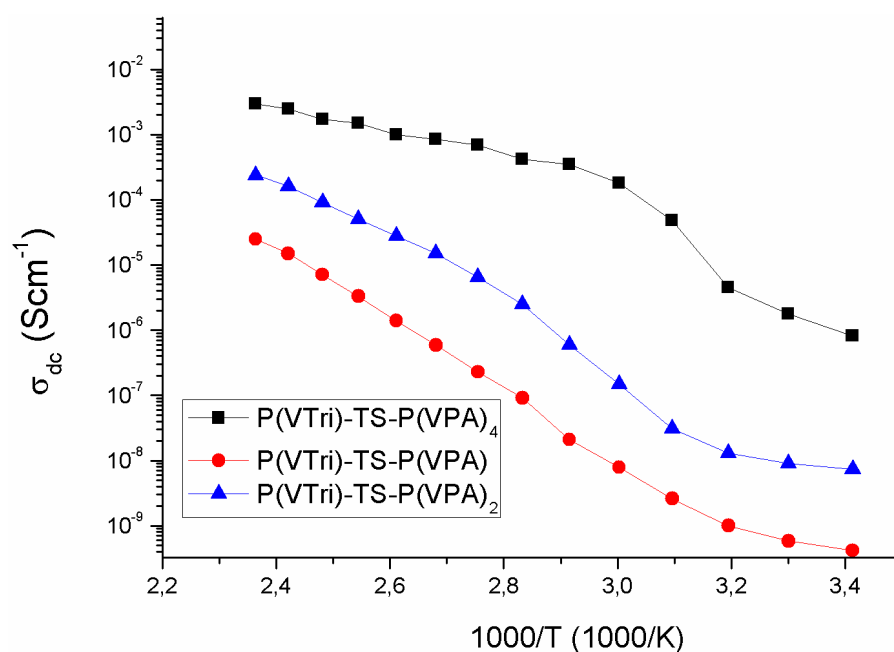
Figure 3.49 DC Conductivity Measurements of P(VTri)-TS-P(VPA) composite membranes versus reciprocal temperature .

From the FT-IR as well as conductivity data, it can be concluded that a major part of proton transport can be provided over both phosphonic acid and sulphonic acid units that are coordinated with azoles. Grotthuss mechanism (structural diffusion) can be the possible pathway for the total proton diffusion. This continuous pathway may convey proton mobility over the –POH groups and sulfate groups that may reduce the energy barrier for

proton transport (see Figure 3.50.). The proton could travel between the phosphonic acid units of P(VPA) and SO$_3$H groups of sulfated titania ionic bonds from one functional group to another (Smitha, Sridhar et al. 2004, Ramirez-Salgado 2007, Macarie and Ilia 2010).
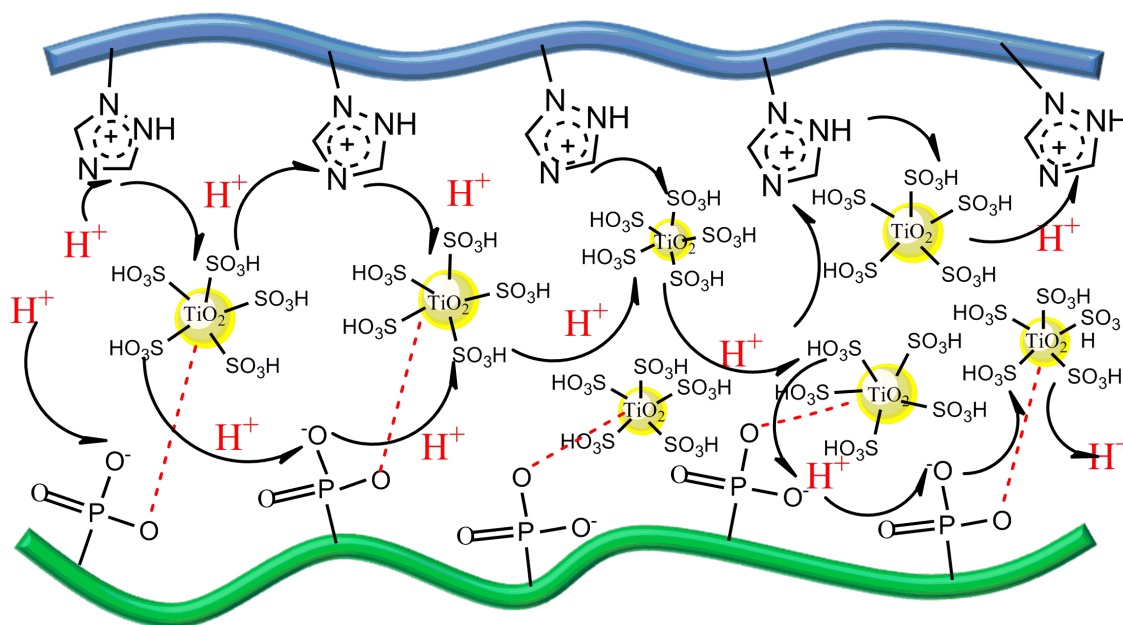
Figure 3.50 DC Conductivity Measurements of P(VTri)-TS-P(VPA) composite membranes versus reciprocal temperature .

3.6 CHARACTERIZATION OF PVA-TS-NMPA NANOCOMPOSITE MEMBRANES

3.6.1 FTIR studies

Figure 3.51 shows the FT-IR spectra of PVA-TS and sulfated nano-titania (TS). FT-IR spectrum of sulfated titanina poly(vinylalcohol) showed a very strong and broad peak centered at 3300 cm^{-1} attributed to the hydroxyl (–OH) group and a peak at 2900 cm^{-1} that correspond to the CH$_2$ asymmetric stretching (Daniliuc, Dekesel et al. 1992) . FT-IR spectra of sulfated nano-titania showed characteristic peaks around 1650 cm^{-1} and at 980-

1250 cm^{-1}. The peaks at 980 - 1250 cm^{-1} were attributed to bidentate sulfate coordination on the titania surface (980-990, 1040, 1130-1150 and 1210-1230 cm^{-1}) (Aslan and Bozkurt 2013). The S=O vibration at 1393 cm^{-1}, can be clearly observed from the sample sulfated nano-titania (Arata and Hino 1990, Navarrete, Lopez et al. 1996, Jiang, Herricks et al. 2003, Celik, Akbey et al. 2008, Sakai, Kajitani et al. 2010).
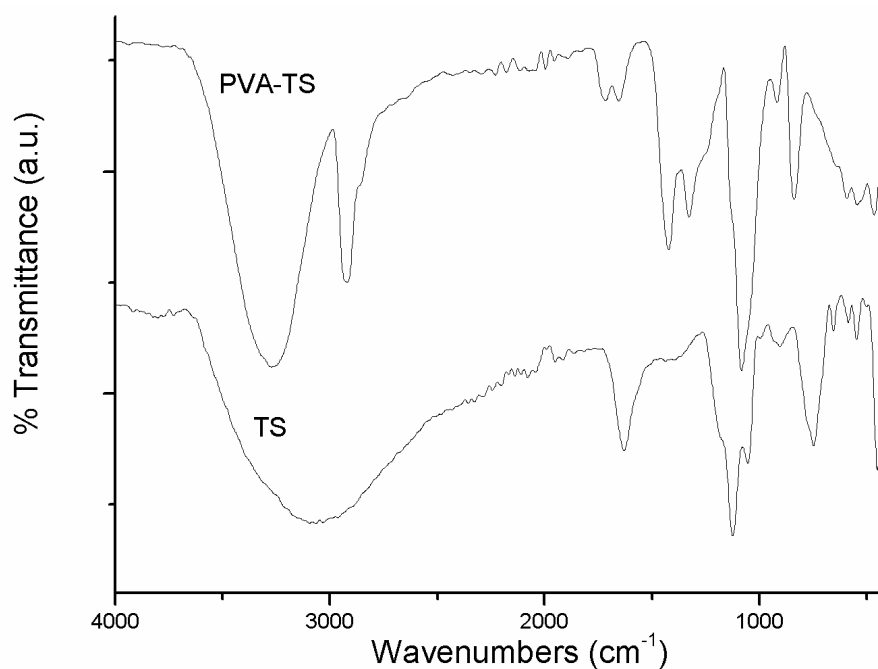
Figure 3.51 FT-IR spectra of the TS and PVA-TS composite membranes.

Figure 3.52 is the FT-IR of the ternary system where the peak at 1150 cm^{-1} corresponds to P=O stretching of NMPA. As can be seen in the PVA-TS-NMPA spectrum the weak peak between 910- 1100 can be attributed to the P–O–Ti and P-O stretching vibrations. The bands at 1330 and 1427 cm^{-1} can be attributed to the weak phosphoryl (PO) frequency and P–C stretching vibrations, respectively (Wu, Hou et al. 2010). It could be deduced from these results that NMPA had replaced the original bidentate position of SO$_3$H and formed chemical bonds with the Ti atom at the titania surface via phosphonate groups. NMPA shows strong bands at 950 cm^{-1} that belong to asymmetric stretching

vibrations of the P-OH group, at 1150 cm^{-1} that corresponds to P=O stretching, and a weak peak around 3500 cm^{-1} was attributed to O-H stretching(Chen, Han et al. 2007). The characteristic peaks of sulfated nano-titania at 980-990, 1040, 1130-1150 and 1210-1230 cm^{-1} are overlapped with the corresponding peaks of phosphonic acid units of host matrix and became more intense. Between 3500 and 2000 cm^{-1} a broadening of the band can be related to hydrogen bonding network formation. Within 1500 - 800 cm^{-1} region, the peaks near 1150 cm^{-1} and 960 cm^{-1} are attributed to characteristic absorptions in the formation of anion NMPA as a consequence of interaction of SO$_3$H interaction(Ma, Zhang et al. 2008). These results confirm successful embedding of bifunctional nano-titania in PVA host matrix (Aslan and Bozkurt 2013)..
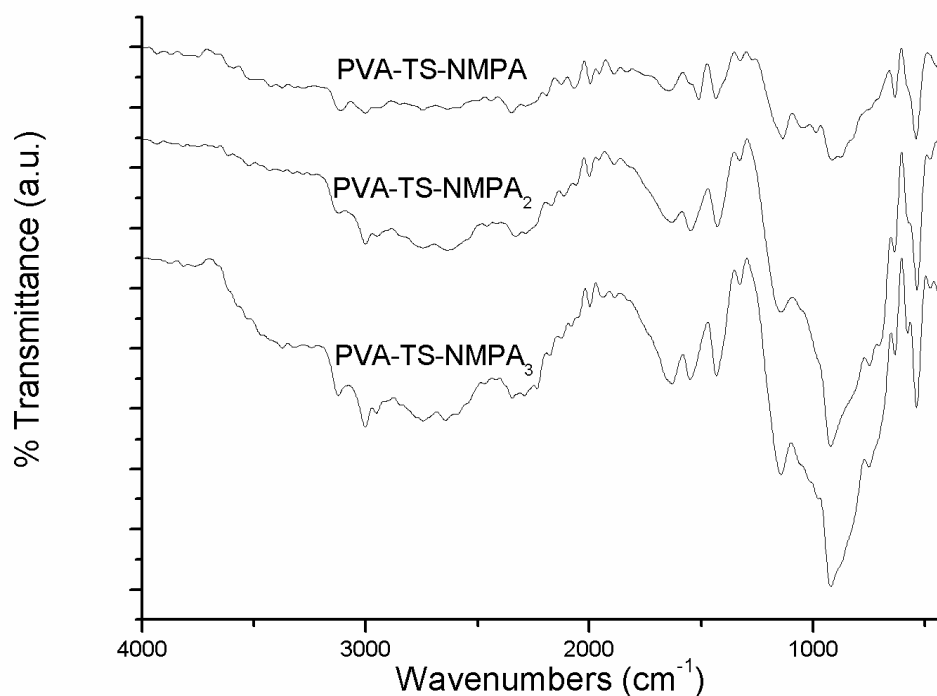
Figure 3.52 FT-IR spectra of the PVA-TS-NMPA composite membranes.

3.6.2   SEM

The micro topography of PVA-TS and PVA-TS-NMPA composite membranes was studied by scanning electron microscopy (SEM) as shown in Figure 3.53 and 3.54. In Figure 3.53, it was observed that sulfated nano-titania were homogenously dispersed and embedded in the PVA matrix.

The SEM micrograph indicates that there was no obvious agglomeration of TS nanoparticles. In comparison with the pure PVA (Peng, Kong et al. 2005) the surface of the PVA-TS-NMPA nanocomposite was smoother (see Figure 3.54). Additionally, due to strong interactions between sulfonic acid groups of sulfated titania and phosponic acid units of NMPA, whereas no phase separation was observed during solvent evaporation. Although micro-domain formation regarding PVA-TS-NMPA complex might have been expected in the final dry membrane such domains did not appear in the SEM micrographs. Figure 3.55. indicates a very good compatibility between PVA and NMPA.Consequently, the micrographs showed that homogeneous films were successfully produced.
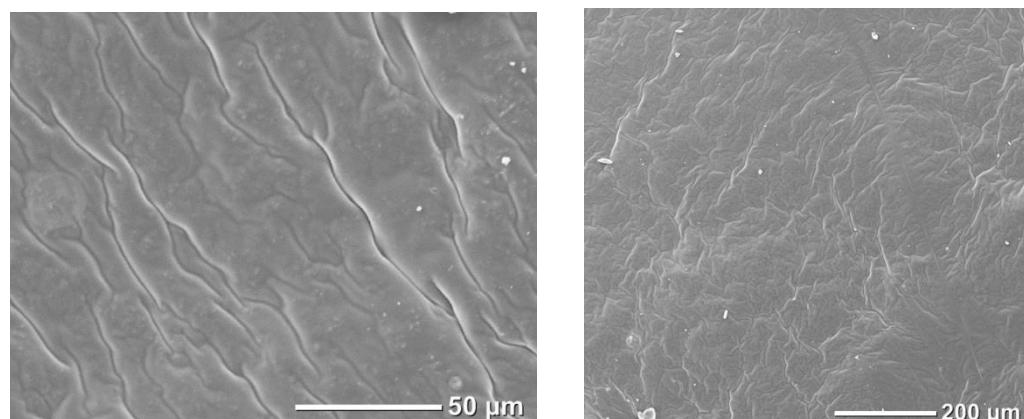
Figure 3.53 SEM micrographs of the PVA-TS surface of composite membranes.
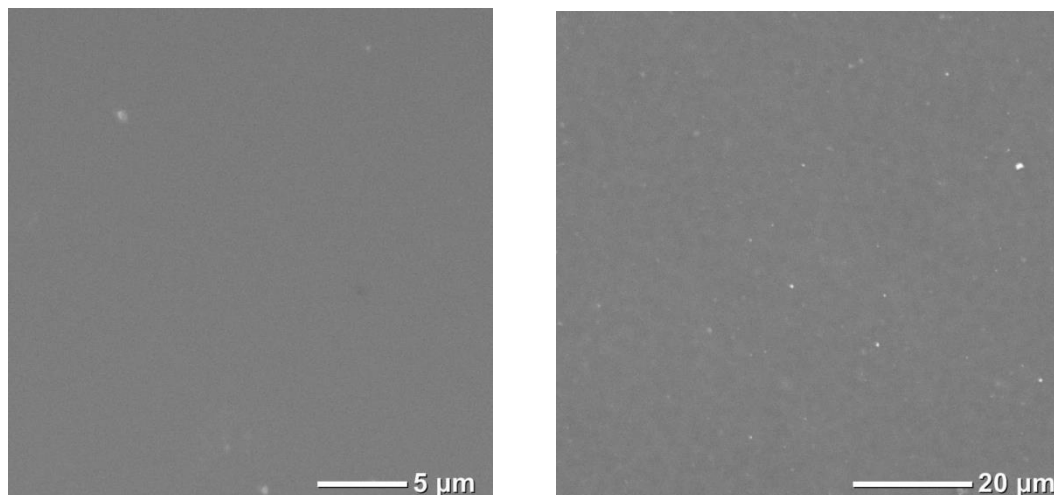
Figure 3.54 SEM micrographs of the PVA-TS-NMPA surface of composite membranes.

3.6.3 Thermal analysis

Table 3.7 lists the glass transition temperatures of the PVA-TS-NMPA$_x$ composite membranes. PVA exhibits a glass transition located at around 72 ^{o}C(Peng, Kong et al. 2005). In the presence of sulfated nano-titania the Tg of PVA shifts to 150 ^{o}C which indicated that sulfated nano-titania prevented segmental motion of the PVA (Aslan and Bozkurt 2013).. The membrane materials PVA-TS-NMPA, PVA-TS-NMPA$_2$ and PVA-TS-NMPA$_3$ have definite obvious glass transition temperatures of 118°C, 100 ^{o}C and 92 ^{o}C, respectively (see Figure 3.55.). Clearly, the results indicated that the glass transition temperatures of the samples shift to lower temperatures as the quantity of NMPA increases. This behavior can be described by the softening effect of NMPA.
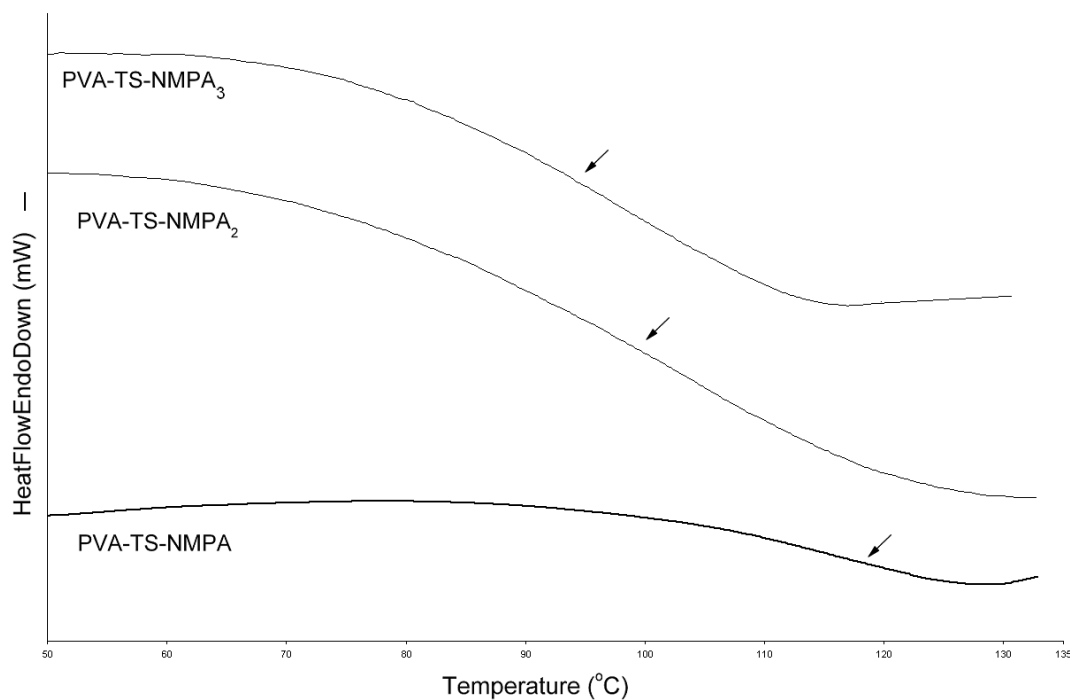
Figure 3.55 DSC curves of PVA-TS-NMPA composite membranes under nitrogen atmosphere at a heating rate of 10 ^{o}C min^{-1}.

Table 3.7 Max. Proton conductivity and Tg (^{o}C) values for the composite membranes.

Sample name	Molar Ratio (PVA/NMPA)	Tg ^{o}C	Max. proton cond. (Scm^{-1})
PVA-TS	-	151 ^{o}C	2 x10^{-6} at 150 ^{o}C
PVA-TS-NMPA	1:1	118 ^{o}C	8.5x10^{-6}at 150 ^{o}C
PVA-TS-NMPA$_2$	1:2	100 ^{o}C	3.1x10^{-4} at 150 ^{o}C
PVA-TS-NMPA$_3$	1:3	92 ^{o}C	**0.003** at 150 ^{o}C

Figure 3.56. shows the thermogravimetry (TG) results of the composite membranes recorded under N_2 atmosphere. The TG graphs show an elusive weight loss up to 150 ^{o}C, which can be attributed to anhydride formation (Park, Shin et al. 2005). It is clear that the dried polymers are thermally stable up to approximately 250 ^{o}C, after which, they decompose. The PVA-TS thermograms indicated that the sulfated titania nanoparticles enhanced the thermal stability of the composite membranes. The degradation temperature of PVA-TS-NMPA nanocomposite polymer membranes is approximately 200 ^{o}C, i.e., slightly lower than that of PVA-TS.
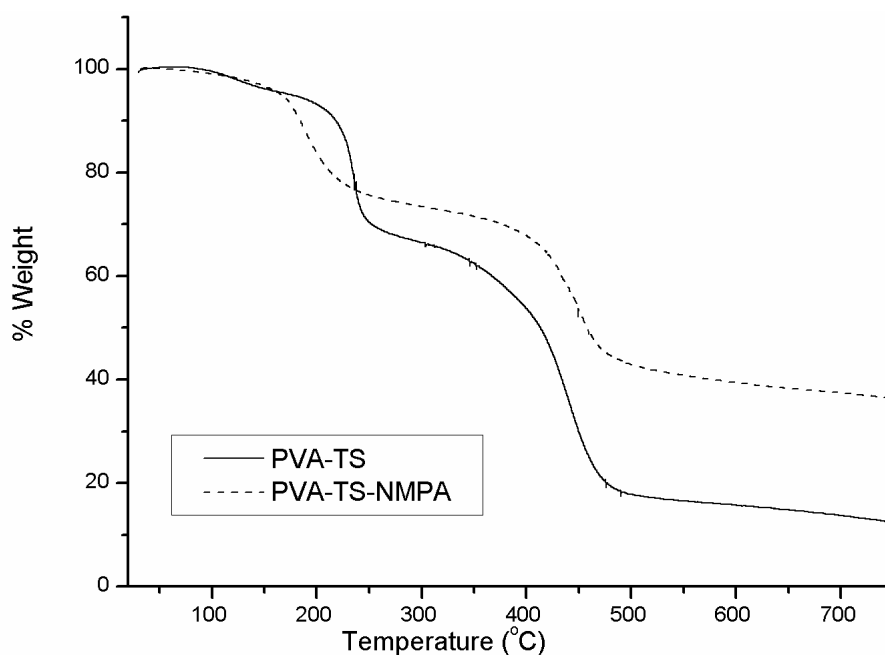
Figure 3.56 TG thermograms of PVPATiO$_2$ (*in situ*) composite membranes recorded at a heating rate of 10 ^{o}C/min under a nitrogen atmosphere.

3.6.4   Water/Methanol Uptake

The water/methanol uptake of the membranes is a major parameter influencing proton conductivity, mechanical property and stability. Solution uptakes of the PVA-TS-NMPA samples are shown in Figure 3.57. As can be seen, water uptake decrease with

increasing NMPA content. The sample PVA-TS has the highest water uptake value (70 %). This result showed that the decreasing swelling character with NMPA content enhanced the mechanical strength, and almost no NMPA dissolved in the solution. The result indicated that the complexation of PVA-TS with NMPA prevented the loss of guest polymer (PVA) to the solution.
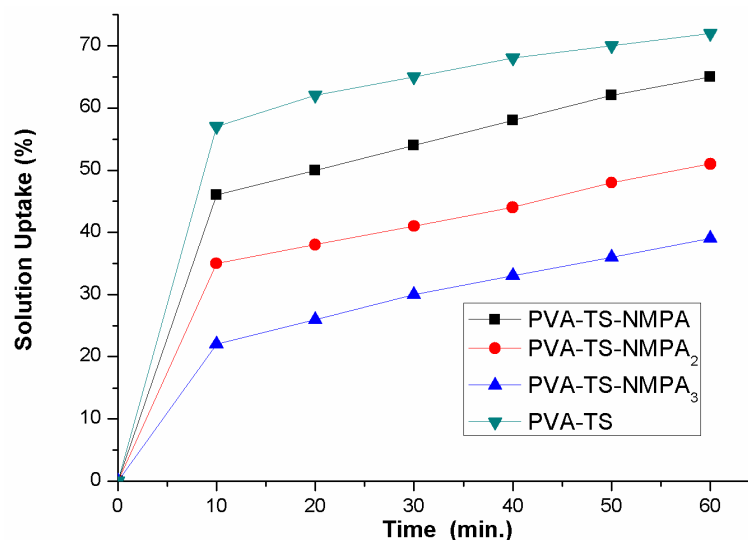
Figure 3.57 Water / Methanole uptake of PVA-TS-NMPA composite membranes.

3.6.5 Proton conductivity

The proton conductivities of PVA-TS and PVA-TS-NMPA anhydrous nanocomposite polymer electrolytes were measured between 20-150 oC. The AC conductivity of PVA-TS-NMPA2 composite membrane is shown in Figure 3.58. The graph includes several regions which are typical for ion conducting polymers. The irregularities between 80-150 oC at the low frequency side correspond to polarization blocking the electrode-electrolyte interface and the conductivity increase at high temperature and high frequencies results from the regular dispersion in polymer electrolytes(Acar, Sen et al. 2009).
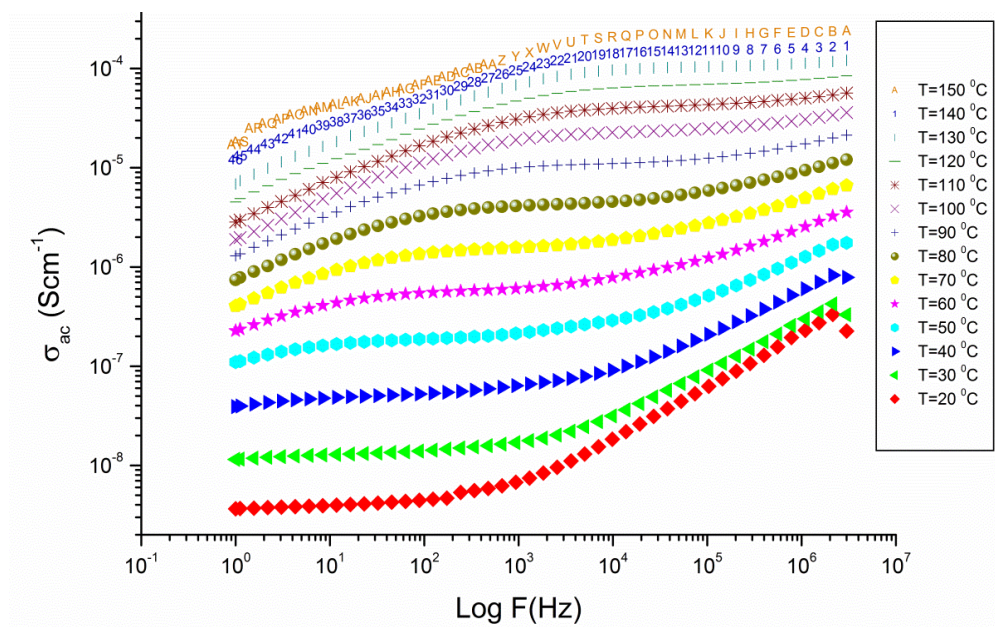
Figure 3.58 AC Conductivity of PVA-TS-NMPA$_2$ composite membranes.

The DC conductivities of anhydrous samples were derived from the plateau regions which are compared in Figure 3.59. Clearly, the proton conductivity of PVA-TS system increases linearly (Arrhenius behavior) with increasing temperature. Max conductivity of PVA with 5% TS is 2 x10^{-6} at 150 ^{o}C
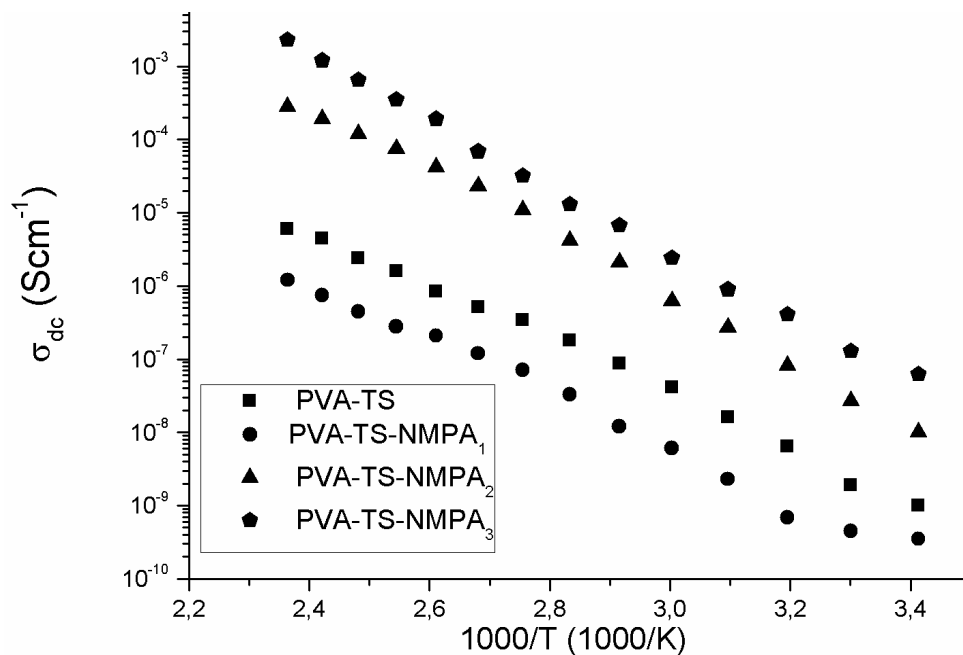
Figure 3.59 DC Conductivity of PVA-TS-NMPA composite membranes.

Previously, it was reported that organophosphorylated titania and chitosan composite membranes exhibit an increased proton conductivity to an acceptable level of 0.01 S cm−1 (RH= 80 %) for DMFC (Wu, Hou et al. 2010). These organophosphorylated titania nanoparticles enhanced the proton conductivity when they were dispersed in the membranes at low temperatures in humidified conditions. In this study, we combined the advantages of phosphonic acid units and sulfonic acid units on the titania surface, which enhanced the proton diffusion under anhydrous conditions.

The conductivity isotherm of PVA-TS-NMPA composite membranes strongly depends on temperature as well as the ratio of NMPA. The proton conductivity of PVA-TS nanocomposite membrane is lower than that of composite membranes with NMPA. The DC conductivity illustrated that the NMPA content increases the conductivity for PVA-TS-NMPA composite membranes. The maximum proton conductivity was measured for PVA-TS-NMPA$_3$ and found to be 0.003 (Scm^{-1}) at 150 ^{o}C, in the dry state. The material with x=3 was considered to be the optimum composition for these series of composite membranes.

Conductivity results showed that the NMPA composition is highly effective on the proton conductivity of the samples in the PVA-TS-NMPA systems.
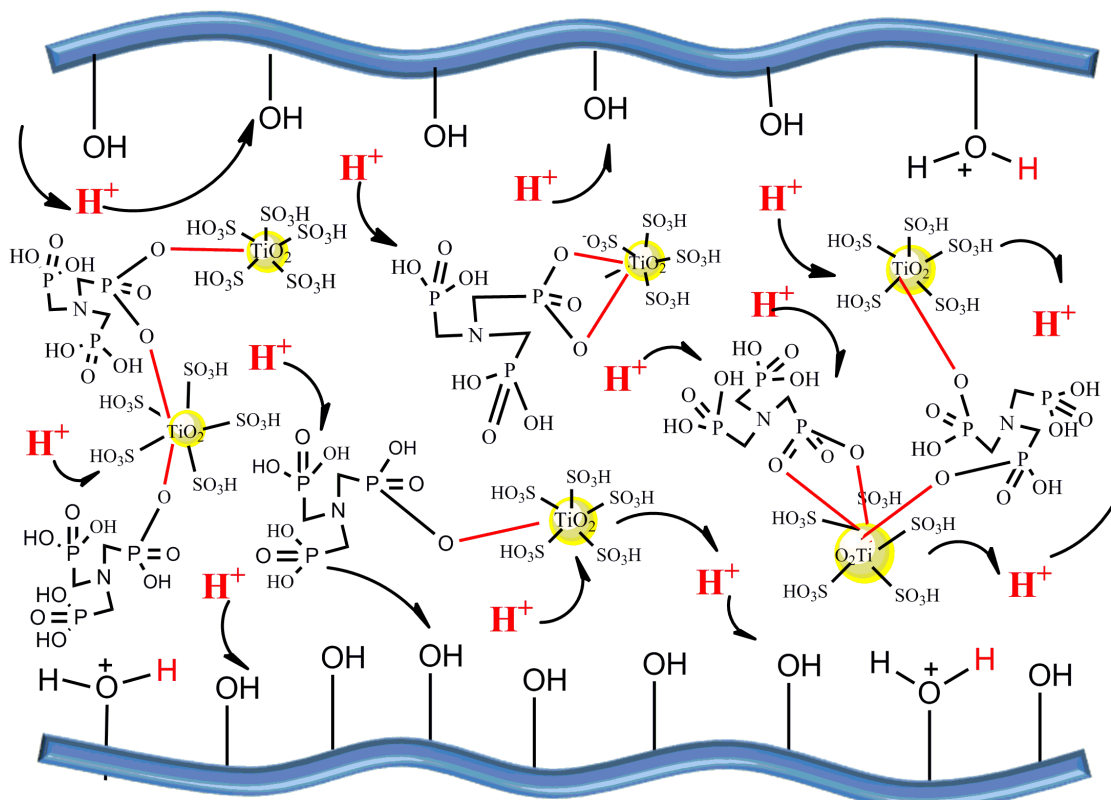
Figure 3.60 Proton transport mechanism of the PVA-TS-NMPA composite membranes.

In the current system, proton transfer can be facilitated by the additional phosphonic acid groups on NMPA. From the FT-IR of composite membranes as well as the conductivity data, it can be concluded that a Grotthuss mechanism (structural diffusion) is the possible pathway for the total proton diffusion (Aslan and Bozkurt 2013). This continuous pathway may convey proton mobility over the –P-OH and sulfonic acid groups may reduce the energy barrier for proton transport (see Figure 3.60). The protons could travel through the ionic functional groups(Smitha, Sridhar et al. 2004, Ramirez-Salgado 2007).

3.7 CHARACTERIZATION OF SPSU-TS-NMPA NANOCOMPOSITE MEMBRANES

3.7.1 FTIR studies

Figure 3.61 and Figure 3.62 are the FTIR spectra of nanocomposite membranes. Fig.ure 3.60 shows the FT-IR spectra of sulfated nanotitania (TS), sulfonated polysulfone (SPSU) and SPSU-TS composite membranes. The signals belonging to SPSU are seen at 690 cm^{-1}, 1041 cm^{-1}, 1103 cm^{-1}, 1149 cm^{-1}, 1238 cm^{-1}, 1485 cm^{-1}, 2950 cm^{-1}, 3110 cm^{-1}, 3500 cm^{-1}(Alberti, Casciola et al. 2005, Chuang, Hsu et al. 2007). In FTIR of SPSU, the presence of -OH peaks at 3500 cm^{-1} and O=S=O stretching vibration of -SO$_3$ groups near 1041 cm^{-1} confirm the sulphonation of PSU. The FT-IR spectrum of sulfated nano-titania shows characteristic peaks around 1650cm^{-1} and at 980-1250 cm^{-1}. The peaks at 980 - 1250 cm^{-1} were attributed to bidentate sulfate coordination on the titania surface (980-990, 1040, 1130-1150 and 1210-1230 cm^{-1}) (Aslan and Bozkurt 2014). These peaks The S=O vibration at 1393 cm^{-1}, can be clearly observed from the sample sulfated nanotitania (Arata and Hino 1990, Navarrete, Lopez et al. 1996, Jiang, Herricks et al. 2003, Celik, Akbey et al. 2008, Sakai, Kajitani et al. 2010).
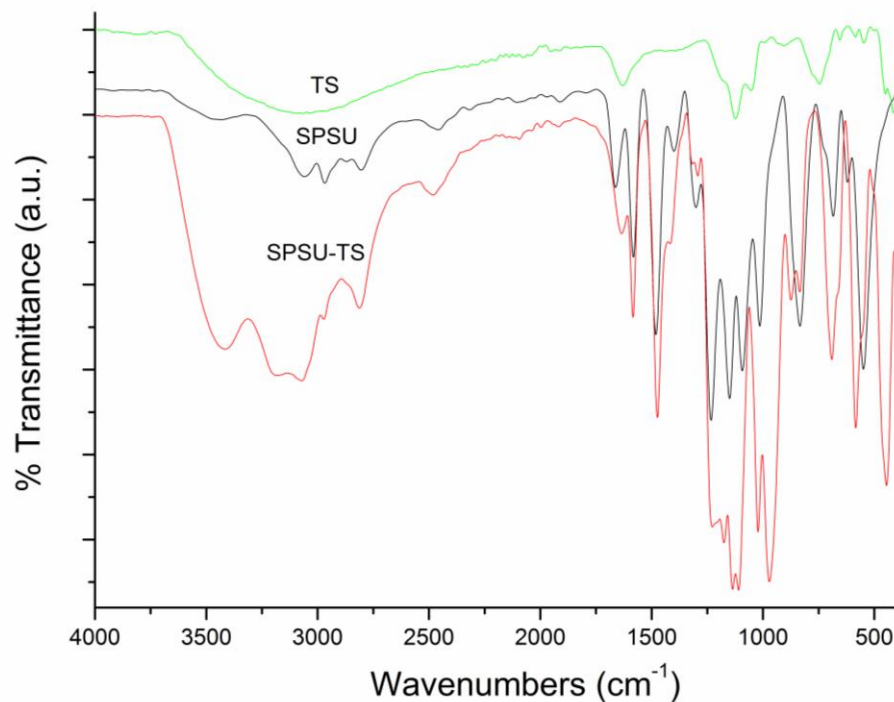
Figure 3.61 FT-IR spectra of the SPSU, TS and SPSU-TS composite membranes.

In Figure 3.61 P=O stretching band is observed at 1150 cm⁻¹. P–O–Ti and P O stretching vibrations are seen at 1075 and 1140 cm⁻¹, respectively (Aslan and Bozkurt 2012). NMPA has strong bands at 1020 - 890 cm⁻¹ it can be attributed to asymmetric stretching vibrations of the P-OH group (Aslan and Bozkurt 2014).. These results prove that the existing of original bidentate position of SO_3H and formed chemical bonds with titania surface via phosphonate groups of NMPA. The weak peak around 3500 cm⁻¹ was attributed to O-H stretching(Chen, Han et al. 2007).

The characteristic peaks of sulfated nanotitania at 980-990, 1040, 1130-1150 and 1210-1230 cm⁻¹ are overlapped with the corresponding peaks of phosphonic acid units of host matrix and became more intense (Aslan and Bozkurt 2014). The peaks at 1150 cm⁻¹, 960 cm⁻¹ and between 1500 - 800 cm⁻¹ demonstrated the formation anion NMPA as a consequence of interaction of SO_3H (Ma, Zhang et al. 2008).
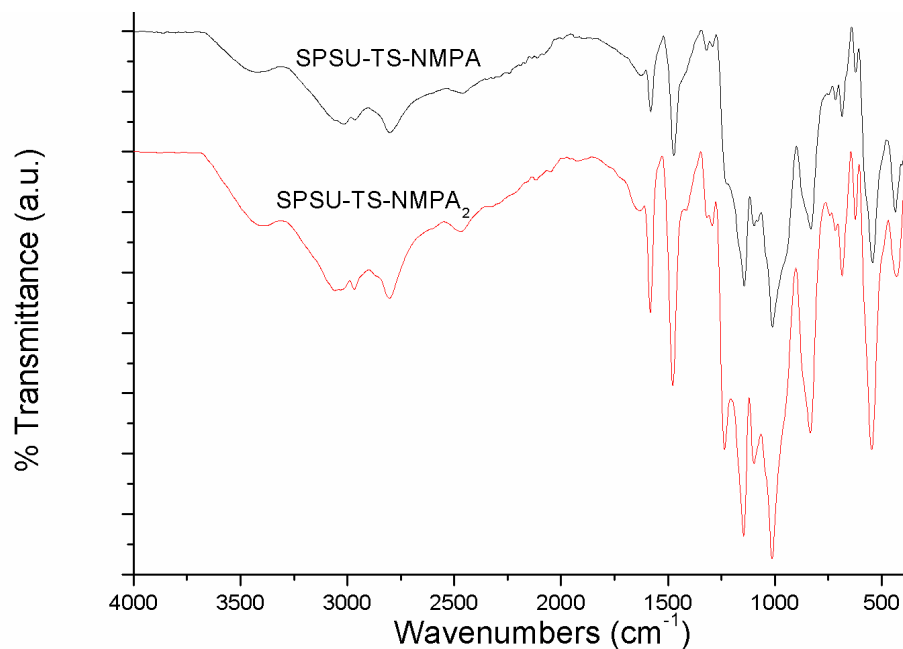
Figure 3.62 FT-IR spectra of the SPSU-TS-NMPA composite membranes.

3.7.2 SEM

The microtopography of SPSU-TS and SPSU-TS-NMPA composite membranes was studied by scanning electron microscopy (SEM) as shown in Figure 3.63. From Figure 3.62a, it was observed that sulfated nano-titania were homogenously dispersed and embedded in the SPSU matrix.

Due to strong interactions between sulfonic acid groups of sulfated titania and phosphonic acid units of NMPA, no phase separation observed during solvent evaporation. In fact, extensive phase separation was prevented by interactions between SPSU and NMPA. Therefore, homogeneous films were produced. Figure 3.63b indicates a very good compatibility between SPSU and NMPA. This result is also consistent with the DSC curves of the impregnated membranes that have no separate T_g transition.

a)
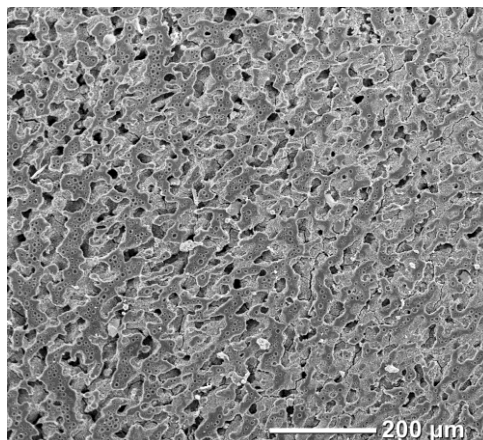
b)
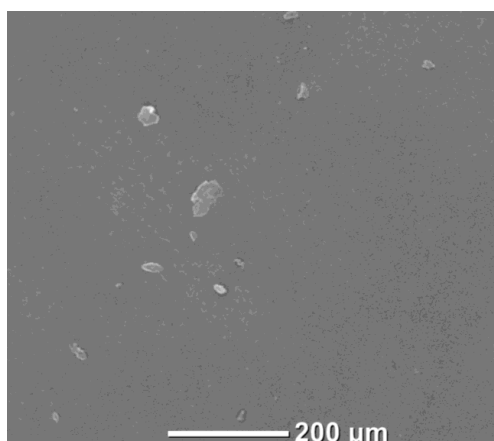
Figure 3.63 SEM micrographs of the surface of composite membranes
(a) SPSU-TS□(b) SPSU-TS-NMPA

3.7.4   Thermal analysis

Table 3.8 lists the glass transition temperatures of the SPSU-TS-NMPA composite membranes. SPSU exhibits a glass transition at around 193 ^{o}C(Lufrano, Baglio et al. 2008). In the presence of sulfated nanotitania Tg of SPSU to 180 ^{o}C. The reason can be attributed to softer effect of SO_3H units in the sulfated nanotitania (Aslan and Bozkurt 2014). The T_g of SPSU-TS-NMPA nanocomposite polymer membranes were measured between 86 ^{o}C and 100 ^{o}C. According to the glass transition temperatures of the nanocomposites

membranes, NMPA has softener effect. The T_g shifted to lower temperatures while the quantity of phosphonic acid groups increases.

Table 3.8 Max. Proton conductivity and Tg (^{o}C) values for the all membranes.

Sample name	Molar Ratio (SPSU/NMPA)	Tg ^{o}C	Max. proton cond. (Scm^{-1})
SPSU-TS	-	180	2 x10^{-5} at 150 ^{o}C
SPSU-NMPA	1:1	110	2x10^{-4} at 150 ^{o}C
SPSU-TS-NMPA	1:1	98	0,002 at 150 ^{o}C
SPSU-TS-NMPA$_2$	1:2	95	3x10^{-4} at 150 ^{o}C
SPSU-TS-NMPA$_3$	1:3	86	4x10^{-5} at 150 ^{o}C

The TGA results were showed in Fiure 3.64. Due to the anhydride formation the TG thermograms have a subtle weight loss up to 150 ^{o}C (Park, Shin et al. 2005). As seen in the TG graphs the nanocomposites membranes thermally stable up to 270 ^{o}C, then they decompose. The thermal stability of the composite membranes decreased after the embedding NMPA into SPSU-TS. This can be attributed to intermolecular condensation of phosphonic acid units as well as titania surface at high temperatures.
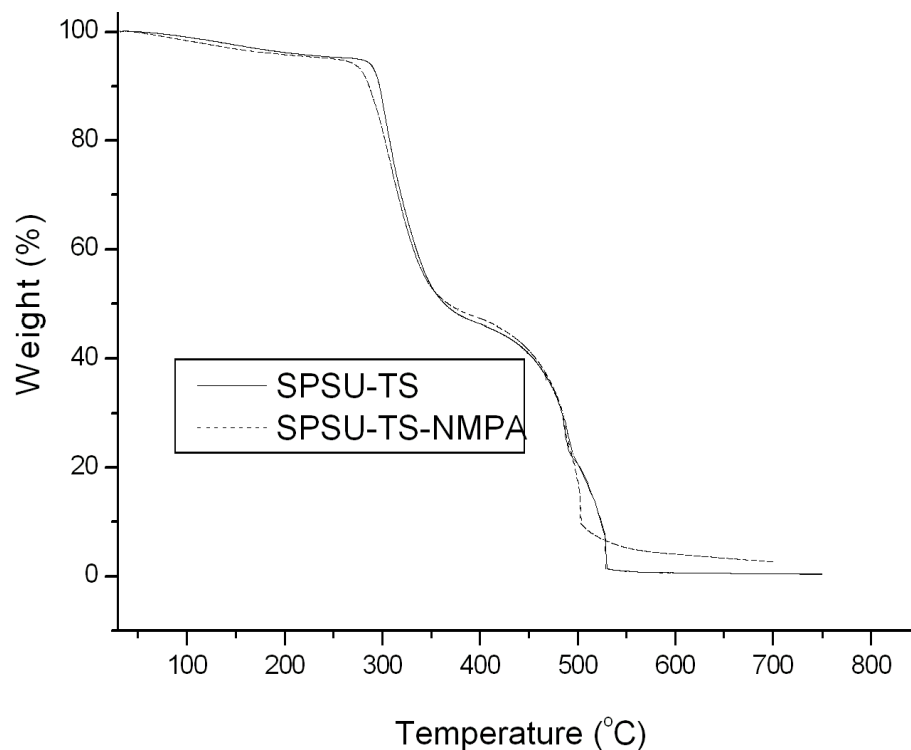
Figure 3.64 Thermogravimetry (Tg) Analysis of SPSU-TS-NMPA composite membranes under nitrogen atmosphere at a heating rate of 10 ^{o}C min^{-1}.

3.7.5   Water Uptake

The water uptake of the membranes is a major parameter influencing proton conductivity, mechanical property and stability. Water uptakes of the SPSU-TS-NMPA samples are shown in Figure 3.65. As can be seen, water uptake increased with decreasing NMPA content due to interaction between phosphonic acid units of NMPA and nanotitania surface. The sample with (1:1) composition has the highest water uptake value (130 %). Although the mechanical strength of the swelled membrane decreased to a certain extent, almost no NMPA dissolved in the solution (Aslan and Bozkurt 2014). The result showed that the complexation of SPSU with NMPA prevented the loss of guest polymer (SPSU) to the solution.
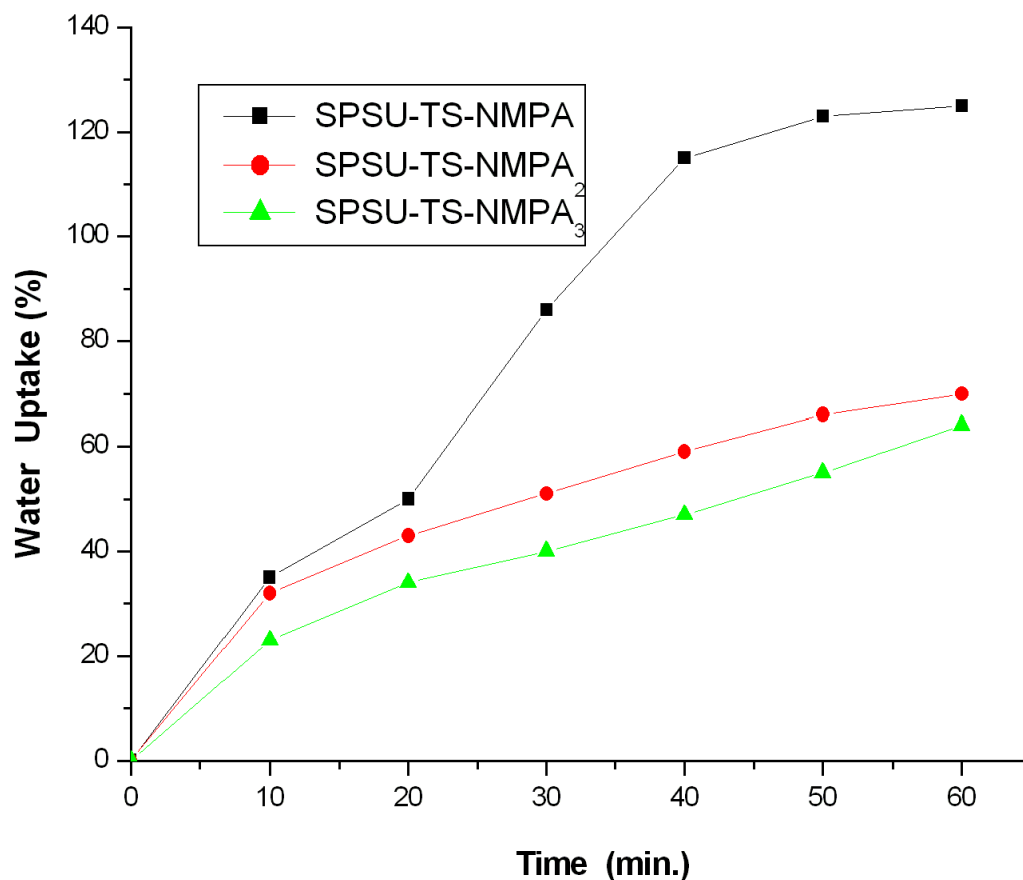
Figure 3.65 Water / Methanole uptake of SPSU-TS-NMPA composite membranes.

3.7.6 Methanol Permeability

Methanol crossover is an important problem for portable methanol fuel cell. In this study, simple homemade diaphragm diffusion cell was used to measure methanol permeability of the composite membranes (Munakata, Chiba et al. 2005, Gasa, Boob et al. 2006). The cell is filled with a pure methanol and the mass flow is recorded as a function of time (see Figure 3.66). Molar methanolflux(J) through SPSU-TS AND SPSU-TS-NMPA blends was calculated according to literature (Boroglu, Celik et al. 2011).

The measured methanol permeability through SPSU-TS and SPSU-TS-NMPA were 1.75×10^{-7} cm^2 s^{-1} and 2×10^{-8} cm^2 s^{-1}, respectively. In previously work, Li et al. reported that methanol permability of the Nafion® 117 membrane was measured as $\sim 10^{-6}$ cm^2 s^{-1}(Li,

Sun et al. 2006). Furthermore, the SPSU-TS-NMPA composite membranes have showed lower methanol crossover than commercial Nafion 112 showed lower methanol crossover than commercial Nafion 112 (Lin, Wycisk et al. 2007, Lin, Wu et al. 2008).
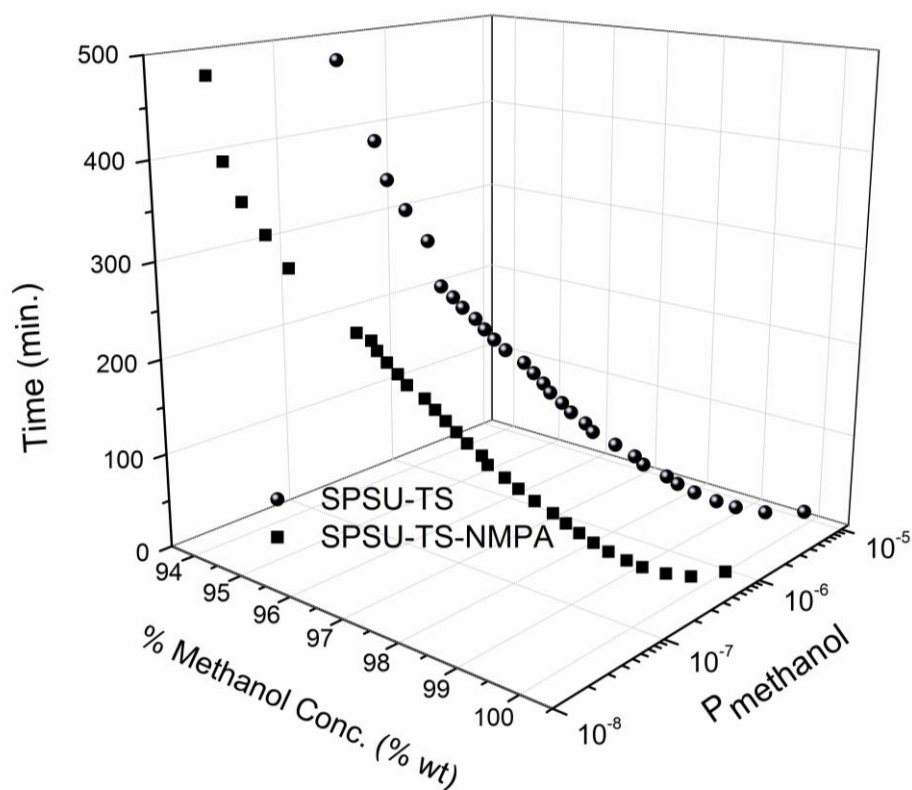
Figure 3.66 Methanole permeability of SPSU-TS-NMPA composite membrane.

3.7.7 Mechanical Analysis

Figure 3.67 shows the results of the dynamic mechanical analysis of SPSU-TS as a function of temperature. At lower temperature, the rigidity of the films is relatively high with a E' plateau in the 10^9 (Pa) regime, which correspond to glass material. When the glass transition is reached, a severe drop in both the *E'* and *E''* values is observed until values are reached which are typical for a highly viscous melt (Aslan and Bozkurt 2014).

Above 225 ^{o}C, E' becomes lager than E'' that may be due to onset of rubber elastic plateau (Bozkurt, Ise et al. 1999, Deimede, Fragou et al. 2000).
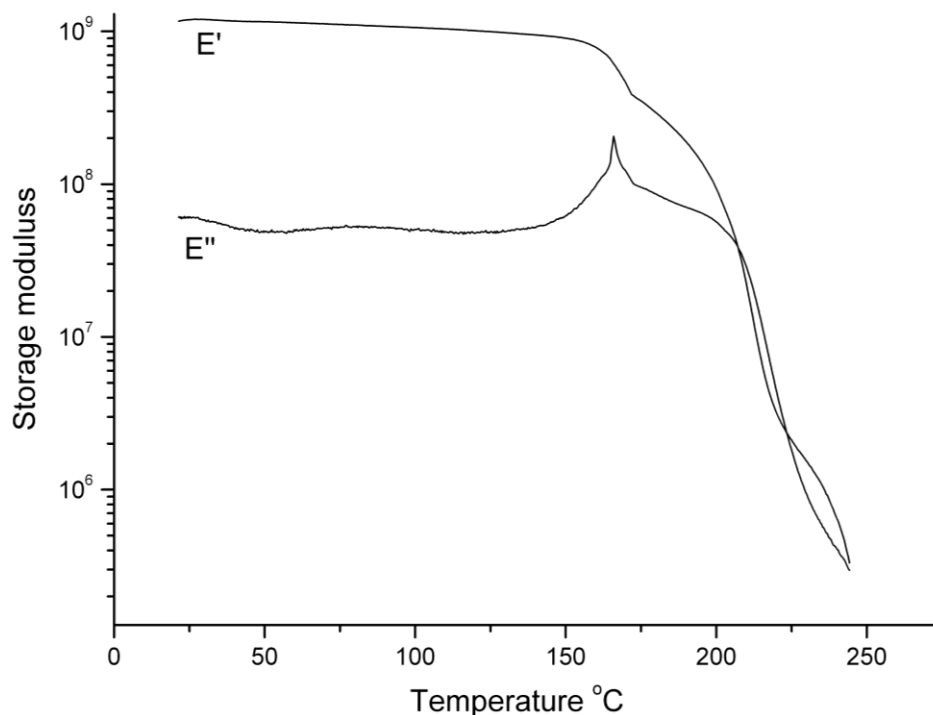
Figure 3.67 Temperature dependence of DMA results for SPSU-TS.

3.7.8   Oxidative Stability

The oxidative stability of the SPSU-TS-NMPA nanocomposite membranes were evaluated in Fenton's reagent (3% H_2O_2 aqueous solution containing 2 ppm $FeSO_4$) (Aslan and Bozkurt 2010). SPSU-TS-NMPA and SPSU-TS-NMPA$_2$ membranes were not soluble in Fenton's reagent, whereas the SPSU-TS-NMPA$_3$ and SPSU-TS-NMPA$_4$ membranes partially dissolved in Fenton's reagent within 24h. The composite membranes which including lower NMPA content have better oxidative stability against Fenton's reagent compared to including high NMPA containing membranes (Aslan and Bozkurt 2014).

3.7.6 Proton conductivity

The AC conductivities, σ_{ac} (ω) of the polymers were measured by using an impedance analyzer.

The proton conductivities of SPSU-TS and SPSU-TS-NMPA anhydrous nanocomposite polymer electrolytes were measured between 20-150 ^{o}C. The AC conductivity of SPSU-TS-NMPA$_x$ composite membrane is shown in Figure 3.68, Figure 3.68 and Figure 3.69.
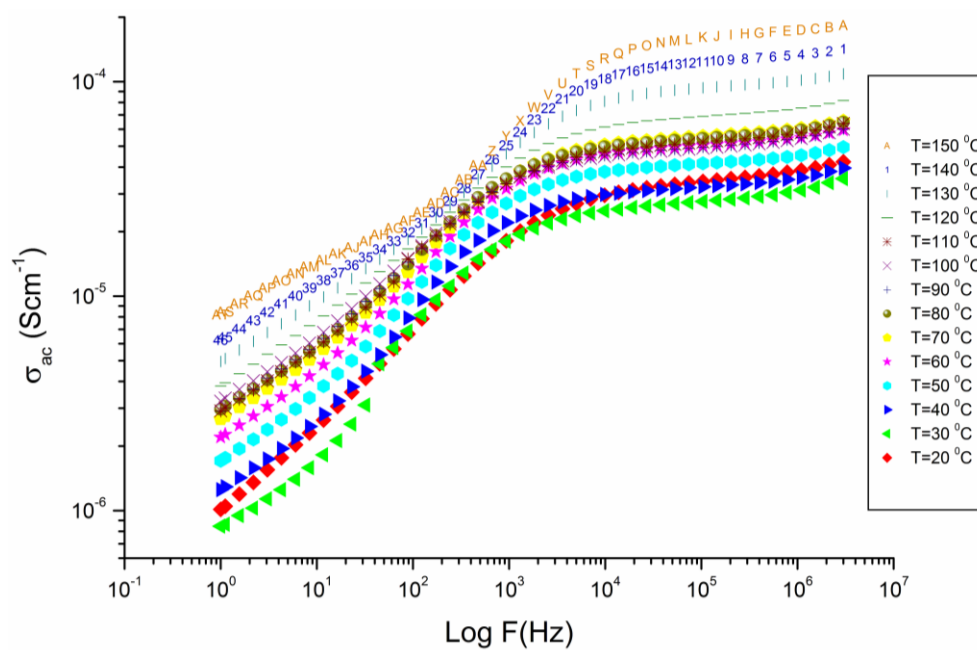
Figure 3.68 AC Conductivity of SPSU-TS-NMPA composite membrane.
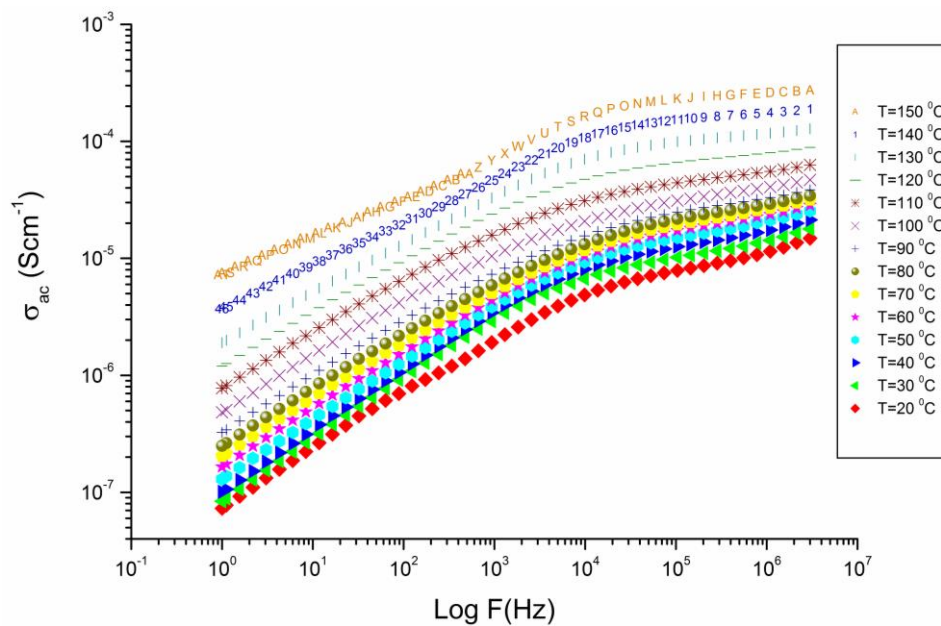
Figure 3.69 AC Conductivity of SPSU-TS-NMPA$_2$ composite membrane.
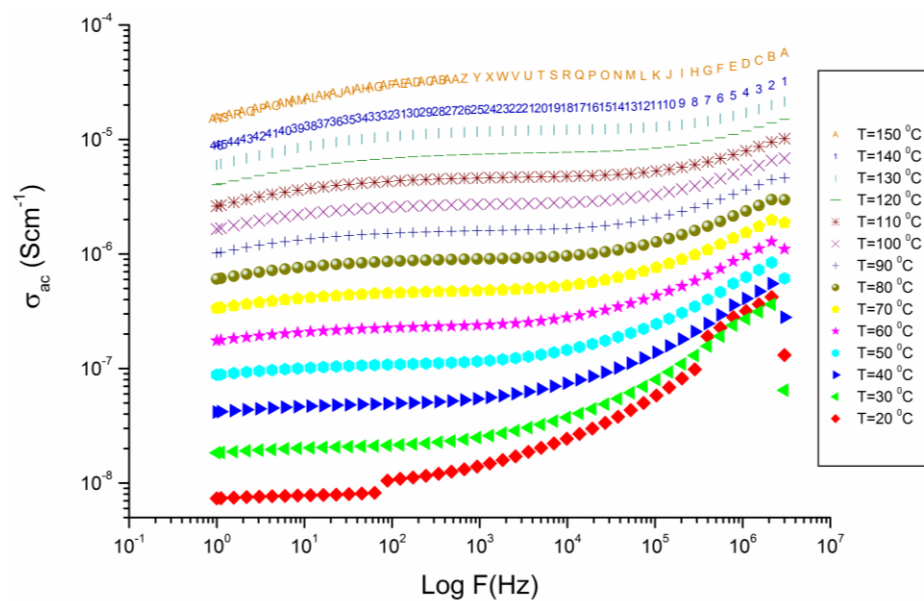
Figure 3.70 AC Conductivity of SPSU-TS-NMPA$_3$ composite membrane.

The proton conductivities of all anhydrous samples were compared in Figur 3.71. The proton conductivity of SPSU increased in the presence of sulfated nanotitania and increasing temperature. There are several studies about the proton conductivity property of SPSU but most of them are in humidified conditions(Lufrano, Baglio et al. 2006, Lufrano, Baglio et al. 2008). For anhydrous proton conductivity sulfonated polysulfone-nitrilotri(methyl triphosphonic acid) composite membrane was measured as $2x10^{-4}$ Scm^{-1} at 150 ^{o}C. Previous works have reported modified titania and polymer composite membranes have an acceptable proton conductivity level for PEMFC application(Aslan and Bozkurt 2012). At low temperatures, these organophosphorylated titania increased the proton conductivity when they embedded in the membranes for humidified conditions.
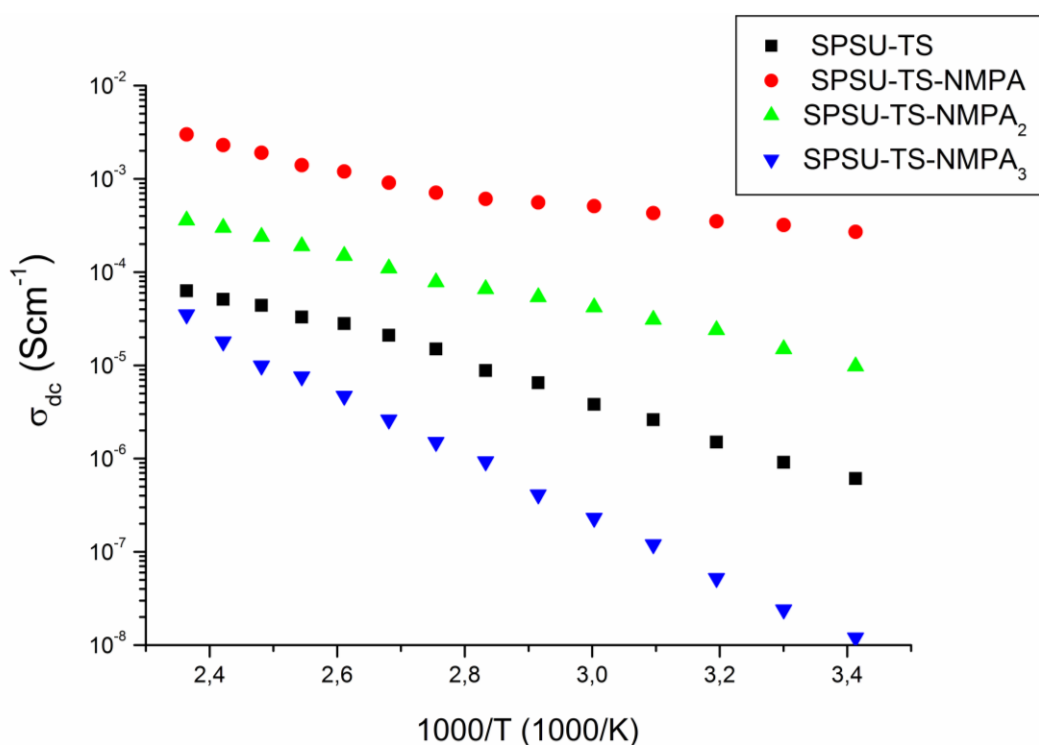
Figure 3.71 DC Conductivity Measurements of SPSU-TS-NMPA composite membranes versus reciprocal temperature.

The conductivity isotherm illustrates that the DC conductivities of SPSU-TS-NMPA composite membranes strongly depends on temperature as well as the ratio of NMPA. However the DC conductivity illustrates that the NMPA content increases the conductivity for SPSU-TS-NMPA and SPSU-TS-NMPA$_2$ composite membrane decreases the conductivity for SPSU-TS-NMPA$_3$. One possible explanation is that complexation may occur between phosphonic acid units of NMPA and SO$_3$H groups of sulfated nanotitania at high ratio of NMPA. Additional reason can be the partial reaction of TS with phosphonic acid units of NMPA resulting in loss of proton sources. Thus, at high NMPA ratio the proton conductivity decreased due to loss of proton by condensation (Aslan and Bozkurt 2014).

The maximum proton conductivity of SPSU-TS-NMPA was measured as 0.002 (Scm^{-1}) at 150 ^{o}C in the dry state. The SPSU-TS-NMPA (x =1) is the optimum composition as the complex polymer electrolyte. When the NMPA composition increased the proton conductivity also increased. The major part of proton transport is provided over both phosphonic acid coordinated with SO$_3$H groups of sulfated titania and sulfonated polysulphone.
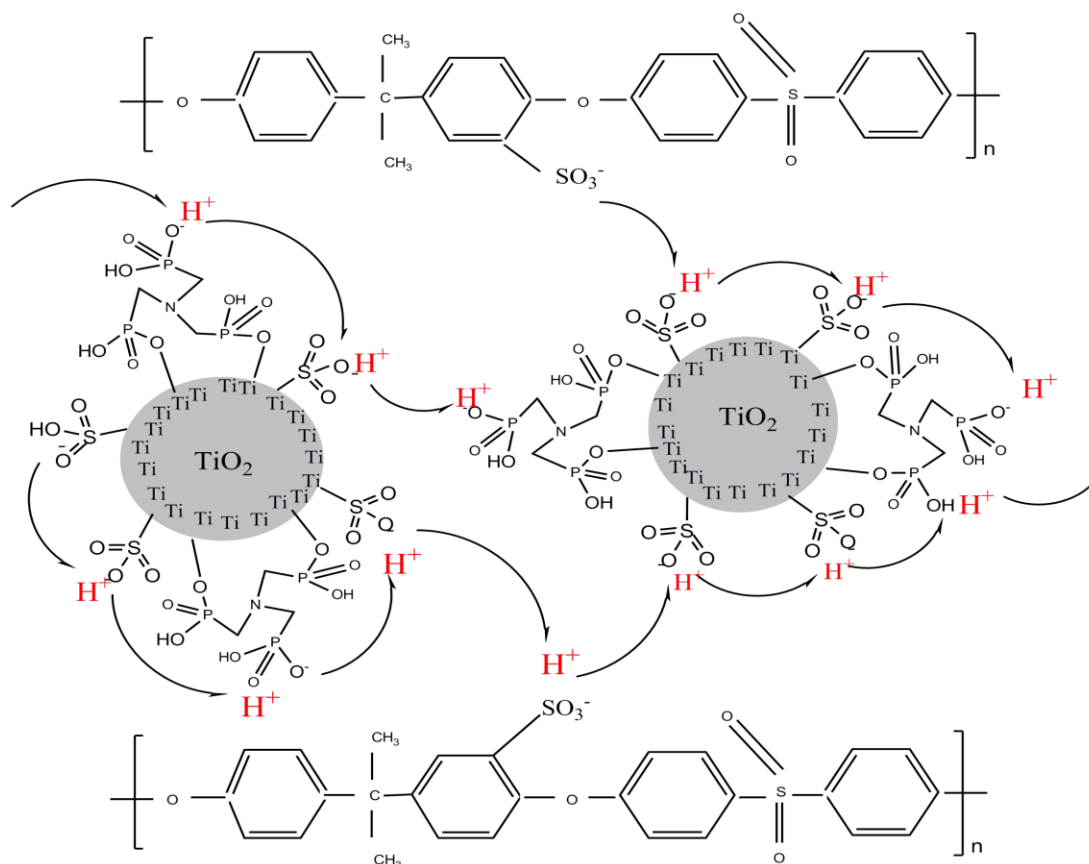
Figure 3.72 The postulate of proton transfer mechanism in SPSU-TS-NMPA composite membranes.

In the SPSU-TS-NMPA membranes, proton transfer can be facilitated by the additional phosphonic acid groups on NMPA. The FTIR result supported that it can be concluded that a Grotthuss mechanism (structural diffusion) is the possible pathway for the total proton diffusion as well as conductivity data. The proton transported via the –POH groups and sulfate groups (see Figure 3.72) (Smitha, Sridhar et al. 2004, Ramirez-Salgado 2007).

3.7.8 Selectivity

Figure 3.73 shows the selectivity parameters of membranes as a function of temperature. The selectivity parameters (Φ) are calculated by using data of proton conductivity and methanol permeability,

$$\Phi \ (S \ s \ cm^{-3}) = \sigma/P_{Methanol} \qquad\qquad (3.8)$$

where σ is the proton conductivity (S cm^{-1}), and $P_{Methanol}$ is the methanol permeability (in cm^2 s^{-1}) through the membrane.

The selectivity for the SPSU-TS-NMPA membrane was 150000 at 150 ^{o}C. It is clearly seen that the SPSU-TS-NMPA show a higher selectivity than Nafion 117 film (which is ca. 50,000) (Vargas, Vargas et al. 1999, Won, Cho et al. 2009).
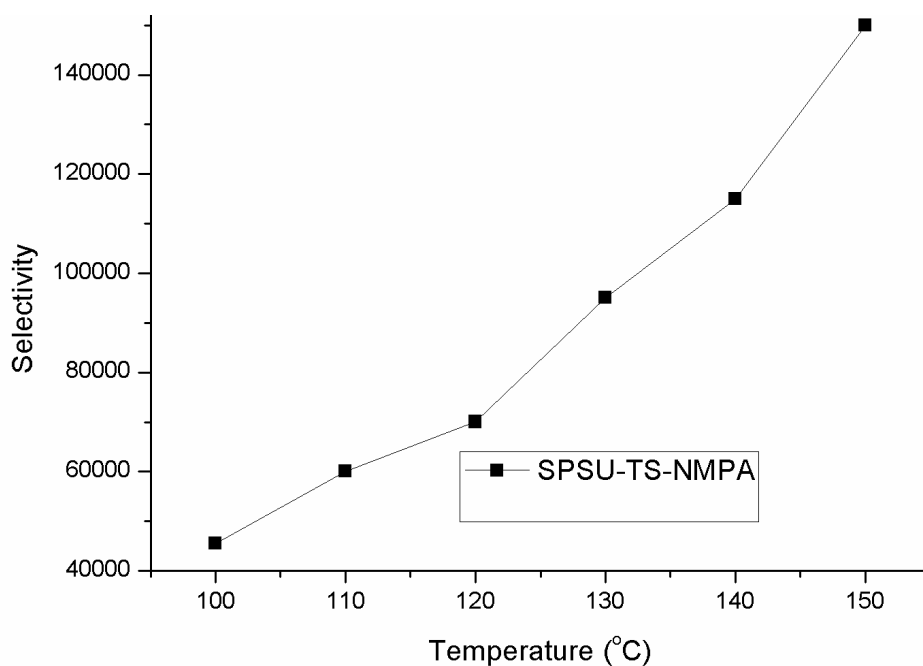
Figure 3.73 Selectivity parameter of SPSU-TS-NMPA composite membrane.

3.8 CHARACTERIZATION OF AZOL GROUPS FUNCTIONAL PGMA GRAFTED HALLOW SILICA SPHERES NANOCOMPOSITE MEMBRANES

3.8.1 Characterizations

In this study azole functional HSS-g-PGMA was produced and immobilization of azole which was verified by elemental analysis. Nitrogen contents of the samples were used to calculate azole ratio of the functional polymers. As illustrated from elemental analysis, more than 80 % of the epoxide rings were opened by azole units.

3.8.2 FT-IR analysis

FT-IR spectra of HSPGMA and azole functional HSPGMA are represented in Figure 3.74. The absorption peaks at 1132 cm^{-1} and 1045 cm^{-1} attributed to Si–O–Si asymmetric stretching (Pu, Pan et al. 2010, Celik, Bozkurt et al. 2012). The peak at 3435 cm^{-1} belonged to Si–OH stretching vibration. A distinctive C=C stretching was displayed at about 1603 cm^{-1}. In the medium and lower energy region, 1700–450 cm^{-1}, small vibrational modes at 1639 and 1386 cm^{-1} are related to C–H stretching characteristic of CH2/CH3, indicating the presence of remaining methoxy groups. The following bands are well established to specific molecular motions that can be taken as the silica fingerprint (Cao and Fischer 1999, Won, Cho et al. 2009, Ma, Lee et al. 2010). The signals at 1220 and 1083 cm^{-1} belong to Si–O stretching. The band centered at 954 cm^{-1} is associated with the stretching mode of non-bridging oxide bands as Si–OH and Si–O−. The band around at 795 cm^{-1} is assigned to the symmetric stretching of the Si–O–Si mode. The lowest frequency modes (550 and 470 cm^{-1}) are associated with the rocking motions perpendicular to the Si–O–Si plane, of the oxygen bridging two adjacent Si atoms that formed the tetra or trisiloxane rings (Chuang, Hsu et al. 2007, Ma, Lee et al. 2010).

Figure 3.74 FT-IR spectra ofHSS-graft-PGMA(HSPGMA), Triazole functional HSS-graft-PGMA (HSPGMA-Tri), Amino-tetrazole functional HSS-graft-PGMA (HSPGMA-Tet) and 5-Amino-Triazole functional HSS-graft-PGMA (HSPGMA-ATri).

In PGMA the carbonyl group gives a strong peak at 1720 cm^{-1} and the strong peaks at 1140 cm^{-1} and 1260 cm^{-1} are attributed to C-O stretching of the ester group(Hirose, Hatakeyama et al. 2002). The absorption at 900 cm^{-1} is assigned to stretching vibration of the epoxy group which disappeared up on azole functionalization (Nanjundan, Unnithan et al. 2005). In the high energy region from 4000 up to 1800 cm^{-1}, the appearance of absorption bands correspond to stretching vibrations of OH, NH and CH$_2$ groups (Aslan and Bozkurt 2010). The signals at 3328 and 3174 cm^{-1} are assigned to NH and OH modes from the ring and the amino groups. Several small bands between 2900 and 2600 cm^{-1} together with 1926 cm^{-1}, belong to aromatic and aliphatic CH modes. The broad band between 2700 and 2300 cm^{-1} has been assigned to an associated N–H mode, intermolecular hydrogen bonded in the form of N–H$\cdots$N hydrogen bonds. Azole functional HSPGMA exhibited a medium absorption at 1577 cm^{-1} and 1450 cm^{-1} due to C=N and C-N stretching of the triazole ring (Angell 1961). The bands below 1800 cm^{-1} are attributed to chains and

ring skeletal vibrations of H–C–H, C O, H–N–H, C–N. The strong signal at $1630 cm^{-1}$ is related to an in-plane deformation mode of NH_2 group, and the ones at 1604 and 1571 cm^{-1} to N–H vibration inplane and C O stretching. The series of five fairly strong absorptions between 1500 and 1300 cm^{-1} assigned to ring vibrations C-N single and double bonds, and also to a deformation mode of CH groups. Additionally except a new absorption at 1640 cm^{-1} coming from amine bending vibration.

Figure 3.75 H_3PO_4 doped HSS-graft-PGMA (HSPGMA-Tri-H_3PO_4) membranes.
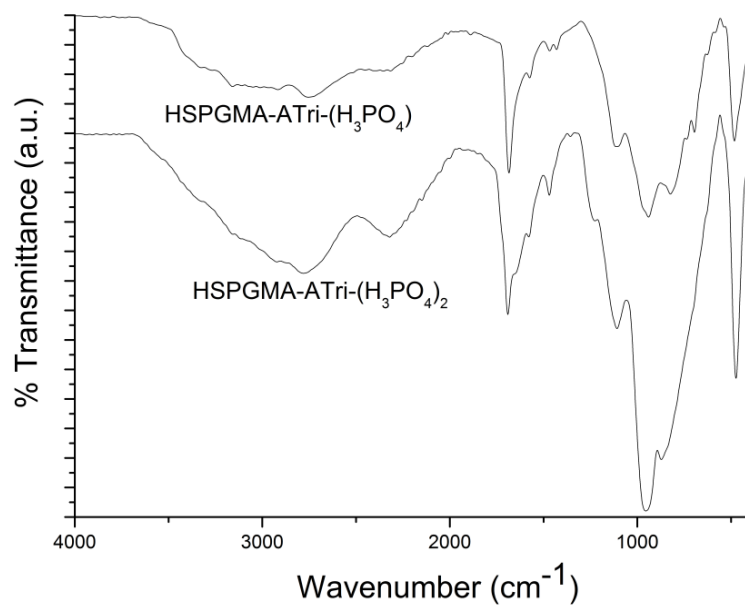
Figure 3.76 H$_3$PO$_4$ doped HSS-graft-PGMA (HSPGMA-ATri-H$_3$PO$_4$) composite membranes.
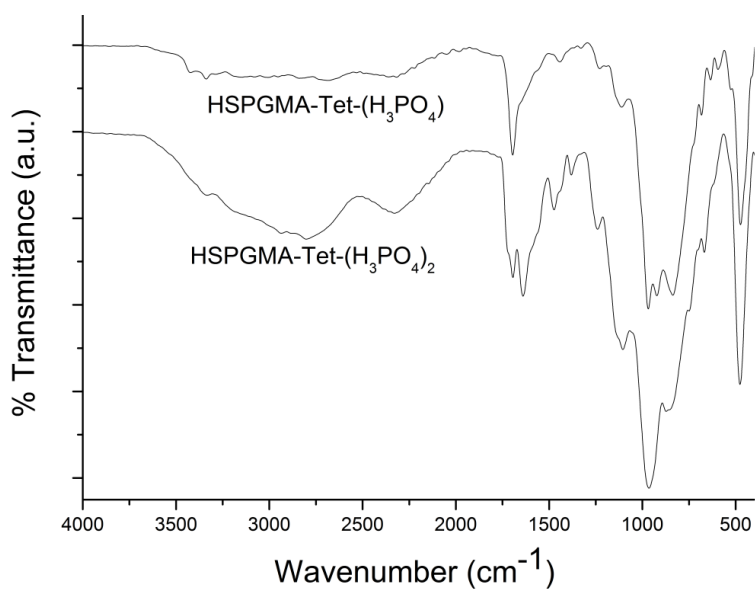
Figure 3.77 H$_3$PO$_4$ doped HSS-graft-PGMA (HSPGMA-Tet -H$_3$PO$_4$) composite membranes.

After doping Azole functional HSPGMA with phosphoric acid the intensity of the peak at 1577 cm^{-1} decreases and the intensity of the peaks at 1510 cm^{-1} and 1450 cm^{-1} increase which may show the protonation of the triazole ring. Additionally, the peak which appears at 3100 cm^{-1} shows the N-H absorption. Doping of HSPGMA-Tri with H$_3$PO$_4$, two strong peaks appear near 500 cm^{-1} and 1000 cm^{-1} which are attributed to PO$_2$ bending vibration of (H$_2$PO$_4{}^{2-}$) and P-O symmetric stretching of H$_3$PO$_4$. The carbonyl stretching band at 1725 cm^{-1} decreases and broadens due to protonation of C=O bond. In addition, the disappearance of the azole ring stretching at 1550 cm^{-1} (C=N) as well as the formation of a broad band at 1940-1960 cm^{-1} may indicate proton exchange reactions (Aslan and Bozkurt 2010).

3.8.3   Surface Morphology

The selected AFM images of membranes are shown in Figure 3.78 and Figure 3.79. When comparing unmodified grafted HSPGMA, bigger granular domains are clearly seen on the surface of azole functional HSPGMA (see Figure 3.78.). Diameter and level of aggregation of the silica particles were determined from AFM images after their grafting with PGMA the surface of HSS (see Figure 3.79.). The average vertical distance (diameter) of original particles was about 350 nm. Determination of average diameter was performed by measuring the cross-section of at least 60 single particles. AFM imaging indicates that no significant aggregation occurred (beside the lateral aggregation caused by capillary forces during drying) when the particles were transferred in DMF from the water medium.
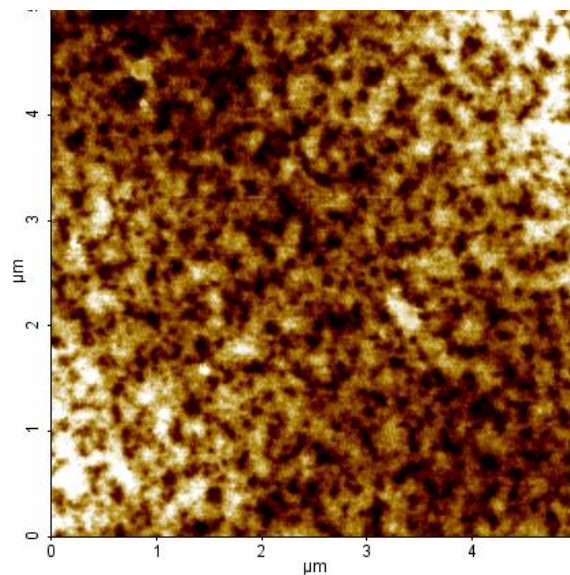
Figure 3.78 AFM micrographs of the surface of HSS-graft-PGMA (HSPGMA) composite membrane.
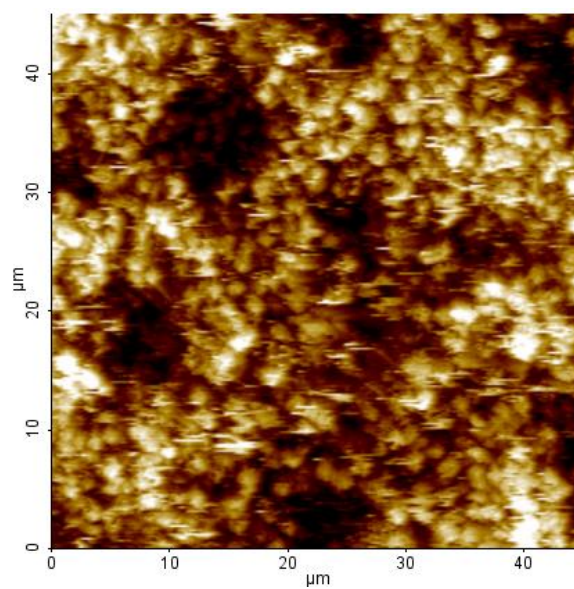
Figure 3.79 AFM micrographs of the surface of Amino-tetrazole functional HSS-graft-PGMA (HSPGMA-Tet) composite membrane.

After grafting of PGMA from the silica nanoparticles, TEM images such as that in Figure 3.80 show the formation of polymer layer on the 350 nm diameter HSS particles. The 100 nm increase in diameter after polymerization suggests that the polymer layer is 100 nm thick. The particle diameter in TEM images is ~50 nm after modification with azole units, indicating a ~100 nm thick polymer layer on the HSS core (see Figure 3.75.). As seen in the Figure 3.74 the particles are not aggregated after the modification.
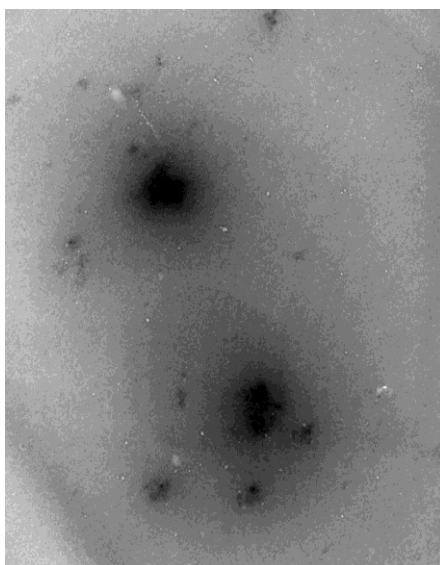
Figure 3.80 TEM pictures of HSS-graft-PGMA(HSPGMA) composite membrane.
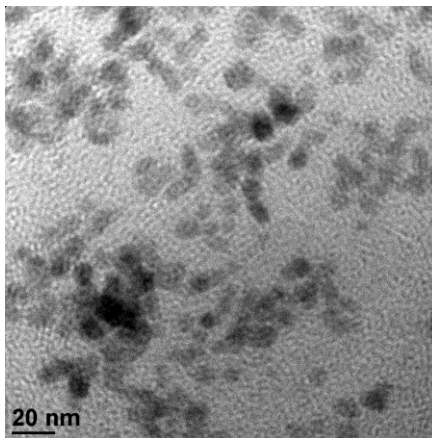
Figure 3.81 TEM pictures of Amino-tetrazole functional HSS-graft-PGMA (HSPGMA-Tet) composite membrane.

Surface morphologies of HSS (see Figure 3.82), HSPGMA (see Figure 3.83), HSPGMA-Tri (see Figure 3.84.), HSPGMA-ATri (see Figure 3.85), and HSPGMA-Tet (see Figure 3.86), materials were investigated by scanning electron microscopy. The grafting on the surface of HSS is clearly seen in Figure 3.76. Here a pronounced difference is seen when comparing the native and the polymer modified particles. It is clearly seen that the polymer covers the particle surface, although growth has also occurred, as seen in the occurrence of some irregularly shaped particles. At higher grafting levels, these particles attach to polymer forming larger porous agglomerates (>100 μm) composed of hallow silica particles (3.5 μm) held together by a weblike polymer structure with micron sized interstitial pores. After azole modification, azole units reduced the interaction of between the polymer chains so HSS particles diverged. Furthermore, no phase separation occurred during solvent evaporation, hence homogeneous films formed.
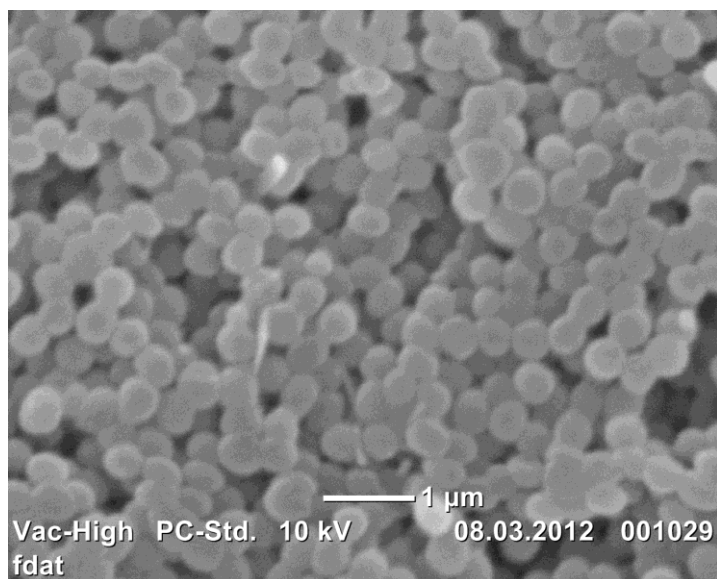
Figure 3.82 SEM pictures of Hallow silica spheres (HSS).
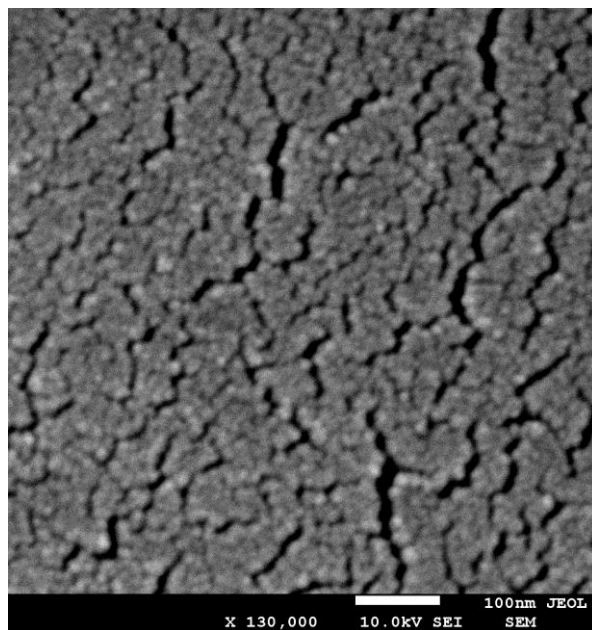
Figure 3.83 SEM pictures of HSS-graft-PGMA composite membrane.
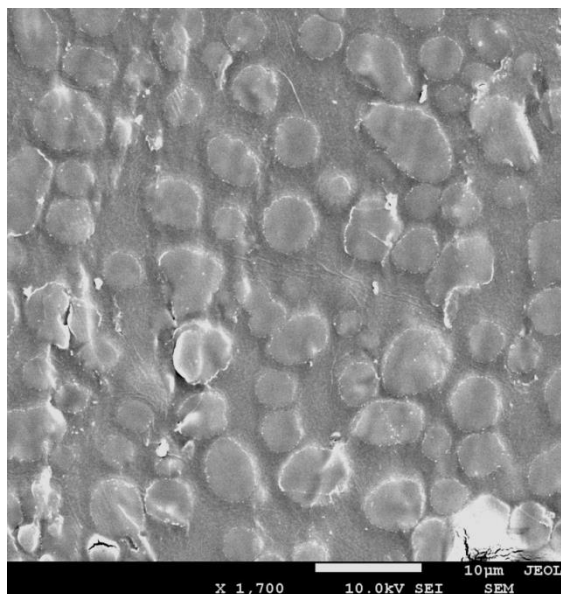
Figure 3.84 SEM pictures of Triazole functional HSS-graft-PGMA (HSPGMA-Tri) composite membrane.
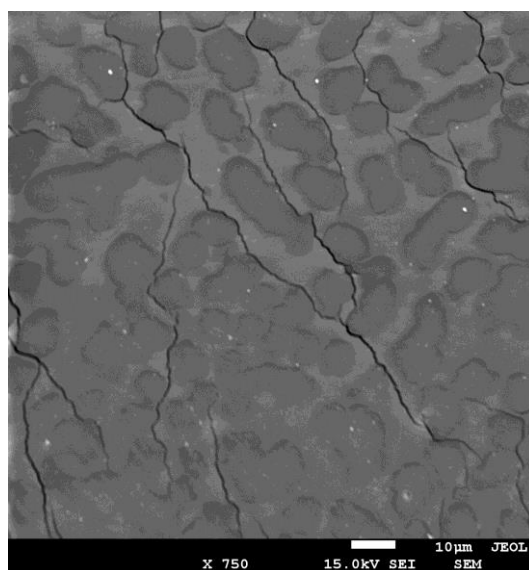
Figure 3.85 SEM pictures of 5-Amino-Triazole functional HSS-graft-PGMA (HSPGMA-ATri) composite membrane.
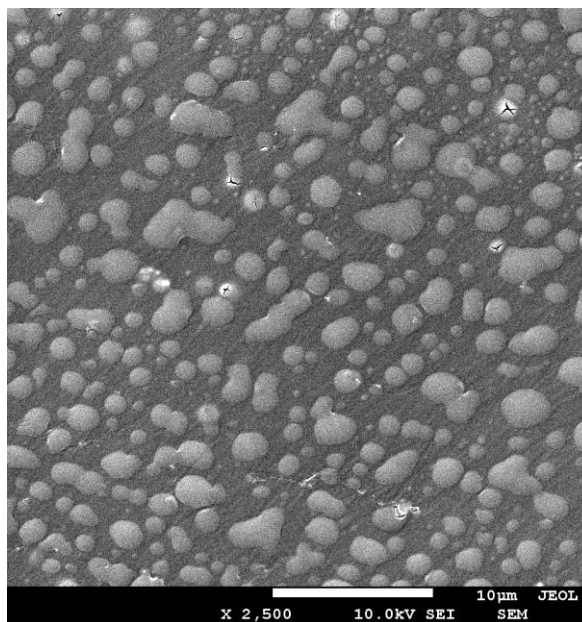
Figure 3.86 SEM pictures of Amino-tetrazole functional HSS-graft-PGMA (HSPGMA-Tet) composite membrane.

3.8.4   Thermal analysis

The glass transition temperature, T_g of the homopolymer PGMA and HSS-g-PGMA were measured as 47 ^{o}C and 80 ^{o}C. Incorporation of grafting HSS particles with polymer matrix would fill the free volumes and would cause need to more energy for starting segmental motions, which would make Tg to increase. Table 3.9 shows the DSC curves of Tri, ATri and Atet functional samples under inert atmosphere at a scan rate of 10 ^{o}C/min. The second curves were evaluated. The melting points of pure Tri and ATri composites are 120 and 157 ^{o}C, respectively. The Tg of triazole functional HSS-graft-PGMA (HSPGMA-Tri) is around 87°C, Tg of 5-Amino-Triazole functional HSS-graft-PGMA (HSPGMA-ATri) is around 92 ^{o}C and Tg of Amino-tetrazole functional HSS-graft-PGMA (HSPGMA-Tet) is 105 ^{o}C. After functionalization with azolic units the Tg of the samples shifted to higher temperatures (Sinirlioglu, Celik et al. 2013).

Table 3.9 Max. Proton conductivity and Tg (^{o}C) values for the all membranes.

Sample name	H_3PO_4 Molar Ratio	Tg ^{o}C	Nitrogen functionalization (%)	Max. proton cond. (Scm^{-1})
HSPGMA	-	80	-	-
HSPGMA-Tri	-	87	94	-
HSPGMA-Tri-(H_3PO_4)	(1:1)	78	-	0.003 Scm^{-1} at 150 ^{o}C
HSPGMA-Tri-$(H_3PO_4)_2$	(1:2)	67	-	0.004 Scm^{-1} at 150 ^{o}C
HSPGMA-ATri	-	92	86	
HSPGMA-ATri-(H_3PO_4)	(1:1)	85	-	0.001 Scm^{-1} at 150 ^{o}C
HSPGMA-ATri-$(H_3PO_4)_2$	(1:2)	70	-	0.006 Scm^{-1} at 150 ^{o}C
HSPGMA-Tet	-	105	90	-
HSPGMA-Tet-(H_3PO_4)	(1:1)	87	-	0.004Scm^{-1} at 150 ^{o}C
HSPGMA-Tet-$(H_3PO_4)_2$	(1:2)	74	-	0.008 Scm^{-1} at 150 ^{o}C
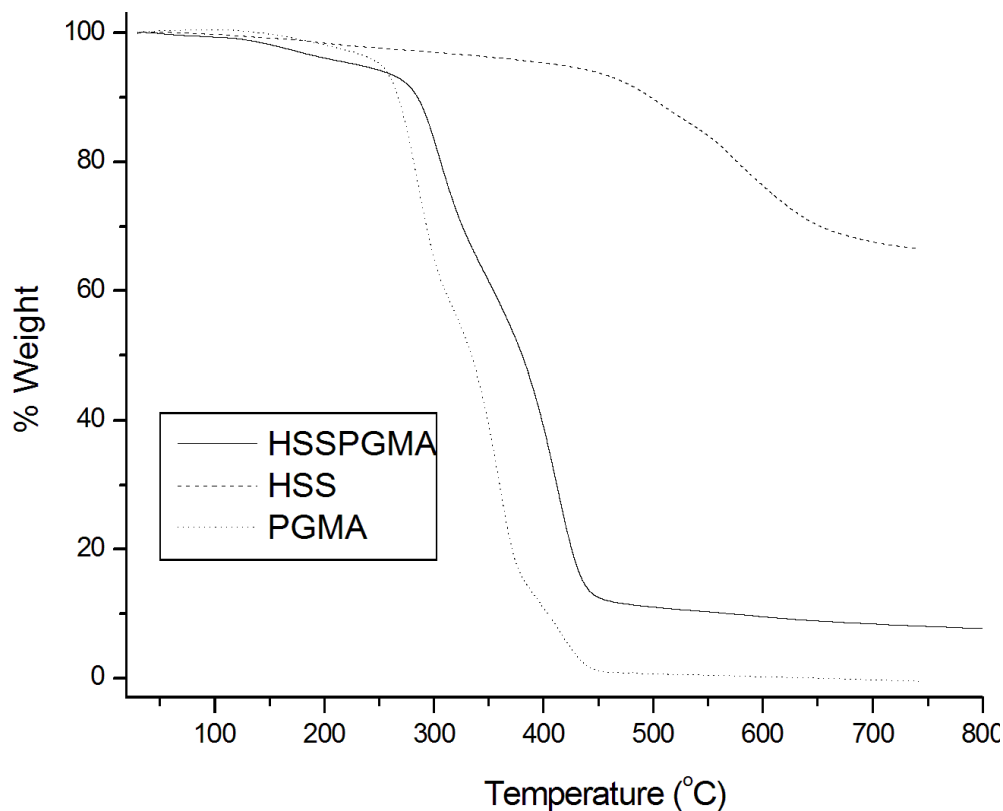
Figure 3.87 Thermogravimetry (Tg) Analysis of HSS, PGMA and HSS-graft-PGMA (HSPGMA) membranes under nitrogen atmosphere at a heating rate of 10 ^{o}C/min.

The weight loss in PGMA occurs in two steps within 200-400 ^{o}C. Figure 3.87 shows the thermograms of HSS, PGMA and PGMA grafting HSS. TGA plots of weight loss versus temperature provide an estimate of the quantity of polymer grown from the nanoparticles. The coated particles consist of both thermally stable compounds that remain in the residue (silica bound to the polymer) and decomposable polymer brushes and initiators that contribute to weight loss. After growth of PGMA from the particle, TGA shows a total weight loss of 90%, which corresponds to a PGMA thickness of ~100 nm. This thickness value agrees reasonably well with the TEM. Reaction of PGMA leads to a total weight loss of 90%, which is consistent with essentially complete reaction between PGMA and HSS. Clearly, PGMA graft HSS is thermally stable up to at least 380 ^{o}C. After 250°C a remarkable weight loss derives from the thermal decomposition of the polymer main chain. The grafting enhanced thermal stability of PGMA.
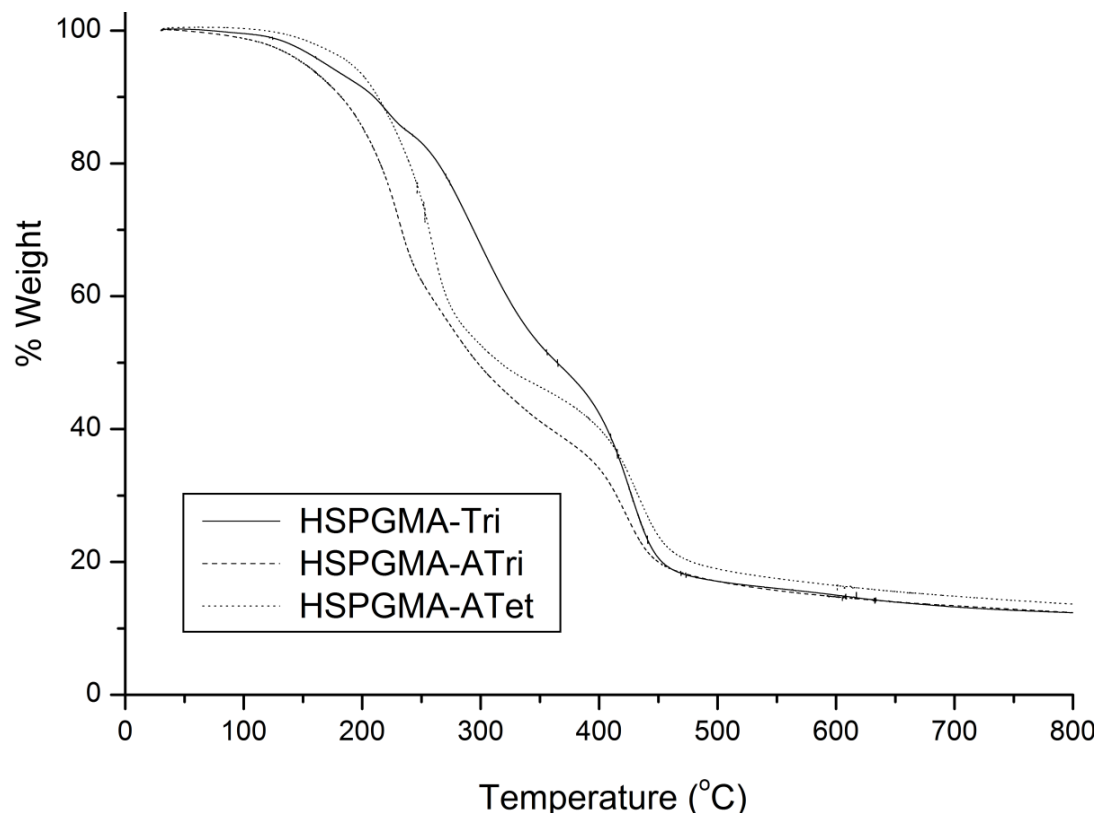
Figure 3.88 Thermogravimetry (Tg) Analysis of Triazole functional HSS-graft-PGMA (HSPGMA-Tri), 5-Amino-Triazole functional HSS-graft-PGMA (HSPGMA-ATri) and Amino-tetrazole functional HSS-graft-PGMA (HSPGMA-Tet) composite membranes under nitrogen atmosphere at a heating rate of 10 ^{o}C/min.

The TG thermograms of azole functional HSSPGMA showed in Figure 3.88. The thermogram of azole functional HSPGMA showed two step decomposition. The weight loss at 200 ^{o}C due to decomposition of azole functional polymer chain after 350 ^{o}C, HSS particles decomposed. The thermal stability of the composite materials decreased with azole functionalization Sinirlioglu, Aslan et al.2013). This also may be attributed to enlarge the grafting nano particle size thus the HSS particles diverged.
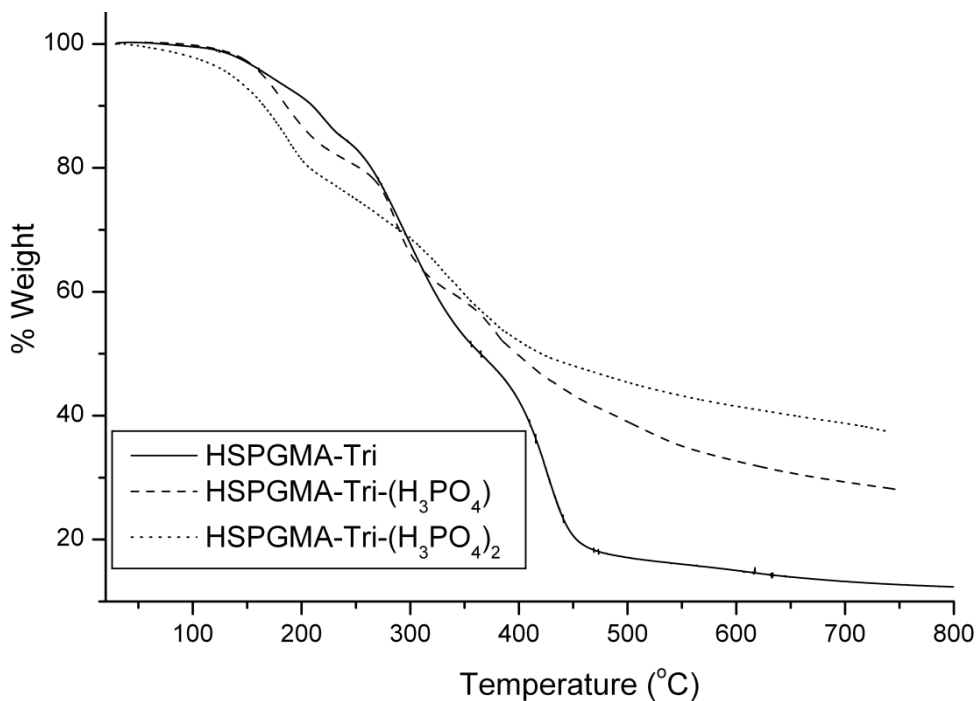
Figure 3.89 TG thermograms of Triazole functional HSS-graft-PGMA (HSPGMA-Tri) recorded at a heating rate of 10 ^{o}C/min under a nitrogen atmosphere.

In Figure 3.88, TG profiles of H_3PO_4 doped triazole functional HSPGMA illustrate no weight change up to approximately 200 ^{o}C. After 200 ^{o}C, can be attributed to water liberation due to the self-condensation of the phosphoric acid and also decomposition the polymer main chain contributes to further weight loss. Clearly, HSPGMA-Tri-$(H_3PO_4)_x$ the materials are thermally stable up to 200 ^{o}C and then they decompose.
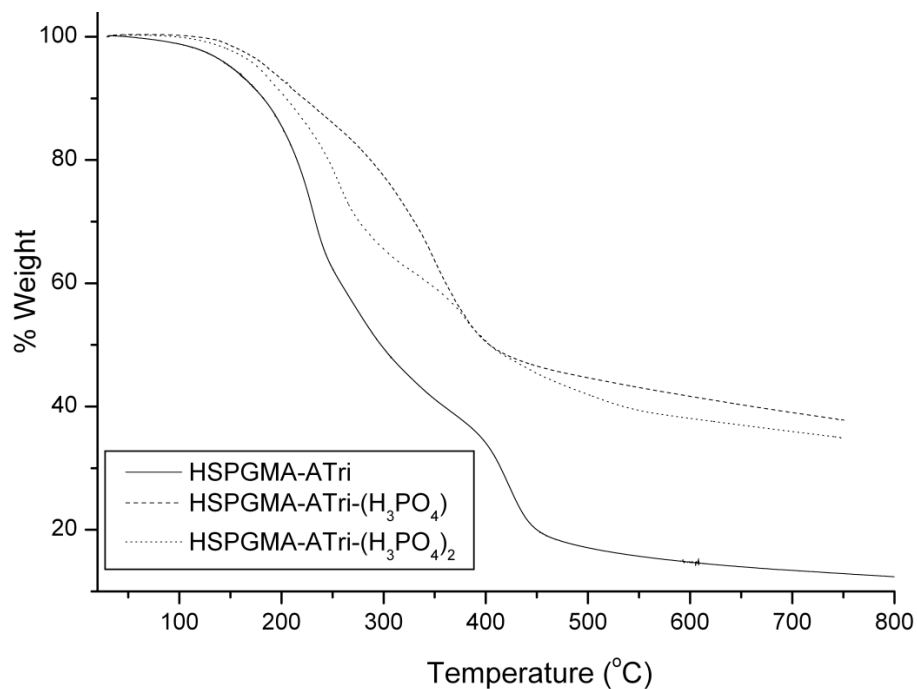
Figure 3.90 Thermogravimetry (Tg) Analysis of .5-Amino-Triazole functional HSS-graft-PGMA (HSPGMA-ATri) membranes under nitrogen atmosphere at a heating rate of 10 ^{o}C/min

In Figure 3.90, TG profiles of H_3PO_4 doped amino-triazole functional HSPGMA illustrate no weight change up to approximately 250 ^{o}C. After 250 ^{o}C, can be attributed to water liberation due to the self-condensation of the phosphoric acid and also decomposition the polymer main chain contributes to further weight loss (Aslan and Bozkurt 2010). Clearly, HSPGMA-ATri-$(H_3PO_4)_x$ the materials are thermally stable up to 250 ^{o}C and then they decompose.
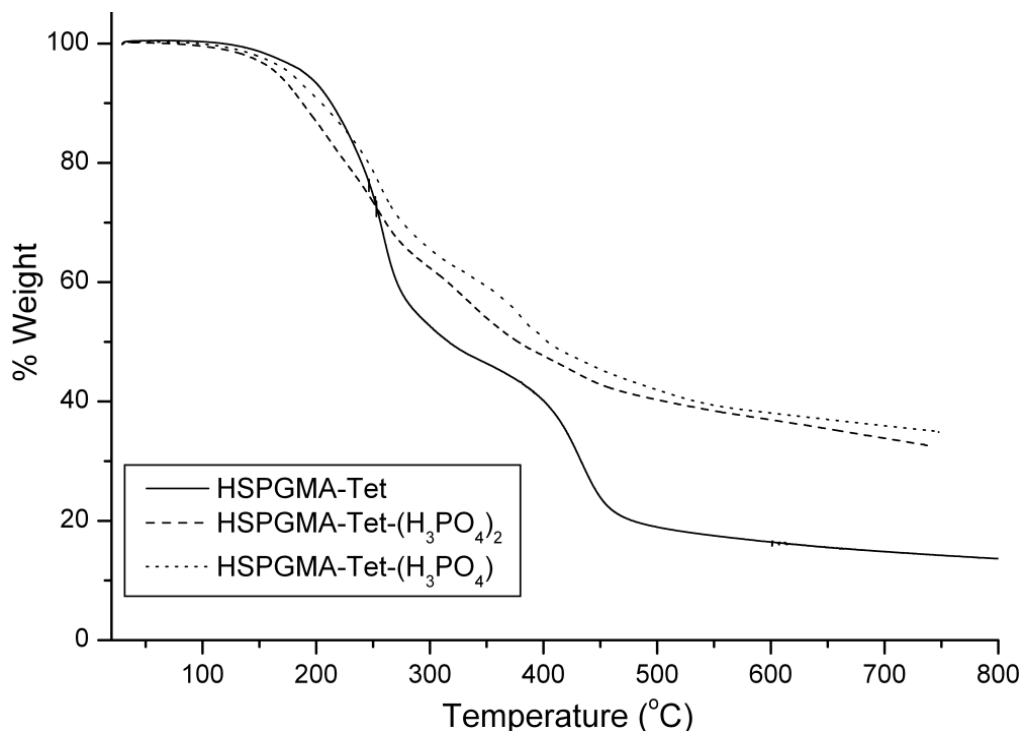
Figure 3.91 Thermogravimetry (Tg) Analysis of Amino-tetrazole functional HSS-graft-PGMA (HSPGMA-Tet) membranes under nitrogen atmosphere at a heating rate of 10 ^{o}C/min.

In Figure 3.91, TG profiles of H_3PO_4 doped amino-tetrazole functional HSPGMA illustrate no weight change up to approximately 250 ^{o}C. After 250 ^{o}C, can be attributed to water liberation due to the self-condensation of the phosphoric acid and also decomposition the polymer main chain contributes to further weight loss. Clearly, HSPGMA-ATet-$(H_3PO_4)_x$ the materials are thermally stable up to 250 ^{o}C and then they decompose.

The doped samples exhibit an insignificant weight change until 200 ^{o}C. The stepwise decomposition above this temperature can be attributed to water liberation due to the self-condensation of the phosphoric acid as well as the decomposition of the polymer(Aslan and Bozkurt 2010).

3.8.5 Proton conductivity

The alternating current (AC) conductivities, σ_{ac} (ω) of the polymers were measured at several temperatures using impedance spectroscopy. The proton conductivities of anhydrous samples were measured from 20 ^{o}C to 150 ^{o}C.
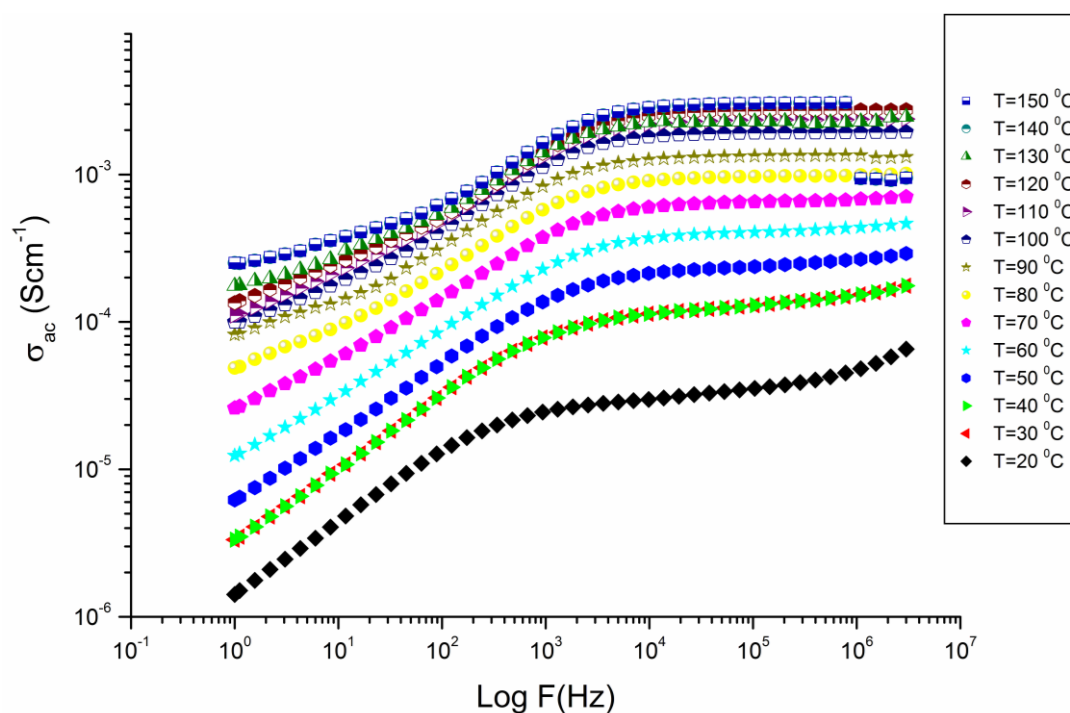
Figure 3.92 AC measurements of H_3PO_4 doped HSS-graft-PGMA HSPGMA-Tri-$(H_3PO_4)_2$ composite membranes versus reciprocal temperature.
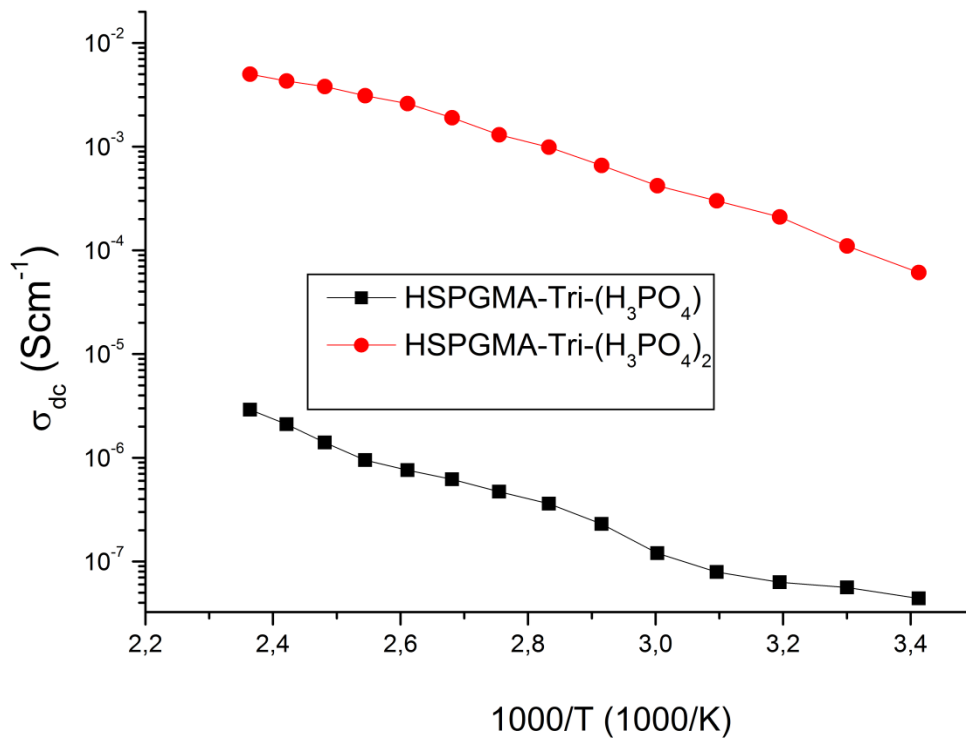
Figure 3.93 DC measurements of H_3PO_4 doped HSS-graft-PGMA (HSPGMA-Tri-H_3PO_4) composite membranes versus reciprocal temperature.

Among phosphoric acid doped HSPGMA-Tri samples HSPGMA-Tri-$(H_3PO_4)_2$ showed the highest proton conductivity of 0.006 Scm^{-1} at 150 ^{o}C in the anhydrous state in Figure 3.93. In the phosphoric acid doped triazole functional HSPGMA systems, the doping ratio is highly effective on the proton conductivity of sample which indicates that major part of proton transport is provided over the H_3PO_4 as well as over azole units.
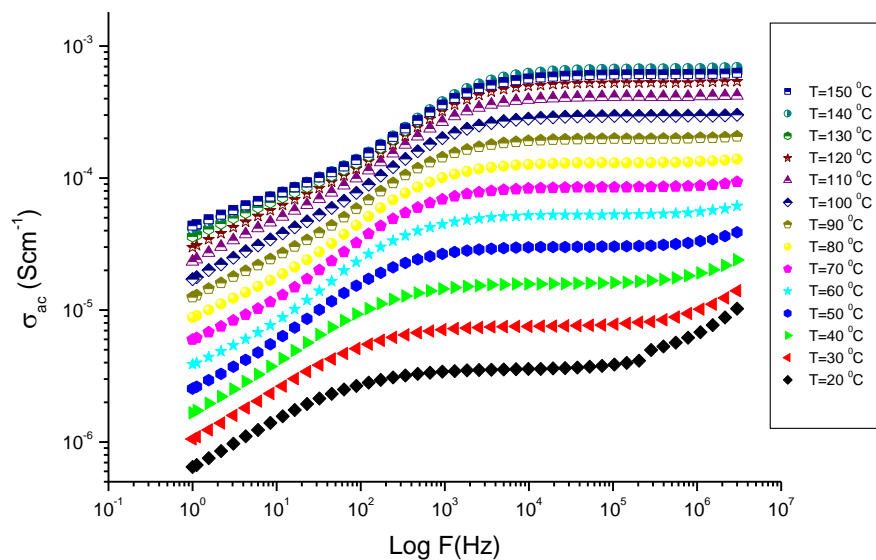
Figure 3.94 AC measurements of H_3PO_4 doped HSS-graft-PGMA (HSPGMA-ATri-H_3PO_4) composite membranes versus reciprocal temperature.
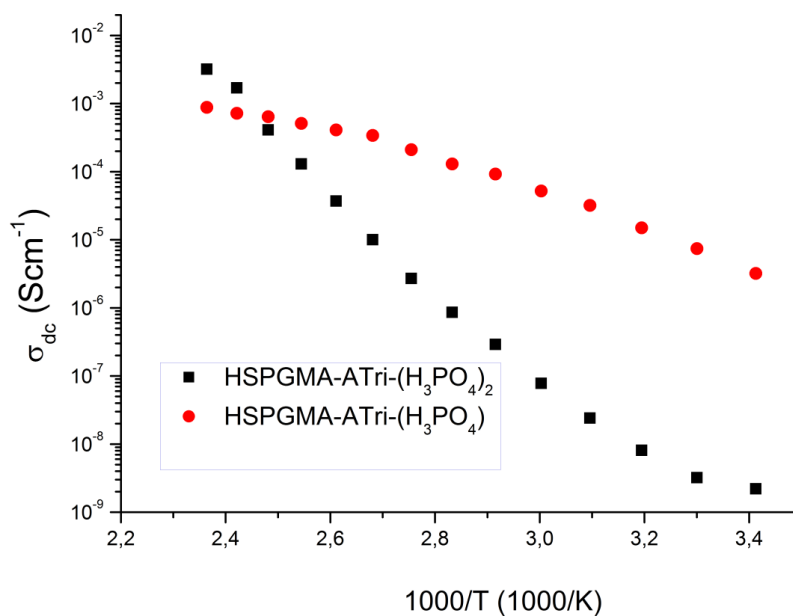
Figure 3.95 DC measurements of H_3PO_4 doped HSS-graft-PGMA (HSPGMA-ATri-H_3PO_4) composite membranes versus reciprocal temperature.

As clearly seen in Figure 3.95 proton conductivity of HSPGMA-ATri-$(H_3PO_4)_2$ was measured as 0.004 Scm^{-1} at 150 ^{o}C under anhydrous conditions. The phosphoric doping ratio of 5-Amino-Triazole functional HSPGMA is not impressed on proton conductivity, for HSPGMA-ATri-(H_3PO_4) proton conductivity was measured as 0.001 Scm^{-1} at 150 ^{o}C under anhydrous conditions.
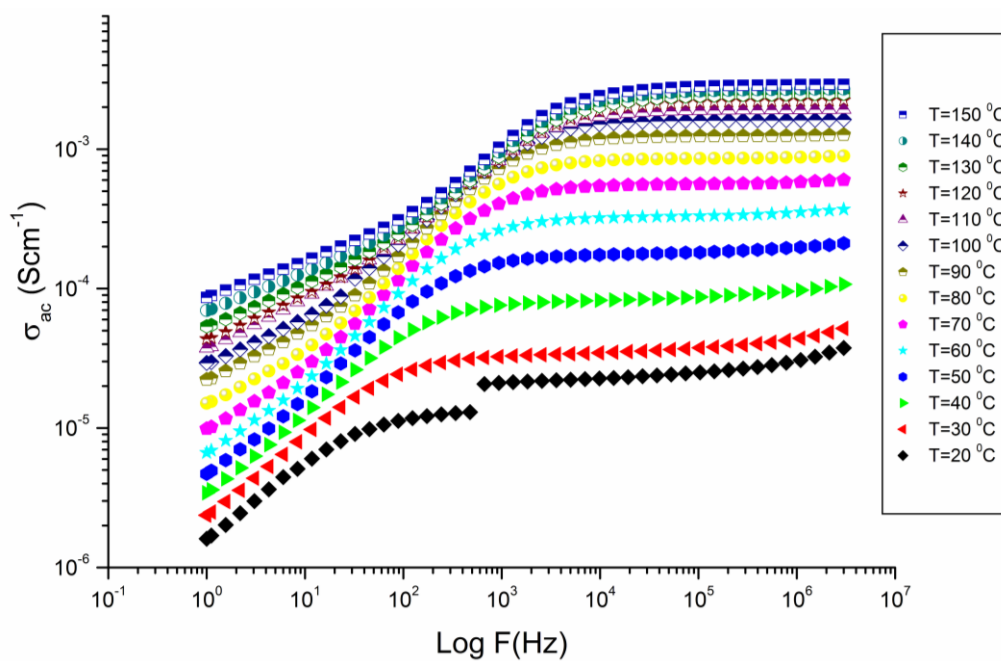
Figure 3.96 AC measurements of H_3PO_4 doped HSS-graft-PGMA (HSPGMA-ATet-H_3PO_4) composite membranes versus reciprocal temperature.
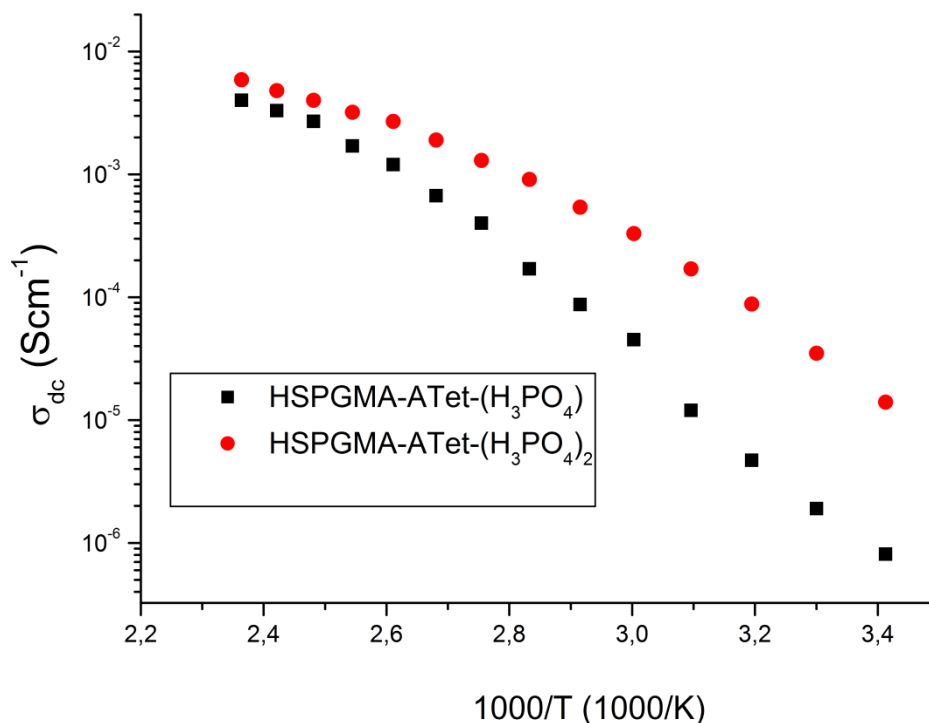
Figure 3.97 DC measurements of H_3PO_4 doped HSS-graft-PGMA (HSPGMA-ATet-H_3PO_4) composite membranes versus reciprocal temperature.

The proton conductivity of HSPGMA-Tet-$(H_3PO_4)_x$ composite membranes was compared in Figure 3.97. Among the phosphoric acid doped Amino-tetrazole functional HSS-graft-PGMA samples HSPGMA-Tet-$(H_3PO_4)_2$ showed the highest proton conductivityof 0.008 at 150 ^{o}C under anhydrous conditions.

Normally, there are two different transport mechanisms that contribute to the proton conductivity in phosphoric acid-doped polymer systems. The first is the structural diffusion (Grotthuss mechanism) in which the conductivity is mainly controlled by proton transport through phosphate ions, i.e. $H_4PO_4^+$, $H_2PO_4^-$ (Grotthuss proton transport). The second is the vehicle mechanism where the protons travel through the material on a neutral or charged "vehicle". Several studies were reported about the contribution of these mechanisms on the proton conductivity of pure phosphoric acid and it was indicated that the former is much more predominant and the conduction mechanism is mainly controlled by the structural diffusion rather than vehicle mechanism. In the current system, the presence of HPO_4^{2-} and

$H_2PO_4^-$ anions implies that the proton diffusion can also occur throughout these ionized species (Dippel, Kreuer et al. 1993).

It seems that the proton hopping from one N–H site to a free nitrogen may contribute to the conductivity of HSPGMA-Azole-$(H_3PO_4)_x$ systems as in the case of imidazole where the long range proton transfer occurs throughout the protonic defects, i.e., protons transport between protonated and unprotonated heterocyclic units (Kreuer 1996, Kreuer, Fuchs et al. 1998, Yan, Yu et al. 2009, Lin, Cheng et al. 2010). In addition, proton hopping from one N–H site to phosphate ions may also contribute to the conductivity.

In azole functional HSS-garft-PGMA systems, the doping of the phosphoric acid is highly effective on the proton conductivity of sample which indicates that major part of proton transport is provided over the H_3PO_4 as well as over azole units.

From the conductivity and FTIR results, it can be concluded that the host matrix, azole functional HSPGMA includes excess phosphoric acid without significant change in the mechanical properties and conductivity occur throughout the material predominantly by Grotthuss mechanism.

3.9 CHARACTERIZATION OF AZOL FUNCTIONAL SIO$_2$ NANOCOMPOSITE MEMBRANES

3.9.1 FTIR studies

FT-IR spectra of azole functional SiO_2 are represented in Fig. 3.98. The absorption peaks at 1132 cm^{-1} and 1045 cm^{-1} attributed to Si–O–Si asymmetric stretching . The peak at 3435 cm^{-1} belonged to Si–OH stretching vibration. A distinctive C=C stretching was displayed at about 1603 cm^{-1}. The following bands are well established to specific molecular motions that can be taken as the silica fingerprint (Cao and Fischer 1999, Won, Cho et al. 2009, Ma, Lee et al. 2010). The signals at 1220 and 1083 cm^{-1} belong to Si–O stretching. The band centered at 954 cm^{-1} is associated with the stretching mode of non-bridging oxide bands as Si–OH and Si–O. The band around at 795 cm^{-1} is assigned to the

symmetric stretching of the Si–O–Si mode. The lowest frequency modes (550 and 470 cm^{-1}) are associated with the rocking motions perpendicular to the Si–O–Si plane, of the oxygen bridging two adjacent Si atoms that formed the tetra or trisiloxane rings (Chuang, Hsu et al. 2007, Ma, Lee et al. 2010).

Figure 3.98 FT-IR spectra of the Tri-SiO$_2$, Tet-SiO$_2$ and Atri- SiO$_2$ composite membranes.

The absorption at 900 cm^{-1} is assigned to stretching vibration of the epoxy group which moved out on azole functionalization (Nanjundan, Unnithan et al. 2005). In the high energy region from 4000 up to 1800 cm^{-1}, the appearance of absorption bands correspond to stretching vibrations of OH, NH and CH$_2$ groups. The signals at 3328 and 3174 cm^{-1} are assigned to NH and OH modes from the ring and the amino groups. Several small bands between 2900 and 2600 cm^{-1} together with 1926 cm^{-1}, belong to aromatic and aliphatic CH modes. The broad band between 2700 and 2300 cm^{-1} has been assigned to an associated N–

H mode, intermolecular hydrogen bonded in the form of N–H···N hydrogen bonds. Azole functional SiO_2 exhibited a medium absorption at 1577 cm^{-1} and 1450 cm^{-1} due to C=N and C-N stretching of the triazole ring (Angell 1961). The bands below 1800 cm^{-1} are attributed to chains and ring skeletal vibrations of H–C–H, C O, H–N–H, C–N. The strong signal at 1630cm^{-1} is related to an in-plane deformation mode of NH_2 group, and the ones at 1604 and 1571 cm^{-1} to N–H vibration inplane and C O stretching. The series of five fairly strong absorptions between 1500 and 1300 cm^{-1} assigned to ring vibrations C-N single and double bonds, and also to a deformation mode of CH groups. Additionally except a new absorption at 1640 cm^{-1} coming from amine bending vibration.

The FTIR spectrum of azole functional SiO_2-PVPA composites show strong bands between 1040-910 cm^{-1} due to asymmetric stretching vibrations of the P-OH group. The peak at 1150 cm^{-1} corresponds to P=O stretching (Çelik et al., 2008: Goktepe et al. 2008). The P–O–H vibration at 930 cm^{-1} decreases as the PVPA ratio increases, indicating the existence of excess acidic protons. Additionally, phosphonic acid units give rise to broad bands with medium intensity between 1700-1590 cm^{-1} and 2850-2750 cm^{-1} region. The band at 918 cm^{-1} is ascribed to vibration of terminal SiOH groups. The broad and strong peak at about 1136 cm^{-1} is attributed to the overlapping of the combined results of the Si-O band vibrations and/or stretching in SiO_2 particles (Ou et al., 1997: Parler et al., 2001). Typical absorption peaks of SiO_2 (1100 and 466 cm^{-1}) did not only overlap by those of PVPA but also shifted to 972 and 440 cm^{-1}, respectively.
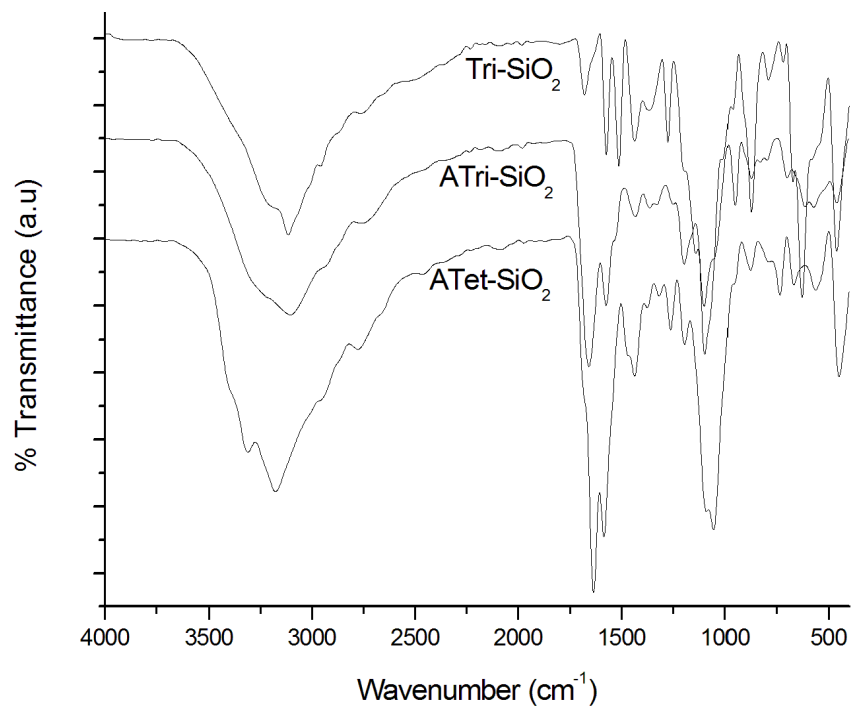
Figure 3.99 FT-IR spectra of the Azol Functional SiO_2-PVPA composite membranes.

3.9.2 SEM

In order to examine the microstructures and nanofiller distribution within the nanocomposites, SEM analysis was conducted. Typical surface SEM photographs of azole functional SiO_2-PVPA nanocomposite membranes were illustrated in Figure 3.98, Figure 3.100 and Figure 3.101. From Figure 3.100 it was observed that azole functional silica were homogenously dispersed and embedded in the PVPA matrix. Moreover, from these figures, it can be seen that PVPA beads and azole functional silica being well distributed throughout the matrix. This result is also consistent with the DSC curves of the impregnated membranes that has no separate T_g transition.
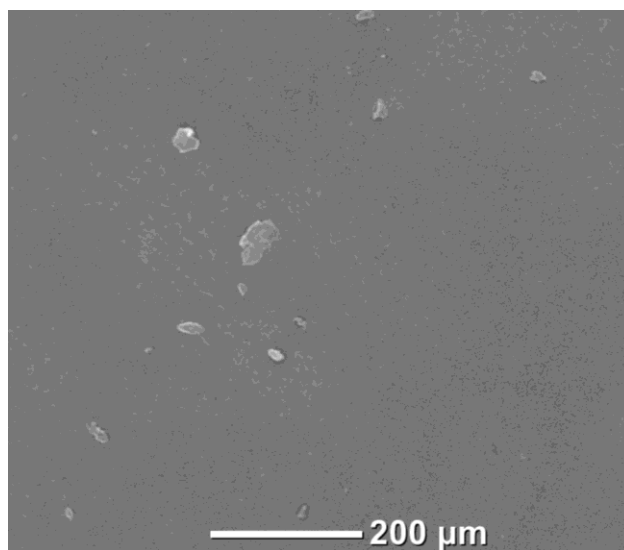
Figure 3.100 The SEM pictures of Tri-SiO$_2$, composite membranes.
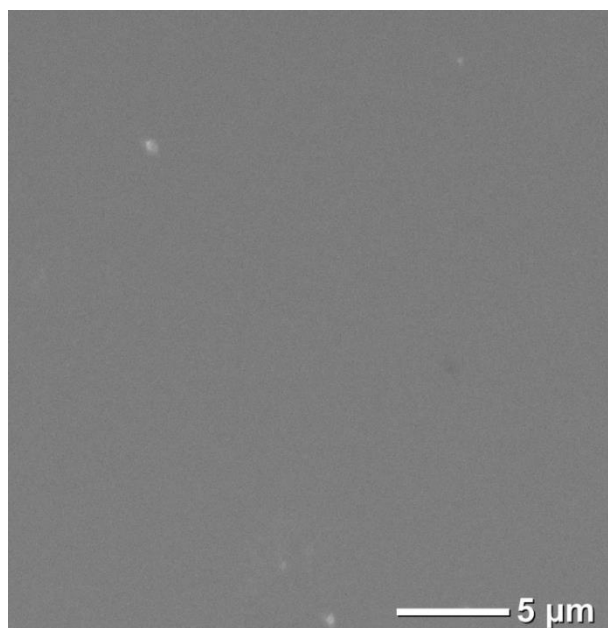
Figure 3.101 The SEM pictures of ATri-SiO$_2$ composite membranes.
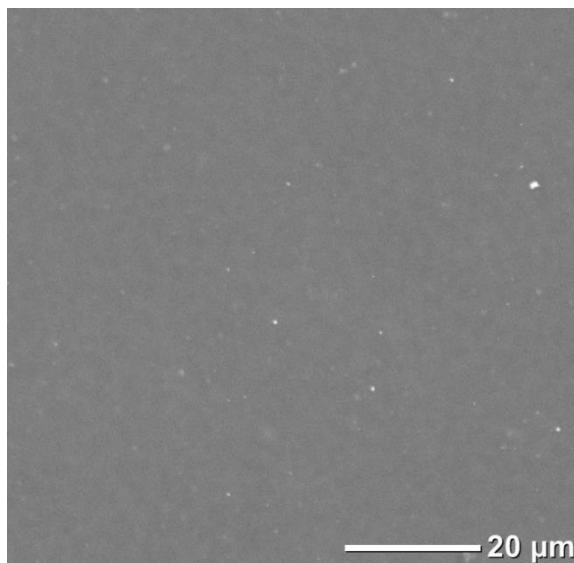
Figure 3.102 The SEM pictures of Tet-SiO$_2$ composite membranes.

3.9.4   Thermal analysis

The glass transition temperature, T_g of the Tri-SiO$_2$, Tet-SiO$_2$ and Atri- SiO$_2$ composite membranes were measured. Incorporation of Tri-SiO$_2$, Tet-SiO$_2$ and Atri- SiO$_2$ with pure Atri, TRi and Tet would fill the free volumes and would cause need to more energy for starting segmental motions, which would make Tg to increase. Table 3.10 shows the DSC curves of Tri, ATri and Atet functional samples under inert atmosphere at a scan rate of 10 ^{o}C/min. The melting points of pure Tri and ATri comopounds are 120 and 157 ^{o}C, respectively. The Tg of triazole functional SiO$_2$ (Tri-SiO$_2$) is around 122°C, Tg of 5-Amino-Triazole functional SiO$_2$ (ATri-SiO$_2$)is around 137 ^{o}C and Tg of Amino-tetrazole functional SiO$_2$ (Tet-SiO$_2$) is 162 ^{o}C. After functionalization on SiO$_2$ surface the Tg of the azolic units shifted to higher temperatures.

Table 3.10 Max. Proton conductivity and Tg (^{o}C) values for the all membranes.

Sample Name	Molar Ratio (mol/mol)	Tg ^{o}C	Max Conductivity (Scm^{-1})
Tri-SiO$_2$	-	122	2.1 x 10^{-5} (Scm^{-1}) at 150 ^{o}C
Atri- SiO$_2$	-	137	2.4 x 10^{-4} (Scm^{-1}) at 150 ^{o}C
Tet-SiO$_2$	-	162	1.3 x 10^{-4} (Scm^{-1}) at 150 ^{o}C
Tri-SiO$_2$-PVPA	1-1	103	1.9 x 10^{-4} (Scm^{-1}) at 150 ^{o}C
Tri-SiO$_2$-PVPA$_2$	1-2	90	8.7 x 10^{-4} (Scm^{-1}) at 150 ^{o}C
Atri- SiO$_2$-PVPA	1-1	80	1.1 x 10^{-4} (Scm^{-1}) at 150 ^{o}C
Atri- SiO$_2$-PVPA$_2$	1-2	63	0.007 (Scm^{-1}) at 150 ^{o}C
Tet-SiO$_2$-PVPA	1-1	88	1.3 x 10^{-4} (Scm^{-1}) at 150 ^{o}C
Tet-SiO$_2$-PVPA$_2$	1-2	76	0.003 (Scm^{-1}) at 150 ^{o}C

Figure 3.103 shows the thermograms of Tri-SiO$_2$, Tet-SiO$_2$ and Atri- SiO$_2$ TGA plots of weight loss versus temperature provide an estimate of the quantity of azol units from the nanoparticles. The functional particles consist of both thermally stable compounds that remain in the residue (silica bound to the azol units) and decomposable brushes and initiators that contribute to weight loss. After functionalization from the particle, TGA shows a total weight loss of 90%, which corresponds to azol units thickness of ∼100 nm. This thickness value agrees reasonably well with the TEM. Reaction of azol functionalization leads to a total weight loss of approximately 90%, which is consistent with essentially complete functionalization between azolic units and silica nano particles. After 250°C a remarkable weight loss derives from the thermal decomposition of the azolic units.
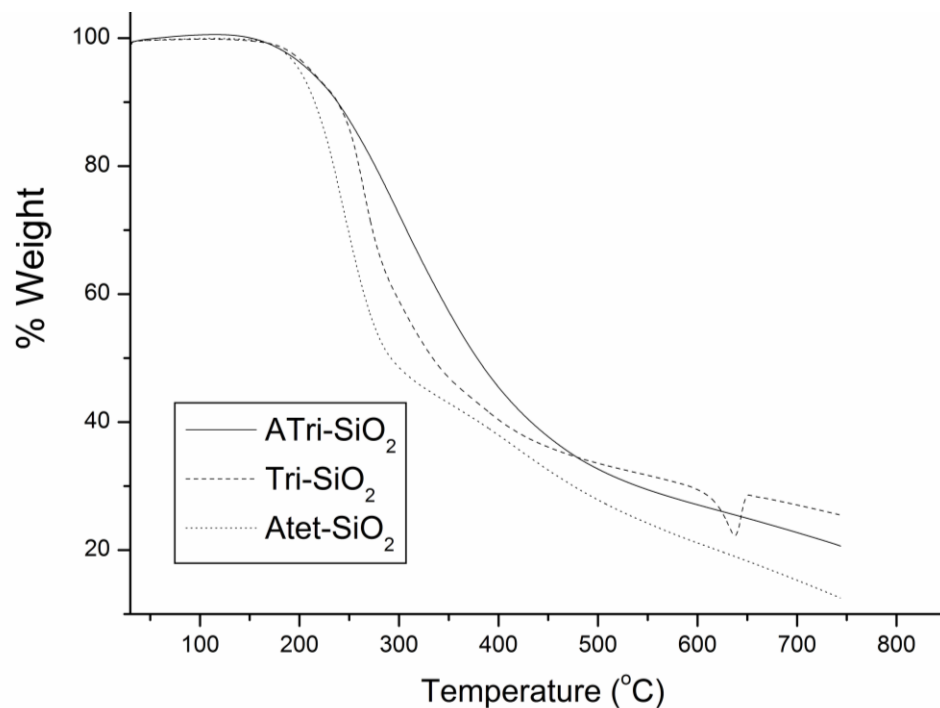
Figure 3.103 TG thermograms of Azol functional SiO_2 recorded at a heating rate of 10 ^{o}C/min under a nitrogen atmosphere.

3.9.7 Proton conductivity

The alternating current (AC) conductivities, σ_{ac} (ω) of the polymers were measured at several temperatures using impedance spectroscopy. The proton conductivities of anhydrous samples were measured from 20 ^{o}C to 150 ^{o}C.
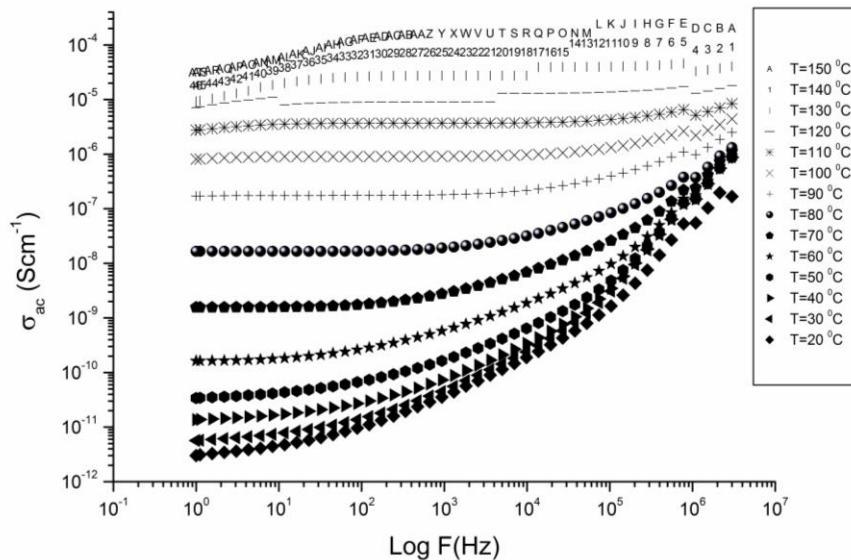
Figure 3.104 AC conductivity of 5-Amino-1,2,4-Triazol functional SiO_2 (ATri-SiO_2) composite membranes
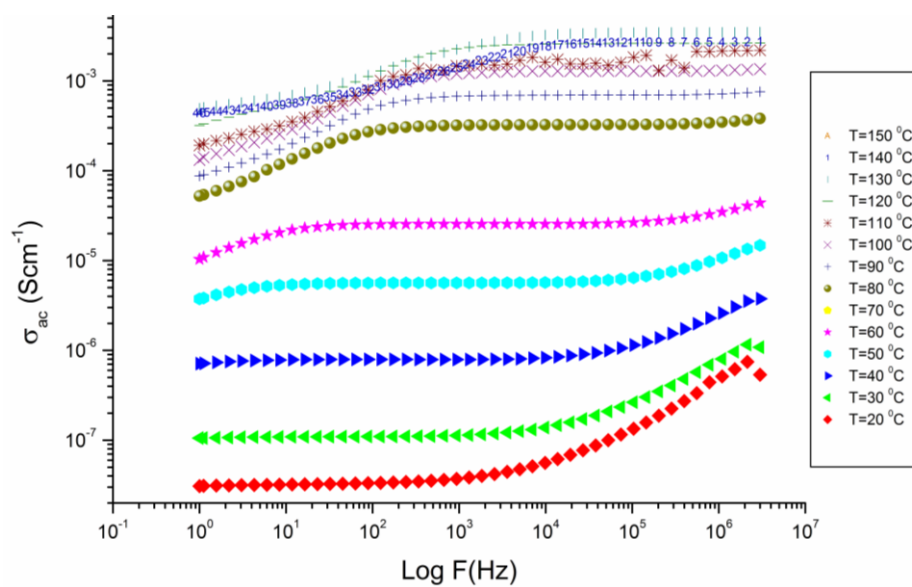
Figure 3.105 AC conductivity of 5-Amino Tetrazol functional SiO_2 (Tet-SiO_2-PVPA) composite membranes.

The AC proton conductivity of composite membranes were showed in Figure 3.104 and Figure 3.105. Among the azol functional SiO_2-PVPA composite membranes showed the highest proton conductivityof 0.008 at 150 ^oC under anhydrous conditions.

Normally, there are two different transport mechanisms that contribute to the proton conductivity in phosphoric acid-doped polymer systems. The first is the structural diffusion (Grotthuss mechanism) in which the conductivity is mainly controlled by proton transport through phosphate ions (Grotthuss proton transport). The second is the vehicle mechanism where the protons travel through the material on a neutral or charged "vehicle". Several studies were reported about the contribution of these mechanisms on the proton conductivity of pure phosphoric acid and it was indicated that the former is much more predominant and the conduction mechanism is mainly controlled by the structural diffusion rather than vehicle mechanism.

It seems that the proton hopping from one N–H site to a free nitrogen may contribute to the conductivity of Azol-SiO_2-PVPA systems as in the case of imidazole where the long range proton transfer occurs throughout the protonic defects, i.e., protons transport between protonated and unprotonated heterocyclic units (Kreuer 1996, Kreuer, Fuchs et al. 1998, Yan, Yu et al. 2009, Lin, Cheng et al. 2010). In addition, proton hopping from one N–H site to phosphate ions may also contribute to the conductivity.

In azole functional Azol-SiO_2 systems, the PVPA ratio highly effective on the proton conductivity of sample which indicates that major part of proton transport is provided over the phosphonic acid units as well as over azole units.

From the conductivity and FTIR results, it can be concluded that the host matrix, azole functional Azol-SiO_2-PVPA composites include excess phosphonic acid without significant change in the mechanical properties and conductivity occur throughout the material predominantly by Grotthuss mechanism

.

CHAPTER 4

CONCLUSIONS

The composite membranes of SiO_2 nanoparticles and PVPA were produced by free radical polymerization. FTIR spectroscopy confirmed that the interaction existed between PVPA and SiO_2. TG analysis showed that the samples are thermally stable up to approximately 200 °C. DSC results illustrated that the Tg of the materials shifted to lower temperatures with increasing SiO_2 content. The AFM study suggests that bigger granules increases RMS roughness, hence it causes to increase effective area of the surface of the membranes. In the anhydrous state, the proton conductivity of PVPA(10)SiO_2 (*in situ*) was found to be 0.009 Scm^{-1} at 120°C. The proton conductivity of PVPA(x)SiO_2 was increased at 50 % relative humidity and reached to 0.08 (Scm^{-1}) for x=10 and 0.007 (Scm^{-1}) for x=15 at 100 ^{o}C. The proton conductivity of PVPA(10)SiO_2 approached to that of humidified Nafion117 membrane at 40 ^{o}C and at the same humidification level. In dried samples, the proton diffusion is expected to occur by the transport of the protons through phosphonic acid units up to certain threshold composition of PVPA. After humidification, the synthesized nanocomposite polymers can be suggested for application in proton exchange membrane fuel cells (PEMFC).

The composite membranes of TiO_2 nanoparticles and PVPA were produced. by free radical polymerization. FTIR spectroscopy confirmed that the interaction existed between PVPA and TiO_2. TG analysis showed that the samples are thermally stable up to approximately 200 °C. DSC results illustrated that the Tg of the materials shifted to higher

temperatures with increasing TiO_2 content. In the anhydrous state, the proton conductivity of PVPA(10)TiO_2 (*in situ*) was found to be 0,004 Scm^{-1} at 120°C. The proton conductivity of is approached to PVPA(10)TiO_2 that of humidified Nafion117 membrane at 40 °C and at the humidified conditions. In this system, the proton diffusion is expected to occur by the transport of the protons through phosphonic acid units up to certain threshold composition of PVPA. The synthesized nano composite polymers can be suggested for application in polymer electrolyte membrane fuel cells (PEMFC).

The composite membranes from sulfated nano-titania and PVPA were produced. FTIR spectroscopy confirmed the existence of complexation between the modified inorganic nanoparticle and host polymer matrix. TG analysis showed that sulfated nano-titania inhibited anhydride formation increasing the thermal stability up to approximately 200 °C. DSC results illustrated that the T_g of the materials shifted to higher temperatures with increasing sulfated nano-titania ratio due to complexation. In the anhydrous state, the proton conductivity of PVPATS$_x$ was found to be 0.03 Scm^{-1} at 150°C. In dried samples, the proton diffusion is expected to occur by the transport of the protons through phosphonic acid units up to certain threshold composition of PVPA. The synthesized nanocomposite polymers can be suggested for application in polymer electrolyte membrane fuel cells (PEMFC).

The composite membranes from sulfated nano-titania and Nafion were produced. FTIR spectroscopy confirmed the existence of complexation between the modified inorganic nanoparticle and host matrix. TG analysis showed that sulfated nano-titania inhibited anhydride formation increasing the thermal stability up to approximately 300 °C. DSC results illustrated that the T_g of the materials shifted to higher temperatures with increasing sulfated nano-titania ratio due to complexation. In the anhydrous state, the proton conductivity of Nafion-TS$_x$ was found to be 0.03 Scm^{-1} at 150°C. In dried samples, the proton diffusion is expected to occur by the transport of the protons through sulfonic acid units up to certain threshold composition of Nafion. The synthesized nanocomposite polymers can be suggested for application in polymer electrolyte membrane fuel cells (PEMFC).

The P(VTri)-TS-P(VPA)$_x$ nanocomposite membranes were produced and their physical properties discussed. The host polymers, Poly(1-vinyl-1,2,4-triazole), P(VTri) and poly(vinyl phosphonic acid), P(VPA) were produced by free radical polymerization of the corresponding monomers. Sulfated nanotitania is more effective for proton conductivity than unmodified nano-titania so that polymer/sulfated nano-titania composite membranes were prepared. The thin films were produced by mixing of P(VPA) with P(VTri)-TS at various concentrations to get P(VTri)-TS-P(VPA)$_x$. FT-IR analysis confirmed the interaction between sulfonic acid units of TS and phosphonic acid units of P(VPA). According to XRD results the crystallite size of the sulfated nano-titania, embeded in P(VTri), was around 10 nm. TG analysis of the nanocomposite membranes showed that the presence of TS inhibited the anhydride formation and shifted the thermally stability up to at approximately 300 $^{\circ}$C. DSC and SEM results illustrated the homogeneity of the nanocomposite materials. In the anhydrous state, the proton conductivity of P(VTri)-TS-P(VPA)$_4$ was 0.003 at 150 $^{\circ}$C. The nanocomposite membranes could be suggested for application in proton exchange membrane fuel cells (PEMFC).

The composite membranes of PVA and bifunctional nanotitania were produced. FT-IR data confirmed the formation of super acid and the strong interaction between the modified inorganic nanoparticle and host polymer matrix. Water uptake study showed that water uptake increased with decreasing NMPA content. The TGA results verified that the presence of sulfated nano-titania in the composite membranes enhanced thermal stability up to approximately 250 $^{\circ}$C. DSC results illustrated that the T$_g$ of the materials shifted to lower temperatures with increasing NMPA content. In the anhydrous state, the proton conductivity of PVA-TS-NMPA was found to be 0.003 Scm^{-1} at 150°C. In dried samples, the proton diffusion is expected to occur by the transport of the protons through phosphonic acid units up to a certain threshold composition of NMPA. The synthesized composite materials have ability to form free standing films with improved mechanical strengths, and therefore, can be suggested for use in proton exchange membrane fuel cell (PEMFC) applications.

The nanocomposite membrane materials were prepared by mechanical mixing of SPSU and NMPA. FTIR spectroscopy confirmed the existence of complexation between

the modified inorganic nanoparticle and host polymer matrix. Water uptake study showed that water uptake increased with decreasing NMPA content due to interaction between phosphonic acid units of NMPA and nanotitania surface. The TG results proved that the nanocomposites membranes thermally stable up to 270°C. DSC results showed that NMPA has softening effect in the membrane materials. In the anhydrous state, the proton conductivity of SPSU-TS-NMPA was found to be 0.002 Scm^{-1} at 150°C. . These composite membranes better physicochemical properties can be suggested for application in polymer electrolyte membrane fuel cells (PEMFC).

The azole functional hollow silica spheres graft poly(glycidyl methacrylate) polymers have been synthesized via two-step methods. HSS was synthesized with hydrolysis of phenyltrimethoxysilane and grafting of Poly(glycidyl methacrylate) on HSS surface was produced by free radical polymerization of GMA. Azole units were immobilized by ring opening of the epoxide ring. Elemental analysis verified azole immobilization about 80 %. The structures of the azole functional PGMA-g-HSS were proved by FT-IR. DSC and SEM results illustrated the homogeneity of the materials. Anhydrous proton conducting properties and thermal properties functional and phosphoric acid doped HSPGMA were investigated. The proton conductivity of the materials increased with phosphoric acid and the temperature. Phosphoric acid doped polymers showed lower Tg values. HSPGMA-Tri-$(H_3PO_4)_2$, HSPGMA-ATri-$(H_3PO_4)_2$, and HSPGMA-Tet-$(H_3PO_4)_2$, showed a maximum water-free proton conductivity of approximately 0.004 Scm^{-1} at 150 ^{0}C, 0.006 Scm^{-1} and 0.008 Scm^{-1} at 150 ^{0}C. Azole functional HSS-g-PGMA membranes can be suggested for application in high temperature polymer electrolyte membrane fuel cells (PEMFC).

The azole functional silica nanoparticles have been synthesized via two-step methods. Silica was synthesized with Scthöber method of TEOS and funcionalized with azol units on silica surface was produced. Azole units were immobilized by ring opening of the epoxide ring. The back titration method was used o determined functionalization. The structures of the azole functional silica were proved by FT-IR. DSC and SEM results illustrated the homogeneity of the materials. Anhydrous proton conducting properties and thermal properties functional materials and PVPA composites were investigated. The proton

conductivity of the Tri-SiO$_2$-PVPA, Tet-SiO$_2$-PVPA and Atri-SiO$_2$-PVPA composite membranes increased with phosphonic acid and the temperature. Azol functional SiO$_2$-PVPA composites showed lower Tg values. Tri-SiO$_2$-PVPA, Tet-SiO$_2$PVPA and Atri-SiO$_2$-PVPA composite membranes showed a maximum water-free proton conductivity of approximately 0.004 Scm^{-1} at 150 ^{0}C, 0.006 Scm^{-1} and 0.008 Scm^{-1} at 150 ^{0}C. Azole functional SiO$_2$-PVPA membranes can be suggested for application in high temperature polymer electrolyte membrane fuel cells (PEMFC).

In this thesis proton conductive nnanocomposite membranes were synthesized with sol-gel and free radical polymerization methods. As expected high proton conductivities were obtained in these studies. The proton transport is explained with Grotthuss mechanism and presence of functional nano particles also contributes the proton conduction which was clearly observed in polymer/nano particles systems. Although pure nano particles have low proton conductivity, it increases with functionalization of nanoparticles due to the increase interaction between functional groups of nanoparticles and polymers. Membrane formability and mechanical stability is very important in fuel cell application and we faced shrinkage problem when we used thin membranes. Therefore these matrices should be converted into thin and nonporous films with more efficient methods.

REFERENCES

Abu-Thabit, N. Y., S. A. Ali and S. M. J. Zaidi, "New highly phosphonated polysulfone membranes for PEM fuel cells.", *Journal of Membrane Science,* Vol. 360(1-2): pp. 26-33, 2010.

Acar, O., U. Sen, A. Bozkurt and A. Ata. "Proton conducting membranes based on Poly(2,5-benzimidazole) (ABPBI)-Poly(vinylphosphonic acid) blends for fuel cells." *International Journal of Hydrogen Energy* Vol. 34(6): pp. 2724-2730, 2009.

Ahmad, Z., M. I. Sarwar and J. E. Mark. "Thermal and mechanical properties of aramid-based titania hybrid composites." *Journal of Applied Polymer Science* Vol. 70(2): pp. 297-302, 1998.

Alahmadi, S. M., S. Mohamad and M. J. Maah "Synthesis and Characterization of Mesoporous Silica Functionalized with Calixarene Derivatives." *Int J Mol Sci* Vol. 13(10) pp. 13726-13736, 2012.

Alberti, G., M. Casciola, M. Pica, T. Tarpanelli and M. Sganappa. "New preparation methods for composite membranes for medium temperature fuel cells based on precursor solutions of insoluble inorganic compounds." *Fuel Cells* Vol. 5(3) pp. 366-374, 2005.

Angell, C. L. "100. An infrared spectroscopic investigation of nucleic acid constituents." *Journal of the Chemical Society* (Resumed)(0): pp. 504-515, 1961.

Arata, K. and M. Hino. "Preparation Of Superacids By Metal-Oxides And Their Catalytic Action." *Materials Chemistry and Physics,* Vol. 26(3-4): pp. 213-237, 1990.

Aslan, A., S. U. Celik and A. Bozkurt "Proton-conducting properties of the membranes based on poly(vinyl phosphonic acid) grafted poly(glycidyl methacrylate)" *Solid State Ionics* Vol. 180: pp. 1240–1245, 2009

Aslan, A. and A. Bozkurt. "Development and characterization of polymer electrolyte membranes based on ionical cross-linked poly(1-vinyl-1,2,4 triazole) and poly(vinylphosphonic acid)." *Journal of Power Sources,* Vol. 191(2): pp. 442-447, 2009.

Aslan, A. and A. Bozkurt. "Bioinspired Blend Membranes Based on Adenine and Guanine Functional Poly(glycidyl methacrylate)." *Langmuir*, Vol. 26(16): pp. 13655-13661, 2010.

Aslan, A. and A. Bozkurt, "Proton conducting properties of ionically cross-linked poly(1-vinyl-1,2,4 triazole) and poly(2-acrylamido-2-methyl-1-propanesulfonic acid) electrolytes." *Polymer Bulletin,* Vol. 66(8), pp. 1099-1110, 2011.

Aslan, A. and A. Bozkurt (2012). "Nanocomposite polymer electrolyte membranes based on poly (vinylphosphonic acid)/sulfated nano-titania." *Journal of Power Sources,* Vol. 217, pp. 158-163.

Aslan, A And A. Bozkurt. "Nanocomposite Polymer Electrolytes Membranes Based On Poly(Vinylphosphonic Acid)/TiO2." *Journal Of Materials Research,* Vol. 27(24), 3091-309,2012

Aslan, A., K. Golcuk And A. Bozkurt. "Nanocomposite Polymer Electrolytes Membranes Based On Poly(Vinylphosphonic Acid)/SiO2." *Journal Of Polymer Research,* Vol. 19(12), 2012.

Aslan, A. And A. Bozkurt "An investigation of proton conductivity of nanocomposite membranes based on sulfated nano-titania and polymer" *Solid State Ionics* Vol. 239, pp. 21–27, 2013.

Aslan, A. And A. Bozkurt "Nanocomposite membranes based on sulfonated polysulfone and sulfated nano-titania/NMPA for proton exchange membrane fuel cells" *Solid State Ionics* Vol. 255: pp. 89–95, 2014

Aslan, A., S. U. Celik, U. Sen, R. Haser and A. Bozkurt. "Intrinsically proton-conducting poly(1-vinyl-1,2,4-triazole)/triflic acid blends." *Electrochimica Acta,* Vol. 54(11) pp. 2957-2961 2009.

Baglio, V., A. S. Arico, A. Di Blasi, V. Antonucci, P. L. Antonucci, S. Licoccia, E. Traversa and F. S. Fiory. "Nafion-TiO2 composite DMFC membranes: physico-chemical properties of the filler versus electrochemical performance." *Electrochimica Acta,* Vol. 50(5), pp. 1241-1246, 2005.

Baglio, V., A. S. Arico, A. Di Blasi, V. Antonucci, P. L. Antonucci, S. Licoccia, E. Traversa and F. S. Fiory. "Nafion-TiO2 composite DMFC membranes: physico-chemical properties of the filler versus electrochemical performance." *Electrochimica Acta,* Vol. 50(5) pp.1241-1246, 2005.

Balazs, A. C., T. Emrick and T. P. Russell. "Nanoparticle polymer composites: Where two small worlds meet." *Science,* Vol. 314(5802) pp. 1107-1110, 2006.

Bao, C., M. G. Ouyang and B. L. Yi. "Analysis of the water and thermal management in proton exchange membrane fuel cell systems." *International Journal of Hydrogen* Energy, Vol. 31(8) pp. 1040-1057, 2006.

Barbir, F. and T. Gómez. "Efficiency and economics of proton exchange membrane (PEM) fuel cells." *International Journal of Hydrogen Energy,* Vol. 21(10) pp. 891-901, 1996.

Bingol, B., W. H. Meyer, M. Wagner and G. Wegner, "Synthesis, microstructure, and acidity of poly (vinylphosphonic acid)." *Macromolecular Rapid Communications,* Vol. 27(20) pp. 1719-1724, 2006.

Boroglu, M. S., S. U. Celik, A. Bozkurt and I. Boz. "The synthesis and characterization of anhydrous proton conducting membranes based on sulfonated poly(vinyl alcohol) and imidazole." *Journal of Membrane Science*, Vol. 375(1-2) pp. 157-164 2011.

Boroglu, M. S., S. U. Celik, A. Bozkurt And I. Boz, "The Synthesis And Characterization Of Anhydrous Proton Conducting Membranes Based On Sulfonated Poly(Vinyl Alcohol) And Imidazole." *Journal Of Membrane Science,* Vol. **375**(1-2) pp. 157-164, 2011.

Bozkurt, A., M. Ise, K. D. Kreuer, W. H. Meyer and G. Wegner. "Proton-conducting polymer electrolytes based on phosphoric acid." *Solid State Ionics* Vol. 125(1-4) pp. 225-233, 1999.

Bozkurt, A., W. H. Meyer and G. Wegner. "PAA/imidazol-based proton conducting polymer electrolytes." *Journal of Power Sources* Vol. 123(2): pp. 126-131.

Cao, X. and G. Fischer (1999). "New infrared spectra and the tautomeric studies of purine and αl-alanine with an innovative sampling technique." *Spectrochimica Acta Part A: Molecular and Biomolecular Spectroscopy* Vol. 55(11) pp. 2329-2342 1993.

Carbone, A., A. Sacca, I. Gatto, R. Pedicini And E. Passalacqua, "Investigation On Composite S-PEEK/H-BETA Meas For Medium Temperature PEFC." International Journal Of Hydrogen Energy Vol. **33**(12): pp.3153-3158, 2008.

Casciola, M., G. Alberti, M. Sganappa and R. Narducci. "On the decay of Nafion proton conductivity at high temperature and relative humidity." *Journal of Power Sources* Vol. 162(1), pp. 141-145, 2006.

Caseri, W. R., "Nanocomposites of polymers and inorganic particles: preparation, structure and properties." *Materials Science and Technology,* Vol. 22(7) pp. 807-817, 2006.

Celik, S. U., A. Aslan and A. Bozkurt, "Phosphoric acid-doped poly(1-vinyl-1,2,4-triazole) as water-free proton conducting polymer electrolytes." *Solid State Ionics* Vol. 179(19-20), pp. 683-688, 2008.

Celik, S. U., A. Bozkurt and S. S. Hosseini. "Alternatives toward proton conductive anhydrous membranes for fuel cells: Heterocyclic protogenic solvents comprising polymer electrolytes." *Progress in Polymer Science* Vol. 37(9) pp. 1265-1291, 2012.

Celik, S. U., U. Akbey, R. Graf, A. Bozkurt and H. W. Spiess (). "Anhydrous proton-conducting properties of triazole-phosphonic acid copolymers: a combined study with MAS NMIR." *Physical Chemistry Chemical Physics* Vol. 10(39) pp. 6058-6066, 2008.

Cendoya, I., D. Lopez, A. Alegria and C. Mijangos . "Dynamic mechanical and dielectrical properties of poly(vinyl alcohol) and poly(vinyl alcohol)-based nanocomposites." *Journal of Polymer Science Part B-Polymer Physics* Vol. 39(17), pp. 1968-1975, 2001.

Chalkova, E., M. B. Pague, M. V. Fedkin, D. J. Wesolowski And S. N. Lvov. "Nafion/Tio2 Proton Conductive Composite Membranes For Pemfcs Operating At Elevated Temperature And Reduced Relative Humidity." *Journal Of The Electrochemical Society* Vol. **152**(6) pp. A1035-A1040, 2005.

Chen, S. Y., C. C. Han, C. H. Tsai, J. Huang and Y. W. Chen-Yang. "Effect of morphological properties of ionic liquid-templated mesoporous anatase TiO2 on performance of PEMFC with Nafion/TiO$_2$ composite membrane at elevated temperature and low relative humidity." *Journal of Power Sources* Vol. 171(2) pp. 363-372, 2007.

Chen, S. Y., C. C. Han, C. H. Tsai, J. Huang and Y. W. Chen-Yang. "Effect of morphological properties of ionic liquid-templated mesoporous anatase TiO2 on performance of PEMFC with Nafion/TiO2 composite membrane at elevated temperature and low relative humidity." *Journal of Power Sources* Vol. 171(2) pp. 363-372, 2007.

Cho, S. A., E. A. Cho, I. H. Oh, H. J. Kim, H. Y. Ha, S. A. Hong and J. B. Ju. "Surface modified Nafion((R)) membrane by ion beam bombardment for fuel cell applications." *Journal of Power Sources* Vol. 155(2) pp. 286-290, 2006.

Chuang, S.-W., S. L.-C. Hsu and Y.-H. Liu. "Synthesis and properties of fluorine-containing polybenzimidazole/silica nanocomposite membranes for proton exchange membrane fuel cells." *Journal of Membrane Science* Vol. 305(1-2) pp. 353-363, 2006.

Chuang, S.-W., S. L.-C. Hsu and Y.-H. Liu. "Synthesis and properties of fluorine-containing polybenzimidazole/silica nanocomposite membranes for proton exchange membrane fuel cells." *Journal of Membrane Science* Vol. 305(1-2) pp. 353-363, 2007.

Croce, F., G. B. Appetecchi, L. Persi and B. Scrosati, "Nanocomposite polymer electrolytes for lithium batteries." *Nature* Vol. 394(6692) pp. 456-458, 1998.

Daniliuc, L., C. Dekesel and C. David. "Intermolecular Interactions In Blends Of Poly(Vinyl Alcohol) With Poly(Acrylic Acid) .1. Ftir And Dsc Studies." *European Polymer Journal* Vol. 28(11) pp. 1365-1371, 1992.

Deimede, V. A., K. V. Fragou, E. G. Koulouri, J. K. Kallitsis and G. A. Voyiatzis. "Miscibility behavior of polyamide 11/sulfonated polysulfone blends using thermal and spectroscopic techniques." Polymer Vol. 41(26) pp. 9095-9101, 2000.

Deng, J. G., X. B. Ding, W. C. Zhang, Y. X. Peng, J. H. Wang, X. P. Long, P. Li and A. S. C. Chan. "Carbon nanotube-polyaniline hybrid materials." *European Polymer Journal* Vol. 38(12) pp. 2497-2501, 2002.

Devrim, Y., S. Erkan, N. Bac and I. Eroglu (2009). "Preparation and characterization of sulfonated polysulfone/titanium dioxide composite membranes for proton exchange membrane fuel cells." *International Journal of Hydrogen Energy* Vol. 34(8) pp. 3467-3475.

Devrim, Y., S. Erkan, N. Baç And I. Eroğlu. "Preparation And Characterization Of Sulfonated Polysulfone/Titanium Dioxide Composite Membranes For Proton Exchange Membrane Fuel Cells." *International Journal Of Hydrogen Energy* Vol. **34**(8) pp. 3467-3475, 2009.

Dippel, T., K. D. Kreuer, J. C. Lassègues and D. Rodriguez. "Proton conductivity in fused phosphoric acid; A 1H/31P PFG-NMR and QNS study." *Solid State Ionics* Vol. 61(1–3) pp. 41-46 1993.

Eikerling, M., A. A. Kornyshev, A. M. Kuznetsov, J. Ulstrup and S. Walbran (). "Mechanisms of proton conductance in polymer electrolyte membranes." *Journal of Physical Chemistry B* Vol. 105(17) pp. 3646-3662, 2001.

Gasa, J. V., S. Boob, R. A. Weiss and M. T. Shaw. "Proton-exchange membranes composed of slightly sulfonated poly(ether ketone ketone) and highly sulfonated crosslinked polystyrene particles." *Journal of Membrane Science* Vol. 269(1-2) pp. 177-186, 2006.

Godovsky, D. Y. Device applications of polymer-nanocomposites. Biopolymers/Pva Hydrogels/Anionic Polymerisation Nanocomposites. A. Abe. *Berlin, Springer-Verlag Berlin.* Vol. 153, pp.163-205, 2000.

Goktepe, F., S. U. Celik and A. Bozkurt "Preparation and the proton conductivity of chitosan/poly(vinyl phosphonic acid) complex polymer electrolytes." *Journal of Non-Crystalline Solids* Vol. 354(30) pp. 3637-3642, 2008.

Gosalawit, R., S. Chirachanchai, S. Shishatskiy And S. P. Nunes. "Sulfonated Montmorillonite/Sulfonated Poly(Ether Ether Ketone) (SMMT/SPEEK) Nanocomposite Membrane For Direct Methanol Fuel Cells (Dmfcs)." *Journal Of Membrane Science* Vol. **323**(2) pp. 337-346, 2008.

Gubler, L., D. Kramer, J. Belack, O. Uensal, T. J. Schmidt and G. G. Scherer. "Celtec-V - A polybenzimidazole-based membrane for the direct methanol fuel cell." *Journal of the Electrochemical Society* Vol. 154(9) pp. B981-B987, 2007.

Hagihara, H., H. Uchida And M. Watanabe. "Preparation Of Highly Dispersed Sio2 And Pt Particles In Nafion (R) 112 For Self-Humidifying Electrolyte Membranes In Fuel Cells." *Electrochimica Acta* Vol. **51**(19): pp. 3979-3985, 2006.

Hah, H. J., J. S. Kim, B. J. Jeon, S. M. Koo And Y. E. Lee. "Simple Preparation Of Monodisperse Hollow Silica Particles Without Using Templates." *Chemical Communications* Vol. (14): pp. 1712-1713, 2003.

Hino, M. And K. Arata. "Reactions Of Butane And Isobutane Catalyzed By Titanium-Oxide Treated With Sulfate Ion - Solid Superacid Catalyst." *Journal Of The Chemical Society-Chemical Communications* Vol. (24): pp. 1148-1149, 1979.

Hino, M. And K. Arata. "Solid Catalysts Treated With Anions - Synthesis Of Solid Superacid Catalyst With Acid Strength Of H0 Less-Than-Or-Equal-To-16.04." *Journal Of The Chemical Society-Chemical Communications* Vol. (18): pp. 851-852, 1980.

Hirose, S., T. Hatakeyama, Y. Izuta and H. Hatakeyama. "TG-FTIR studies on lignin-based polycaprolactones." *Journal of Thermal Analysis and Calorimetry* Vol. 70(3): pp. 853-860, 2002.

Hogarth, W. H. J., J. C. D. da Costa and G. Q. Lu. "Solid acid membranes for high temperature (> 140 degrees C) proton exchange membrane fuel cells." *Journal of Power Sources* Vol. 142(1-2) pp. 223-237, 2005.

Jalani, N. H., K. Dunn and R. Datta. "Synthesis and characterization of Nafion (R)-MO2 (M = Zr, Si, Ti) nanocomposite membranes for higher temperature PEM fuel cells." *Electrochimica Acta* Vol. 51(3): pp. 553-560, 2005.

Jiang, X. C., T. Herricks and Y. N. Xia. "Monodispersed spherical colloids of titania: Synthesis, characterization, and crystallization." *Advanced Materials* Vol. 15(14): pp. 1205, 2003.

Jin, Y., S. Qiao, J. C. D. da Costa, B. J. Wood, B. P. Ladewig and G. Q. Lu . "Hydrolytically stable phosphorylated hybrid silicas for proton conduction." *Advanced Functional Materials* Vol. 17(16): pp. 3304-3311,2007.

Jun, Y., H. Zarrin, M. Fowler And Z. Chen. "Functionalized Titania Nanotube Composite Membranes For High Temperature Proton Exchange Membrane Fuel Cells." *International Journal Of Hydrogen Energy* Vol. **36**(10): pp. 6073-6081, 2011.

Kaltbeitzel, A., S. Schauff, H. Steininger, B. Bingoel, G. Brunklaus, W. H. Meyer and H. W. Spiess "Water sorption of poly(vinylphosphonic acid) and its influence on proton conductivity." *Solid State Ionics* Vol. 178 (7-10): pp. 469-474, 2007.

Kickelbick, G. "Concepts for the incorporation of inorganic building blocks into organic polymers on a nanoscale." *Progress in Polymer Science* Vol. 28(1): pp. 83-114, 2003.

Kim, J.-D., T. Mori, S. Hayashi and I. Honma. "Anhydrous proton-conducting properties of Nafion-1,2,4-triazole and Nafion-benzimidazole membranes for polymer electrolyte fuel cells." *Journal of the Electrochemical Society* Vol. 154(4): pp. A290-A294, 2007.

Kobayashi, T., M. Rikukawa, K. Sanui and N. Ogata "Proton-conducting polymers derived from poly(ether-etherketone) and poly(4-phenoxybenzoyl-1,4-phenylene)." Solid State Ionics Vol. 106(3–4): pp. 219-225, 1998.

Kreuer, K. D. "On the development of proton conducting polymer membranes for hydrogen and methanol fuel cells." *Journal of Membrane Science* Vol. 185(1): pp. 29-39, 2009.

Kreuer, K. D., A. Fuchs, M. Ise, M. Spaeth and J. Maier. "Imidazole and pyrazole-based proton conducting polymers and liquids." Electrochimica Acta Vol. 43(10–11): pp. 1281-1288, 1998.

Kreuer, K.-D. "Proton Conductivity: Materials and Applications." *Chemistry of Materials* Vol. 8(3): pp. 610-641, 1996.

Krishnamoorti, R. and R. A. Vaia "Polymer nanocomposites." *Journal of Polymer Science Part B-Polymer Physics* Vol. 45(24): pp. 3252-3256, 2007.

Kumar, R. V., R. Elgamiel, Y. Diamant, A. Gedanken and J. Norwig "Sonochemical preparation and characterization of nanocrystalline copper oxide embedded in poly(vinyl alcohol) and its effect on crystal growth of copper oxide." *Langmuir* Vol. 17(5): pp. 1406-1410, 2001.

Lee, Y. J., B. Bingoel, T. Murakhtina, D. Sebastiani, W. H. Meyer, G. Wegner and H. W. Spiess "High-resolution solid-state NMR studies of poly(vinyl phosphonic acid) proton-conducting polymer: Molecular structure and proton dynamics." *Journal of Physical Chemistry* B 111(33): pp. 9711-9721, 2007.

Li, C. N., G. Q. Sun, S. Z. Ren, J. Liu, Q. Wang, Z. M. Wu, H. Sun and W. Jin "Casting Nafion-sulfonated organosilica nano-composite membranes used in direct methanol fuel cells." *Journal of Membrane Science* Vol. 272(1-2): pp. 50-57, 2006.

Li, S. W., Z. Zhou, Y. L. Zhang, M. L. Liu and W. Li "1H-1,2,4-triazole: An effective solvent for proton-conducting electrolytes." *Chemistry of Materials* Vol.17(24): pp. 5884-5886, 2005.

Lin, B., S. Cheng, L. Qiu, F. Yan, S. Shang and J. Lu "Protic Ionic Liquid-Based Hybrid Proton-Conducting Membranes for Anhydrous Proton Exchange Membrane Application." *Chemistry of Materials* Vol. 22(5): pp. 1807-1813, 2010.

Lin, H., Y. Watanabe, M. Kimura, K. Hanabusa and H. Shirai "Preparation of magnetic poly(vinyl alcohol) (PVA) materials by in situ synthesis of magnetite in a PVA matrix." *Journal of Applied Polymer Science* Vol. 87(8): pp. 1239-1247, 2003.

Lin, J., P. H. Wu, R. Wycisk, A. Trivisonno and P. N. Pintauro "Direct methanol fuel cell operation with pre-stretched recast Nafion (R)." *Journal of Power Sources* Vol. 183(2) pp. 491-497, 2008.

Lin, J., R. Wycisk, P. N. Pintauro and M. Kellner "Stretched recast Nafion for direct methanol fuel cells." *Electrochemical and Solid State Letters* Vol. 10(1): pp. B19-B22, 2007.

Liu, J., J. Li, Y. Ma, F. Chen And G. Zhao "Synthesis, Characterization And Aqueous Self-Assembly Of Octenyl-Succinate Oat B-Glucan." *Journal Of Agricultural And Food Chemistry,* 2013.

Liu, Z. L., B. Guo, J. C. Huang, L. Hong, M. Han And L. M. Gan "Nano-Tio2-Coated Polymer Electrolyte Membranes For Direct Methanol Fuel Cells." *Journal Of Power Sources* Vol. 157(1): pp. 207-211, 2006.

Lufrano, F., V. Baglio, P. Staiti, A. S. Arico and V. Antonucci "Development and characterization of sulfonated polysulfone membranes for direct methanol fuel cells." *Desalination* Vol. 199(1–3): pp. 283-285, 2006.

Lufrano, F., V. Baglio, P. Staiti, A. S. Arico and V. Antonucci "Polymer electrolytes based on sulfonated polysulfone for direct methanol fuel cells." *Journal of Power Sources* Vol. 179(1): pp. 34-41, 2008.

Ma, T. Y., X. J. Zhang, G. S. Shao, J. L. Cao and Z. Y. Yuan "Ordered macroporous titanium phosphonate materials: Synthesis, photocatalytic activity, and heavy metal ion adsorption." *Journal of Physical Chemistry C,* Vol. 112(8): pp. 3090-3096, 2008.

Ma, X.-k., N.-H. Lee, H.-J. Oh, J.-W. Kim, C.-K. Rhee, K.-S. Park and S.-J. Kim "Surface modification and characterization of highly dispersed silica nanoparticles by a cationic surfactant." *Colloids and Surfaces A: Physicochemical and Engineering Aspects* Vol. 358(1–3): pp. 172-176, 2010.

Macarie, L. and G. Ilia. "Poly(vinylphosphonic acid) and its derivatives." *Progress in Polymer Science* Vol. 35(8): pp. 1078-1092, 2010.

Mallakpour, S. and A. Barati (2011). "Efficient preparation of hybrid nanocomposite coatings based on poly(vinyl alcohol) and silane coupling agent modified TiO2 nanoparticles." *Progress in Organic Coatings* Vol. 71(4): pp. 391-398.

Marini, M., B. Pourabbas, F. Pilati and P. Fabbri "Functionally modified core-shell silica nanoparticles by one-pot synthesis." *Colloids and Surfaces A: Physicochemical and Engineering Aspects* Vol. 317(1–3): pp. 473-481, 2008.

Mauritz, K. A. And C. K. Jones "Novel Poly(Normal-Butyl Methacrylate) Titanium-Oxide Alloys Produced By The Sol-Gel Process For Titanium Alkoxides." Journal Of Applied Polymer Science Vol. 40(7-8): pp. 1401-1420, 1990.

Mckeen, J. C., Y. S. Yan And M. E. Davis "Proton Conductivity In Sulfonic Acid-Functionalized Zeolite Beta: Effect Of Hydroxyl Group." *Chemistry Of Materials* Vol. **20**(12): pp. 3791-3793, 2008.

Moskwiak, M., I. Giska, R. Borkowska, A. Zalewska, M. Marczewski, H. Marczewska and W. Wieczorek "Physico- and electrochemistry of composite electrolytes based on PEODME-LiTFSI with TiO2." *Journal of Power Sources* Vol. 159(1): pp. 443-448, 2006.

Munakata, H., H. Chiba and K. Kanamura "Enhancement on proton conductivity of inorganic–organic composite electrolyte membrane by addition of sulfonic acid group." *Solid State Ionics* Vol. 176(31–34): pp. 2445-2450, 2005.

Munakata, H., H. Chiba And K. Kanamura "Enhancement On Proton Conductivity Of Inorganic–Organic Composite Electrolyte Membrane By Addition Of Sulfonic Acid Group." Solid State Ionics Vol. **176**(31–34): pp. 2445-2450, 2005.

Nagarale, R. K., W. Shin and P. K. Singh "Progress in ionic organic-inorganic composite membranes for fuel cell applications." *Polymer Chemistry* Vol. 1(4): pp. 388-408, 2010.

Nakane, K., T. Yamashita, K. Iwakura and F. Suzuki "Properties and structure of poly(vinyl alcohol)/silica composites." *Journal of Applied Polymer Science* Vol. 74(1): pp. 133-138, 1999.

Nanjundan, S., C. S. Unnithan, C. S. J. Selvamalar and A. Penlidis "Homopolymer of 4-benzoylphenyl methacrylate and its copolymers with glycidyl methacrylate: synthesis, characterization, monomer reactivity ratios and application as adhesives." *Reactive and Functional Polymers* Vol. 62(1): pp. 11-24, 2005.

Navarrete, J., T. Lopez, R. Gomez and F. Figueras "Surface acidity of sulfated TiO2-SiO2 sol-gels." *Langmuir* Vol. 12(18): pp. 4385-4390, 1996.

Nogami, M., H. Matsushita, Y. Goto And T. Kasuga "A Sol-Gel-Derived Class As A Fuel Cell Electrolyte." *Advanced Materials* **12**(18): pp. 1370-1372, 2000.

Ou, D. L. and A. B. Seddon "Near- and mid-infrared spectroscopy of sol-gel derived ormosils: Vinyl and phenyl silicates." *Journal of Non-Crystalline Solids* Vol. 210(2-3): pp. 187-203, 1997.

Ozden, S., S. U. Celik and A. Bozkurt "Synthesis and Proton Conductivity Studies of Polystyrene-Based Triazole Functional Polymer Membranes." *Journal of Polymer Science Part a-Polymer Chemistry* Vol. 48(22): pp. 4974-4980, 2010.

Pandey, G. P., S. A. Hashmi And R. C. Agrawal "Hot-Press Synthesized Polyethylene Oxide Based Proton Conducting Nanocomposite Polymer Electrolyte Dispersed With Sio2 Nanoparticles." *Solid State Ionics* Vol. **179**(15-16): pp. 543-549, 2008.

Park, H. B., H. S. Shin, Y. M. Lee and J. W. Rhim "Annealing effect of sulfonated polysulfone ionomer membranes on proton conductivity and methanol transport." *Journal of Membrane Science* Vol. 247(1-2): pp. 103-110, 2005.

Parler, C. M., J. A. Ritter and M. D. Amiridis. "Infrared spectroscopic study of sol-gel derived mixed-metal oxides." Journal of Non-Crystalline Solids Vol. 279(2-3): pp. 119-125, 2001.

Peighambardoust, S. J. and B. Pourabbas "Preparation and characterization of Nylon-6/PPy/MMT composite of nanocomposite." *Journal of Applied Polymer Science* Vol. 106(1): pp. 697-705, 2007.

Peng, Z., L. X. Kong and S. D. Li "Thermal properties and morphology of a poly(vinyl alcohol)/silica nanocomposite prepared with a self-assembled monolayer technique." *Journal of Applied Polymer Science* Vol. 96(4): pp. 1436-1442, 2005.

Pielaszek, R. "FW1/5/4/5M method for determination of the grain size distibution form powder diffraction line profile." *Journal of Alloys and Compounds* Vol. 382(1-2): pp. 128-132, 2004.

Pu, H., H. Pan, Y. Qin, D. Wan and J. Yuan "Phosphonic acid-functionalized hollow silica spheres by nitroxide mediated polymerization." *Materials Letters* Vol. 64(13): pp. 1510-1512, 2010.

Qian, X. F., J. Yin, J. C. Huang, Y. F. Yang, X. X. Guo and Z. K. Zhu"The preparation and characterization of PVA/Ag2S nanocomposite." *Materials Chemistry and Physics* Vol. 68(1-3): pp. 95-97, 2001.

Rahman, I. A., P. Vejayakumaran, C. S. Sipaut, J. Ismail, M. A. Bakar, R. Adnan and C. K. Chee "An optimized sol–gel synthesis of stable primary equivalent silica particles." *Colloids and Surfaces A: Physicochemical and Engineering Aspects* Vol. 294(1–3): pp. 102-110, 2007.

Ramirez-Salgado, J. "Study of basic biopolymer as proton membrane for fuel cell systems." *Electrochimica Acta* Vol. 52(11): pp. 3766-3778, 2007.

Rao, K. S., K. El-Hami, T. Kodaki, K. Matsushige and K. Makino "A novel method for synthesis of silica nanoparticles." *Journal of Colloid and Interface Science* Vol. 289(1): pp. 125-131, 2005.

Ren, S. Z., G. Q. Sun, C. N. Li, S. Q. Song, Q. Xin And X. F. Yang "Sulfated Zirconia-Nafion Composite Membranes For Higher Temperature Direct Methanol Fuel Cells." *Journal Of Power Sources* Vol. **157**(2): pp. 724-726, 2006.

Rusanov, A. L., P. V. Kostoglodov, M. J. M. Abadie, V. Y. Voytekunas and D. Y. Likhachev Proton-Conducting Polymers and Membranes Carrying Phosphonic Acid Groups. *Fuel Cells* Ii. G. G. Scherer. Vol. 216: pp. 125-155, 2008.

Saccà, A., A. Carbone, E. Passalacqua, A. D'Epifanio, S. Licoccia, E. Traversa, E. Sala, F. Traini And R. Ornelas "Nafion–Tio2 Hybrid Membranes For Medium Temperature Polymer Electrolyte Fuel Cells (Pefcs)." *Journal Of Power Sources* Vol. **152**(0): pp. 16-21, 2005.

Sakai, T., S. Kajitani, S.-J. Kim, J.-i. Hamagami, H. Oda, M. Matsuka, H. Matsumoto and T. Ishihara "Proton conduction properties of hydrous sulfated nano-titania synthesized by hydrolysis of titanyl sulfate." *Solid State Ionics* Vol. 181(39-40): pp. 1746-1749, 2010.

Sakai, T., S.-J. Kim, S. Kajitani, J.-i. Hamagami, H. Oda, M. Matsuka, T. Ishihara and H. Matsumoto (). "Proton conduction properties of nano-titania modified by sulfuric acid impregnation." *Journal of Solid State Electrochemistry* Vol. 16(6): pp. 2055-2059, 2012.

Santiago, E. I., R. A. Isidoro, M. A. Dresch, B. R. Matos, M. Linardi And F. C. Fonseca "Nafion-Tio2 Hybrid Electrolytes For Stable Operation Of PEM Fuel Cells At High Temperature." *Electrochimica Acta* Vol. **54**(16): pp. 4111-4117, 2009.

Schadler, L. S., S. K. Kumar, B. C. Benicewicz, S. L. Lewis and S. E. Harton "Designed interfaces in polymer nanocomposites: A fundamental viewpoint." *Mrs Bulletin* Vol. 32(4) pp. 335-340, 2007.

Schaefer, D. W. and R. S. Justice "How nano are nanocomposites?" *Macromolecules* Vol. 40(24): pp. 8501-8517, 2007.

Schuster, M. E. and W. H. Meyer "Anhydrous proton-conducting polymers." *Annual Review of Materials Research* Vol. 33: pp. 233-261, 2003.

Schuster, M., T. Rager, A. Noda, K. D. Kreuer and J. Maier "About the choice of the protogenic group in PEM separator materials for intermediate temperature, low humidity operation: A critical comparison of sulfonic acid, phosphonic acid and imidazole functionalized model compounds." *Fuel Cells* Vol. 5(3) pp. 355-365, 2005.

Sedin, D. L. and K. L. Rowlen "Influence of tip size on AFM roughness measurements." *Applied Surface Science* Vol. 182(1-2): pp. 40-48, 2001.

Sevil, F. and A. Bozkurt (2004). "Proton conducting polymer electrolytes on the basis of poly (vinylphosphonic acid) and imidazole." *Journal of Physics and Chemistry of Solids* Vol. 65(10): pp. 1659-1662.

Sinirlioglu, D. Celik S.U, Muftuoglu A.E. and Bozkurt A. "Proton Conducting Copolymer Electrolytes Based on Vinyl Phosphonic Acid and 5-(Methacrylamido)tetrazole", *Macromolecular Chemistry and Physics*, 2013.

Sinirlioglu, D.Aslan A., Muftuoglu A.E. and Bozkurt A. "Synthesis and Proton Conductivity Studies of Methacrylate/Methacrylamide-Based Azole Functional Novel Polymer Electrolytes" 39915(1-8), 2013

Smitha, B., S. Sridhar and A. A. Khan "Polyelectrolyte complexes of chitosan and poly(acrylic acid) as proton exchange membranes for fuel cells." *Macromolecules* Vol. 37(6): pp. 2233-2239, 2004.

Smitha, B., S. Sridhar and A. A. Khan "Solid polymer electrolyte membranes for fuel cell applications - a review." *Journal of Membrane Science* Vol. 259(1-2): pp. 10-26, 2005.

Steininger, H., M. Schuster, K. D. Kreuer, A. Kaltbeitzel, B. Bingoel, W. H. Meyer, S. Schauff, G. Brunklaus, J. Maier and H. W. Spiess "Intermediate temperature proton conductors for PEM fuel cells based on phosphonic acid as protogenic group: A progress report." *Physical Chemistry Chemical Physics* Vol. 9(15): pp. 1764-1773, 2007.

Stöber, W., A. Fink and E. Bohn "Controlled growth of monodisperse silica spheres in the micron size range." Journal of Colloid and Interface Science Vol. 26(1) pp. 62-69, 1968.

Strawhecker, K. E. and E. Manias "Structure and properties of poly(vinyl alcohol)/Na+ montmorillonite nanocomposites." *Chemistry of Materials* Vol. 12(10) pp. 2943-2949, 2000.

Suryani And Y.-L. Liu "Preparation And Properties Of Nanocomposite Membranes Of Polybenzimidazole/Sulfonated Silica Nanoparticles For Proton Exchange Membranes." *Journal Of Membrane Science* Vol. **332**(1–2) pp. 121-128, 2009.

Takimoto, N., L. Wu, A. Ohira, Y. Takeoka and M. Rikukawa "Hydration behavior of perfluorinated and hydrocarbon-type proton exchange membranes: Relationship between morphology and proton conduction." *Polymer* Vol. 50(2) pp. 534-540, 2009.

Taniguchi, Y., K. Shirai, H. Saitoh, T. Yamauchi and N. Tsubokawa "Postgrafting of vinyl polymers onto hyperbranched poly(amidoamine)-grafted nano-sized silica surface." *Polymer* Vol. 46(8) pp. 2541-2547, 2005.

Trakanprapai, C., V. Esposito, S. Licoccia and E. Traversa "Alternative chemical route to mesoporous titania from a titanatrane complex." *Journal of Materials Research* Vol. 20(1) pp. 128-134, 2005.

Tripathi, B. P., A. Saxena and V. K. Shahi "Phosphonic acid grafted bis(4-gamma-aminopropyldiethoxysilylphenyl) sulfone (APDSPS)-poly(vinyl alcohol) cross-linked polyelectrolyte membrane impervious to methanol." *Journal of Membrane Science* Vol. 318(1-2) pp. 288-297, 2008.

Tsyalkovsky, V., V. Klep, K. Ramaratnam, R. Lupitskyy, S. Minko And I. Luzinov "Fluorescent Reactive Core–Shell Composite Nanoparticles With A High Surface Concentration Of Epoxy Functionalities." Chemistry Of Materials Vol. **20**(1) pp. 317-325, 2007.

Tuncer, E., I. Sauers, D. R. James, A. R. Ellis, M. P. Paranthaman, A. Goyal And K. L. More "Enhancement Of Dielectric Strength In Nanocomposites." *Nanotechnology* Vol. **18**(32) pp. 325704, 2007.

Uchida, H., Y. Ueno, H. Hagihara and M. Watanabe "Self-humidifying electrolyte membranes for fuel cells - Preparation of highly dispersed TiO2 particles in Nafion 112." *Journal of the Electrochemical Society* Vol. 150(1) pp. A57-A62, 2003.

Venckatesh, R., K. Balachandaran And R. Sivaraj "Synthesis And Characterization Of Nano Tio2-Sio2: PVA Composite - A Novel Route." *International Nano Letters* Vol. **2**(1) pp. 1-5, 2012.

Wagner, T., A. Manhart, N. Deniz, A. Kaltbeitzel, M. Wagner, G. Brunklaus and W. H. Meyer "Vinylphosphonic Acid Homo- and Block Copolymers." *Macromolecular Chemistry and Physics* Vol. 210(22) pp. 1903-1914, 2009.

Wang, H. T., B. A. Holmberg, L. M. Huang, Z. B. Wang, A. Mitra, J. M. Norbeck and Y. S. Yan "Nafion-bifunctional silica composite proton conductive membranes." *Journal of Materials Chemistry* Vol. 12(4) pp. 834-837, 2002.

Wang, J., H. Zhang, Z. Jiang, X. Yang And L. Mao "Tuning The Performance Of Direct Methanol Fuel Cell Membranes By Embedding Multifunctional Inorganic Submicrospheres Into Polymer Matrix." *Journal Of Power Sources* Vol. 188(1): pp. 64-74, 2009.

Wang, K., S. McDermid, J. Li, N. Kremliakova, P. Kozak, C. Song, Y. Tang, J. Zhang and J. Zhang "Preparation and performance of nano silica/Nafion composite membrane for proton exchange membrane fuel cells." *Journal of Power Sources* Vol. 184(1): pp. 99-103, 2008.

Watanabe, M., H. Uchida, Y. Seki, M. Emori and P. Stonehart "Self-humidifying polymer electrolyte membranes for fuel cells." *Journal of the Electrochemical Society* Vol. 143(12): pp. 3847-3852, 1996.

Wejrzanowski, T., R. Pielaszek, A. Opalinska, H. Matysiak, W. Lojkowski and K. J. Kurzydlowski "Quantitative methods for nanopowders characterization." *Applied Surface Science* Vol. 253(1): pp. 204-208, 2006.

Wen, J. Y. And J. E. Mark "Sol-Gel Preparation Of Composites Of Poly(Dimethylsiloxane) With Sio2 And Sio2/Tio2 And Their Mechanical-Properties." *Polymer Journal* Vol. 27(5) pp. 492-502, 1995.

Weston, J. E. And B. C. H. Steele "Effects Of Inert Fillers On The Mechanical And Electrochemical Properties Of Lithium Salt Poly (Ethylene-Oxide) Polymer Electrolytes." *Solid State Ionics* Vol. 7(1): pp. 75-79, 1982.

Won, J., H. Cho and Y. Kang "The effect of annealing on sSEBS/polyrotaxanes electrolyte membranes for direct methanol fuel cells." *Macromolecular Research* Vol. 17(10): pp. 729-733, 2009.

Wu, H., B. Zheng, X. Zheng, J. Wang, W. Yuan and Z. Jiang. "Surface-modified Y zeolite-filled chitosan membrane for direct methanol fuel cell." *Journal of Power Sources* Vol. 173(2): pp. 842-852, 2007.

Wu, H., W. Hou, J. Wang, L. Xiao and Z. Jiang "Preparation and properties of hybrid direct methanol fuel cell membranes by embedding organophosphorylated titania submicrospheres into a chitosan polymer matrix." *Journal of Power Sources* Vol. 195(13): pp. 4104-4113, 2010.

Yan, F., S. Yu, X. Zhang, L. Qiu, F. Chu, J. You and J. Lu "Enhanced Proton Conduction in Polymer Electrolyte Membranes as Synthesized by Polymerization of Protic Ionic Liquid-Based Microemulsions." *Chemistry of Materials* Vol. 21(8): pp. 1480-1484, 2009.

Yang, C. C. And S. J. Lin. "Preparation Of Composite Alkaline Polymer Electrolyte." *Materials Letters* Vol. **57**(4): pp. 873-881, 2002.

Yang, C., S. Srinivasan, A. S. Arico, P. Creti, V. Baglio and V. Antonucci. "Composition Nafion/zirconium phosphate membranes for direct methanol fuel cell operation at high temperature." *Electrochemical and Solid State Letters* Vol. 4(4): pp. A31-A34, 2001.

Yang, C.-C., S.-J. Chiu, K.-T. Lee, W.-C. Chien, C.-T. Lin and C.-A. Huang, "Study of poly(vinyl alcohol)/titanium oxide composite polymer membranes and their application on alkaline direct alcohol fuel cell." *Journal of Power Sources* Vol. 184(1): pp. 44-51 2008.

Yu, Y. H., C. Y. Lin, J. M. Yeh and W. H. Lin. "Preparation and properties of poly(vinyl alcohol)-clay nanocomposite materials." *Polymer* Vol. 44(12) pp. 3553-3560, 2003.

Zhang, H., X. Li, C. Zhao, T. Fu, Y. Shi and H. Na. "Composite membranes based on highly sulfonated PEEK and PBI: Morphology characteristics and performance." *Journal of Membrane Science* Vol. 308(1-2): pp. 66-74, 2008.

APPENDIX A

DECLARATION STATEMENT FOR THE ORIGINALITY OF THE THESIS, FURTHER STUDIES AND PUBLICATIONS FROM THESIS WORK

A.1 DECLARATION STATEMENT FOR THE ORIGINALITY OF THE THESIS

I hereby declare that this thesis comprises my original work. No material in this thesis has been previously published and written by another person, except where due reference is made in the text of the thesis. I further declare that this thesis contains no material which has been submitted for a degree or diploma or other qualifications at any other university.

Signature:

Date:February, 4 2014

A.2 FURTHER STUDIES

Functional nanoparticles for biomedical applications and nanocomposite materials for biomedical applications.

A.3 PUBLICATIONS FROM THESIS WORK

Academic Journals

- **Ayşe Aslan,** Kurtuluş Gölcük, Ayhan Bozkurt, " Nanocomposite polymer electrolytes membranes based on Poly(vinylphosphonic acid)/SiO2" Journal of Polymer Research (2012)
- **Ayşe Aslan**, Ayhan Bozkurt "Nanocomposite polymer electrolyte membranes based on poly (vinylphosphonic acid)/sulfated nano-titania. Journal of Power Sources 2012;217:158-163. "
- **Ayşe Aslan**, Ayhan Bozkurt "An investigation of proton conductivity of nanocomposite membranes based on sulfated nano-titania and polymer" Solid State Ionics 2013;239:21–27"
- **Ayşe Aslan**, Ayhan Bozkurt "Nanocomposite polymer electrolyte membranes based on poly(vinylphosphonic acid)/TiO2 nanoparticles" Journal of Materials Research, 27 (2012) 3090-3095.
- **Ayşe Aslan**, Ayhan Bozkurt "Preparation of Proton Conducting Membranes Containing Bifunctional Titania Nanoparticles" Journal of Nanoparticle Research 2013
- **Ayşe Aslan**, Ayhan Bozkurt "Nanocomposite Membranes Based on Sulfonated Polysulfone and Sulfated Nano-Titania / NMPA for Proton Exchange Membrane Fuel Cells" Solid State Ionics (accepted manuscript)
- **Ayşe Aslan**, Ayhan Bozkurt "Novel Polymer Grafted Hollow Silica Nano-Spheres As Proton Exchange Membranes" Langmuir(under review)

Other studies

- **Ayşe Aslan**, Ayhan Bozkurt "As an Alternative Membrane: Functional NanoParticles/Polymer Composites Membranes for Proton Exchange Membrane Fuel Cells (PEMFC)" Advanced Materials Research Vol. 716 (2013) pp 98-102

Conference Proceedings

- **Ayşe Aslan**, Ayhan Bozkurt,"Nanocomposite Polymer Electrolytes Membranes Based on Poly(vinylphosphonic acid) / SiO$_2$", Nano TR 8 Hacettepe Üniversitesi, Ankara 8. Türkiye Nanobilim-Nanoteknoloji Kongresi-Nano TR8 Haz. 2012

- **Ayşe Aslan**, Ayhan Bozkurt, "Preparation of Composite Membranes Containing Bifunctional Titania Nanoparticles for PEMFC", First International Chemistry & Chemical Engineering Conference, 18–21 April 2013, Qafqaz University, Baku, Azerbaijan, First International Chemistry & Chemical Engineering Conference Abstract&Proceedings, pp.64

- Ayhan Bozkurt, **Ayşe Aslan**, "As an Alternative Membrane: Functional NanoParticles/Polymer Composites Membranes for Proton Exchange Membrane Fuel Cells (PEMFC)" 2nd International Conference on Materials Science & Technology (ICMST 2013) Hong Kong, April 11-12, 2013, Advanced Materials Research Vol. 716 (2013) pp 98-102

- **Ayşe Aslan**, Sevim Ünügür Çelik, Ayhan Bozkurt "Boron, Siloxane and Nano Titania Containing Polymer Electolytes for Poton Exchange Membrane Fuel Cells (PEMFC)" Energy Matters Koç University, İstanbul 5 Dec. 2012 Energy Matters Conference.

A.4 PATENTS FROM THESIS WORK

- Azol Fonksiyonel SiO$_2$ Nanoparçacıkların Üretilmesi Ve Kanser Hücrelerine Olan Etkisi

APPENDIX B

Curriculum Vitae

Name&Surname: Ayşe ASLAN

E-mail: ayseaslan44@gmail.com

Adress: Fatih Univesity, Chemistry Department

Büyükçekmece, İstanbul

EDUCATION

- PhD, Fatih University, Chemistry, İstanbul
- MS, Fatih University, Chemistry-2009, İstanbul
    Thesis: Ayşe Aslan "The Production of Anhydrous Proton Conducting Biomembranes for Polymer Electrolyte Membrane Fuel Cell Applications"
- BS, İnönü University Chemistry-2006, Malatya

AWARDS AND HONORS

- Ranked 1st in Chemistry, İnönü University, June 2006
- Received full scholarship for MS degree studies from 2228 TUBITAK-BIDEB scholarship programme (2006-2009)
- Received full scholarship for MS degree studies from 2228 TUBITAK-BIDEB scholarship programme (2009-2014)

- Received full university scholarship for graduate studies in Chemistry at Fatih University, (2006 - 2009)
- Received full university scholarship for graduate studies in Chemistry at FatihUniversity, (2009 - 2013)

Experience

- Research/ Assistant, Fatih University, Sept. 2007- …

Research Interests

- Anhydrous Proton Conducting Polymer Membranes
- Li-polymer Batteries
- Biocomposite membranes
- Nano materials

Research Projects

- Polimer Elektrolit Membran Yakıt Hücrelerinde (PEMFC) Kullanım Amaçlı Proton İletken Nemsiz Membranların Üretilmesi, TÜBİTAK (108T103), 2009-2010, Araştırmacı.
- Azol Fonksiyonel Gruplar İçeren Akrilik Polimer Membranların Üretilmesi ve Karakterizasyonları, BAP, 2011-2012, Araştırmacı
- Polimer Nanokompozit Membranların üretilmesi ve Proton İletkenlik Özelliklerinin İncelenmesi BAP, 2009-2010, Araştırmacı

Publications:

Academic Journals

- **Ayşe Aslan**, Sevim Ünügür Çelik, Ayhan Bozkurt, "Proton-conducting properties of the membranes based on poly(vinyl phosphonic acid) grafted poly(glycidyl methacrylate)" Solid State Ionics, 180 (2009) 1240–1245
- **Ayşe Aslan,** Sevim Ü. Çelik, Ünal Şen, Resul Haser, Ayhan Bozkurt, "Intrinsically proton-conducting poly(1-vinyl-1,2,4-triazole)/triflic acid blends", Electrochimica Acta, Vol. 54, No. 11, Apr. 2009, pp. 2957-2961

- Sevim Ü. Çelik, **Ayşe Aslan,** Ayhan Bozkurt , "Phosphoric acid-doped poly(1-vinyl-1,2,4-triazole) as water-free proton conducting polymer electrolytes", Solid State Ionics, Vol. 179, No. 19-20, Aug. 2008, pp. 683-688

- Zehra Durmus, Hüseyin Kavas, Muhammet Sadaka Toprak, Abdülhadi Baykal,Tuba Gürkaynak Altınçekic, **Ayşe Aslan**, Ayhan Bozkurt, Sedat Coşgun, "l-lysine coated iron oxide nanoparticles: Synthesis, structural and conductivity characterization" Journal of Alloys and Compounds 484 (2009) 371–376

- **Ayşe Aslan**, Ayhan Bozkurt, "Development and characterization of polymer electrolyte membranes based on ionical cross-linked poly(1-vinyl-1,2,4 triazole) and poly(vinylphosphonic acid)" Journal of Power Sources 191 (2009) 442–447

- **Ayşe Aslan**, Ünal Şen, Ayhan Bozkurt, "Preparation, Properties, and Characterization of Polymer Electrolyte Membranes Based on Poly(1-vinyl-1,2,4 triazole) and Poly(styrene sulfonic acid)" Journal of The Electrochemical Society, 156, 10, B1112-B1116 (2009)

- Hüseyin Kavas, Zehra Durmus, Abdülhadi Baykal, **Ayşe Aslan**, Ayhan Bozkurt, Muhammet Sadaka Toprak, "Synthesis and conductivity evaluation of PVTri–Fe_3O_4 nanocomposite" Journal of Non-Crystalline Solids Volume 356, Issues 9-10, (2010), Pages 484-489

- Zehra Durmus, Hüseyin Kavas, Ebubekir Karaoğlu, Hüseyin Sozeri, **Ayşe Aslan**, Abdülhadi Baykal, Poly(vinyl phosphonic acid) (PVPA)–$BaFe_{12}O_{19}$ nanocomposite Journal of Superconductivity and Novel Magnetism Vol. 25, Jan. 2012, pp. 1185-1193

- **Ayşe Aslan**, Ayhan Bozkurt, "Bioinspired Blend Membranes Based on Adenine and Guanine Functional Poly(glycidyl methacrylate)" Langmuir 2010, 26(16), 13655–13661

- **Ayşe Aslan**, Ayhan Bozkurt, "Proton conducting properties of ionically cross-linked poly(1-vinyl-1,2,4 triazole) and poly(2-acrylamido-2-methyl-1-propanesulfonic acid) electrolytes" Polymer Bulletin 2012; 66(8):1099-1110

- Z. Durmus, H. Erdemi, **A. Aslan**, M.S. Toprak, H. Sozeri, A. Baykal, "Synthesis and characterization of poly(vinyl phosphonic acid) (PVPA)–Fe3O4 nanocomposite" Polyhedron 30 (2011) 419–426.

- **Ayşe Aslan,** Kurtuluş Gölcük, Ayhan Bozkurt, " Nanocomposite polymer electrolytes membranes based on Poly(vinylphosphonic acid)/SiO2" Journal of Polymer Research (2012)

- **Ayşe Aslan**, Ayhan Bozkurt "Nanocomposite polymer electrolyte membranes based on poly (vinylphosphonic acid)/sulfated nano-titania. Journal of Power Sources 2012;217:158-163. "

- **Ayşe Aslan**, Ayhan Bozkurt "An investigation of proton conductivity of nanocomposite membranes based on sulfated nano-titania and polymer" Solid State Ionics 2013;239:21–27"

- **Ayşe Aslan**, Ayhan Bozkurt "Nanocomposite polymer electrolyte membranes based on poly(vinylphosphonic acid)/TiO2 nanoparticles" Journal of Materials Research, 27 (2012) 3090-3095.

- **Ayşe Aslan**, Ayhan Bozkurt "Preparation of Proton Conducting Membranes Containing Bifunctional Titania Nanoparticles" Journal of Nanoparticle Research 2013

- **Ayşe Aslan**, Ayhan Bozkurt "Nanocomposite Membranes Based on Sulfonated Polysulfone and Sulfated Nano-Titania / NMPA for Proton Exchange Membrane Fuel Cells" Solid State Ionics (accepted manuscript)

- **Ayşe Aslan**, Ayhan Bozkurt "Novel Polymer Grafted Hollow Silica Nano-Spheres As Proton Exchange Membranes" Langmuir(under review)

- Deniz Sinirlioglu, **Ayse Aslan**, Ali Ekrem Muftuoglu, Ayhan Bozkurt, "Synthesis and Proton Conductivity Studies of Methacrylate / Methacrylamide Based Azole Functional Novel Polymer Electrolytes" Journal of Applied Polymer Science

Other studies

- **Ayşe Aslan**, Ayhan Bozkurt   "As an Alternative Membrane: Functional NanoParticles/Polymer Composites Membranes for Proton Exchange Membrane Fuel Cells (PEMFC)" Advanced Materials Research Vol. 716 (2013) pp 98-102

Proceedings&Posters

- **Ayşe Aslan,** Ayhan Bozkurt, Polimer Elektrolit Membran Yakıt Hücrelerinin Uygulamaları İçin Nemsiz Proton İletken Biomembranların Üretilmesi, IV.Ulusal Hidrojen Enerjisi Kongresi 2009,

- Sevim Ünügür Çelik, **Ayşe Aslan**, Ayhan Bozkurt, "Poli(Glisidil metakrilat-g-vinil fosfonik asit) kopolimerinin sentezlenmesi ve proton iletkenlik

özelliklerinin İncelenmesi", Iv.Ulusal Hidrojen Enerjisi Kongresi (Uhk 2009) Ve Sergisi, Kocaeli/Türkiye, Oct. 2009 Iv. Ulusal Hidrojen Enerjisi Kongresi (Uhk 2009) Ve Sergisi, Bildiri Kitabı, pp.75

- **Ayşe Aslan**, Ayhan Bozkurt Polimer Elektrolit Membran Yakıt Hücresi Uygulamaları İçin Poli(1-Vinil-1,2,4 triazol) / Poli(stiren sülfonik asit) Bazlı Kompozit Membranların Üretilmesi ve Karakterizasyonu, III. Polimer Kongresi ve Sergisi, Kocaeli Üniversitesi, May. 2010 III. Polimer Kongresi ve Sergisi

- Sevim Ünügür Çelik, **Ayşe Aslan**, Ayhan Bozkurt, Ümit Akbey, Robert Graf, Hans W. Spiess, "Proton conducting polymer electrolytes based on 1-vinyl-1,2,4-triazole and vinylphosphonic acid", 10 th European Symposium on Polymer Blends, Dresden/Almanya, Mar. 2010, Book of Abstracts, pp.65

- **Ayşe Aslan**, Sevim Ünügür Çelik, Ünal Şen, Ayhan Bozkurt, "Preparation and Characterization of Polymer Electrolyte Membranes Based on Poly(1-Vinyl-1,2,4 triazole) and Poly(styrene sulfonic acid)", 10 th European Symposium on Polymer Blends", Dresden/ Almanya, Mar. 2010, Book of Abstracts, pp.155

- **Ayşe Aslan**, Ayhan Bozkurt,"Nanocomposite Polymer Electrolytes Membranes Based on Poly(vinylphosphonic acid) / SiO_2", Nano TR 8 Hacettepe Üniversitesi, Ankara 8. Türkiye Nanobilim-Nanoteknoloji Kongresi-Nano TR8 Haz. 2012

- **Ayşe Aslan**, Ayhan Bozkurt, "Preparation of Composite Membranes Containing Bifunctional Titania Nanoparticles for PEMFC", First International Chemistry & Chemical Engineering Conference, 18–21 April 2013, Qafqaz University, Baku, Azerbaijan, First International Chemistry & Chemical Engineering Conference Abstract&Proceedings, pp.64

- Ayhan Bozkurt, **Ayşe Aslan**, "As an Alternative Membrane: Functional NanoParticles/Polymer Composites Membranes for Proton Exchange Membrane Fuel Cells (PEMFC)" 2nd International Conference on Materials Science & Technology (ICMST 2013) Hong Kong, April 11-12, 2013, Advanced Materials Research Vol. 716 (2013) pp 98-102

- **Ayşe Aslan**, Sevim Ünügür Çelik, Ayhan Bozkurt "Boron, Siloxane and Nano Titania Containing Polymer Electrolytes for Poton Exchange Membrane Fuel Cells (PEMFC)" Energy Matters Koç University, İstanbul 5 Dec. 2012 Energy Matters Conference.